UNIVERSITÀ DEGLI STUDI DI TRIESTE
e
UNIVERSITÀ CA' FOSCARI DI VENEZIA

XXXI CICLO DEL DOTTORATO DI RICERCA IN

CHIMICA

Integration of bioinformatics analysis and experimental biocatalysis for a comprehensive approach to the synthesis of renewable polyesters

Settore scientifico-disciplinare: CHIM/06 CHIMICA ORGANICA

DOTTORANDO / A
MARCO CESPUGLI

COORDINATORE
PROF. BARBARA MILANI

SUPERVISORE DI TESI
PROF. LUCIA GARDOSSI

ANNO ACCADEMICO 2017/2018

Table of contents

Abstract

The rising demand for advanced polyesters, displaying new functional properties, has boosted the development of new biocatalysed routes for polymer synthesis, where enzymes concretely respond to the challenge of combining benign conditions with high selectivity and efficient catalysis. Enzymes are attractive sustainable alternatives to toxic catalysts used in polycondensation, such as metal catalysts and tin in particular. Moreover, they enable the synthesis of functional polyesters that are otherwise not easily accessible by using traditional chemical routes.

Enzymes add higher value to bio-based polymers by catalysing not only their selective functionalization but also their synthesis under mild and controlled conditions.

The aim of the present thesis is to integrate experimental and bioinformatics approaches in order to study new biocatalysts to be used in polycondensations.

Aliphatic polyesters are among the most widely used biodegradable polymers. Typically, such polymers are produced by means of polycondensation reactions which make use of toxic metal catalysts with the risk of product contamination, making them not suitable for the use in the production of materials of biomedical interest. More importantly, traditional metal-based catalysts are less selective in comparison to enzymes, making difficult the synthesis of functional polyesters displaying complex structures.

A valid alternative to metal catalysts is represented by enzymes. Biocatalyst recyclability and avoidance of product contamination are usually obtained via enzyme immobilization on solid carriers. Nowadays, non-renewable petrochemical-based supports are used for this purpose, namely methacrylic and styrenic resins. In this thesis (Chapter 3), rice husk - a waste product of rice milling available worldwide at a negligible price - has been explored as an innovative and fully renewable lignocellulosic carrier endowed with morphological complexity and chemical versatility that makes it prone to multiple and benign chemo-enzymatic modifications. A comparison of chemical and enzymatic methods for the functionalization of rice husk has been carried out, enabling the development of a renewable immobilization carrier suitable for responding to the looming challenge of green chemistry. The enzymatic method relies on laccase oxidation using laccase from *Trametes spec.* and TEMPO-radical mediator, followed by the insertion of a diamine spacer[1]. As compared to the classical cellulose oxidation performed via sodium periodate, the enzymatic method offers the advantage of preserving the morphology of rice husk, as demonstrated by SEM

microscopy. Laccase oxidation also assures benign operative conditions. *Candida antarctica* Lipase B, and two commercially available formulations of asparaginase, were immobilized and tested. In the first case, the lipase was successfully applied in the polycondensation of the biobased monomer dimethyl itaconate whereas the immobilized asparaginases were applied in the hydrolysis of asparagine, a precursor of the toxic acrylamide in food. In addition, lignin removal via alkaline hydrogen peroxide bleaching has been tested as a method for increasing the specific activity of the immobilized formulation.

While lipases being the most common alternative for polycondensation reactions, our research group focused on the study of a novel class of serine hydrolases to be used in these kind of reactions, namely the cutinases[2]. The cutinase class proved to catalyse the efficient polycondensation of biobased monomers working in mild conditions in terms of pressure and temperature[3]. A thorough bioinformatics study was carried out based on GRID-based BioGPS descriptors (Chapter 4). BioGPS allowed to project a selection of cutinases on a Unsupervised Pattern Cognition Analysis (UPCA) model previously published by this research group[4], confirming that the pre-organized physicochemical environment in the active site of Cutinase 1 from *Thermobifida cellulosilytica* is very similar to the one of *Candida antarctica* Lipase B, while offering increased capabilities in terms of the size of the substrate accepted, thanks to a superficial and wide active site. The said software was used also to generate the "catalophor" of different serine hydrolase subfamilies, enabling to extract the structural features that distinguish the various sub-families of serine hydrolases. Exploiting the "catalophor" tool and molecular dynamics studies it was possible to shed light on the particular behaviour that makes cutinases an advantageous biocatalyst to be used in polycondensation reactions.

1. Objectives and outline

The present work is part of a wider context aimed to the development of renewable solutions for the synthesis of high added value green-polyesters carried forward by the Laboratory of Applied and Computational Biocatalysis (LACB) of the University of Trieste. More specifically, we focused on the valorisation of rice husk, an inexpensive composite material derived as a waste of the industrial processing of rice[5]. The high worldwide availability, the particular physicochemical features and the high percentage of polymeric organic matrix prone to be functionalized, make the said lignocellulosic material an option for producing carriers for enzyme immobilization with the potential to be used in industrial processes, where recyclability of the biocatalyst and cost-effective solutions in terms of process design play a central role. The possibility of introducing functionalizable chemical groups on the cellulose fraction of rice husk paves the way to the exploitation of this material for a wide range of opportunities, in particular the replacement of methacrylic and styrenic resins.

The Laboratory of Applied and Computational Biocatalysis studied rice husk as an immobilization carrier for various enzymes including enzymes belonging to the classes of lipases, invertases, proteases and cutinases[3,5]. Various techniques were tested for the immobilization, including physical adsorption, cross-linking and covalent immobilization using tailored functional groups. For this purpose, the rice husk was chemically treated in order to functionalize the cellulosic component.

A characterization of the starting material was carried out in order to clarify the morphology and the physical properties of the rice husk and how they can be exploited the enzyme immobilization. Subsequently, the functionalization and immobilization technique was tested with *Candida antarctica* lipase B (CaLB) and with asparaginase. Lipase immobilization plays an important role in the research carried out at LACB because of their involvement in the synthesis of high added value polyesters starting from renewable monomers; full renewability of the synthetic process – from the choice of the immobilization carrier to the selection of monomers – is the main goal. Various chemical modification methods of rice husk aiming to obtain the best yield in terms of protein loading and enzyme activity will be commented, including oxidation by sodium periodate and laccase and pre-treatment with alkaline hydrogen peroxide to increase the immobilization yield.

Another key aspect for the efficient use of enzymes for industrial purposes, with particular attention to biocatalysed polycondensations, is the selection of a suitable enzyme to be used in the synthetic process. Our previous computational investigations disclosed how two

cutinases employed in polycondensation, namely *Humicola insolens* cutinase (HiC) and cutinase 1 from *Thermobifida cellulosilytica* (Thc_cut1), share common features with CaLB. For example, the hydrophobicity of their surface is a consequence of the insolubility of their natural substrates[3,6]. Moreover, the BioGPS-based calculation of the "catalophor" of entire enzyme sub-families, coupled with molecular dynamics simulations allowed to shed light on the structural features of a dataset of serine hydrolases, where cutinases play a central role as regards the biocatalysed polycondensations. The calculation of the "catalophor" tool helps to identify the most important physicochemical features of the active sites responsible of establishing an interaction with the substrate.

Cutinases are enzymes of particular interest because, unlike CaLB and most lipases, the catalytic Ser of the considered cutinases is not buried in a deep funnel shape active site but the active site is rather superficial and accessible to solvents and substrates[6]. In the case of Thc_cut1, the wider and more accessible active site, along with efficiency under milder and less strictly anhydrous conditions represent crucial features for the development of strategies for polymer synthesis and modification, as well as for the design of optimized hydrolases starting from the Thc_cut1 scaffold[3].

When cutinases are compared to lipases and CaLB in particular, it is important to consider that industry has been making a wide use of lipases - especially in detergent formulations- since several decades, therefore pushing the scientific research towards the optimization of stability, activity and expression of these biocatalysts. Similar efforts would be needed for transforming selected promising cutinases into efficient industrial biocatalysts in the current optics of developing a sustainable bioeconomy.

2. Background

2.1 The role of enzymes in the bioeconomy

During the last 150 years, the global industrial economy has always pursued a linear approach that consists of gathering resources, transforming them into products and their disposal after usage. In terms of volume, that caused the extraction of 65 billion tons of raw materials[7]; taking into account that 3 billion of new consumers are expected to reach the market by 2030, it is clear that an economic model like this is no more sustainable. The economic cost of raw materials and their extraction is now constantly increasing because the descending trend of the XX century has been broken[8]. Another key point is the slowdown of agricultural productivity due to the worsening of soil quality caused by overexploitation.

These kinds of issues can be efficiently faced by circular bioeconomy with the valorisation of waste materials. The aim of circular bioeconomy is, in fact, reintegrate waste in the production process, treating them as valuable resources and establishing a virtuous cycle where the waste is transformed into high added value starting material. Circular bioeconomy represents a great change of paradigm where the concept of "end of life" is replaced by recycling, removing in particular the need of bringing back in the biosphere toxic chemicals and not environmentally friendly materials; this kind of approach requires a redesign of materials, products and business models[7] that aims to make extensive use of renewable resources with a particular focus to those parts of the product that cannot be recycled, and that should be recovered and brought back to the production cycle.

In the big vision of circular bioeconomy, chemistry obviously plays a central role. The target of sustainable chemistry is redefining synthetic processes and products in order to minimize the environmental impact while maximizing the possibility of recycling and re-usage. To that extent, the green chemistry offers the practical tools needed to put in place this paradigmatic and holistic change, which must start from research labs to reach the big industrial production. The philosophy of the green chemistry could be summarised in the twelve principles here reported:

- Avoiding waste production is more favourable than handling their disposal;
- Synthetic methodologies should be tuned to allow the maximum yield;
- Where possible, unharmful and non-polluting substances should be used;
- Chemicals employed should be carefully selected to avoid toxic substances production throughout the entire life cycle of the product;

- Volatile chemicals usage reduction (i.e. solvents);
- Energetic requirements should be assessed taking into account the economic and environmental impact. Synthetic methodologies at environmental pressure and temperature should be encouraged;
- Renewable matters should be preferred;
- Production of side products should be avoided or limited;
- The use of catalysts should be encouraged;
- Chemicals should be designed to not cause environmental harm after their disposal and should be subject to natural biodegradative processes;
- Analytical procedures should be designed to avoid the real-time formation of toxic substances;
- Chemicals should be chosen based on their safety in terms of explosions or accidental release in the environment.

Biocatalysis fits very well the above-mentioned principles and can represent a good synthetic methodology to push for the creation of environmentally compatible, cost-effective and innovative products.

2.2 Biocatalysis

Biocatalysis refers to use natural catalysts, such as enzymes or microorganisms, to perform chemical transformations[9]. Biocatalysis is a broad science whose comprehensive definition requires a multidisciplinary approach that involves molecular biology, biochemistry, organic chemistry, engineering and others[10].

Enzymatic reactions have been exploited since the dawn of the history of man for beer, cheese and other foods productions and also for the treatment of leather and silk. The industrial use of biocatalysis started 30 years ago, thanks to the recombinant DNA technology, driving to the synthesis of high added value chemicals: the so-called fine chemicals. Nowadays biocatalytic methodologies are extensively used in different fields, spacing from the pharmaceutical and food industry to textile and medical sectors.

Lowering the activation energy of a chemical transformation, enzymes are able to boost reaction rate to several orders of magnitude, enabling obtaining low environmental and economic impact products, reducing the use of non-renewable resources and avoiding or limiting the formation of toxic by-products.

The main advantages of biocatalysts are that they are biodegradable and non-toxic for the humans and for the environment, their usage enables working in a reasonable range of pressure and temperature conditions and the use of metals and organic solvents can be avoided. Another important feature of enzymes is their chemo- regio- and stereoselectivity; for this reason, they are often used for the synthesis of chiral molecules (i.e. steroids).

Biocatalysis also have some drawbacks. If recombinant DNA technology paved the way to a broad availability of these catalysts, enzymes still remain not so stable (i.e. easily losing activity because of temperature, mechanical stress, pH), the procedure of development and process optimization represents a major obstacle and, lastly, not every chemical reaction could be catalysed by known enzymes.

2.3 Biocatalysed synthesis of aliphatic polyesters

Aliphatic polyesters are among the most widely used biodegradable polymers. Typically, such polymers are produced by means of polycondensation reactions which make use of metal catalysts as manganese, zinc, calcium, cobalt, magnesium acetates and antimuonium and titan oxides[11]. Their toxicity and the risk of product contamination by the catalyst, make them not suitable for the use in the production of materials of biomedical interest. More importantly, traditional metal-based catalysts are less selective in comparison to enzymes, making hard the synthesis of functional polyesters displaying complex structures. For example, the use of monomers with three or more functional groups can lead to uncontrolled polymerization and branching. Usually, chemical polycondensations are carried out at high temperatures (180-280 °C) in order to reduce the viscosity of the system, with the side effect of promoting the formation of by-products. In addition, such temperatures must be avoided in presence non-thermostable monomers bearing functional groups like siloxanes, epoxides, vinylic groups.

In 1980 enzymatic polycondensation was introduced as a technique that makes use of an isolated enzyme to catalyse the polyesterification process[12]. The biocatalysed polymerization can be based on polycondensation or ring-opening polymerization of lactones (ROP). More specifically, these reactions can be further split in diacids and their esters polycondensations with diols and polycondensations of hydroxy acids and their esters with themselves (self-polycondensation).

Biocatalysed polycondensations have been extensively used in the industry in the last 20 years because other than being eco-friendly processes, they bring multiple advantages in comparison to the classical chemical synthesis[13]:

- high catalytic activity (turnover number);

- mild reaction conditions;

- high chemo-regio-enantio selectivity;

- low by-products formation;

However, there are also some drawbacks in the use of immobilized enzymes:

- biocatalyst are often unstable

- there is a low choice in terms of available enzymes

- cost-effectiveness

- time and costs needed for the development of an industrial biocatalysed process

The modern immobilization and protein engineering techniques allow to overcome most of the mentioned disadvantages, providing a wide number of high performance and cost-effective biocatalysts[14].

2.4 Lipases and cutinases as a tool for the synthesis of green polyesters

100 years ago, the physician C. Eijkmann discovered that some bacteria are able to produce and secrete lipases, enzymes belonging to the family of serine hydrolases that turned out to be stable in organic media. This finding had important practical applications in the field of organic chemistry.

Nowadays, lipases are broadly studied and largely employed in the industry due to the ease of preparation starting from fungi and bacteria. No cofactors are needed for their activity, and they are able to catalyse esterifications and transesterifications also in organic media[15]. Lipases (EC 3.1.1.3) are defined as long chain (10+ C) triacylglycerol carboxylesterases. Hydrolysing short-chain lipids is more typical of esterases, but very often lipases are able to hydrolyse them too[16].

Originally, two key requirements were pointed out to define what exactly characterise an enzyme with lipolytic activity as a lipase:

1. The enzyme must be activated when in correspondence of an oil/water interface and its activity must increase when triglycerides are in form of an emulsion. This behaviour is called interfacial activation;

2. The enzyme shall have a superficial and mobile peptide loop covering the active site and called lid. That structure is displaced when the substrate approaches[16]. Recently researchers have established that this definition is not completely correct because of

the existence of interfacial activation-lacking lipases as some lipases from *Pseudomonas* and *Candida antarctica* lipase B.

Our research group addressed also cutinases, another serine hydrolase sub-family, to be efficiently used in polycondensation reactions in thin-film, solvent-free conditions, while employing rice husk as a carrier for enzyme immobilization and enabling for the first time a fully renewable synthesis of polyesters[3,6]. In a precedent work of this group, a multivariate fractional design demonstrated that Cutinase 1 from *Thermobifida cellulosilytica* (Thc_cut1) is able to catalyse the synthesis of biobased aliphatic polyesters in mild conditions, offering some advantages in comparison with CaLB. In particular, the reaction can take place at mild environmental conditions; notably, the activity of Thc_cut1 is higher at environmental pressure and at low temperature (50 °C), increasing the sustainability of the process. In addition, Thc_cut1 has a superficial active site capable of accepting larger substrates in comparison to CaLB (Figure 1).
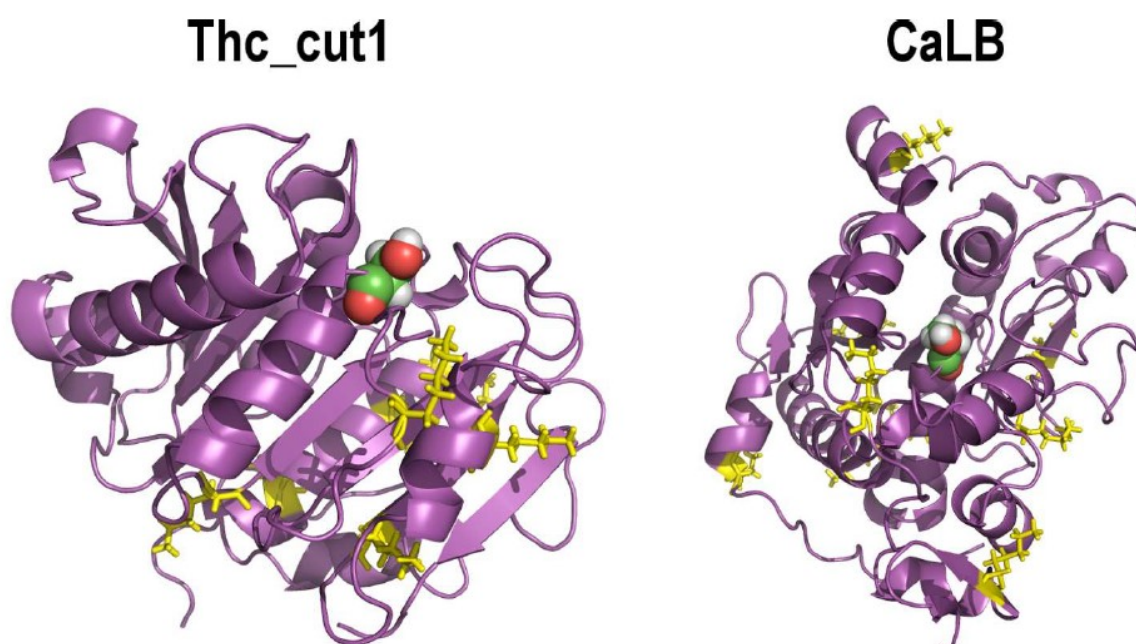
Figure 1: Cutinase 1 from Thermobifida cellulosilytica (Thc_cut1) and Candida antarctica lipase B. Lys residues are represented in yellow and are targeted by covalent enzyme immobilization. Catalytic serine, shown in spheres, occupies a more superficial position in Thc_cut1. (Pellis et al. 2015)

2.5 Catalytic mechanism of serine hydrolases

Lipases and cutinases are serine hydrolases presenting a catalytic triad composed of serine, histidine and aspartic or glutamic acid. The catalytic mechanism starts with the nucleophilic attack of the oxygen on the sidechain of the serine to the carbonyl on the ester moiety of the

substrate. The tetrahedral intermediate presents a negative charge stabilized b H-bond interaction formed with the so-called oxyanion hole. Conversely, the charge on the protonated histidine is stabilized by an H-bond with the acid catalyst of the catalytic triad. Consequently, a proton transfer involving histidine and the alkoxy of the ester is carried out, leading to the release of the alcohol with the simultaneous formation of the acyl-enzyme intermediate.

The acyl-enzyme intermediate is then deacylated thanks to the reaction with a new nucleophile (i.e. water, alcohols, amines). The histidine of the active site extract a proton from the above-mentioned nucleophile and the hydroxyl anion reacts with the acyl-enzyme carbonyl. A second tetrahedral intermediate is formed an stabilized by the oxyanion hole. In the last step, the histidine loses a proton that is accepted by the serine with the simultaneous release of the product and active site environment regeneration[16] (Figure 2).
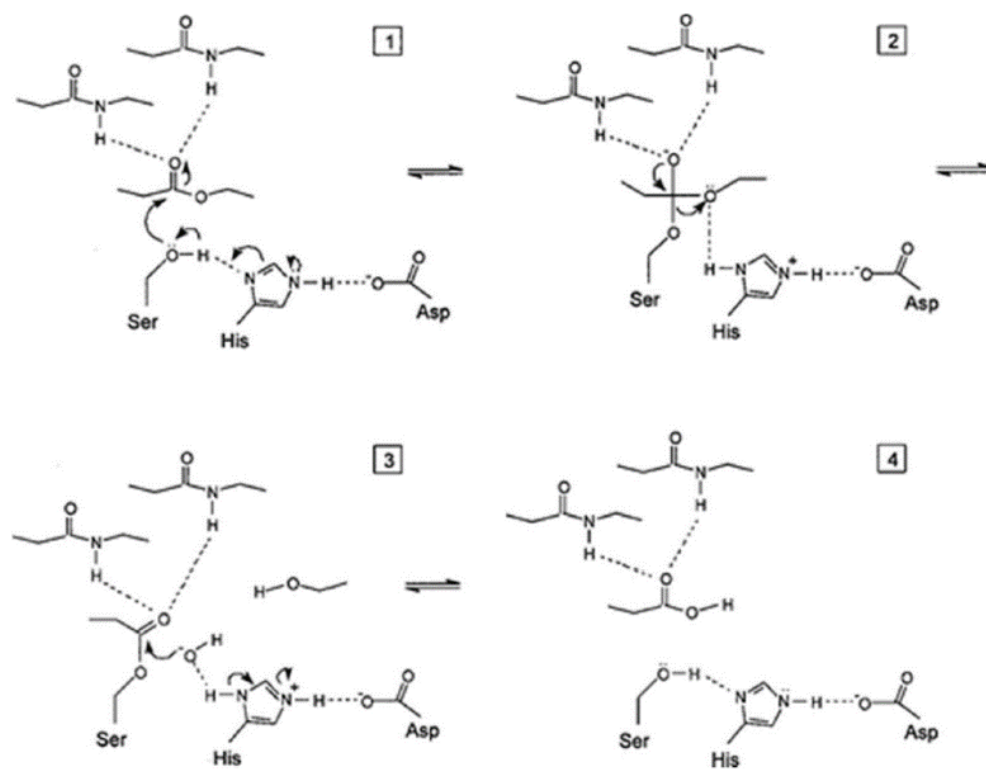
Figure 2. Reaction mechanism of a typical lipase (Jaeger et al. 1999)

2.6 Polyesterification reactions and enzyme immobilization

Lipase B from the yeast *Candida antarctica* is one of the most used lipases in various fields like chemistry, pharmaceutical and food industries[17]. As its name suggests, the yeast was discovered in the Antarctica during a research that aimed to find out new enzymes to be used

in the formulation of detergents. The yeast produces two isoenzymes; lipase A (CaLA) activity depends on calcium ions and is highly thermostable, on the other hand, lipase B activity does not rely on the presence of metal ions in the reaction media but it is much less thermostable. Furthermore, lipase A is active on a broad spectrum of triglycerides and is not much active towards non-natural ester substrates. Both the isoenzymes are produced via cloning and expression of the lipase codifying genes in *Aspergillus oryzae* cells[18].

CaLB is a robust and organic solvent friendly enzyme of 317 amino acids, with a molecular mass of 33 kDa. Its deactivation starts at temperatures higher than 60 °C. If immobilized on a solid support it is able to withstand harsher conditions like polar organic solvents, low water activity media, alkaline pH and higher temperatures. To date, CaLB is produced both in free and in immobilized form by the companies Novozym, Roche Diagnostics, Almac, Chiral Vision and Syncore Laboratories[19].

Furthermore, CaLB (Figure 3) is to be considered a hybrid between a lipase and an esterase because – compared with other lipases – this enzyme is much less conformationally mobile and does not present a clear interfacial activation[20]. The narrow active site is buried in the enzyme structure, and the catalytic triad is represented by Ser105, Asp187 and His224. The oxyanion hole forming amino acids are Thr40, Gln106.
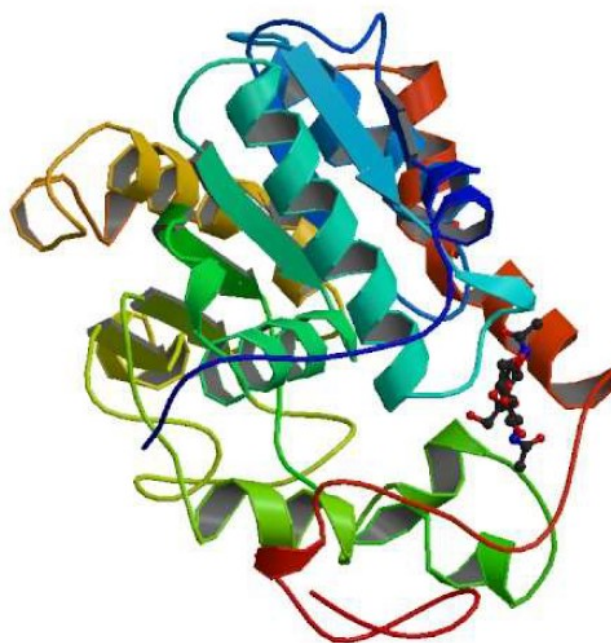
Figure 3. Lipase B from *Candida antarctica* (Uppenberg et al. 1994)

To date, CaLB is one of the most suitable enzymes in polyesterification reactions because of its favourable stability and catalytical features.

The enzymatic synthesis of polyesters requires immobilized biocatalysts because the use of a water suspension of the protein is not compatible with the formation of polyesters, driving the reaction towards hydrolysis rather than synthesis. Working with immobilized enzymes also avoids product contamination, protein aggregation and limits denaturation while enabling biocatalyst recycling after product separation.

The enzyme carriers commonly used for protein immobilization are methacrylic resins of petrochemical derivation. Their usage has clearly the drawback of the environmental impact associated with the production and disposal of such carriers. Life-cycle Assessment (LCA) analysis pointed out that a great contribution to acidification and eutrophication events is given by the usage of methacrylic resins in fermentative processes involving enzymes. In particular, it has been calculated that, for each kg of immobilized biocatalyst, 16 to 25 kg of carbon dioxide are produced and 117-207 MJ of non-renewable energy are consumed. However, because of their cost-effectiveness, petrochemical carriers are still extensively used[21].

The majority of the examples of polyesterification reported in the literature make use of CaLB in its commercial formulation Novozym 435, where the enzyme is immobilized by adsorption over methacrylic beads[22–24].

Novozyme 435 has been widely used on solvent-free systems or in presence of organic solvents. As reported by Binns[25], the viscosity of polycondensation products and the need of mechanical stirring are so stressful for the support that adsorbed enzyme detachment is easily noticed, due to the weak enzyme-support interactions. To overcome this issue, our research group[26] proposed the covalent immobilization on methacrylic resins with epoxy moieties (Figure 4).
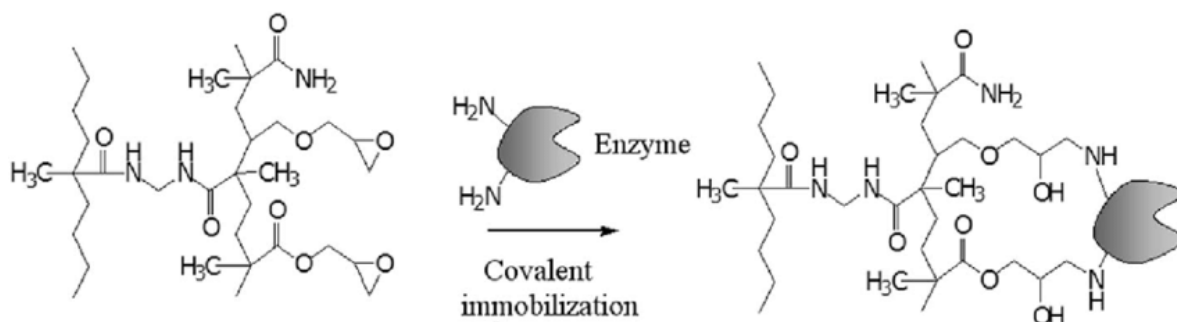
Figure 4. Enzyme immobilization on epoxy-functionalized carriers (Hanefeld U., Gardossi L. et al. 2009)

In this thesis, particular emphasis will be given to cutinases as an interesting substitute of lipases in polycondensation reactions, a full overview of this topic will be provided in the next chapters. As stated before, cutinases are a very interesting class of serine hydrolases that show unparalleled advantages when it comes to the synthesis of polyesters. A thorough review article on cutinases will be reported here and it will be accompanied with an in-depth bioinformatics study tailored to compare cutinases with other serine hydrolases classes.

3. Rice husk as a renewable and inexpensive solution for enzyme immobilization

3.1 Manuscript: Rice Husk as an Inexpensive Renewable Immobilization Carrier for Biocatalysts Employed in the Food, Cosmetic and Polymer Sectors

Nowadays, immobilized enzymes are not much widely used in industrial processes due to the fact that the cost of the biocatalyst is not a critical factor in the planning of a synthesis on an industrial scale[27]. However, as pointed out in the preceding paragraph, immobilized enzymes are mandatory in certain cases (i.e. polyesterification in solvent-free medium), their usage enables also recyclability of the support that can be used for additional reaction cycles and avoids product contamination with important use cases in the cosmetic and pharma sectors[28].

In the perspective of achieving fully renewable and sustainable bio-based products, the overall viability of the biocatalytic process has to be considered, and Life-cycle Assessment (LCA) demonstrated that the nature of immobilization carriers is a critical point in evaluating the sustainability of a biocatalysed process. Methacrylic resins represent the primary greenhouse gas emission source for immobilized enzymes (51-83%) because of the fossil-based raw materials, namely glycidyl methacrylate and ethylene dimethyl acrylate[21].

Natural biopolymers from agricultural waste may represent attractive alternatives responding to the pressing challenges of a circular bioeconomy as long as they are largely available at low prices. On a global scale, rice husk (RH) is one of the highest-volume agricultural residues. For every 4 tons of rice harvested, 1 ton of RH is produced, amounting to 120 million tons per year that are in large part not valorised.

In a previous study[5] our research group explored the potential of milled RH as a carrier for enzyme immobilization of several enzymes. A minimal pre-treatment of the raw material was necessary and different routes to achieve efficient and stable immobilization were tested exploiting the different components of RH (cellulose, hemicellulose, silica and lignin). CaLB immobilized on RH was tested in polyesterification reactions demonstrating its competitivity with commercial styrenic and methacrylic preparations.

In the following work, rice husk as a green, novel and inexpensive carrier will be explored for the covalent immobilization of *Candida antarctica* Lipase B (CaLB) and of two asparaginases. The said manuscript lays the foundation for the improvement of the immobilization technique on rice husk that will be treated in the following paragraph, where a chemoenzymatic approach was exploited to obtain an immobilized formulation of CaLB.

Rice Husk as an Inexpensive Renewable Immobilization Carrier for Biocatalysts Employed in the Food, Cosmetic and Polymer Sectors

Marco Cespugli [1], Simone Lotteria [1], Luciano Navarini [2], Valentina Lonzarich [2], Lorenzo Del Terra [2], Francesca Vita [3], Marina Zweyer [4], Giovanna Baldini [4], Valerio Ferrario [1], Cynthia Ebert [1] and Lucia Gardossi [1,*]

[1] Laboratory of Applied and Computational Biocatalysis, Dipartimento di Scienze Chimiche e Farmaceutiche, Università degli Studi di Trieste, Via Licio Giorgieri 1, 34127 Trieste, Italy; marco.cespugli@phd.units.it (M.C.); lotteria.simone@hotmail.it (S.L.); valerio.ferrario@gmail.com (V.F.); ebert@units.it (C.E.)
[2] illycaffè S.p.A., via Flavia 110, 34147 Trieste, Italy; luciano.navarini@illy.com (L.N.); valentina.lonzarich@illy.com (V.L.); lorenzo.delterra@illy.com (L.D.T.)
[3] Department of Life Science, University of Trieste, 34127 Trieste, Italy; vita@units.it
[4] Department of Medical, Surgical, and Health Sciences, University of Trieste, 34149 Trieste, Italy; marinazweyer@gmail.com (M.Z.); baldini@units.it (G.B.)
* Correspondence: gardossi@units.it; Tel.: +39-040-5583947

Abstract: The high cost and environmental impact of fossil-based organic carriers represent a critical bottleneck to their use in large-scale industrial processes. The present study demonstrates the applicability of rice husk as inexpensive renewable carrier for the immobilization of enzymes applicable sectors where the covalent anchorage of the protein is a pre-requisite for preventing protein contamination while assuring the recyclability. Rice husk was oxidized and then functionalized with a di-amino spacer. The morphological characterization shed light on the properties that affect the functionalization processes. Lipase B from *Candida antarctica* (CaLB) and two commercial asparaginases were immobilized covalently achieving higher immobilization yield than previously reported. All enzymes were immobilized also on commercial epoxy methacrylic resins and the CaLB immobilized on rice husk demonstrated a higher efficiency in the solvent-free polycondensation of dimethylitaconate. CaLB on rice husk appears particularly suitable for applications in highly viscous processes because of the unusual combination of its low density and remarkable mechanical robustness. In the case of the two asparaginases, the biocatalyst immobilized on rice husk performed in aqueous solution at least as efficiently as the enzyme immobilized on methacrylic resins, although the rice husk loaded a lower amount of protein.

Keywords: covalent immobilization of enzymes; rice husk; polycondensation; CaLB; itaconic acid; aspartase; acrylamide; aspartase; renewable carriers; biomass

1. Introduction

Immobilized biocatalysts have the potential of enabling continuous processing, lowering production costs and waste stream generation. Moreover, prevention of protein contamination is one further motivation that induces food and cosmetic sectors to employ immobilized biocatalysts [1]. Nevertheless, immobilized enzymes represent only a minor fraction of the overall enzyme market and the number of immobilized enzymes used on a scale larger than 10 kton per year is limited [2]. The development of immobilized enzymes for applications in the food sector and in the production

of large volume chemicals must carefully consider both costs and sustainability issues. Inexpensive carriers and protocols, together with high reusability, are the factors that will determine the success of immobilized enzymes. Woodley and co-workers [3] demonstrated that, if considered a carrier with a cost of $50/kg, the carrier represents the largest contribution to the final cost, although the cost of some carriers available on the market for enzyme immobilization (e.g., methacrylic resins) can be 2–5 fold higher.

Furthermore, environmental factors and stringent regulations [4] are gaining increasing relevance in determining the overall viability of the biocatalytic process. Indeed, Life Cycle Analysis (LCA) [5] of biocatalyzed processes disclosed that the fossil-based raw materials of epoxy methacrylic resins represent the primary source of greenhouse gas emission for the immobilized enzymes. It is evident that in order to promote a wider uptake of immobilized enzymes for the production of high-volume and low-cost sustainable products, new carriers and immobilization strategies are needed [6].

Natural biopolymers from biomass represent attractive alternatives and on a global scale, the two highest-volume agricultural residues are rice husk (RH) and sugarcane bagasse [7]. Rice husk production accounts for around 120 Mt per year and only 20 Mt are currently used.

The literature reports a large number of studies where renewable materials or biopolymers have been used as economical and sustainable immobilization carriers [8] and recently we have also reported some preliminary results on the use of rice husk (RH) as a carrier for biocatalyst immobilization [9]. This natural and robust composite material is made of lignin, cellulose, hemicellulose and SiO_2 [10]. RH responds also to the pressing challenges of a circular economy, since it can be re-utilized at the end of its proposed industrial application [11]. Moreover, as natural composite material, it has the subsidiary advantage that it is subjected to less stringent legislative constraints even after chemical modification [12].

The milled RH requires minimal pre-treatment and it is applicable in both physical and covalent immobilization protocols and under various process conditions. Lipase B from *Candida antarctica* (CaLB), a protease and an invertase have been previously immobilized covalently on RH oxidized with $NaIO_4$ and functionalized with the spacer hexamethylenediamine (HMDA). The method exploits the nucleophilic reactivity of the lysine residues on the surface of the enzymes. Nevertheless, the low protein loading (<50%) indicated the need of further optimization. The present study addresses the problem of improving the percentage of protein loaded on the functionalized RH and aims at understanding the morphological factors that affect the chemical modification of this complex natural composite material. CaLB and two commercial asparaginases were selected for the immobilization and application of the biocatalysts in reaction of practical interest in solvent-free but also aqueous systems. The results here reported set the basis for the full exploitation of this versatile renewable biomass for the covalent anchoring of proteins and as functional material in general [13–16].

2. Results and Discussion

2.1. Morphological Characterization of the Rice Husk

The rice husk used in the present study derives from Italian rice varieties and its composition in terms of SiO_2, lignin cellulose and pentosanes was previously determined [10]. Figure 1 reports the Scanning Electron Microscopy (SEM) images of the entire cuticle of the RH before the milling.
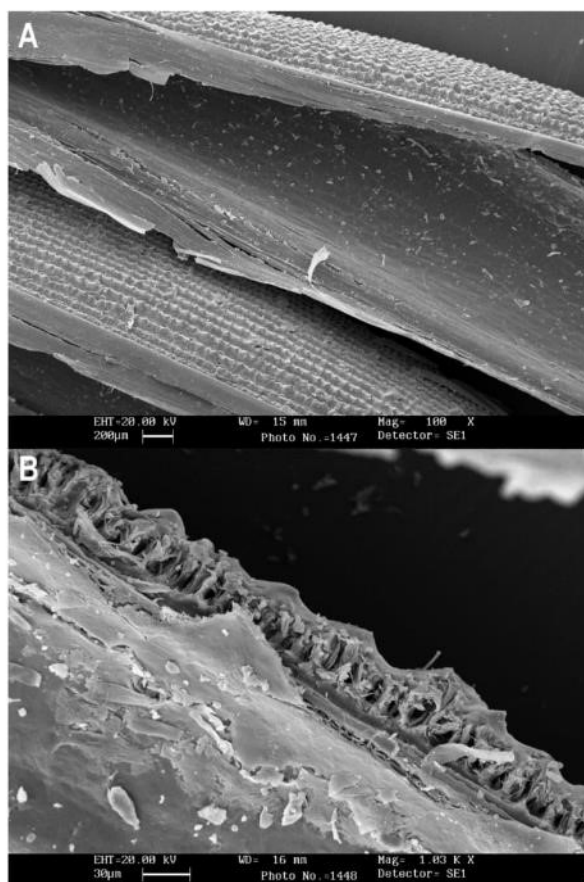
Figure 1. Scanning electron micrographs of rice husk fibers at different orders of magnification: (**A**) View of the external and internal surface; (**B**) internal section exposing the tracheids.

The rice husk has morphological differences between internal and external surfaces. The outer surface of the husk is very rough and presents linear ripples with a conical shape that run regularly along the whole surface. The outer surface contains a higher concentration of SiO_2 that confers stiffness and resistance towards external agents [17]. The internal surface, on the other hand, is smoother and consists of a larger quantity of cellulose.

The first step of the study was the detailed characterization of fractions of the milled RH differing in size (200–400 μm and 100–200 μm) using microscopy analysis (Figures 2–4). SEM microscopy (Figure 2) indicates that the material retains the typical morphology of the internal and external surface, probably because of the toughness conferred by the silica. Indeed, the milling of RH is feasible only by knife-mill devices whereas ball mill systems resulted inefficient. Therefore, most of the fragments expose only the lateral tubular structure as a result of the cutting of the stiff surface. Figure 2c,f provides details of the internal organization of RH, with the fibrous tubular structures of tracheids that form the mechanical skeleton of the material and have the function of transporting water and nutrients in the plant cell wall [18]. The matured dead plant cells retained only the lignocellulosic vascular structure.
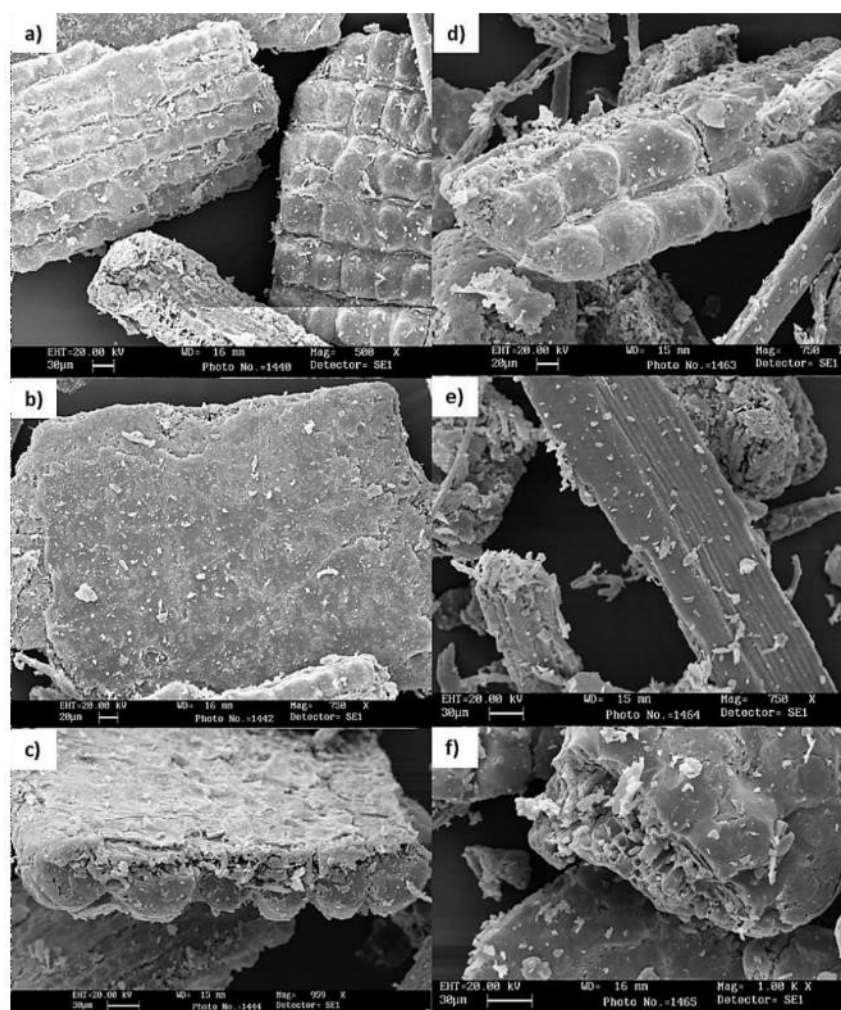
Figure 2. SEM images of: (**a**–**c**) Milled rice husk with particle size 200–400 μm; (**d**–**f**) milled rice husk with particle size 100–200 μm.

Bright field light microscopy (Figure 3) illustrates the tubular structures of tracheids and the external layer of SiO_2 that confers strength and rigidity to RH. Fluorescence microscopy (Figure 4a–c) shows how the material is endowed with autofluorescence especially in the blue (λ = 450–480 nm) and green range (λ = 510–520 nm). These are the typical wavelengths of the lignin, which composes the lignocellulosic biomasses [19]. Moreover, some restricted spots with autofluorescence in the red range (λ = 660–680 nm) are most probably ascribable to some residual chloroplasts [20]. Finally, the phase contrast image shows a single RH fragment that underwent a partial exposure of the inner cellulosic surface and highlights the regions where the lignin and the SiO_2 are more concentrated.
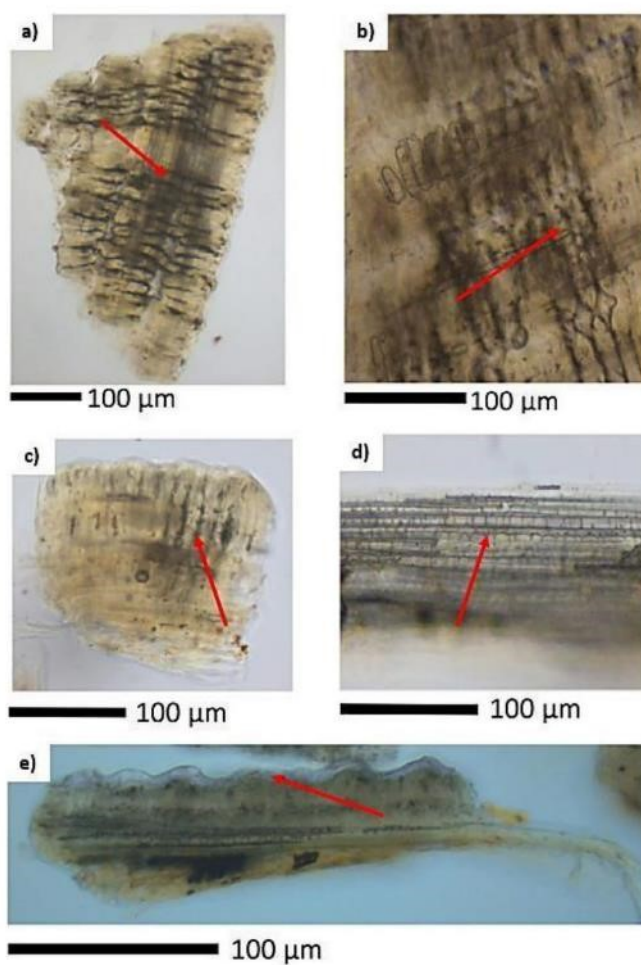
Figure 3. Bright field light microscopy images highlighting the tubular structure of tracheids (red arrows): (**a**,**b**) Milled rice husk (RH) with average size of 200–400 µm; (**c**,**d**) milled RH with average size of 100–200 µm; (**e**) detail of the external siliceous layer of a fragment of milled RH.
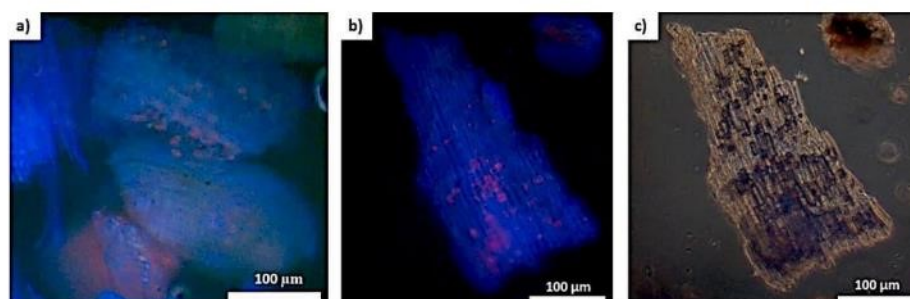
Figure 4. Milled RH (fragments with average size of 200–400 µm): (**a**,**b**) Fluorescence microscopy, (**c**) phase contrast image.

The data of mercury intrusion porosimetry (Table 1) indicates that the milling causes an increase of the porosity because of the exposure of the lignocellulosic tubular structures of tracheids.

Table 1. Comparison of porosity of RH before and after milling. Data were obtained by means of mercury intrusion porosimetry.

Material	Total Volume Intrusion (mL/g)	Total Pores Volume (m^2/g)	Average Pore Diameter (μm)	Porosity (%)
RH	0.2829	26.0	0.044	30.0
Milled RH (200–400 μm)	0.3889	17.3	0.090	37.9

Overall, the characterization of the RH and its fragments indicates that it is mandatory to increase the exposure of the lignocellulosic fraction of the tracheids in order to have access to a chemical substrate suitable for the derivatization and the covalent anchoring of proteins. The attack of the cellulosic component can occur at the level of the cut edges of the fragments or in regions that underwent the partial removal of the outer layer composed by lignin and SiO_2. It is also evident that the lignin fraction is poorly accessible due to the SiO_2 coating.

The activation of the surface was accomplished by oxidizing the cellulose with $NaIO_4$ as previously described [10]. The method preserves the glycoside bond while the oxidative cleavage of the glucose unit leads to a five-term di-aldehyde, which resemble in its chemical structure the glutaraldehyde, a largely employed reagent for the protein crosslinking as well as for enzyme immobilization (see Electronic Supplementary Information—ESI, Figure S1). Notably, reports on the use of oxidized carbohydrates for crosslinking established practical procedures, but never disclosed the molecular basis for the cross-linking of proteins. The formation of an imine-linkage with primary amino groups of Lys side chain was suspected to be the first step of the cross-linking by subsequent reductive amination [21]. In the case of dextran polyaldehyde, one-step cross-linking was first reported by Kobayashi and co-workers [22], demonstrating the possibility of obtaining rather stable products without reduction. Indeed, studies on the glutaraldehyde reactivity reported little or no reversibility of the imino bond formation within a pH range of 7–9 [23]. Moreover, the occurrence of unsaturated Michael addition products has been reported at basic pH [24].

The oxidation of RH [25] was carried out using the milled RH with a particulate size between 200 and 400 μm and the formation of the carbonyl groups was evaluated by titration (see ESI Figure S2) with hydroxylamine [26,27]. Moreover, the incidence of any subsequent oxidation of the carbonyl group to carboxylic acid was quantitatively evaluated (see ESI Figure S3) by means of a conductimetric titration [27,28]. The results obtained from the oxidation of the cellulose component of the rice husk by treatment with a 0.2 M $NaIO_4$ solution for 22 h are reported in Figure 5.

There is an increase of carbonyl groups of more than 380%, whereas carboxylic groups increase about 66%. Of course, some oxidative modification of the lignin cannot be excluded although the microscopic characterization indicates that SiO_2 covers most of the lignin, which appears poorly accessible (Figure 4).

2.2. Functionalization of RH with Amine Groups and Immobilization of CaLB

Upon oxidation of the cellulose, amine functional groups were inserted using hexamethylenediamine (HMDA) [10,29]. The functionalized RH was used for the covalent immobilization of CaLB, one of the most widely employed enzymes in oleo-chemical, cosmetic and food sectors. Its structure and superficial properties are illustrated in Figure 6.
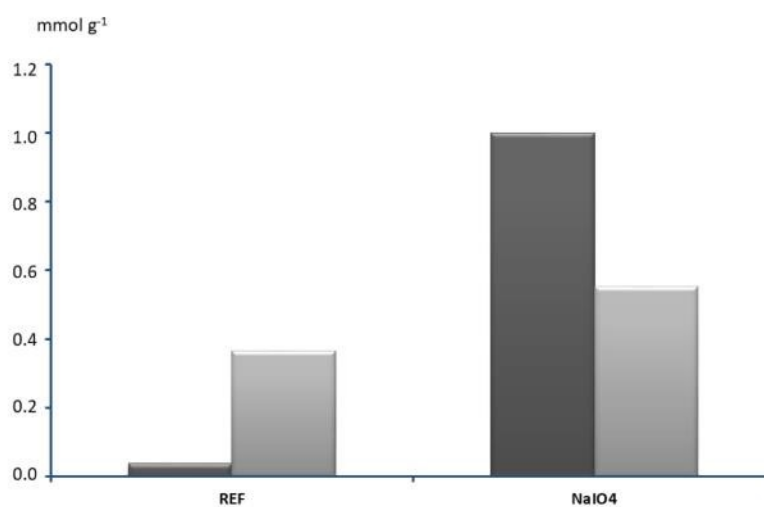
Figure 5. Comparison of the content (mmol·g^{-1}) of carbonyl (light gray) and carboxylic groups (black) in samples of milled RH before and after different oxidative treatment.
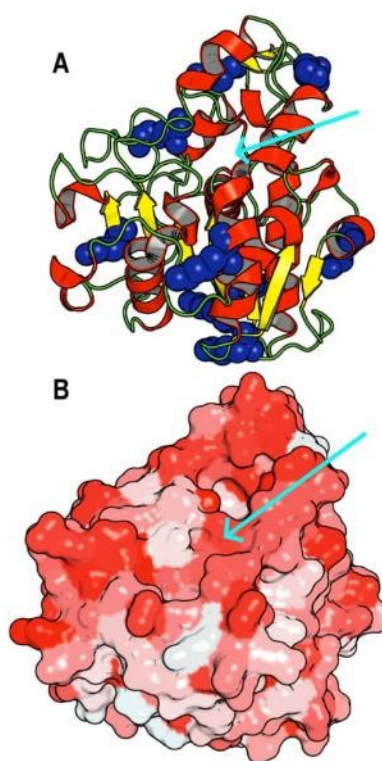
Figure 6. Analysis of the 3D structure of lipase B from *Candida antarctica* (CaLB, PDB: 1TCA). (**A**) The active site entrance is indicated by a cyan arrow while the superficial Lys are highlighted in blue spheres on the secondary structure of the enzyme. (**B**) The color of designates the hydrophobicity of the surface, going from white (hydrophilic) to red (hydrophobic).

Prior to lipase immobilization, the amine groups were activated for 5 h with a solution of glutaraldehyde (GA) in phosphate buffer. Finally, the activated carrier was incubated for 24 or 48 h in a solution of 10,000 U $g_{carrier}$ $^{-1}$ in 0.5 M phosphate buffer at pH 8 (Figure 7). A solution of PEG3000 was also added in order to improve the stability of the enzyme throughout the immobilization procedure [10]. The pH was selected in order to maintain deprotonated a sufficient fraction of the primary amine residues of the Lys thus allowing the reaction with the reactive groups present on the solid support. Moreover, the imine bond presents little or no reversibility as well the formation of Michael addition products [23].
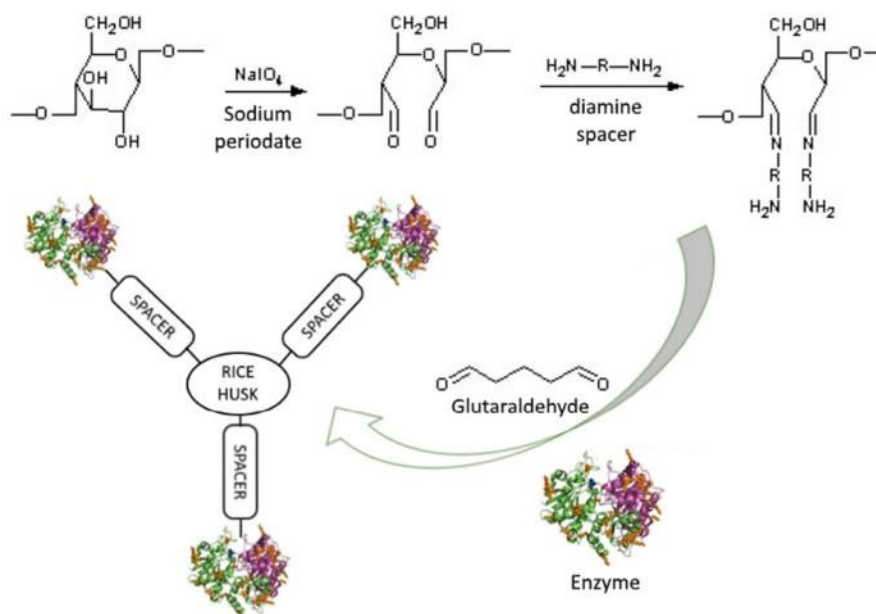
Figure 7. Schematic illustration of the oxidation and functionalization of the cellulosic fraction of RH for the covalent immobilization of CaLB.

In parallel, CaLB was also immobilized on the epoxy methacrylic resin EC-EP/S (size 100–300 μm). The actual anchorage of the CaLB through covalent bonding was verified for all immobilized biocatalysts by filtering the immobilized biocatalyst at the end of the hydrolytic assay and then by titrating the residual enzymatic activity in the supernatant using additional tributyrin. The data showed that no residual activity was detected in the filtered emulsion, as a proof that all the immobilized enzyme was covalently bound on the support (see ESI Figure S4). The recyclability of the CaLB immobilized on RH was also tested for 10 hydrolytic cycles (see ESI Figure S5) confirming the robustness of the formulation, as previously reported [9,10]. The properties of the different enzymatic formulations are reported in Table 2.

It is noteworthy that the extension of the immobilization time from 24 to 48 h led to an increase of the protein loaded on the RH from 33 to 72%. The need of a longer incubation time is ascribable to a slow adsorption of the enzyme to the RH [10], whereas it is widely demonstrated that the hydrophobic regions on CaLB induces a fast adsorption of the enzyme on hydrophobic organic resins [1]. Furthermore, the formation of the imino bond requires longer reaction times than the nucleophilic attack of the amine group to the epoxy ring of the EC-EP resins. Indeed, the loading of only 10,000 U of CaLB led to an expressed enzymatic activity of 316 tributyrin Units (TBU), comparable

22

to that previously reported by employing 25,000 U $g_{carrier}^{-1}$, and this result indicates that one gram of the functionalized RH carrier is already saturated with 10,000 U of CaLB.

Table 2. Properties of different formulations of covalently immobilized CaLB.

Carrier	Function Group	Immobilization Time (h)	Enzymatic U Loaded [a] (U $g_{carrier}^{-1}$)	Immobilized Protein [b] (%)	Hydrolytic Activity [a] (U g^{-1})
Oxidized Rice Husk	Amine (HMDA + GA)	24	25,000 [c]	35	317
Oxidized Rice Husk	Amine (HMDA + GA)	24	10,000	33	178
Oxidized Rice Husk	Amine (HMDA + GA)	48	10,000	72	316
Methacrylic EC-EP/S	Epoxy	24	10,000	95	709

[a] Units expressed as tributyrin hydrolytic activity referred to g of dry immobilized biocatalyst. [b] Amount of protein that was actually immobilized on the carrier, calculated by subtracting from the total amount of protein offered to the carrier the protein still present in solution at the end of the immobilization procedure. [c] Data previously reported [10].

Figure 8 reports a comparison of the morphology of the milled rice husk and the commercial epoxy activated methacrylic resins EC-EP/S (size 100–300 μm) that were selected for comparison. The milled RH has a very inhomogeneous morphology, with particles of various shapes.
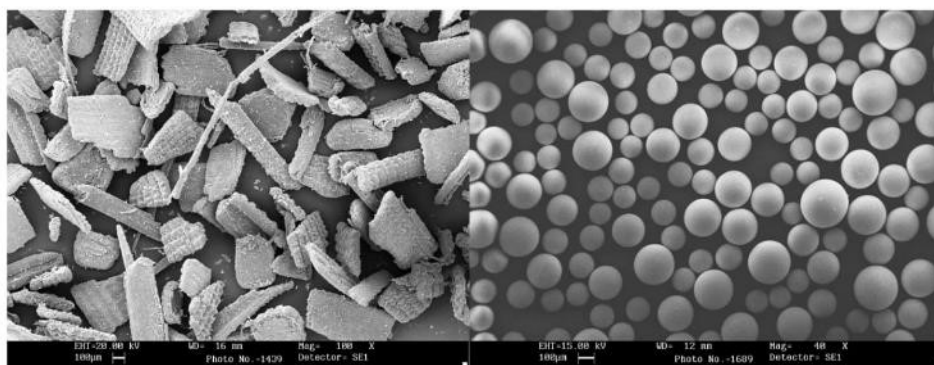
Figure 8. SEM images of: (**a**) Milled rice husk with average particle size 200–400 μm; (**b**) Sepabeads EC-EP epoxy methacrylic resin beads with average particle size 100–300 μm.

The comparison with a CaLB formulation prepared using a known procedure [10] and employing the commercial epoxy resin EC-EP/S (100–300 μm) shows that the epoxy group allows for faster immobilization protocols and, as expected, the percentage of loaded protein is close to 100% leading also to higher hydrolytic activities. The discrepancy between the two data obtained with EC-EP/S is due to the use of two different batches of the resin.

Despite the lower loading capacity, the functionalized RH is suitable for applications in bulk viscous polycondensation processes [30,31]. We have already demonstrated that the severe mass transfer limitations of these reactions can be overcome by maximizing the dispersion of the enzyme over a wide surface of the carrier rather than by increasing the loading of the biocatalyst. Moreover, any attempt to apply vigorous mixing systems while using methacrylic carriers resulted in the mechanical damage of the resins. In the present study, the polycondensation was carried out using a thin-film system that preserves the integrity of both the RH and the EC-EP resin [10,30,31].

The different formulations of covalently immobilized CaLB were used upon drying (see experimental) and in all cases, the water content of the formulations was <12% (*w/w*). Interestingly, despite the lower loading capacity, the RH-CaLB resulted more efficient in the solvent-free polycondensation of two bio-based monomers, dimethylitaconate (DMI) and 1,4-butandiol (BDO) to obtain poly(1,4-butylene itaconate) [30,31] (Figure 9 and Table 3). Enzymatically synthesized polyesters

23

with moderate MW are of interest for the cosmetic sector as film forming or for improving sensorial quality [32] but they find also applications as adhesives or pre-polymers prone to further chemical modifications [33,34]. More specifically, the derivatives of itaconic acid are gaining attention for the potential applications in dental materials, elastomers, drug-delivery and other biomedical and biotechnological applications [35]. Notably, the chemical polycondensation of itaconic acid leads to isomerization and radical cross-linking of the vinyl group under the conventional harsh reaction conditions (T > 150 °C). Therefore, the enzymatic polycondensation carried out at 50 °C appears as a convenient route for preserving the vinyl group throughout the synthetic process [31].
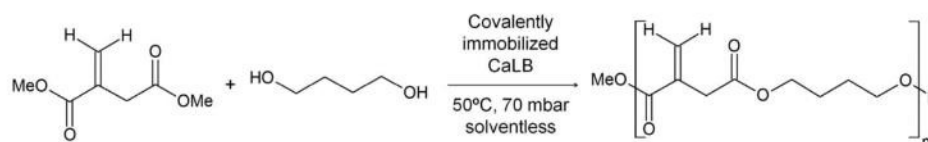
Figure 9. Solvent-free polycondensation catalyzed by CaLB covalently immobilized on RH.

The results in Table 3 and Figure 10 show that CaLB on rice husk and CaLB on methacrylic resin lead to comparable conversion and Mw values, although in the first case the polycondensation employed about half of the enzymatic units. The data indicate that the enzymatic preparation of CaLB on RH can be effectively employed for the sustainable synthesis of short bio-based polyesters with controlled structures. Nuclear Magnetic Resonance (NMR) characterization (see details in ESI Figures S6–S11) demonstrated that the enzymatic synthesis at 50 °C preserves all vinyl groups, thus making them available for further functionalization [31].

Table 3. Comparison of the results obtained by the polycondensation reaction catalyzed by the two different preparations of immobilized CaLB. Enzymatic units refers to tributyrin hydrolytic activity. Reaction were monitored by ^{1}H-NMR. Details are available in ESI.

Biocatalyst	U $g_{monomers}^{-1}$	Reaction Time (h)	Conversion (%)
CaLB RH	158	24	69
		48	87
		72	92
CaLB EC-EP/S	297	24	70
		48	87
		72	88

Notably, the use of a low amount of lipase (158 U $g_{monomer}^{-1}$) but dispersed on a wide amount of RH carrier (corresponding to 50% w/w) allowed also to overcome the low electrophilicity of the conjugated acyl group of the dimethylitaconate. Previously reported attempts [31] of synthetizing poly(1,4-butylene itaconate) using 240 U $g_{monomer}^{-1}$ of CaLB immobilized on EC-EP but concentrated in a smaller volume of carrier (10% w/w) led to the formation only of the trimer ABA where the diol (A) is acylated by the fast reacting carbons of two DMI units (B). Under such conditions only 5% of the slow reacting acyl group reacted, thus preventing the elongation of the polymeric chain.

One possible explanation of the higher efficiency of the RH as immobilization carrier resides in its lower density (0.4 g mL^{-1}) compared to methacrylic resins (>1.1 g mL^{-1} as stated by the producer). The two polycondensation reactions were carried out using an equal weight of the two immobilized formulations (50% w/w on monomers basis). Therefore, the volume available for the immobilization of the lipase is more than double in the case of RH. Indeed, the data confirm the previous observations [30] that mass transfer limitations can be overcome in viscous systems by distributing a limited amount of enzymatic units on a large volume of carrier. On that respect, the common paradigm of biocatalysis that calls for highly loaded and highly active biocatalysts appears not applicable to viscous systems.

Although the diameter of a single enzyme molecule is <10 nm and the pores of EC-EP/S (average pore diameter 10–20 nm), in principle, should be accessible to single enzyme molecules, the viscous reaction mixture has access only to the portion of CaLB immobilized on the outer surface of the carrier [30].
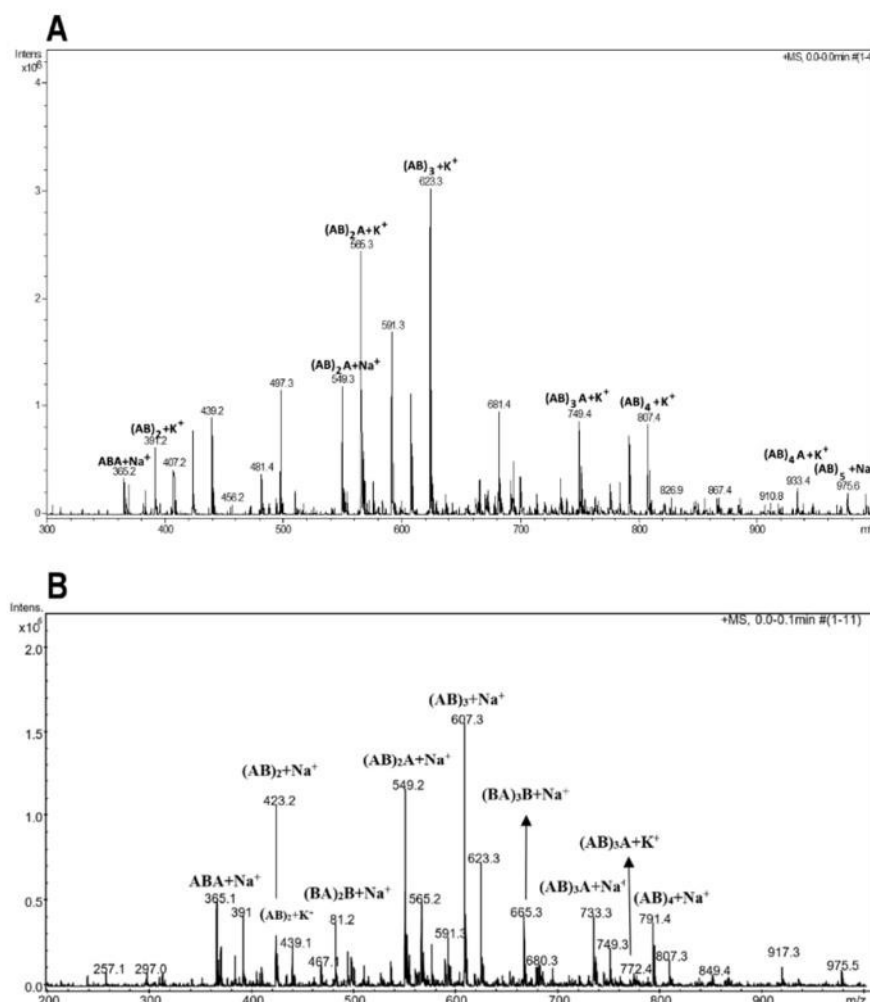
Figure 10. Electron Spry Ionization Mass Spectrometry (ESI-MS) positive ion mass spectra of the solvent-free enzymatic polycondensation products of dimethyl itaconate (DMI) with 1,4-butanediol (BDO) after 72 h. Top: Reaction catalyzed by CaLB on rice husk. Bottom: Reaction catalyzed by CaLB on EC-EP/S. A = BDO; B = DMI.

The role of the porosity of RH is more complex: Although the SEM images (Figure 2f) show that the opening of tracheids is quite wide (3–10 μm), these deep and straight channels (Figure 2e) are accessible only from the cut edges of the RH fragments. Therefore, this type of internal structure of RH (average pore diameter 90 nm, Table 1) is hardly comparable with the macroporosity of common silicate or methacrylic carriers. Further studies will be necessary for describing the localization of the enzymes molecules on the macropores of RH and also on its external surface.

For instance, Gross and co-workers analyzed by Infra Red (IR) imaging the localization of CaLB in Novozymes 435 [36], the biocatalyst most widely employed for polycondensation and made of a macroporous resin of poly-methyl methacrylate (Lewatit VP OC 1600). They showed that the protein is localized in an external shell of the bead with a thickness of 80–100 μm and that the distribution of CaLB is not uniform throughout this shell. However, in such case, the lipase was immobilized through physical adsorption, which makes the comparison with RH behavior even more difficult.

In order to evaluate the applicability of the CaLB covalently immobilized on RH, this formulation was also applied to the solvent-free synthesis of propyl laurate at 55 °C, a reaction system without relevant mass transfer limitations. In that case, the activity of CaLB-RH (expressed as μmol of propyl laurate formed by 1 g of immobilized biocatalyst in minute) was of 592 ± 24 μmol g^{-1} min^{-1}. The CaLB on EC-EP led to 2395 ± 41 μmol g^{-1} min^{-1}, demonstrating a higher efficiency of the mesoporous methacrylic resin in this kind of synthetic process. In conclusion, the efficiency of the two formulations of covalently immobilized CaLB depends strongly on the physical chemical properties of the reaction system.

2.3. Covalent Immobilization of Asparaginases on Functionalized Rice Husk

The study moved its focus to the application of functionalized RH as a carrier for the immobilization of asparaginases, which catalyze the hydrolysis of asparagine to aspartic acid. The enzyme is considered an effective means for reducing the formation of acrylamide in foods by degrading its precursor asparagine [37]. Upon heat treatments, asparagine undergoes condensation with reducing sugars then promoting a cascade of reactions that lead to the formation of acrylamide. Acrylamide is classified as "probably carcinogenic to humans" and the discovery of high levels of acrylamide in many common food products has intensified the research towards possible solutions of the problem [38] and to the development of commercially available food grade asparaginases enzymes.

Asparaginases are classified as asparagine starch hydrolase, namely amidases, with EC code (3.5.1.1.) The asparaginases from *Erwinia chrysanthemi* and *Escherichia coli* are currently in clinical use as effective drugs in the treatment of leukemia and several studies have already addressed the immobilization of asparaginases for clinical applications on supports such as magnetic nanoparticles [39], epoxy activated Sepharose [40] and protein micro particles [41]. The literature reports that asparaginases are tetramers of identical subunits, with molecular mass in the range of 140–160 kDa [41,42]. Each of the four active sites is located between the N- and C-terminal domains of two adjacent monomers. Thus, the tetramer can be treated as a dimer of dimers. Despite this fact, the active enzyme is always a tetramer. Each monomer consists of 327 residues. Therefore, the enzyme results to be rather large. Nine residues have been identified as essential within the active site because they are involved in substrate recognition and catalysis. The hydrolytic mechanism involves a residue endowed with nucleophilic activity (threonine 12 in the case of asparaginase from *Pyrococcus horikoshii*) within the active site [43].

The present study was carried out by combining the structural and functional analysis of two asparaginases commercialized by Novozymes. Acrylaway L is produced by the cloning of an asparaginase gene from *Aspergillus oryzae* in the same microorganism, although genetically modified, whereas Acrylaway High-T is obtained by cloning an unmodified gene into the genetically modified *Bacillus subtilis*. It must be noted that only the enzyme contained in the preparation Acrylaway L is potentially glycosylated as it is produced by a eukaryotic organism. The presence of large glycans (generally 8–30 units of mannoses) on the protein surface creates wide hydrophilic regions that affect the interactions of the enzyme with the outer environment or the immobilization carriers.

The two enzymes were evaluated in terms of protein concentration, presence of stabilizers, possible post-translational modifications (glycosylation) and all the factors that could influence their immobilization and final use. The asparaginases were immobilized covalently on RH and EC-EP/S resins to comply with EFSA (European Food Safety Authority) regulations regarding the use of

enzymes in food processing and more specifically the two asparaginases were immobilized covalently to guarantee the control of any contamination of the food by the enzyme [44].

The structure of the asparaginases from *Erwinia chrysantemi* was selected from the Protein Data Bank [45] as a model of reference for a general analysis of the structural features of asparaginases enzymes. Figure 11 shows the hydrophobic and hydrophilic areas of the protein surface, responsible for the preliminary physical interactions with the solid support and the distribution of the nucleophilic Lys residues, responsible for the covalent bonds with the carriers.
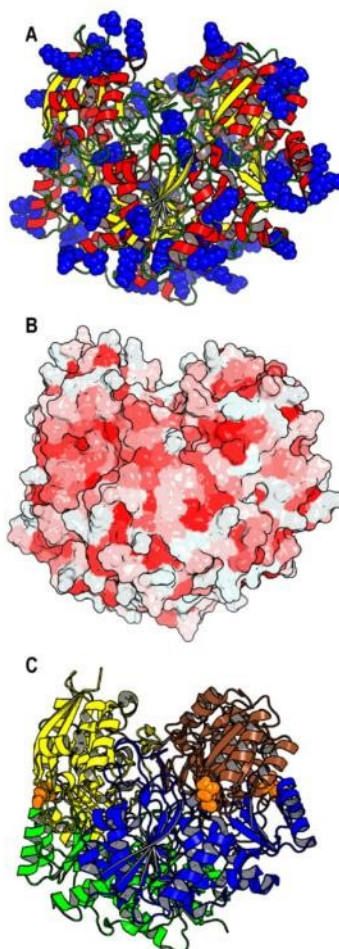
Figure 11. Analysis of the 3D structure of asparaginase from *Erwinia chrysantemi* in tetrameric form (PDB 1O7J). (**A**) The superficial Lys of the enzyme are highlighted in blue spheres on the secondary structure of the enzyme. (**B**) The colors of the enzyme surface indicate hydrophilic areas (white) and hydrophobic regions (red). (**C**) The tetrameric structure with each monomer colored differently while the glycosylation sites are highlighted in orange sphere mode.

The enzyme surface presents significant hydrophobic areas, which are generally absent in hydrolases such as proteases and amidases but widely present in lipases [46]. The potential N-glycosylation sites were also identified by analyzing the primary structure of the enzyme (see ESI Figure S12). They are located in each subunit (Figure 11C) in areas adjacent to the opening of the

active site. Generally, the glycans have the role of masking hydrophobic regions exposed to the bulk aqueous environment, thus preventing protein aggregation [47].

As illustrated in Figure 11, the enzyme has a large number of lysine residues and they are mostly disposed on the opposite side in respect to the opening of the active site. This element, although referred to a model structure, indicates that the asparaginase from *Erwinia chrysanthemi* is favorable for being covalently immobilized and achieving multi-point anchorage with correct orientation and free access to the active site.

The protocols for the covalent immobilization of the two asparaginases on the functionalized rice husk were developed by adjusting the two enzymatic solutions at the same protein concentration (3.40 mg/mL) to compare the affinity of the two enzymes for the carrier. The activity was tested for 10 cycles, in order to evaluate also the recyclability of the biocatalyst. The two asparaginases were also immobilized on EC-EP/S resins. The results of the characterization of the four preparations are reported in Table 4. Enzyme performance was determined by evaluating the amount of asparagine hydrolyzed by the immobilized enzymes after 30 min at 40 °C.

Table 4. Properties of the two asparaginase immobilized covalently on the functionalized rice husk and on EC-EP/S resins. The enzyme performance was determined by evaluating the amount of asparagine hydrolyzed after 30 min of incubation at 40 °C.

Carrier	Asparaginase	Loaded Protein (mg·g$_{carrier}$$^{-1}$)	Actual Loaded Protein %	Actual Loaded Protein (mg·g$_{carrier}$$^{-1}$)	Hydrolyzed Asparagine (%)	Hydrolyzed Asparagine after 10 Cycles (%)
EC-EP/S	Acrylaway L	26.8	72	12.3	100	100
	Acrylaway High-T	26.8	93	24.9	100	98.5
RH	Acrylaway L	17.9	44	7.9	100	100
	Acrylaway High-T	17.9	38	6.8	93	86.5

The different immobilization yields obtained with the two asparaginases indicates that the hydrophobic and hydrophilic interactions play important roles in favoring the initial adsorption of the enzyme on the support. Acrylaway L is a glycosylated asparaginase and therefore more hydrophilic. This characteristic translates in a lower immobilization yield on the methacrylic epoxy resin (72%) whereas the less hydrophilic Acrylaway High-T adsorbs and binds readily (93%) on the same hydrophobic resin. An opposite trend, although less marked, can be observed in the case of the immobilization on RH.

All immobilized biocatalysts expressed an excellent efficiency, especially those immobilized on rice husk that proved able to hydrolyze quantitatively the acrylamide in solution for 10 cycles of treatment. Notably, the amount of protein loaded on the methacrylic resins was about double as compared to the formulations obtained with RH. This indicates that the lower loading capacity of the functionalized RH is counterbalanced by an excellent dispersion of the light RH carrier in the aqueous solution and favorable access to the enzyme.

3. Materials and Methods

3.1. Materials

Samples of rice husk (*Carnaroli* type) were kindly donated by Riseria Cusaro (S.r.L.) (Binasco, Italy) and derive from Italian rice varieties. The organic composition, previously determined [10], is the following: 46.5% cellulose, 31.9% lignin and 22.1% of pentosanes (hemicellulose). SiO_2 constitutes about 20% of the global weight. The milled RH has a water adsorption capacity of 42.6% *w/w*, determined by weight difference. Lipase B from *Candida antarctica* (CaLB, batch LCN02115 with an activity of 4005 U mL^{-1}), Asparaginases Acrylaway L (minimum activity stated by producer: 3500 ASNU/g) and Acrylaway High-T (minimum activity stated by the producer: 6000 TASU/g) were purchased from Novozymes (Bagsvaerd, Denmark). The protein content of Acrylaway L and

Acrylaway High-T, determined independently by the Bradford test using serum bovine albumin as standard, was 5.77 and 3.04 mg. mL^{-1} respectively. The solvents were standard laboratory grade. Alcohol, organic acid, and other reagents were purchased from either Aldrich Chemical Co. (Milwaukee, Wisconsin, United States) or Sigma-Aldrich (St. Louis, MO, USA) and used as received if not otherwise specified. Sepabeads EC-EP/S were purchased from Resindion (Milano, Italy). Product features as from the producer: Oxirane content: Minimum 100 µmol/g wet; Median pore diameter: 10–20 nm. Water retention: 55–65%.

3.2. Grinding and Sieving

Rice husk was milled using a Rotor mill ZM 200 (Retsch Cusaro (S.r.L.), Bergamo, Italy). The raw material was separated by size using four different sieves of 450, 250, 200 and 100 µm, respectively. The wet particles were weighed and then dried in an oven at 120 °C for 6 h. The density of RH before milling was 0.153 g mL^{-1} whereas the milled RH (size 0.2–0.4 mm) had a density of 0.437 g mL^{-1}. Porosity was determined using mercury porosimetry.

3.3. SEM Microscopy

Samples were metallized with the S150A Sputter Coater instrument (Edwards High Vacuum, Crawley, West Sussex, UK) before being observed with the Leica Stereoscan 430i scanning electron microscope (Leica Cambridge Ltd., Cambridge, UK) integrated with an Si detector (Li) PENTAFET PLUS TM, with an ATW TM window (Oxford Instruments, Oxfordshire, England) for microanalysis.

3.4. Light and Fluorescence Microscopy

Rice husk was put on glass slides, mounted with Canada balsam (Sigma-Aldrich, St. Louis, MO, USA) and kept under vacuum for a few minutes to remove air bubbles. Specimens for epifluorescence were mounted with glycerol and DABCO (1,4-Diazobicyclo-(2,2,2)octane (Sigma-Aldrich St. Louis, MO, USA).

Rice husk slides were observed with a Zeiss Axiophot microscope (Oberkochen, Germany) using transmission light or epifluorescence and micrographs were collected by a ProgRes CFcool camera (Jenoptic, Jena, Germany).

3.5. ^{1}H-NMR Spectra Related to Polycondensation of DMA and BDO

Spectra were recorded on a JEOL Ex-270 spectrometer (JEOL, Tokyo, Japan) operating (270 MHz). The solvent was $CDCl_3$ if not otherwise specified.

3.6. Thin Layer Chromatography (TLC)

Polycondensation was monitored on silica gel glass plates 20×20 cm (Macherey-Nagel, Düren, Deutschland). The spots were visualized by treating the silica plates with a solution mixture of $KMnO_4/KOH$ (1.25/0.5%). The components were separated employing ethyl acetate as mobile phase.

3.7. Electrospray Ionization Mass Spectrometry (ESI-MS)

The crude reaction mixtures were analyzed on Esquire 4000 ESI-MS ion trap Bruker instrument (Karlsruhe, Germany) electrospray positive ionization by generating the ions in an acidic environment. Around 10 mg of sample was dissolved in 1 mL methanol containing 0.1% v. v^{-1} formic acid. The generated ions were positively charged with the m z^{-1} ratio falling in the range of 100–1000. The subsequent process of deconvolution allows the reconstruction of the mass peaks of the chemical species derived from the analysis of the peaks generated.

3.8. Moisture Determination

A sample of 1.0 g of rice husk (A) was weighed in a tarred weighing bottle. It was dried for 2 h in an oven at 105 ± 5 °C, cooled in a desiccator, and then the stopper was opened in order to equalize the air pressure and weigh. The bottle was replaced again in the oven for 1 h. The process was repeated, followed by cooling and weighing as above for successive periods until constant weight (B) was reached. Moisture content % = $[(A - B)/A] \times 100$.

3.9. Titrations

Potentiometric titrations and pH measurements were performed using a Graphic DL50 Mettler Toledo automatic titrator. Conductimetric measurements were performed using a Conductivitymeter CDM 92 (Sigma-Aldrich St. Louis, MO, USA).

3.10. Lipase Hydrolytic Activity (Tributyrin Assay)

The activity of enzymatic preparations was assayed by following the tributyrin hydrolysis and by titrating, with 0.1 M sodium hydroxide (NaOH), the butyric acid that was released during the hydrolysis. An emulsion composed of 1.5 mL tributyrin, 5.1 mL gum arabic emulsifier (0.6% w/v) and 23.4 mL water was prepared in order to obtain a final molarity of tributyrin of 0.17 M. Successively, 2 mL of 0.1 M sodium-phosphate buffer (Nap), pH 7.0, was added to 30 mL of tributyrin emulsion and the mixture was incubated in a thermostatted vessel at 30 °C, equipped with a mechanical stirrer. After pH stabilization, 100 mg of immobilized biocatalyst or 0.005 mL CaLB native solution was added. The consumption of 0.1 M NaOH was monitored for 14 min. One unit of activity was defined as the amount of immobilized enzyme required to produce 1 μmol of butyric acid per min at 30 °C. One tributyrin unit (TBU) of lipase activity was defined as the amount of enzyme which liberated 1 μmol of butyric acid per minute under the given assay conditions.

3.11. Asparaginase Assay

L-Asparagine (Sigma A0884-25G, St. Louis, MO, USA) was dissolved in deionized water at a concentration of 100 mg L^{-1}. A total of 0.5 mg of immobilized asparaginase was added to 1 mL of this solution and was placed in 2 mL Eppendorf tubes. To obtain the previously mentioned amount of enzyme, 200 μL (volume of the storage buffer in which the immobilization matrix was carefully re-suspended) was used in the case of enzymes immobilized on resin. For enzymes immobilized on rice husks, the volume used was double (400 μL). After 30 min under stirring at 250 rpm on an orbital shaker at 40° C, the immobilized enzyme was recovered by centrifugation (Beckman-Coulter Allegra 64R centrifuge, Indianapolis, IN, USA, F2402H rotor, 17,000 rpm, 3 min, RT (21 °C)). At the end of the centrifugation, the concentration of asparagine was measured in the supernatant. Afterward, 1 mL of fresh asparagine solution was added to the precipitated enzyme for the next assay cycle. The procedure was repeated 9 times, for a total of 10 consecutive cycles of use of each enzyme sample. The determination of asparagine was carried out according to the procedures described by the EZ-faast® kit for amino acids (Phenomenex) by GC/MS Agilent Technologies (Santa Clara, CA, USA), equipped with a 10 m ZB-AAA capillary column, 0.25 mm thick film. A total of 100 μl of sample in the presence of 20 nmol of norvaline as internal standard were cleaned up through an ion exchange resin. The amino acids were released from the resin through *n*-propanol used as an eluting medium. The samples were then derivatized through propyl chloroformate, which allowed the alkylation of the amino and the esterification of the carboxylic group of each amino acid simultaneously. The sample preparation was in accordance with the procedures described by Phenomenex in the usage of the EZ-faast® kit for amino acids determination. Compounds were eluted by a He gas flow of 1 ml/min in splitless mode and separated using a 10 m ZB-AAA capillary column (film thickness 0.25 μm). The oven temperature was initially set at 110 °C, held for 1 min, increased to 160 °C at 25 °C/min, held for 1 min, then to 205 °C at a rate of 15 °C/min. The mass spectrometer was set to electron impact

mode (MS-EI) generated at 70 eV and mass spectra were collected in full scan mode, collecting ions from 39 to 500 m/z.

3.12. FT-IR

FT-IR spectra were recorded with a 2000 NIR FT-Raman spectrophotometer (Perkin Elmer, Roadgau, Germany). The samples, after drying in a desiccator, were reduced to powder with KBr and a tablet was prepared by pressing a force of 10 tons for 2 min. The spectra were recorded in a 4000–400 cm^{-1} spectral range and with a resolution of 2 cm^{-1}.

3.13. UV-Vis

UV-Vis spectra were recorded using a two-ray Lambda 35 spectrophotometer (Perkin Elmer, Rodgau, Germany) and a two-beam V-550 spectrophotometer (JASCO, Pfungstadt, Germany).

3.14. Determination of the Content of Carbonyl Groups

The content of carbonyl groups was determined by reaction with hydroxylamine chlorhydrate. This reacted with the hydroxylamine forming an oxime and the hydrochloric acid released was then titrated with sodium hydroxide. In 25 min of a 0.25 M solution of hydroxylamine and chlorhydrate, the pH was brought to 3.20 ± 0.05 with HCl. About 200 mg of rice husk of hydrated oxidized rice was added to the solution and the suspension was allowed to react for 2 h under stirring. After this time, the reaction was titrated with 0.1 M NaOH to bring the pH back to 3.20. At the end of the titration, the mixture was fed and the rice husk was dried for 6 h in an oven at 120 °C to determine the exact anhydrous weight of the analyzed sample.

To remove any interferences, a white consisting of a non-oxidized rice husk was treated with the same method, which was previously washed 6 times with an ethanol mixture:Water 50:50. Each measurement was performed twice. The content of carbonyl groups was calculated using the following formula:

$$\text{mmol aldehyde}/g_{\text{carrier}} = (V_{\text{NaOH}} \times C_{\text{NaOH}})/m_{\text{dry carrier}}$$

where V_{NaOH} is the volume in mL necessary to adjust the pH of the mixture to 3.20, C_{NaOH} is the concentration of NaOH (0.1 mmol/mL) and $m_{\text{dry carrier}}$ is the mass in grams of the anhydrous samples.

3.15. Determination of the Content of Carboxylic Groups with the Conductimetric Method

About 100 mg of sample was suspended in a beaker containing about 70 mL of 0.01 M HCl. The suspension was left under magnetic stirring for 30 min and subsequently titrated with 0.1 M NaOH. At the end of the titration, the suspension was filtered and the sample was dried for 6 h in an oven at 120 °C to determine the exact weight. As a reference, a solution consisting of 70 mL of 0.01 M HCl was titrated.

The content of carboxylic groups ($\text{mmol}_{\text{COOH}}/g_{\text{sample}}$) was determined with the following formula:

$$\text{carboxylic groups} = C_{\text{NaOH}} \times (V_1 - V_2)/m_{\text{sample}}$$

where CNaOH is the concentration of NaOH (0.1 mmol/mL), V_1 and V_2 are the volumes (mL) of NaOH necessary to control the weak acid present in the mixture (see ESI) and m_{sample} is the mass (g) of the anhydrous sample. The value of the carboxyl group contents was calculated on an average of two measures and it is reported with the standard deviation.

3.16. Oxidation of Rice Husk with Sodium Periodate

A total of 2 g of rice husk (particle size 200–400 μm) previously washed with a mixture of H$_2$O:ethanol 50:50 (3 × 3 mL) was placed in a syringe with septum. Then, 50 mL of a 0.20 M NaIO$_4$

solution was added and the mixture was allowed to react under stirring on the blood rotator for 22 h in the dark and at 25 °C. The solid support became dark brown. At the end of the reaction, the rice husk was filtered and rinsed with deionized water (3 × 10 mL) until neutrality.

3.17. Functionalization of Oxidized Rice Husk with HMDA Diamine Spacer

A total of 40 mL of a 0.9 M solution of hexamethylenediamine in methanol was added to the oxidized rice husk (200 mg) and the mixture was allowed to react for 72 h at 25 °C by stirring on the blood rotator. After this time, the rice husk was filtered and washed with methanol (2 × 40 mL).

3.18. Activation of Amine Functionalized Rice Husk with Glutaraldehyde Prior to Immobilization

Prior to immobilization, the amine-functionalized rice husk (200 mg) was activated by adding 50 mL of a 1.25% (v/v) glutaraldehyde solution in 0.05 M phosphate buffer at pH 8 and the suspension was allowed to react for 5 h at 25 °C. At the end of activation, the rice husk was filtered and washed with 0.05 M phosphate buffer at pH 8 (2 × 50 mL).

3.19. Determination of the Leaching of the Enzymes after Covalent Immobilization

At the end of the test for enzymatic activity, the biocatalyst was removed by filtration and 500 µL of the filtrate was taken, which were subjected to the enzymatic activity assay with tributyrin hydrolysis.

3.20. Immobilization of the CaLB on the Rice Husks Oxidized with Metaperiodate and Functionalized with Diamine Spacer

A total of 0.2 g of rice husk functionalized according to the procedure described above was placed in a syringe with septum. A 900 U/mL solution of Lipozyme CaLB was prepared in a vial by diluting the commercial preparation (4005 U/mL) in 0.5 M phosphate buffer at pH 8.

Immobilization was carried out by adding the enzymatic solution to the activate the rice husk to have a theoretical enzyme loading of 10,000 TBU $g_{carrier}^{-1}$. Then, 0.5 mL of a 2 mg/mL solution of PEG-3000 in phosphate buffer 0.5 M at pH 8 was added and the mixture was allowed to react at 25 °C on a rotating wheel for 24 or 48 h as stated in Table 2. After immobilization, the preparation was filtered and washed with 0.02 M phosphate buffer at pH 8 (6 × 1.2 mL), rinsed with acetone (4 × 1 mL) and dried on the septum of the syringe under vacuum (740 mbar). The preparation was transferred in a vial and stored in the fridge at 4 °C.

3.21. Immobilization of the CaLB on EC-EP/S Epoxy Methacrylic Resins

A total of 1.0 g of EC-EP/S epoxy resins (average particle size 100–300 µm) and washed once with 5 mL of deionized water were placed in a syringe with septum.

A 900 U/mL solution of Lipozyme CaLB was prepared in a vial by diluting the commercial preparation (4005 U/mL) in 0.5 M phosphate buffer at pH 8. Then, 11.4 mL of this solution was taken and added to the syringe containing the resin, so as to have a theoretical enzyme loading of 10,000 TBU $g_{carrier}^{-1}$. The mixture was allowed to react at 25 °C on a rotating wheel. After 24 h, the preparation was filtered and washed with 0.02 M phosphate buffer at pH 8 (6 × 3 mL). In order to quench the unreacted epoxy groups, the enzymatic preparation was incubated for 24 h with 15 mL of a saturated solution of glycine. Afterwards, the immobilized biocatalyst was filtered and washed with 0.02 M phosphate buffer at pH 8 (6 × 1 mL), then rinsed with acetone (3 × 3 mL) and dried on the septum of the syringe under vacuum (740 mbar for 30 min. The biocatalyst was transferred in a vial and stored at 4 °C.

3.22. Lipase Catalyzed Synthesis of Propyl Laurate

A total of 1.2 g of lauric acid (6 mmol) and 0.45 mL of 1-propanol (6 mmol) were placed in a 20 mL vial. The solution was thermostatted at 55 °C and kept under stirring (250 rpm) in an orbital shaker.

A sample (0.1 mL) was collected at t = 0 and weighed in a beaker. About 50 mg of biocatalyst were added to the initial solution and the mixture was left under stirring for 15 min. At regular intervals, 0.1 mL of the mixture were collected, weighed in a beaker and subsequently diluted in beakers with 7 mL of ethanol under continuous magnetic stirring. Three drops of phenolphthalein solution were added as an indicator. The samples were then titrated with a 0.1 M solution of KOH in ethanol until a persistent color change (light pink). The measurements were made in duplicate. One unit of activity (U/$g_{biocatalyst}$) of the biocatalyst is defined as the amount of immobilized enzyme necessary to produce 1 µmol of propyl laurate in one minute at 55 °C without solvent.

3.23. Solvent-Free Polycondensation of Dimethyl Itaconate with 1,4-butandiol Catalyzed by CaLB Immobilized on Epoxy Methacrylic Resins

A total of 16 mmol (2.4950 g) of dimethyl itaconate, 8 mmol (0.7310 g) of 1,4 butanediol and the immobilized enzyme (50% w/w; 297 U $g_{monomer}^{-1}$) were transferred to a 100 mL flask connected to a rotary evaporator at 200 rpm. A pressure of 70 mbar and a water bath temperature of 50 °C was applied. After 6 h, another 8 mmol of BDO were added and the mixture was left to react for 72 h. The enzyme was removed from the mixture by vacuum filtration and washing with dichloromethane. The solvent was subsequently removed under reduced pressure (600–500 mbar). The reaction product appears colorless and viscous. The characterization of the reaction product was carried out by 1H-NMR spectroscopy (see ESI) by dissolving the sample in deuterated chloroform (CDCl3) and by ESI mass spectrometry. The conversion was calculated by 1H-NMR, taking into account the signal relative to methylene in α to the hydroxyl in 1,4-butanediol and the signal of the same methylene in the esterification product [30]. The raw product was also solubilized in tetrahydrofuran (THF) and analyzed by Gel Permeation Chromatography (GPC).

3.24. Solvent-Free Polycondensation of Dimethyl Itaconate with 1,4-butandiol Catalyzed by CaLB Immobilized on Functionalized Rice Husk

A total of 8 mmol (1.2485 g) of dimethyl itaconate, 4 mmol (0.3600 g) of 1,4 butanediol and the immobilized enzyme (50% w/w; 158 U $g_{monomer}^{-1}$) was transferred to a 25 mL flask connected to a rotary evaporator at 200 rpm. The reaction was carried out as described in the paragraph above.

3.25. Lipase Hydrolytic Activity Assay for Determining Tributyrin Units (TBU)

The activity of enzymatic preparations was assayed by following the tributyrin hydrolysis and by titrating with 0.1 M sodium hydroxide (NaOH), the butyric acid that is released during the hydrolysis. An emulsion composed of 1.5 mL tributyrin, 5.1 mL gum arabic emulsifier (0.6% w v^{-1}) and 23.4 mL water was prepared in order to obtain a final molarity of tributyrin of 0.17 M. Successively, 2 mL of 0.1 M sodium-phosphate buffer (Nap) pH 7.0 was added to 30 mL of tributyrin emulsion and the mixture was incubated in a thermostatted vessel at 30 °C, equipped with a mechanical stirrer. After pH stabilization, 100 mg of immobilized biocatalyst or 0.005 mL CaLB native solution was added. The consumption of 0.1 M NaOH was monitored for 14 min. One unit of activity was defined as the amount of immobilized enzyme required to produce 1 mmol of butyric acid per min at 30 °C. One unit (U) of lipase activity was defined as the amount of enzyme which liberated 1 mmol of butyric acid per minute under the given assay conditions.

3.26. Immobilization of Acrylaway L on Activated Rice Husk

In order to exclude the protein concentration as a variable between the two asparaginase preparations, it was decided to operate Acrylaway L (5.77 mg/mL) at the same enzymatic concentration of Acrylaway High-T (3.04 mg/mL). In a vial containing 3.1 mL of Acrylaway L, corresponding to 17.9 mg $g_{carrier}^{-1}$, 1.25 mL of 2 mg/mL solution of PEG-3000 was added in 0.5 M of phosphate buffer at pH 8, and the pH was adjusted to 8 by adding, under stirring, 0.1 M NaOH. The enzymatic solution thus prepared was added to the syringe containing 0.5 g of functionalized rice husk and the mixture

was allowed to react at room temperature by stirring on the blood rotator. After 48 h, the preparation was filtered and washed with 0.02 M phosphate buffer at pH 8 (6 × 3 mL). The biocatalyst was transferred into a vial and suspended in a 70:30 mixture of glycerol: 0.02 M phosphate buffer at pH 8.

3.27. Immobilization of Acrylaway High-T on Activated Rice Husk

A total of 5.9 mL of Acrylaway High-T (26.8 mg of protein) was placed in a vial and 1.25 mL of a solution 2 mg/mL of PEG-3000 in 0.5 M phosphate buffer at pH 8 was added. The pH was adjusted to 8 by adding, under stirring, 0.1 M NaOH. The enzyme solution thus prepared was added in the syringe containing 0.5 g of rice husk functionalized as described above. The mixture was allowed to react at 25 °C by stirring on a rotating wheel. After 48 h the amount of immobilized protein (%) was determined and the preparation was filtered and washed with phosphate buffer 0.02 M pH 8 (6 × 3 mL). The biocatalyst was transferred into a vial and suspended in a 70:30 mixture of glycerol in 0.02 M phosphate buffer at pH 8.

3.28. Immobilization of Acrylaway L on EC-EP/S Resins

A total of 1 g of EC-EP/S epoxy resin (particle size 100–300 µm) was weighed in a test tube with filter. The resin was washed 3 times with 4 mL of deionized water. An enzymatic solution of Acrylaway L at a concentration of 3.4 mg/mL was prepared in a vial by adding 4.3 mL of 0.5 M phosphate buffer at pH 8 to 3.6 mL of Acrylaway L. The pH was adjusted to 8 by adding, under stirring, 0.1 M NaOH and the enzymatic solution thus prepared was added to the tube containing the resin. The suspension was allowed to react on a rotating wheel at 25 °C. After 24 h the preparation was filtered and washed with 0.02 M phosphate buffer at pH 8 (6 × 3 mL). The biocatalyst was transferred into a vial and suspended in a 70:30 mixture of glycerol:phosphate buffer of 0.02 M at pH 8.

3.29. Immobilization of Acrylaway High-T on EC-EP/S Resins

A total of 1 g of epoxy resin (particle size 100–300 µm) was weighed in a test tube with filter. The resin was washed 3 times with 4 mL of deionized water. Then, 7.7 mL of Acrylaway High-T (26.8 mg of protein) was added to a vial, the pH was adjusted to 8 by adding, under stirring, 0.1 M NaOH, and the thus prepared enzymatic solution was added to the test tube containing the resin. The immobilization was carried out as described in the previous paragraph.

3.30. Determination of Water Content in Enzymatic Preparations

A known amount of biocatalyst was placed on an aluminum plate and the sample was dried for 6 h in an oven at 120 °C. The water content (% w/w) was determined by determining the difference in weight before and after the drying procedure.

3.31. Computational Construction of 3D Models and Analysis of the Surface of Asparaginases

Protein structures were visualized and recorded using the PyMOL software (2.0 version). The 3D structures used for the hydrophobicity comparisons were retrieved from PDB. The representation and the calculation of the hydrophobic enzyme surfaces were performed by GRID mapping, using two different probes describing and quantifying different interactions: WATER (dipolar interactions and hydrogen bond formation), DRY (hydrophobic interactions) [46]. The N-glycosylation sites were determined using the open source software available at http://www.cbs.dtu.dk/services/NetNGlyc/. Details are available in the ESI.

4. Conclusions

In the present study, we have demonstrated the applicability of functionalized rice husk as a carrier for the covalent immobilization of lipase B from *Candida antarctica* (CaLB) and two asparaginases. This new renewable and inexpensive carrier, although not optimized, proved to be more efficient

than the fossil-based commercial methacrylic resins in the solvent-free synthesis of poly(1,4-butylene itaconate) catalyzed by CaLB. Although the micro-porosity of rice husk cannot be exploited for loading the enzymes, this composite material appears a suitable solution for highly viscous systems, having severe mass transfer limitations. Data demonstrate that, by dispersing the enzyme on the outer surface of a large volume of inexpensive carrier, the maximum mass transfer is achieved. Overall, the remarkable robustness of the milled RH associated with a low density (0.4 g mL^{-1} vs. 1.1 g mL^{-1} of methacrylic resins) appear as the main features that affect the performance of this renewable carrier. The functionalized rice husk was also efficiently used in aqueous solutions as carrier for asparaginases enzymes, which catalyzed the hydrolysis of the precursor of acrylamide, a toxic side product of various types of food. The covalently immobilized enzymes demonstrated optimal dispersibility and recyclability. The morphological characterization of RH provides the basis for further optimization studies. As appears from microscopy analysis, the cellulosic surface available for oxidation and further functionalization is rather limited in the milled rice husk. In addition, the lignin fraction is prevalently masked by a SiO$_2$ layer, which confers mechanical resistance to the material notwithstanding its very low density. The possibility of immobilizing enzymes on large volumes of inexpensive renewable carriers opens new perspectives for overcoming the environmental impact of fossil-based carriers, while boosting the economic viability of processes nowadays hampered by the high cost of immobilized biocatalysts.

Supplementary Materials: The following are available online at http://www.mdpi.com/2073-4344/8/10/471/s1, Figures S1–S11.

Conflicts of Interest: The Authors declare no conflict of interest.

References

1. Cantone, S.; Spizzo, P.; Fattor, D.; Ferrario, V.; Ebert, C.; Gardossi, L. Lipases for bio-based chemistry-Efficient immobilised biocatalysts for competitive biocatalysed processes. *Chem. Today* **2012**, *30*, 10–14. [CrossRef]
2. Di Cosimo, R.; McAuliffe, J.; Poulose, A.J.; Bohlmann, G. Industrial use of immobilized enzymes. *Chem. Soc. Rev.* **2013**, *42*, 6437–6474. [CrossRef] [PubMed]
3. Tufvesson, P.; Lima-Ramos, J.; Nordblad, M.; Woodley, J.M. Guidelines and Cost Analysis for Catalyst Production in Biocatalytic Processes. *Org. Process Res. Dev.* **2011**, *15*, 266–274. [CrossRef]
4. Liu, Y.; Andryszkiewicz, M.; Peña, R. Outcome of a public consultation on the draft Statement on Exposure Assessment of Food Enzymes. *EFSA Support. Publ.* **2016**, *13*, 1106E. [CrossRef]
5. Pellis, A.; Cantone, S.; Ebert, C.; Gardossi, L. Evolving biocatalysis to meet bioeconomy challenges and opportunities. *New Biotechnol.* **2017**, *40*, 154–169. [CrossRef] [PubMed]
6. Cantone, S.; Ferrario, V.; Corici, L.; Ebert, C.; Fattor, D.; Spizzo, P.; Gardossi, L. Efficient immobilisation of industrial biocatalysts: Criteria and constraints for the selection of organic polymeric carriers and immobilisation methods. *Chem. Soc. Rev.* **2013**, *42*, 6262–6276. [CrossRef] [PubMed]
7. Ravindran, R.; Jaiswal, A.K. Exploitation of food industry waste for high-value products. *Trends Biotechnol.* **2016**, *34*, 58–69. [CrossRef] [PubMed]
8. Sheldon, R.A. Enzyme Immobilization: The Quest for Optimum Performance. *Adv. Synth. Catal.* **2007**, *349*, 1289–1307. [CrossRef]

9. Pellis, A.; Ferrario, V.; Cespugli, M.; Corici, L.; Guarneri, A.; Zartl, B.; Herrero Acero, E.; Ebert, C.; Guebitz, G.M.; Gardossi, L. Fully renewable polyesters via polycondensation catalyzed by Thermobifida cellulosilytica cutinase 1: An integrated approach. *Green Chem.* **2017**, *19*, 490–502. [CrossRef]

10. Corici, L.; Ferrario, V.; Pellis, A.; Ebert, C.; Lotteria, S.; Cantone, S.; Voinovich, D.; Gardossi, L. Large scale applications of immobilized enzymes call for sustainable and inexpensive solutions: Rice husks as renewable alternatives to fossil-based organic resins. *RSC Adv.* **2016**, *6*, 63256–63270. [CrossRef]

11. Contreras, L.M.; Schelle, H.; Sebrango, C.R.; Pereda, I. Methane potential and biodegradability of rice straw, rice husk and rice residues from the drying. *Water Sci. Technol.* **2012**, *65*, 1142–1149. [CrossRef] [PubMed]

12. Available online: https://echa.europa.eu/regulations/reach (accessed on 23 March 2018).

13. Wartelle, L.H.; Marshall, W.E. Quaternized agricultural by-products as anion exchange resins. *J. Environ. Manag.* **2005**, *78*, 157–162. [CrossRef] [PubMed]

14. Prado, H.J.; Matulewicz, M.C. Cationization of polysaccharides: A path to greener derivatives with many industrial applications. *Eur. Polym. J.* **2014**, *52*, 53–75. [CrossRef]

15. Sud, D.; Mahajan, G.; Kaur, M.P. Agricultural waste material as potential adsorbent for sequestering heavy metal ions from aqueous solutions—A review. *Bioresour. Technol.* **2008**, *14*, 6017–6602. [CrossRef] [PubMed]

16. Tantrakulsiri, J.; Jeyashoke, N.; Krisanangkura, K.J. Utilization of rice hull ash as a support material for immobilization of Candida cylindracea lipase. *Am. Oil Chem. Soc.* **1997**, *74*, 173–175. [CrossRef]

17. Park, B.; Wi, G.S.; Lee, H.K.; Singh, P.A.; Yoon, T.; Kim, S.Y. Characterization of anatomical features and silica distribution in rice husk using microscopic and micro-analytical techniques. *Biomass Bioenergy* **2003**, *25*, 319–327. [CrossRef]

18. Coletta, C.V.; Rezende, V.C.; da Conceicao, F.R.; Polikarpov, I.; Giumaraes, G.E.F. Mapping the lignin distribution in pretreated sugarcane bagasse by confocal and fluorescence lifetime imaging microscopy. *Biotechnol. Biofuels* **2013**, *6*, 43. [CrossRef] [PubMed]

19. Chen, B.; Hu, J.; Miller, M.E.; Xie, W.; Cai, M.; Gross, A.R. Candida antarctica lipase B chemically immobilized on epoxy-activated micro- and nanobeads: Catalysts for polyester synthesis. *Biomacromolecules* **2008**, *9*, 463–471. [CrossRef] [PubMed]

20. Kodama, Y. Time Gating of Chloroplast Autofluorescence Allows Clearer Fluorescence Imaging in Planta. *PLoS ONE* **2016**, *11*, e0152484. [CrossRef] [PubMed]

21. Schoevaart, R.; Siebum, A.; Van Rantwijk, F.; Sheldon, R.; Kieboom, T. Glutaraldehyde Cross-link Analogues from Carbohydrates. *Starch* **2005**, *57*, 161–165. [CrossRef]

22. Kobayashi, M.; Takatsu, K. Cross-linked stabilization of trypsin with dextran-dialdehyde. *Biosci. Biotech. Biochem.* **1994**, *58*, 275–278. [CrossRef]

23. Migneault, I.; Dartiguenave, C.; Bertrand, M.J.; Waldron, K.C. Glutaraldehyde: Behavior in aqueous solution, reaction with proteins, and application to enzyme crosslinking. *Biotechniques.* **2014**, *37*, 798–802. [CrossRef] [PubMed]

24. Tashima, T.; Imai, M.; Kuroda, Y.; Yagi, S.; Nakagawa, T. Structure of a New Oligomer of Glutaraldehyde Produced by Aldol Condensation Reaction. *J. Org. Chem.* **1991**, *2*, 694–697. [CrossRef]

25. Guigo, N.; Mazeau, K.; Putaux, J.L.; Heux, L. Surface modification of cellulose microfibrils by periodate oxidation and subsequent reductive amination with benzylamine: A topochemical study. *Cellulose* **2014**, *21*, 4119–4133. [CrossRef]

26. Zhao, H.; Heindel, D.N. Determination of degree of substitution of formyl groups in polyaldehyde dextran by the hydroxylamine hydrochloride method. *Pharm. Res.* **1991**, *8*, 400–402. [CrossRef] [PubMed]

27. Habibi, Y.; Chanzy, H.; Vignon, M.R. TEMPO-mediated surface oxidation of cellulose whiskers. *Cellulose* **2006**, *13*, 679–687. [CrossRef]

28. Perez, S.D.; Montanari, S.; Vignon, M.R. TEMPO-mediated oxidation of cellulose III. *Biomacromolecules* **2003**, *4*, 1417–1425. [CrossRef] [PubMed]

29. Monsan, P. Enzymes Immobilized on a Solid Support Containing Cellulose and Lignin. U.S. Patent 4405715, 20 September 1983.

30. Pellis, A.; Corici, L.; Sinigoi, L.; D'Amelio, N.; Fattor, D.; Ferrario, V.; Ebert, C.; Gardossi, L. Towards feasible and scalable solvent-free enzymatic polycondensations: Integrating robust biocatalysts with thin film reactions. *Green Chem.* **2015**, *17*, 1756–1766. [CrossRef]

36

31. Corici, L.; Pellis, A.; Ferrario, V.; Ebert, E.; Cantone, S.; Gardossi, L. Understanding Potentials and Restrictions of Solvent-Free Enzymatic Polycondensation of Itaconic Acid: An Experimental and Computational Analysis. *Adv. Synth. Catal.* **2015**, *357*, 1763–1774. [CrossRef]

32. Ansorge-Schumacher, M.B.; Thum, O. Immobilised lipases in the cosmetics industry. *Chem. Soc. Rev.* **2013**, *42*, 6475–6490. [CrossRef] [PubMed]

33. Pellis, A.; Acero, E.H.; Gardossi, L.; Ferrario, V.; Guebitz, G.M. Renewable building blocks for sustainable polyesters: New biotechnological routes for greener plastics. *Polym. Int.* **2016**, *65*, 861–871. [CrossRef]

34. Pellis, A.; Guarneri, A.; Brandauer, M.; Herrero Acero, E.; Peerlings, H.; Gardossi, L.; Guebitz, G.M. Exploring mild enzymatic sustainable routes for the synthesis of bio-degradable aromatic-aliphatic oligoesters. *Biotechnol. J.* **2016**, *11*, 642–647. [CrossRef] [PubMed]

35. Robert, T.; Friebel, S. Itaconic acid—A versatile building block for renewable polyesters with enhanced functionality. *Green Chem.* **2016**, *18*, 2922–2934. [CrossRef]

36. Miller, L.M.; Mei, Y.; Gao, W.; Gross, R.A. Imaging the distribution of immobilized enzymes using infrared micro-spectroscopy. *Biomacromolecules* **2003**, *4*, 70–74. [CrossRef]

37. Hendriksen, H.V.; Kornbrust, B.A.; Ostergaard, P.R.; Stringer, M.A. Evaluating the Potential for Enzymatic Acrylamide Mitigation in a Range of Food Products Using an Asparaginase from Aspergillus oryzae. *J. Agric. Food Chem.* **2009**, *57*, 4168–4176. [CrossRef] [PubMed]

38. Wilson, K.M.; Rimm, E.B.; Thompson, K.M.; Mucci, L.A. Dietary acrylamide and cancer risk in humans: A review. *J. Verbrauch. Lebensm.* **2006**, *1*, 19–27. [CrossRef]

39. Teodor, E.; Litescu, S.C.; Lazar, V.; Somoghi, R. Hydrogel-magnetic nanoparticles with immobilized L-asparaginase for biomedical applications. *J. Mater. Sci. Mater. Med.* **2009**, *20*, 1307–1314. [CrossRef] [PubMed]

40. Kotzia, G.A.; Labrou, N.E. L-Asparaginase from Erwinia Chrysanthemi 3937: Cloning, expression and characterization. *J. Biotechnol.* **2006**, *127*, 657–669. [CrossRef] [PubMed]

41. Zhang, Y.Q.; Tao, M.L.; Shen, W.D.; Zhou, Y.Z.; Ding, Y.; Ma, Y.; Zhou, W.L. Immobilization of l-asparaginase on the microparticles of the natural silk sericin protein and its characters. *Biomaterials* **2004**, *25*, 3751–3759. [CrossRef] [PubMed]

42. Aung, H.P.; Bocola, M.; Schleper, S.; Röhm, K.H. Dynamics of a mobile loop at the active site of Escherichia coli asparaginase. *Biochim. Biophys. Acta* **2000**, *1481*, 349–359. [CrossRef]

43. Yao, M.; Yasutake, Y.; Morita, H.; Tanaka, I. Structure of the type I L-asparaginase from the hyperthermophilic archaeon Pyrococcus horikoshii at 2.16 Å resolution. *Acta Crystallogr. D* **2005**, *61*, 294–301. [CrossRef] [PubMed]

44. European Food Safety Authority. *Technical Report of EFSA: Explanatory Note on the Guidance of the Scientific Panel of Food Contact Material, Enzymes, Flavourings and Processing Aids (CEF) on the Submission of a Dossier on Food Enzymes*; EFSA Supporting Publication: Parma, Italy, 2014; EN-689; Available online: www.efsa.europa.eu (accessed on 28 July 2018).

45. Aghaiypour, K.; Wlodawer, A.; Lubkowski, J. Structural basis for the activity and substrate specificity of Erwinia chrysanthemi L-asparaginase. *Biochemistry* **2001**, *40*, 5655–5664. [CrossRef] [PubMed]

46. Ferrario, V.; Ebert, C.; Knapic, L.; Fattor, D.; Basso, A.; Spizzo, P.; Gardossi, L. Conformational changes of lipases in aqueous media: A comparative computational study and experimental implications. *Adv. Synth. Catal.* **2011**, *353*, 2466–2480. [CrossRef]

47. Basso, A.; Braiuca, P.; Cantone, S.; Ebert, C.; Linda, P.; Spizzo, P.; Caimi, P.; Hanefeld, U.; Degrassi, G.; Gardossi, L. In silico analysis of enzyme surface and glycosylation effect as a tool for efficient covalent immobilization of CalB and PGA on Sepabeads®. *Adv. Synth. Catal.* **2007**, *349*, 877–886. [CrossRef]

3.2 Biocatalyzed activation of rice husk by means of laccases

In order to continue the work described in the previous manuscript and to avoid the use of the hazardous and ecotoxic sodium periodate, "laccase-mediator system" oxidation was explored as an alternative route to chemical oxidation.

Laccases (EC 1.10.3.2) are copper-containing oxidase and contain at least 4 copper atoms. Laccases are common in various organisms like bacteria, plants, insects and fungi and could have different functions based on the organism they belong to[29]. Copper atoms are classified in 3 types based on the coordination of their bonds (Figure 5).
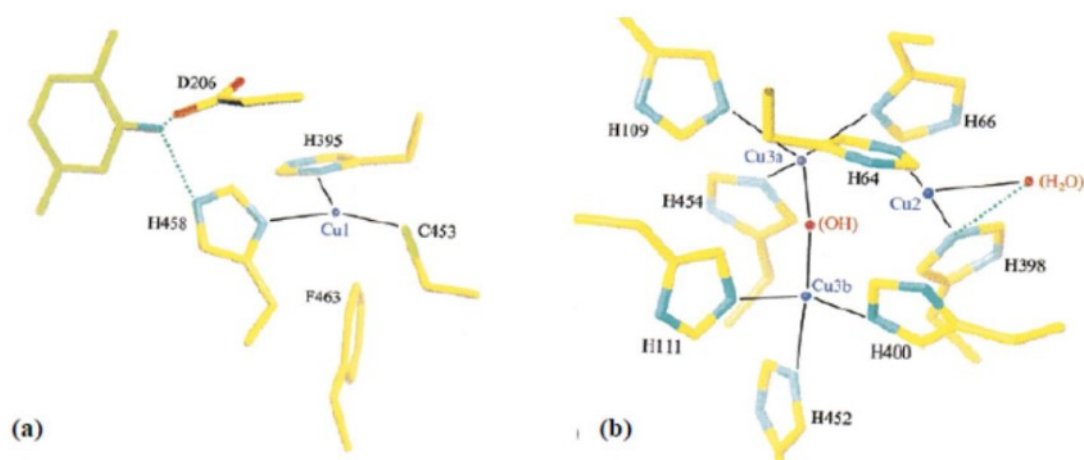
Figure 5. Catalytic site of *Trametes vescicolor* and coordination bonds. **a)** Type one copper (T1); **b)** trinuclear cluster

Type one copper (T1) presents a trigonal geometry with a free axial position prone to substrate interaction. Equatorial positions establish coordination bonds with two histidine residues and a cysteine, while the fourth could be variable[30].

The redox potential of T1 copper depends on the organism producing the enzyme: in fungal laccases, the redox potential is 700-900 mV, while on plant laccases it is typically lower (330-500 mV) and this difference is caused by the different coordination of T1 copper[31]. T1 copper atom is responsible for the blue colour of laccases and of the substrate oxidation.

T2 copper is not detectable in the visible spectrum and is coordinated by two histidine residues. T3 coppers establish a binuclear centre with a band of absorbance at 330 nm in the oxidized form and are coordinated with 6 histidine residues next to the T2 copper. This molecular architecture is responsible for the reduction of molecular oxygen by the production of water.

Laccases are active on a wide range of substrates, in particular they oxidize *p*-diphenols, polyphenols, and aminic compounds. Their usage is sustainable because they require oxygen as an electron acceptor and produce only water as a by-product.

Non-phenolic compounds are often not oxidized by laccases because of their low redox potential. Furthermore, big molecules that cannot reach the active site (i.e. lignin) cannot be oxidized[32]. To overcome this drawback, a mediator with the function of moving oxidative species outside from the enzyme to the substrate can be used. A mediator is usually a small molecule that acts as an electron shuttle, it is oxidized by the enzyme, moves away from the active site and, in turn, oxidize the substrate (Figure 6).

A redox mediator should fulfil some conditions: it must be a small molecule able to generate stable radical species, should not interfere with the catalytic activity of the enzyme while allowing the in situ recyclability and, finally, it should be cost-effective[33]. The system consisting of laccase and mediator is called *laccase-mediator system* (LMS). Many natural and synthetic mediators are reported in the literature, and they could easily be used as redox mediators for laccases[34].
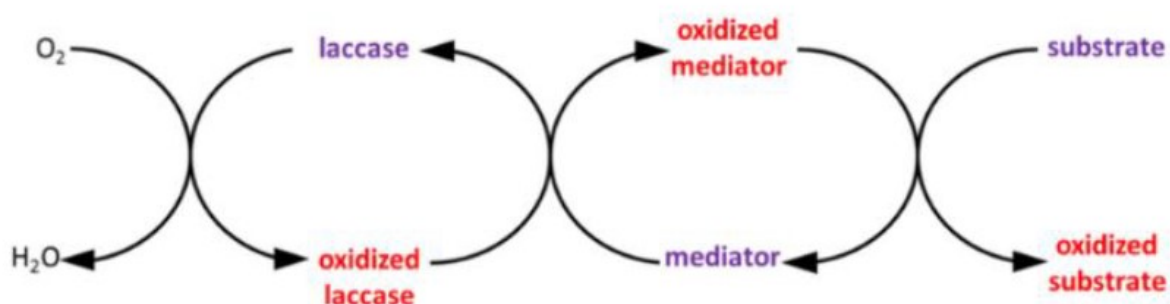
Figure 6. Laccase-mediator system reaction scheme. Oxygen reduction is coupled with substrate oxidation[35].

Laccases can be used for the valorisation of lignocellulosic materials via depolymerization of lignin allowing for a more efficient further conversion of the monomers for the production of biofuels[36] and also for selective grafting of small organic molecules over the surface of the material[37]. Furthermore, it has been reported that laccase-mediator systems enable the oxidation of the glycoside units of cellulose. The selective oxidation of the cellulose fraction of lignocellulosic materials takes place in the presence of (2,2,6,6-Tetramethylpiperidin-1-yl)oxyl radical, the so-called TEMPO-radical[38].
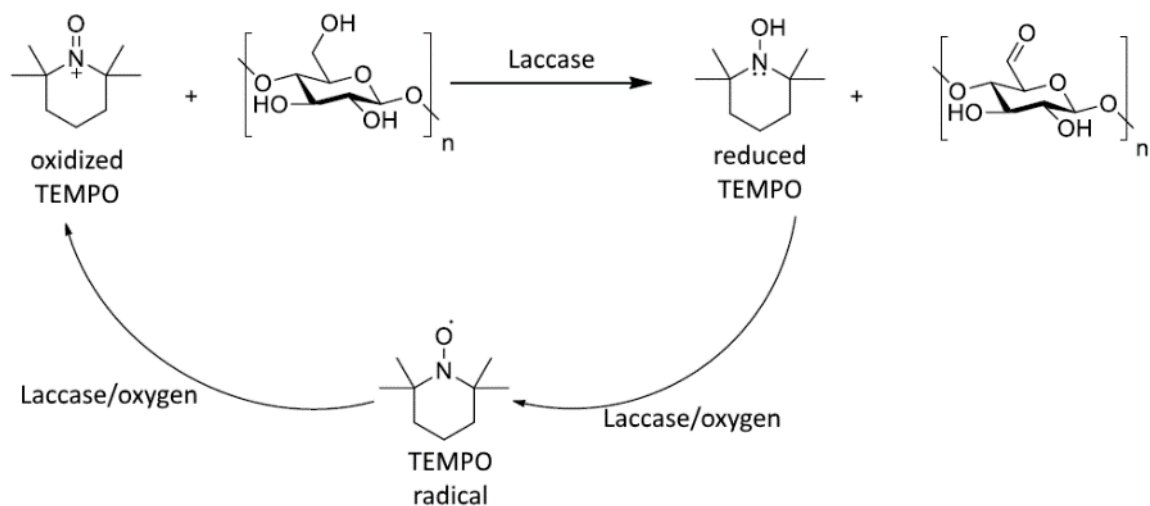
Figure 7. Cellulose oxidation scheme by laccase/TEMPO system

Laccase oxidizes TEMPO radical to an oxo-ammonium cation that, in turn, selectively oxidizes the C_6 hydroxyl of the glycosidic ring forming an aldehyde via heterolytic cleavage. The neo-formed aldehydic moiety can react again with nearby hydroxyl groups to form a hemiketal or could be further oxidized to carboxylic acid (Figure 7).

The above-mentioned approach is a more environmentally friendly route for the oxidation of cellulose and, in particular, for the activation of rice husk. Non-green alternatives are represented by TEMPO/NaOCl/NaBr system[39] or by sodium periodate as a powerful oxidizing agent[38]. Cellulose activation with carbonyl groups makes the material prone to coupling with organic molecules or biomolecules such as enzymes.

3.2.1 Oxidation of milled rice husk using a laccase-mediator system[35]

Following the oxidation of rice husk by means of sodium periodate[1,5], the first oxidation attempt with the laccase-mediator system has been carried out using milled rice husk with a particle size of 0.2-0.4 mm. The oxidation was carried out using laccase from *Trametes species* and Novozym laccase S1003 according to the protocol of Patel and co-workers[38].

The procedure, reported in the experimental section, consists in a 48 hours treatment of rice husk at environmental pressure and 25°C with a 0.1 M pH 5 citrate buffer solution containing 10 mM TEMPO radical and different amounts of laccase from *Trametes spec.* (here called with its commercial name "Laccase C", the enzyme is produced by ASA-spezialenzyme). Air was insufflated in the reaction mixture to provide the oxygen needed for the catalytic activity. After work-up, the content of carbonyl groups was assessed via hydroxylamine chlorhydrate assay[40] and compared rice husk oxidized by 0.2 M sodium-periodate.
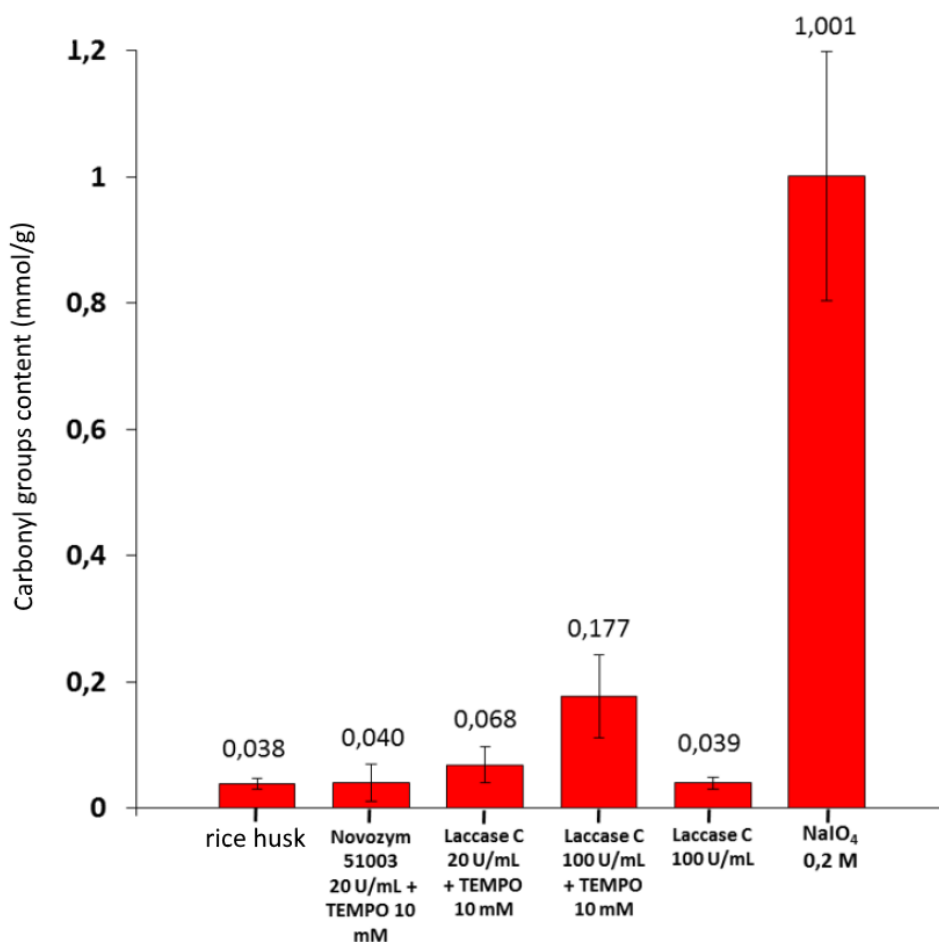
Figure 8. Carbonyl content in oxidized rice husk samples[35].

Oxidation by sodium periodate was more effective in terms of carbonyl content detected (Figure 8). This data was expected because with sodium periodate two carbonyl groups per glycosidic ring are introduced, whereas in the case of LMS oxidation one single carbonyl group per glycosidic ring is formed. Oxidation by 100 U/mL of laccase C gave the best results, leading to 350% increase of carbonyl groups if compared with the blank experiment (rice husk treated in the same conditions without adding laccase). The use of a mediator has proven to be necessary to reach a reasonable concentration of carbonyl groups, laccase C without mediator is in fact not able to oxidize rice husk.

CaLB immobilization via diamine spacer on rice husk activated by laccase

Upon oxidation of the cellulose fraction, amine groups were inserted by treating the oxidized material with a hexamethylenediamine (HMDA) solution. Prior to CaLB immobilization, a reaction step with a glutaraldehyde solution was performed to introduce carbonyl moieties prone to react with amine groups on the surface of the enzyme (Figure 9). A diluted solution

of Lypozyme CaLB was used for the 48 hours immobilization together with a concentration of 10,000 TBU/g_{RH} (TBU=enzyme units assessed with tributyrin hydrolysis).
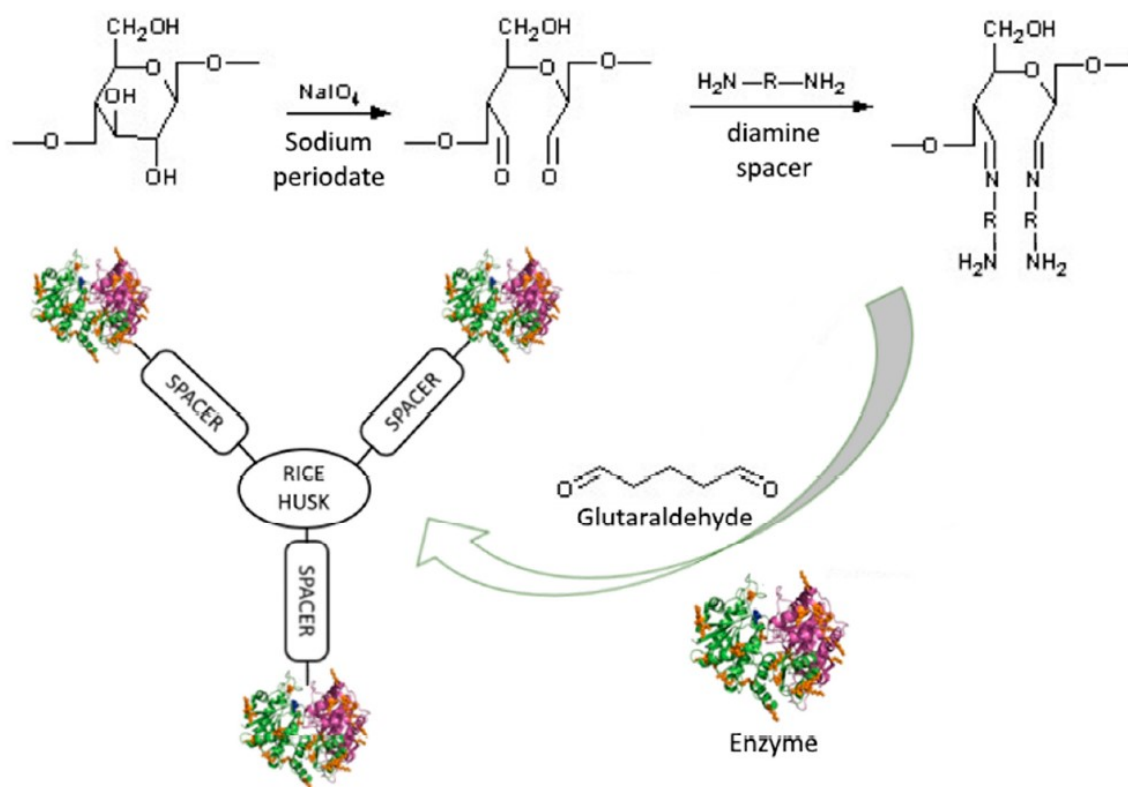
Figure 9. Schematic illustration of the oxidation and functionalization of the cellulosic fraction of RH for the covalent immobilization of CaLB[1].

Characterization of enzyme activity after immobilization

The immobilized CaLB formulation has been assessed in terms of protein loading, hydrolytic activity and synthetic activity (Table 1).

Sample	loading %	hydrolytic activity (U/g)	synthetic activity (U/g)
laccase C-RH(HMDA+GA)	17	56 ± 25	198 ± 8
NaIO$_4$-RH (HMDA+GA)[35]	72	316	592 ± 24

Table 1. Immobilization yield of laccase C oxidized rice husk and sodium periodate-oxidized rice husk after diamine linker attachment and enzyme immobilization

Enzyme leaching was verified in both preparations and was absent. The data here reported clearly shows that laccase C oxidation of rice husk is less effective than sodium periodate in terms of protein immobilization and enzyme activity. The reason lies in the poor number of carbonyl groups obtained with laccase C but there is also a second reason related to the fact that sodium periodate is able to alter the structure of the lignocellulosic matrix enhancing enzyme accessibility. SEM microscopy pointed out that chemical oxidation by means of

sodium periodate was more aggressive in terms of physical degradation of the material on both the inner and the outer surface, laccase oxidation was milder and preserved the structure of rice husk, in particular the outer surface because of its higher content in silica that protects the inner matrix from the oxidative action of the enzyme[1,41].

The higher efficiency of sodium periodate in terms of cellulose functionalization could be justified by the fact that it generates highly reactive glutaraldehyde-like dialdehydic 5-terms rings[42] (Figure 10).
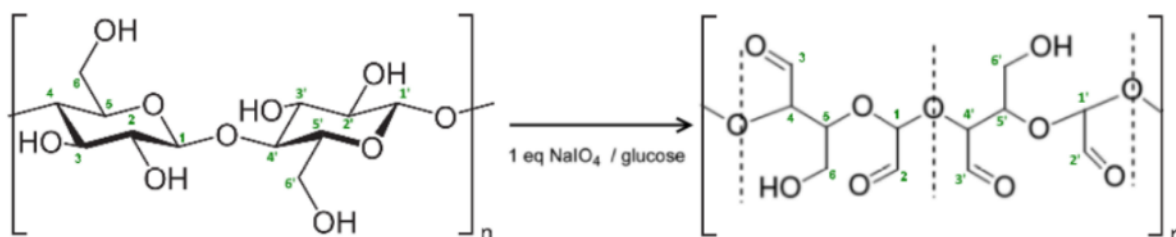
Figure 10. Dialdehyde compound originated form glycosidic ring-opening following sodium periodate oxidation of carbohydrates with 1-4 β glycosidic bonds. Carbons are numbered to ease interpretation. Dialdehyde unit is formed by 2, 1, 4', 3' carbons.

Such structures are more reactive than the single aldehyde group introduced by LMS oxidation because they can lead to the formation of a wide spectrum of stable compounds in the presence of nucleophilic amines. As stated in the thorough review of Migneault on glutaraldehyde reactivity[42], aldolic condensations, Michael reactions and pyridinium ion formation can easily take please in these conditions, contributing to the efficient immobilization of proteins when glutaraldehyde is added to the reaction medium and reacts with the glutaraldehyde-like compounds formed on the cellulose chain.

3.2.2 *Delignification of rice husk by hydrogen peroxide/ammonium hydroxide*

In order to improve the immobilization yield and the consequent catalytic activity of the immobilized preparation, different approaches targeted to increase the surface availability were explored. Preliminary data on sodium periodate-oxidized rice husk indicated that using 10,000 U_{TBU} of CaLB with an immobilization time of 48 hours, 72% protein loading can be achieved and catalytical activity is retained[5]. On the other hand, LMS oxidized rice husk presents only 17% of protein loading and lower catalytical activity. For this reasons, new routes were explored in order to improve the functionalization of the rice husk while avoiding the use of periodate.

Delignification of the lignocellulosic matrix is important to enhance the accessibility of the cellulose. Diferulic linkages between cellulose and lignin are promptly broken by an oxidative pre-treatment[43] in order to expose a higher fraction of cellulose ready to be functionalized in the subsequent carbonyl addition step. Furthermore, lignin removal increases the hydrophilicity of the material.

A possible pre-treatment of rice husk that can be effective to increase the surface availability is the one proposed by Kim S.B. (Kim S.B. et al. 1996) who developed a bleaching technique called ARP-H (ammonia recycled percolation with hydrogen peroxide) to be used on herbaceous biomass. The reaction was carried out at 170 °C in a packed-bed reactor where aqueous ammonia is recycled in a continuous cycle. The authors reported 80% degradation of hemicellulose, that led to the production of xylose, and the complete removal of lignin (94-99%). The obtained residue contained mostly glucans in the form of alpha cellulose. In the work of Kim S.B. et al.[44] aqueous ammonia was reported to have delignificant properties and to cause the hydrolysis of the glucuronic esters responsible for the lignin-hemicellulose matrix integrity[45]. Hydrogen peroxide has a synergic effect that increases the aggressive effect towards the lignocellulosic material. Since cellulose is not attacked by the oxidative process, it can be assumed that also in rice husk the cellulose fraction remains unaltered, paving the way to further functionalization.

$$H_2O_2 = H^+ + HOO^-$$

$$H_2O_2 + HOO^- = \cdot OH + O_2^- \cdot + H_2O$$
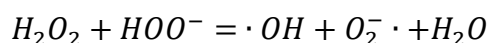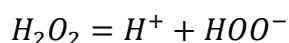
Scheme 1. Hydrogen peroxide decomposition in alkaline conditions

During the spontaneous hydrogen peroxide decomposition (Scheme 1), the hydroperoxide anion produced is unable to directly depolymerize lignin, while the hydroxyl radical is a powerful oxidant responsible for lignin and hemicellulose depolymerisation. The formation of this radical depends on the pH of the reaction mixture: alkaline conditions promote the formation of the hydroperoxide anion via the neutralization of H^+ ions. The produced anion promptly reacts with hydrogen peroxide to form the radical species[44]. Hydrogen peroxide decomposition with ammonia has been reported to follow a first-order kinetic depending on its concentration[46]. The formation of the radical is pH dependent and the optimal pH to achieve delignification with an alkaline hydrogen peroxide solution was reported to be 11.5[43].

Other studies reporting various approaches to depolymerization of lignin in lignocellulosic materials via ammonia and hydrogen peroxide were taken into account to acquire a clear

understanding of the dynamics of the entire process. Zhao and co-workers[43] tested different variants of a lignin and cellulose depolymerizing treatment on corn, namely ammonia fibre expansion (AFEX). The reaction took place with high pressure and high-temperature liquid ammonia, leading to the degradation of the lignocellulose matrix. For enzyme immobilization purposes this technique is clearly too aggressive because the original morphologic structure and mechanical resistance of the raw material should be retained for practical applications.

A patent of M. Vezzani[47] reported an industrial scale treatment for the oxidation of starch-based materials and such procedure was adapted for the purpose of this study at lab scale. In the said patent, 5-20% w/v hydrogen peroxide was used together with 5-20% w/v ammonium hydroxide to obtain starch oxidation at <30° C temperature in a cylindrical rotary reactor, with a continuous feed of reactants and starch. This treatment, at least at lab scale, has proved to be inefficient in terms of lignin removal and did not cause the introduction of extra carbonyl groups. The reason lies in the lower reactivity of aqueous ammonia at low temperatures whereas high temperatures and anhydrous liquid ammonia at high pressure are more effective for this kind of treatments.

Delignification of rice husk and characterization

Rice husk with a particle size of 0.2-0.4 mm was treated with an alkaline hydrogen peroxide solution varying the concentration of the two reactants. The concentration of both starting solutions of aqueous ammonia and hydrogen peroxide was 30%, properly diluted to obtain different reaction mixtures. Hydrogen peroxide was added in the range of 0-8% w/v. Exceeding 8% hydrogen peroxide in an ammonium hydroxide solution could be dangerous because of the high reactivity of the mixture (Figure 11).

Figure 11. Rice husk samples treated with the ammonium hydroxide (15%) and hydrogen peroxide mixture. From left to the right hydrogen peroxide concentration increases. Slight colour change is noticeable.

After the said treatment, the material was oxidized with 1.0 U/mg laccase C and TEMPO radical (10 Mm). The carbonyl content was assessed in duplicate with hydroxylamine chlorhydrate carbonyl assay. Water retaining capability was evaluated gravimetrically (Table 2, Figure 12).

Sample	H_2O_2 % w/v	NH_3 % w/v	Water absorption % w/w	Recovered material %w/w	Original carbonyl content µmol/g	Carbonyl content after oxidation µmol/g
15AHPN0	0	15.0	46,4	73,4	0	0
15AHPN2	2.0	15.0	47,8	77,4	n.d.	n.d.
15AHPN4	4.0	15.0	48,6	73,0	14,5±9,5	33,7±8,5
15AHPN6	6.0	15.0	45,8	63,6	n.d.	n.d.
15AHPN8	8.0	15.0	48,9	71,8	112,2±54,1	187,6±12,4
22AHPN0	0	22.0	44,9	80,6	4,6±3,5	83,2±34,3
22AHPN2	2.0	22.0	45,1	78,8	n.d.	n.d.
22AHPN4	4.0	22.0	47,2	78,0	0	257,0±34,6
22AHPN6	6.0	22.0	48,5	75,6	n.d.	n.d.
22AHPN8	8.0	22.0	48,3	76,4	44,0±22,9	129,3±16,2

Table 2. Ammonium hydroxide/hydrogen peroxide pre-treatment of rice husk. Composition of the reactive mixture is shown and characterisation of the resulting material is reported. Experiments were named based on the following syntax: "%NH_3 *AHP* %H_2O_2". The carbonyl content of samples marked as "n.d." was not assessed.
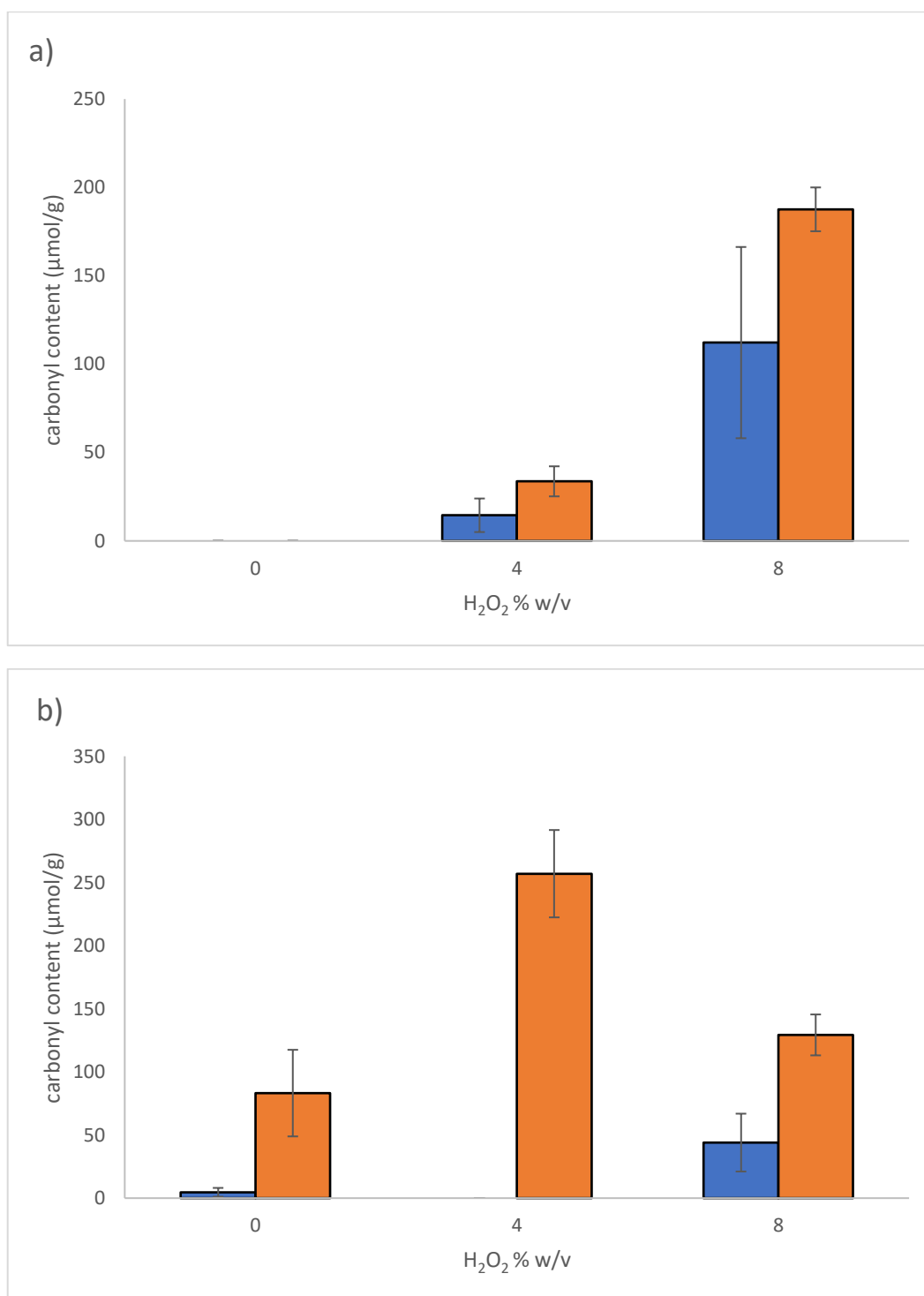
Figure 12. Graphical representation of the variation of carbonyl content after treatment. Blue: before biocatalysed oxidation; orange: after biocatalysed oxidation. **a)** 15% ammonium hydroxide; **b)** 22% ammonium hydroxide.

Carbonyl content quantification indicates that in the set of experiments with 15% w/v of ammonium hydroxide this treatment is able to introduce a quantifiable amount of carbonyl groups, that increases after oxidation by laccase C.

By using 22% ammonium hydroxide conflicting results were obtained. in particular, sample 22AHP4 showed an unexpectedly high carbonyl content after laccase C oxidation starting from a complete absence of carbonyl groups.

In general, after oxidation the overall content of carbonyl groups increases. Although sample 22AHPN4 showed a higher carbonyl content after oxidation, 15AHPN8 was used for the further experiments because of the better consistency of its carbonyl content value among the other samples.

No additional remarks can be made looking at the percentage of material recovered (average of 75%) at the water retainment capability (average is 47%).

CaLB immobilization and testing

In accordance with the immobilization protocol previously reported, prior to enzyme immobilization, the rice husk was activated with glutaraldehyde and diamine linker.

As mentioned before, this experiment was carried out on sample 15AHPN8 oxidized by laccase C.

Enzyme loading was set at 10,000 TBU/g_{RH} as in the previous experiments. No leaching was observed in any of the formulations. The loading and activity data showed no appreciable improvement in comparison with the rice husk oxidized only by laccase without alkaline hydrogen peroxide pre-treatment (Table 3).

Sample	loading %	hydrolytic activity (U/g)	synthetic activity (U/g)
15AHPN8 (LMS)	17.2	60.2 ± 2.7	181.7 ± 23.2

Table 3. Immobilization yield of rice husk pre-treated by ammonia/hydrogen peroxide after laccase C oxidation, diamine linker attachment and enzyme immobilization

3.2.3 *Delignification of rice husk by hydrogen peroxide/sodium hydroxide*

Alkaline hydrogen peroxide treatment with sodium hydroxide instead of ammonium hydroxide was successfully used on rice husk at environmental pressure to make the material more hydrolysable by enzymes in a work of Diaz et al.[48]. The authors developed an optimized method of this oxidation working in different conditions to maximize the disruption of the cellulose matrix. Pressure and temperature proved to be critical parameters,

and 90° C at 28 bar was the best operative conditions to work with. The authors pointed out that complete lignin removal is very important in the biocatalysed hydrolysis of rice husk because lignin-cellulose bonds prevent the enzyme to reach the inner parts of the matrix, leading to low hydrolysis yields, the same behaviour can be expected in terms of laccase accessibility in our oxidative process. In the case of enzyme immobilization, it can be argued that accessing an area as wide as possible is critical for obtaining good protein loading and consequent enzyme activity. Diaz and co-workers proved that their treatment is effective to enhance the accessibility of enzymes to rice husk.

According to Wang and co-workers[49], hemicellulose is easily degraded without using harsh chemical conditions, whereas the cellulose of rice husk, which is in the form of crystalline microfibrils, is reluctant to degradation. Although this behaviour of cellulose can be seen as a drawback due to the fact that the goal of the study of Wang was the complete depolymerization of the material, in the case of enzyme immobilization it is an advantage because the three-dimensional structure of the rice husk is to be retained. Wang and co-workers treated rice husk with 8% w/v sodium hydroxide and 5% w/v hydrogen peroxide at 80 °C obtaining 92% lignin removal and the complete disappearing of acetyl signals in FT-IR spectroscopy associated with hemicellulose xylanes.

Therefore, in the present study, milder conditions were adopted in order to obtain lignin removal avoiding the damage of the three-dimensional structure of rice husk.

Delignification of rice husk and characterization

Rice husk with a granulometry of 0.2-0.4 mm was treated with an 8% hydrogen peroxide solution using sodium hydroxide to adjust the pH at 11.5 (Figure 13-14). The reaction proceeded 4 hours at 50 °C with the production of abundant foam testifying an environment more aggressive than the one obtained mixing hydrogen peroxide with ammonium hydroxide. The treated material appears as a slightly yellow powder. There is a significant weight loss due to the complete removal of lignin in the operative conditions. Water retaining capabilities were greatly increased (Table 4).

Figure 13. Blank reaction on the left (sodium hydroxide). Rice husk treated by alkaline hydrogen peroxide on the right (sodium hydroxide/hydrogen peroxide)

Figure 14. Raw whole rice husk on the left. Whole rice husk treated by alkaline hydrogen peroxide on the right (sodium hydroxide/hydrogen peroxide)
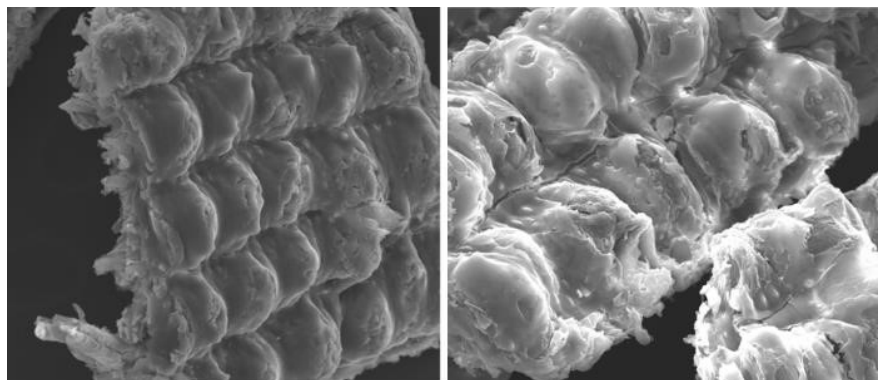
SEM microscopy showed that the overall structure of rice husk was preserved, while signs of chemical abrasion were detected on the external surface, in this way exposing the inner tracheids to the reaction media, increasing water retaining capability (Figure 15).

Figure 15. SEM microscopy images of the outer surface of rice husk before (left) and after (right) alkaline hydrogen peroxide pre-treatment.

In the same way, a batch of non-milled rice husk was produced to be compared with the milled version in terms of hygroscopicity and carbonyl content after oxidation from laccase C. In parallel the treatment was carried out also by avoiding the use of hydrogen peroxide.

Sample	water absorption % w/w	recovered material % w/w
RH	55.2	96.0
RH-AHP blank	37.1 ± 1.8	94.9 ± 0.70
RH-AHP	64.25 ± 1.6	40.0 ± 11.8
RH(whole)-AHP	72.1	60.1

Table 4 Characterisation of raw rice husk and AHP (sodium hydroxide) rice husk.

Recovery and water absorption data show that the treatment causes a significant weight loss and an increase in water retaining capability attributable to lignin and silica removal[50]. FT-ATR spectroscopy confirmed the disappearance of lignin[51] (Figure 16). It is noteworthy that in blank reactions, where only sodium hydroxide was used, the hygroscopicity of the material was lower.
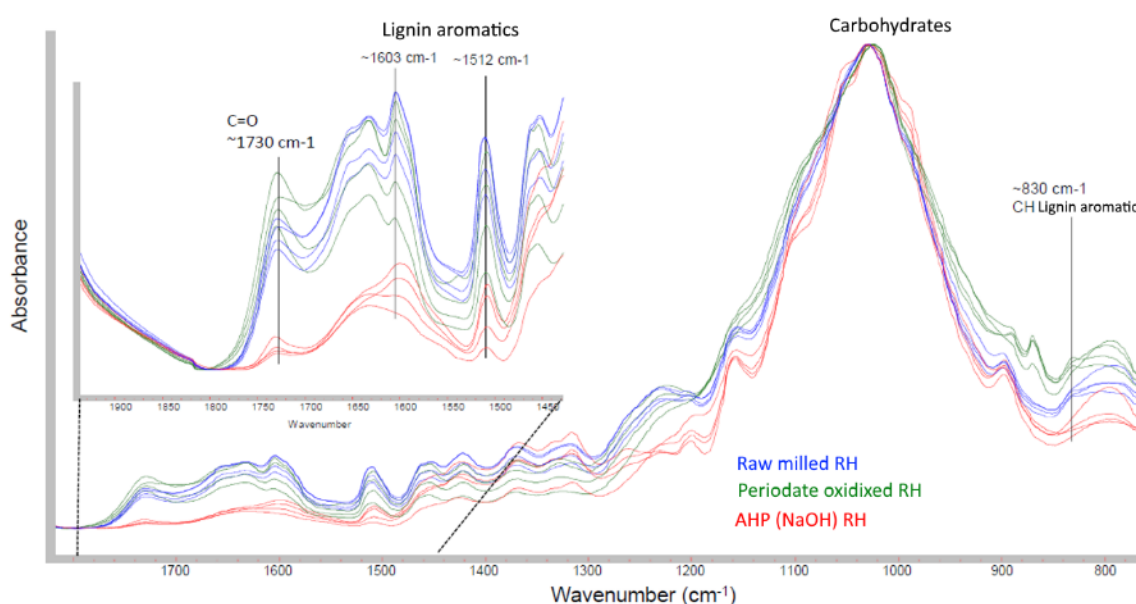
Figure 16. FT-ATR characterisation of rice husk, periodate-oxidized rice husk and AHP (NaOH) rice husk.

After the treatment, the material was oxidized with laccase C and TEMPO and the carbonyl content was assessed in duplicate using the hydroxylamine chlorhydrate carbonyl assay

(Table 5). As a blank reaction, the same procedure was applied to a sample of milled rice husk that underwent no pre-treatment.

Sample	Laccase C U/mg$_{RH}$	Carbonyl continent μmol/g
RH	0	0
	0.2	117±9,5
	1.0	160±2,4
RH-AHP	0	0
	0.2	88±4,0
	1.0	152±7,5

Table 5. Carbonyl content of raw milled rice husk and AHP (NaOH) rice husk oxidized with different laccase C concentrations.
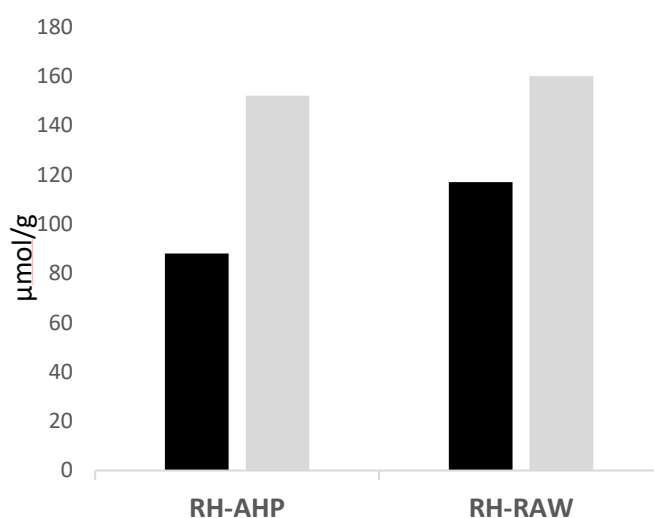
Figure 17. Graphical representation of carbonyl content in raw rice husk and AHP (NaOH) rice husk after LMS treatment with laccase C 0.2 U/mg (black) and 1.0 U/mg (grey).

The data (Figure 17) shows that the AHP pre-treatment had no substantial effect in promoting the increase in carbonyl content, which rather varies as a function of the concentration of the laccase. The obtained values are also very similar to the ones calculated with AHP treatment in ammonium hydroxide. Nevertheless, AHP pre-treatment increases the hygroscopicity of the material, exposing a wider surface of rice husk to the enzyme in the immobilization step.

CaLB immobilization and testing

In accordance with the immobilization protocol previously reported, enzyme immobilization was carried out after HMDA coupling and activation with glutaraldehyde.

The experiment was carried out on an AHP-treated sample treated with laccase 1.0 U/mg$_{RH}$ because of the higher carbonyl content and on an AHP-treated sample not oxidized with the laccase-mediator system. Enzyme loading was set at 10,000 TBU/g$_{RH}$ as in the previous experiments. No leaching was detected in any sample, testifying the covalent immobilization of the enzyme (Table 6).

Sample	loading %	hydrolytic activity (U/g)	synthetic activity (U/g)
RH-AHP	12.5	50.3 ± 2.7	216.0 ± 16.0
RH-AHP + LMS 1 U/mg$_{RH}$	23.0	70.4 ± 7	263 ± 7

Table 6. Immobilization yield of rice husk pre-treated with sodium hydroxide/hydrogen peroxide raw and after laccase C oxidation, diamine linker attachment and enzyme immobilization.

3.2.4   Comparison of the pre-treatment methods

Among the tested protocols, AHP pre-treatment with sodium hydroxide resulted to be able to increase the loaded protein and enzyme activity when followed by LMS oxidation. It is noteworthy that sodium hydroxide AHP rice husk not oxidized with laccase, despite having a lower protein loading, showed a comparable activity with raw rice husk oxidized with laccase (**Table 7**), this fact can be explained with 1) adsorption of laccase during the LMS oxidation step; 2) higher lipase activity on AHP-treated rice husk because of the higher available surface that allows a better enzyme accessibility by the substrate.

Sample	loading %	hydrolytic activity (U/g)	synthetic activity (U/g)
RH sodium hydroxide + hydrogen peroxide	12.5	50.3 ± 2.7	216.0 ± 16.0
RH sodium hydroxide + hydrogen peroxide, LMS oxidized	23.0	70.4 ± 7	263 ± 7
RH ammonium hydroxide + hydrogen peroxide, LMS oxidized	17.2	60.2 ± 2.7	181.7 ± 23.2
RH LMS oxidized	17	56 ± 25	198 ± 8
RH sodium periodate-oxidized[1]	72	316	592 ± 24

Table 7. Comprehensive table of all the immobilized formulations of CaLB on rice husk.

Notwithstanding sodium periodate oxidation showed the best immobilization yield and hydrolytic activity, alkaline hydrogen peroxide pre-treatment using sodium hydroxide proved to increase hydrolytic activity and synthetic activity in comparison with raw rice husk treated directly with laccase, while increasing also water retaining capability of the material. The achievement of a hygroscopic rice husk opens new routes for the full exploitation of this inexpensive composite material because this fact can be an advantage especially on biocatalysed polycondensation, where water removal from the reaction medium is critical in driving the reaction towards the formation of products. The widening of the inner space of rice husk was proved also by measuring the density of the material. In fact, raw milled rice husk has a density[5] of 0.437 g ml^{-1} while sodium hydroxide/hydrogen peroxide pre-treated rice husk has a density of 0.294 g ml^{-1} corresponding to a decrease in density of the 33% imputable to the loss of lignin.

4. Structure-based bioinformatics analysis of cutinases and other serine hydrolases

4.1 Manuscript: Nature Inspired Solutions for Polymers: Will Cutinase Enzymes Make Polyesters and Polyamides Greener?

While exploring the various aspects of fully renewable synthesis of polyesters, our research group focused in particular on a sub-family of promising serine hydrolases, namely cutinases, able to catalyse the polycondensation of renewable aliphatic monomers under solvent-free and thin-film conditions[26]. A multivariate factorial design carried out by this group[3] demonstrated that, if compared with lipase B from *Candida antarctica* (CaLB), cutinase 1 from *Thermobifida cellulosilytica* (Thc_cut1) is less sensitive to the presence of water in the system and is able to work in mild conditions (50 °C; 535 mbar), increasing the overall sustainability of the process. The following review discusses the particular features of cutinases and how they can be exploited in the production of synthetic polyesters and polyamides.

Nature Inspired Solutions for Polymers: Will Cutinase Enzymes Make Polyesters and Polyamides Greener?

Valerio Ferrario [1], Alessandro Pellis [2], Marco Cespugli [1], Georg M. Guebitz [1,3] and Lucia Gardossi [1,*]

[1] Laboratory of Applied and Computational Biocatalysis, Dipartimento di Scienze Chimiche e Farmaceutiche, Università degli Studi di Trieste, Piazzale Europa 1, 34127 Trieste, Italy; valerio.ferrario@gmail.com (V.F.); marco.cespugli@phd.units.it (M.C.); guebitz@boku.ac.at (G.M.G.)

[2] Department of Agrobiotechnology, University of Natural Resources and Life Sciences, Vienna, Konrad Lorenz Strasse 20, 3430 Tulln an der Donau, Austria; alessandro.pellis@gmail.com

[3] Division of enzymes & polymers, Austrian Centre of Industrial Biotechnology, Konrad Lorenz Strasse 20, 3430 Tulln an der Donau, Austria

* Correspondence: gardossi@units.it; Tel.: +39-040-558-3103

Abstract: The polymer and plastic sectors are under the urge of mitigating their environmental impact. The need for novel and more benign catalysts for polyester synthesis or targeted functionalization led, in recent years, to an increasing interest towards cutinases due to their natural ability to hydrolyze ester bonds in cutin, a natural polymer. In this review, the most recent advances in the synthesis and hydrolysis of various classes of polyesters and polyamides are discussed with a critical focus on the actual perspectives of applying enzymatic technologies for practical industrial purposes. More specifically, cutinase enzymes are compared to lipases and, in particular, to lipase B from *Candida antarctica*, the biocatalyst most widely employed in polymer chemistry so far. Computational and bioinformatics studies suggest that the natural role of cutinases in attacking natural polymers confer some essential features for processing also synthetic polyesters and polyamides.

Keywords: cutinases; enzymatic polyesters synthesis; green polymer synthesis; enzymatic polymer hydrolysis

1. Introduction

There is robust evidence that the next generation of polyesters and polyamides calls for a change of standard aiming at mitigating the environmental impact and natural capital cost of polymer production and processing in general [1,2]. A closer integration between chemistry and biotechnologies is expected to boost the change of the scenario. Due to their remarkable selectivity and catalytic efficiency under mild conditions, enzymes are an attractive and sustainable alternative to toxic catalysts used in the polycondensation of functional monomers such as itaconic acid, which suffer from isomerization or cross-linking under the harsh conditions required by conventional chemical processes that employ organo-catalysts [3]. The possibility to use enzymes for the polyester synthesis has been known since the 1990s and has also been industrially applied by Baxenden Chemicals (UK) for the production, later dismissed, of highly regular structures of polymers. On the other hand, especially for the biomedical sector, enzymatic modification of polyesters represents a milder and selective alternative to chemical or physical treatments aimed at introducing chemical functionalities to the surface of polymers while retaining their bulk properties [2].

In nature, cutinases have evolved in some fungi responsible for plant pathologies where these enzymes attack and hydrolyze cutin, a complex hydrophobic polyester. Even though cutinases were discovered more than 40 years ago and tested in a number of technological applications, only more recently have they been proposed as biocatalytic tools for the polymer sector [2]. Indeed, a comprehensive review by Gross et al. published in 2010 discussed the potential of a number of hydrolases to catalyze polyester synthesis through condensation of an array of substrates, focusing the attention on the challenges of the biocatalytic technologies. [4] Out of the 30 synthetic processes reviewed by Gross, 21 were catalyzed by *Candida antarctica* lipase B (CaLB), an industrial biocatalyst already applied in different chemical and pharmaceutical processes. Only two cases reported the use of one single cutinase, namely *Humicola insolens* cutinase (HiC). In the light of the most relevant advances of the last five years achieved through the application of cutinases to polymer chemistry, we now present an analysis that extends the focus also to the hydrolysis and functionalization of various classes of polyesters and polyamides. The review intends to provide also a critical comparison between CaLB and the fungal cutinases recently applied in polymer chemistry: HiC, cutinase 1 from *Thermobifida cellulosilytica* (Thc_cut1) and *Fusarium solani pisi* cutinase (Fsp). For the first time, the biocatalysts are rationally compared also on the basis of structural, computational, and bioinformatics analysis. Finally, a frank analysis of future perspectives for the practical application of these biocatalysts for productive processes is presented.

2. The Cutinase Family

Cutinases (EC 3.1.1.74) are members of the serine hydrolases superfamily comprising the typical Ser-His-Asp catalytic triad and the oxyanion hole, common features shared by other superfamily members such as lipases, esterases, proteases, and amidases [5]. The natural substrate of cutinase is cutin, one of the main polymeric components (together with cutan) of the plant cuticle, which covers all aerial surfaces of higher plants [6,7]. Cutin is a three-dimensional insoluble hydrophobic polyester composed of hydroxyl and hydroxyepoxy fatty acids (usually carrying one to three hydroxyl groups). The most common components of cutin are derivatives of saturated palmitic (C16) or stearic (C18) acid [8]. In vitro, cutinases are able to catalyze ester hydrolysis reactions (in an aqueous environment), as well as esterifications and transesterifications (anhydrous conditions) of large and small molecules. Therefore, they have been proposed as alternative catalysts to lipases and, in particular, to the widely employed and studied lipase B from *C. antarctica* (CaLB) [9,10].

Since their discovery, cutinases have been investigated for applications in different sectors such as food, chemical, detergent, environmental, and textile industries [11,12]. In the food sector, cutinases are applied for the treatment of cutin-rich vegetables, fruits, and berries to achieve partial cutin hydrolysis and thus improve water permeability, an important parameter for food drying and, ultimately, conservation. Additionally, the increased permeability is exploited for delivering sweeteners, flavor enhancers, preservatives and stabilizer into the fruits or vegetables [5,13]. Cutinases can also be applied for improving the extractability of plant polyphenols from macerated fruit and vegetable materials [14]. Moreover, cutinases can be applied in the flavors industry. In particular, it was reported that *Fusarium solani pisi* cutinase has a potential for the production of concentrated cheese flavors [15].

In the chemical industry, the synthesis of alkyl esters by cutinases has been reported when used in organic media or low water activity environment. Alkyl esters are essential building blocks for the pharmaceutical and cosmetic sectors. In particular, the selectivity of *Fusarium solani pisi* cutinase was investigated in the context of the esterification of different alcohols with acids (ethyl butyrate, ethyl oleate, ethyl decanoate, hexyl decanoate, etc.) [16]. The *Fusarium solani pisi* cutinase was also tested for the production of biodiesel, through the transesterification of small molecules, as well as the synthesis of surfactants [17,18]. Cutinases can be utilized in laundry and dishwashing applications as lipolytic enzymes to remove fats. For example, it was shown that the *Fusarium solani pisi* cutinase is superior in fat removal when compared to the detergent lipase Lipolase™ [19]. Cutinases are also used in detergents for de-pilling during washing of polyester fabrics [1]. The *Fusarium solani pisi* cutinase

has been also suggested for the degradation of various phthalates, such as dipentyl phthalate, butyl benzyl phthalate, and di-(2-ethylhexyl)-phthalate by ester hydrolysis [20–22]. In the textile industry, cutinases have been applied for the hydrolysis of the cutin residues on natural fibers such as cotton and wool. Cutin removal improves the wettability of the fiber, which then facilitates uniform dyeing and finishing. Cutinases from *Pseudomonas mendocina*, from *Fusarium solani pisi* and from *Thermobifida fusca* were widely tested for this purpose [23].

Cutinases are produced by plants, bacteria, and fungi (commonly phytopathogenic). Plant cutinases are less investigated since their isolation, maintenance, and cultivation are much more complicated when compared to the microbial analogs [6]. Fungal cutinases are extracellular enzymes expressed and secreted for the cutin hydrolysis during plant infection, where the cuticle depolymerization represents one of the first steps [24]. Fatty acids released during enzymatic hydrolysis of cutin represent a carbon source for cellular growth [6]. The first isolated cutinase was purified already in the 1970s from the *Fusarium solani* growing on cutin as a sole carbon source [25]. Nevertheless, this enzyme class is still relatively 'young' with just few members that have been deeply investigated for their catalytic potential. Cutinases have been subsequently isolated, often recombinantly expressed and characterized from different microorganisms. Microbial cutinases currently isolated and characterized with a known gene sequence and molar masses are listed in Table 1.

Table 1. Isolated and characterized microbial cutinases. For each entry the microbial source is indicated as well as the molar masses.

Source	Molar Masses (kDa)	Ref.
Alternaria brassicicola	26	[26]
Aspergillus nidulans	29	[27]
Aspergillus niger	22.8	[28]
Aspergillus oryzae	19.6	[29]
Botrytis cinerea	18	[30]
Colletotrichum capsici	23.7	[31]
Colletotrichum gloeosporioides	40	[32]
Colletotrichum kahawae	21	[32]
Coprinopsis cinerea	29.6	[33]
Cryptococcus sp.	21.2	[34]
Fusarium oxysporum	23.4	[35]
Fusarium roseum culmorum	24.3	[36]
Fusarium solani	20.8	[37]
Glomerella cingulata	21.1	[38]
Helminthosporium sativum	25	[39]
Humicola insolens	20.3	[40]
Magnaporthe grisea	24.3	[41]
Monilinia fructicola	18.6	[42]
Pennicillium citrinum	14.1	[43]
Pseudomonas putida	30	[44]
Pyrenopeziza brassicae	21	[45]
Rhizoctonia solani	19.8	[46]
Saccharomonospora virdis	30.3	[47]
Thermobifida alba	33.5	[48]
Thermobifida cellulosilytica	30.8	[10]
Thermobifida fusca	30.8	[49]
Thielavia terrestris	27	[50]
Trichoderma reesei	27.3	[51]
Tropaeolum majus	40	[52]
Venturia inaequalis	21.7	[53]

From the structural point of view, cutinases are the smallest family of the α/β hydrolases superfamily [6]. Considering their biocatalytical use as lipase alternatives, differences and similarities of these two enzyme classes have been recently investigated with the aid of computational

methodologies. Cutinases and lipases share, as a common feature, the hydrophobicity of their surface, as a consequence of the insolubility of their natural substrates [10]. Unlike CaLB and most lipases, the catalytic Ser of cutinases is not buried into a deep funnel shape active site, rather the active site is superficial and accessible to solvents and substrates even in absence of any hydrophobic interface [10]. In addition, the active site accessibility of most lipases is regulated by conformational changes involving the lid domain which exposes the active site upon interfacial activation [54]. In this sense, cutinases appear to be more similar to *C. antarctica* lipase B (CaLB) (Figure 1) which is considered as an unconventional lipase also because it lacks the mobile lid which is not susceptible to any relevant structural rearrangements [54]. On that respect, the dynamic behavior of two cutinases, namely *Humicola insolens* cutinase (HiC) and cutinase 1 from *Thermobifida cellulosilytica* (Thc_cut1) were compared with CaLB by performing MD simulations in explicit water and toluene environments [10]. The study confirmed similarities in the dynamic behavior of CaLB and Thc_cut1 since both enzymes had really stable scaffold in both simulated solvents. On the other hand, HiC showed two flexible domains (Figure 1c) able to influence the active site accessibility which is similar to the behavior of other typical lipases [10]. A similar "breath-like" movement at the active site opening was also pointed out for the cutinase from *Fusarium solani* [37].
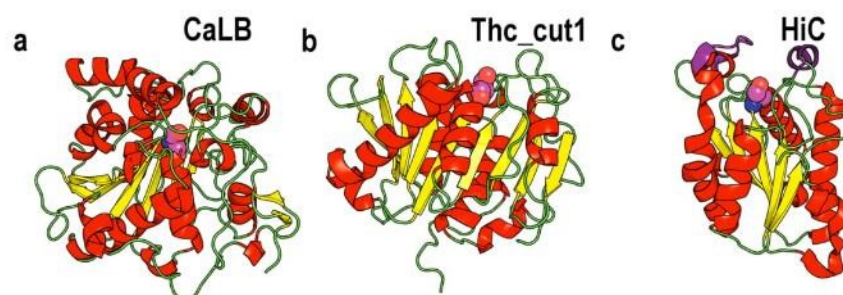
Figure 1. Representation of the 3D structures of two cutinases in comparison with CaLB: (**a**) CaLB (PDB 1TCA); (**b**) Thc_cut1 (Homology model); (**c**) HiC (PDB 4OYY). Structures are represented in cartoon mode and colored according to their secondary structure; the catalytic serine of each enzyme is highlighted in sphere mode. The mobile domains affecting active site accessibility of HiC are colored in violet.

Similarities between CaLB and Thc_cut1 are not just limited to their surface properties and dynamic behavior but are also evident by considering their active site properties. Features such as ability of establishing H bonds and hydrophobic-hydrophilic balance were recently analyzed quantitatively by means of a bioinformatics method based on BioGPS molecular descriptors (Global Positioning System in Biological Space) and multivariate statistical analysis [55,56]. The method allows for functional structural correlation by comparing three-dimensional structures rather than protein sequences, and it makes any structural alignment unnecessary. The bioinformatic analysis pointed out how two cutinases, HiC and Thc_cut1, are classified in between the lipase and esterase families [56]. Accordingly, cutinases are not just active on cutin, but they also hydrolyze suberin (a "waxy" polyester and main component of cork) and are also able to hydrolyze a variety of synthetic esters and show activity on short- and long-chains of emulsified triacylglycerols [6]. Moreover, in analogy to lipases and esterases, when applied in low water activity environment, cutinases are also able to catalyze esterification and transesterification reactions [56].

3. Cutinases as Biocatalysts for Polymerization Reactions

For several decades, the demand for polymers and plastics has grown at a faster rate than for any other group of bulk materials, and expectations are that this trend will continue until

2020. Biocatalytical strategies are promising solutions to mitigate the environmental impact of polymerization technologies currently used [2].

Enzymes are attractive sustainable alternatives to toxic catalysts traditionally used in polymerization reactions, such as metal catalysts and tin in particular. The objective of enzymatic polymerization is not the synthesis of high molecular weight polymers but rather opportunity to produce functionalized as well biodegradable polymers with controlled architecture through highly selective processes at mild temperatures ranging between 40 and 90 °C, whereas conventional polymerizations are carried out at $T > 150$ °C with particular reference to organo-catalysts employed in the production of itaconic acid polyesters [56,57]. Enzymatic synthesis generally leads to polymers with moderate molar masses when compared to products obtainable via conventional chemical synthesis, but this drawback has been circumvented by using a two-step procedure, where an initial enzymatic polymerization leads to oligomers and a second step is carried out at higher temperature and/or lower pressure after removal of the biocatalyst [2]. Furthermore, the synthesis of oligomers and short telechelics pre-polymers with functional ends represents an effective strategy for obtaining polymers with higher molecular weight [58].

Actually, most of the studies related to enzymatic polymerization make use of lipases, and in particular CaLB which is one of the most widely used enzymes in industry and the 'yardstick' for comparison in academia [3,59].

The use of cutinases HiC, Fsp, and Thc_cut1 for polymerization reactions was explored only in the last decade in synthetic reactions reported in Figure 2.

Cutinase-catalyzed polycondensation was reported for the first time in 2007, when HiC was used for polyester synthesis using different diacids and diols [60]. Polycondensation reactions were performed in solvent-free environment and under vacuum (10 mm Hg) at 70 °C using an adsorbed preparation of HiC on previously lyophilized Lewatit beads (similar to the commercial preparation Novozym® 435 where CaLB is adsorbed on the same polymeric carrier) [60]. In particular, adipic acid was tested in polycondensation reactions with 1,4-butanediol, 1,6-hexanediol, and 1,8-octanediol (Figure 2a) leading to M_n ranging from 2700 to 12,000 Da. A more rigid diol, 1,4-cyclohexanedimethanol, was polymerized with adipic, succinic, suberic, and sebacic acids (from C_4 to C_{10}) (Figure 2b) leading to M_n from 900 to 19,000 Da according to the diacid chain lenght [60]. Results demonstrated the ability of HiC to perform polycondensation with each tested monomer and showed a preference for longest acids or diols chains: adipic acid with 1,8-butanediol and 1,4-cyclohexanedimethanol with sebacic acid gave higher polymerization degrees. In the same work, HiC was also reported able to perform ring-opening polymerizations of lactones both in toluene and in solvent-free conditions (Figure 3) leading to polymers with M_n of 24,900 and 16,000 Da respectively.

In another publication, where HiC was covalently immobilized on Amberzyme oxirane, the preference of HiC for long chain substrates was confirmed. Its selectivity was compared again with the commercial preparation of CaLB Novozym® 435 which shows higher substrate promiscuity; moreover, HiC proved to be able to perform homo-polymerization of ω-hydroxyalkanoic acids (Figure 2c) [61].

Cutinase-catalyzed Polycondensation reactions

a) Polyesters from diacids/diesters and linear diols
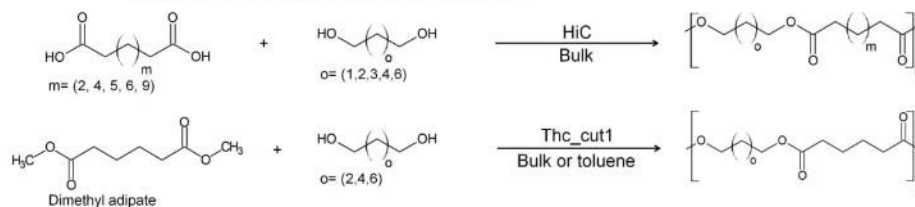
b) Polyesters from diacids and cyclic diols
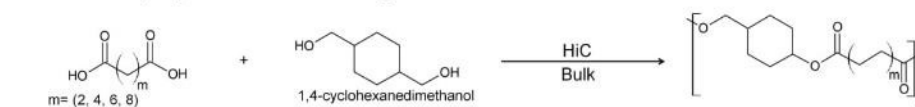
c) Polyesters from ω-hydroxyalkanoic acids

d) Polyamides from diesters and linear diamines

e) Polyamides from aliphatic and aromatic monomers

Figure 2. Schematic representation of polymer synthesis catalyzed by the different cutinases and discussed in the present section. Fsp: *Fusarium solani* pisi cutinase; HiC: *Humicola insolens* cutina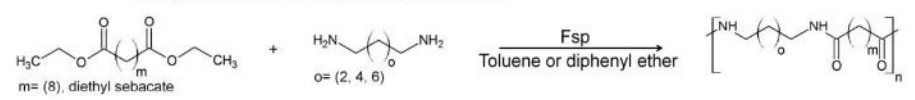se; Thc_cut1: *Thermobifida cellulosilytica* cutinase 1. 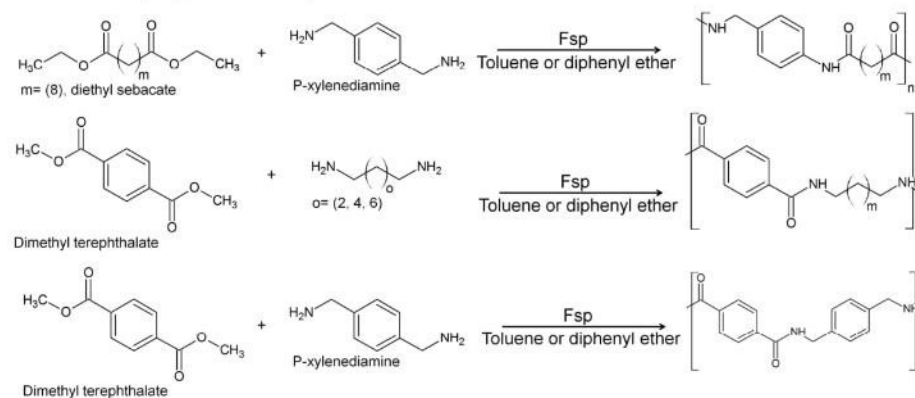(**a**) polyesters from diacids/diesters and linear diols; (**b**) polyesters from diacids and cyclic diols; (**c**) polyesters from ω-hydroxyalkanoic acids; (**d**) polyamides from diesters and linear diamines; (**e**) polyamides from aliphatic and aromatic monomers.
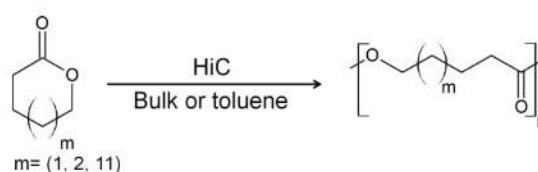
Figure 3. Schematic representation of Ring Opening Polymerizations (ROP) catalyzed by HiC both in toluene and solvent free conditions.

More recently, the activities of CaLB and HiC were also compared with another cutinase, namely Thc_cut1. Both HiC and Thc_cut1 were covalently immobilized on EC-EP Sepabeads as well as CaLB which was also employed in its commercial preparation (Novozym® 435) [10]. All the biocatalysts were tested for polycondensation of dimethyl adipate with 1,4-butanediol or 1,8-octanediol using a thin film solvent-free system under reduced pressure (100 kPa) at 70 °C (Figure 2a). The best performances in terms of conversion and molar masses of the products were obtained by using Thc_cut1 that led to a 86% monomer conversion and M_n of around 1000 Da while CaLB gave a conversion of 76% and a M_n of only 528 Da [10]. Interestingly, the polycondensation catalyzed by HiC gave no observable products, in disagreement to what was previously reported [60]. The substrate acceptance of Thc_cut1 was further investigated, catalyzing the polycondensations of dimethyl adipate with 1,4-butanediol, 1,6-hexanediol, 1,8-octanediol, and 1,12-dodecandiol [10]. It is noteworthy that, in solvent-free conditions, Thc_cut1 showed a preference for short chain diol and the reaction with 1,4-butanediol gave better conversions; on the other hand, the same tests with 1,4-butanediol, 1,6-hexanediol, and 1,8-octanediol were repeated using toluene as solvent produced very similar results in terms of reaction conversion (around 18% after 24 h of reaction), indicating that the higher conversion with 1,4-butanediol might be induced by viscosity and mass transfer effect which have to be carefully considered in this kind of investigation. The attenuation of the mass transfer issues using a solvent demonstrated indeed that Thc_cut1 does not have relevant preference in the use of 1,4-butanediol, 1,6-hexanediol, and 1,8-octanediol [10,56]. Furthermore, a new enzyme preparation, where Thc_cut1 was immobilized on a fully renewable support based on rice husk, was used for the polycondensation of dimethyl adipate with 1,4-butanediol and 1,8-octanediol. The reaction conditions were optimized by a fractional factorial design and finally, such Thc_cut1 preparation was able to reach conversions, considering monomer consumption, as high as 89% [56]. Also, it is remarkable to note that the activity of Thc_cut1 did not decrease after lyophilization.

CaLB was also compared with Fsp in a different polymerization reaction for the obtainment of polyamides. CaLB was tested in its commercial form (Novozym® 435), while Fsp was adsorbed on Lewatit beads (similar to Novozym® 435) and as CLEA (Cross Linked Enzyme Aggregates) [62]. Fsp and CaLB were able to catalyze polyamide formation of diethyl sebacate with 1,8-diaminooctane, 1,6-hexanediamine and 1,4-butanediamine (Figure 2d). The assays were conducted at 70 °C using toluene or diphenyl ether as solvents. The best conversions were obtained by CLEA Fsp (>50%) followed by CaLB (around 45%), whereas Fsp adsorbed on Lewatit gave lower monomer conversions (<25%) [62]. The same enzyme preparations were also tested for the polymerization of aromatic amides: enzymatic syntheses of oligo(p-xylylene sebacamide) and oligo(octamethylene terephthalamide) were successfully performed whereas in this case, CaLB led to better products than CLEA Fsp when 1,8-diaminoctane was used as diamine (Figure 2e) [63].

In general, the immobilization of the biocatalyst is mandatory in these synthetic processes for several reasons: (1) to avoid the aggregation of the hydrophilic enzyme molecules; (2) to recycle the expensive enzyme; and (3) to prevent the contamination of product by the enzyme protein [2,3]. Considering the data reported in literature, it must be noted that results in terms of molecular weight of polymerization products might be affected by detachment and dispersion of the enzyme when not covalently supported as demonstrated in previous studies [64]. In addition to adsorbed preparation

with consequently problematic leaching, the mechanical strength of CLEAs preparations still has to be demonstrated on an industrially relevant scale [65].

A critical parameter in the performance of an immobilized enzyme is indeed the spatial distribution of the enzyme and substrate within a macroporous resin. The enzyme distribution of CaLB immobilized within a macroporous polymer matrix revealed that the enzyme is localized in an external shell of the bead with a thickness of ~100 μm. Furthermore, it was found that CaLB secondary structure was not altered by immobilization.

Unlike CaLB, polystyrene molecules of similar molecular weight diffuse easily throughout Novozym 435 beads. Scanning Electron Micrograph (SEM) images of the beads showed that the average pore size is 10 times larger than CaLB or polystyrene molecules, implying that there is no physical barrier to enzyme or substrate diffusion throughout the beads [65].

In the case of enzymatic polycondensation and more specifically in solvent-free systems, the viscosity of reaction mixtures makes the diffusion of substrates and pre-polymers into the pores highly unlikely [59]. The porosity of carriers seems to play a negligible role in the process design, rather, porosity might induce the risk of undesired occlusion by substrates and products, thus limiting the efficiency of the enzyme. This assumption is also supported by recent data obtained in polycondensation catalyzed by hydrolases immobilized on rice husk [59,66]. Although the enzymes (CaLB and Thc_cut1) were immobilized only on the surface either through adsorption-crosslinking or covalent bonding, the polyester synthesis proceeded with comparable rates and conversion as in the case of the macroporous methacrylic resins. Indeed, it was demonstrated that the most efficient reaction systems for biocatalyzed viscous reactions employed enzymes homogeneously dispersed on large volumes of carriers.

4. Cutinases as Biocatalysts for Polymers Hydrolysis

The ability of some enzymes to hydrolyze polymer molecules is under investigation as a possible solution for the increasing awareness of the world-wide problems associated with plastic pollution since conventional chemical recycling approaches are energy-consuming and cost-intensive methods requiring large-scale degradation processes for an economical application [67]. On the other hand, the ability of enzymes to hydrolyze polymers can be exploited for structural fine-tuning and for controlling the degree of polymer functionalization by operating under mild conditions [57]. The possibility to perform partial hydrolysis on the outer layer of the polymer can be exploited for changing the superficial properties in terms of hydrophobicity/hydrophilicity balance, obtaining reactive groups for successive modifications, and changing the polymer biocompatibility just to name a few [68–70].

The ability of some lipases to hydrolyze polyesters has been known since 1967, and among them, the most widely used and studied one is again the lipase B from *C. antarctica* (CaLB) [2,71]. During the last 10 years, with the aim to expand the biocatalytical tools for polymer hydrolysis and modification, several cutinases have been tested for their ability to hydrolyze polyesters (Table 2).

Table 2. Polyesters and polyamides that were hydrolyzed via cutinase-catalyzed reactions.

Polymer	Enzyme	Ref.
Poly(ethylene terephthalate) (PET)	*Thermobifida cellulosilytica*	[72,73]
	Thermobifida fusca *Thermobifida alba*	[67]
	Thielavia terrestris	[74]
	Humicola insolens *Pseudomonas mendocina* *Fusarium solani*	[75]
	Penicillum mendocin *Penicillum citrinum*	[69,74]

Table 2. *Cont.*

Polymer	Enzyme	Ref.
Poly(L-lactic acid) (PLA)	*Humicola insolens* *Thermobifida halotolerans*	[70,76] [77]
Poly(ethylene furanoate) (PEF)	*Thermobifida cellulosilytica*	[78]
Poly(butylene adipate-*co*-terephthalate) (PBAT)	*Humicola insolens* *Thermobifida cellulosilytica*	[79]
Poly(caprolactone) (PCL)	*Thielavia terrestris*	[79]
Poly(butylene succinate) (PBS)	*Thielavia terrestris* *Aspergillus oryzae* *Fusarium solani* *Humicola insolens* *Alternaria brassicicola*	[79]
Polyamide 6,6	*Fusarium solani*	[80]

The scientific work was focused on the hydrolysis of the most relevant industrial polymers, in particular poly(ethylene terephthalate) (PET). Cutinases from various *Thermobifida* species demonstrated a good selectivity on PET [72,73]. More in detail, cutinases from *Thermobifida cellulosilytica*, *Thermobifida fusca*, and *Thermobifida alba* demonstrated an ability to hydrolyze PET. Even though all these *Thermobifida* cutinases turned out to be very similar in their sequences, they differed in PET hydrolysis activities. Besides, it is important to notice that products released from PET hydrolysis were shown to have an inhibitory effect on the activity of *Thermobifida fusca* cutinase [67]. In addition, modeling analysis suggests that the hydrolysis efficiencies among *Thermobifida* cutinases are influenced by the electrostatic properties in the enzyme regions surrounding the active site entrance, thus affecting the essential sorption processes on the water-insoluble PET [81]. In that respect, with the aim of improving the hydrolytic performances of the cutinase 1 from *Thermobifida cellulosilytica* against PET, the polyhydroxyalkanoate binding module from *Alcaligenes faecalis* was fused to the cutinase obtaining a three-fold increase of the PET hydrolysis release products [81]. The validity of such an approach was further confirmed by other mutagenesis experiments where the regions in proximity to the active site of cutinases from *Thermobifida fusca* and from *Fusarium solani pisi* were mutated for changing the superficial hydrophobicity: mutants turned out to have improved PET hydrolytic performances [82,83]. Other cutinases able to perform PET hydrolysis are those from *Humicola insolens*, *Thielavia terrestris*, *Pseudomonas mendocina*, and *Penicillum citrinum* [69,74]. Notably, *Humicola insolens* cutinase demonstrated high hydrolytic activity due to its stability after prolonged incubation at 70 °C, which corresponds to an optimal hydrolysis temperature, being very close to the T_g of PET. At this temperature, the enzyme benefits from higher mobility of the polyester chains in the amorphous phase, thus increasing the enzyme accessibility to the ester bonds [67]. The most commonly used conditions are enzyme concentrations between 2 and 5 μM and T ranging from 50 to 70 °C, depending on the enzyme thermal stability.

Just a few reports investigate the hydrolysis of different polymers using cutinases. Among them, cutinase 1 from *Thermobifida cellulosilytica* was able to successfully hydrolyze poly(ethylene furanoate) (PEF), new environmentally-friendly polyesters [78]. The cutinase from *Thielavia terrestris* was reported to hydrolyze also poly(caprolactone) and poly(butylene succinate) (PBS) at a rate of 203 mg/h per mg of protein, and 56 mg/h per mg of protein, respectively [74]. Hydrolytic activities on PBS were reported also for cutinases from *Fusarium solani*, from *Aspergillus oryzae*, from *Alternaria brassicicola*, and from *Humicola insolens* [74]. The latter was also reported to be active in the hydrolysis of poly(lactic acid) as well as cutinases from *Thermobifida halotolerans* [70,77]. Finally, cutinase from *Fusarium solani* is currently reported as the only cutinase able to hydrolyze Polyamide 6,6 [80].

5. Conclusions and Future Perspectives

The polymer industry is under pressure to innovating towards more sustainable processes and enzymes represent a formidable tool for conferring unique targeted properties to polyesters and polyamides, while meeting greener criteria. Nevertheless, the replacement of conventional catalysts and chemical synthetic methodologies with biocatalysts on an industrial scale has not taken place yet, since enzymatic processes require to be further optimized both in terms of economic and technological performances. After more than one decade of extensive investigations of the application of lipase CaLB in polyester/polyamide synthesis and modification, recent studies showed that cutinases are endowed with specific properties that make such enzymes promising biocatalysts for translating lab reactions into processes of practical and industrial relevance.

Computational and bioinformatics investigations disclosed how cutinases represent an enzyme class in between lipases and esterases. Interestingly, the same is also applicable to *C. antarctica* lipase B, suggesting, for the first time, some criteria for identifying biocatalysts applicable to polyester synthesis and hydrolysis. In the case of cutinases, the wider and more accessible active site, along with differences in terms of substrate specificity efficiency under milder and less strictly anhydrous conditions represent crucial features for succeeding in the hard task of producing highly structured and effective polyesters on industrial scale.

However, when cutinases are compared to lipases and CaLB in particular, it is important to consider that industry has been making wide use of lipases—especially in detergent formulations—for several decades, therefore pushing the scientific research towards the optimization of stability, activity, and expression of these biocatalysts. Similar efforts would be needed for transforming selected promising cutinases into efficient industrial catalysts. The use of cutinases for the mild and controlled hydrolysis and functionalization of polymer surfaces will get closer to an industrial scale when the expression and the selection of the best variants (deriving from rational design or directed evolution) will be optimized and scaled for tailored applications on commercial polymers.

Furthermore, studies are still needed to verify the applicability of cutinases to a wide array of substrates of industrial interest, such as sensitive functionalized moieties for the obtainment of higher-value polymers carrying lateral functionalities, or renewable monomers for the production of biobased polymers for the cosmetic and the pharmaceutical industry where the obtainment of short oligomers is desired in order to be utilized in various formulations (e.g., nano capsules) [84]. Processes catalyzed by enzymes and whole cells will, in the coming years, be major players for global sustainability. In this sense, the industrial need of robust and heterogeneous biocatalysts to be recovered and reused makes immobilization procedures a key step of practical relevance; it is noteworthy that, also in the perspective of substituting petrol-based carriers that are currently on the market, immobilization technologies recently developed with cheap, stable, and renewable rice husks are of particular interest [66].

In conclusion, cutinases represent promising and selective biocatalytic tools for polyester chemistry, but their potentials still need to be fully exploited through an industrially driven perspective. In an industry moving more and more towards a circular economy [85] and an atomic economy where each compound derived from the process needs to be recycled, enzymes and whole cell transformations will, in the coming years, be a major player for global sustainability.

Author Contributions: V.F., A.P., and M.C. wrote the paper, G.M.G. and L.G. conceived and corrected the manuscript.

Conflicts of Interest: The authors declare no conflict of interest.

References

1. Guebitz, G.M.; Cavaco-Paulo, A. Enzymes go big: Surface hydrolysis and functionalisation of synthetic polymers. *Trends Biotechnol.* **2008**, *46*, 32–38. [CrossRef] [PubMed]
2. Pellis, A.; Herrero Acero, E.; Ferrario, V.; Ribitsch, D.; Guebitz, G.M.; Gardossi, L. The closure of the cycle: Enzymatic synthesis and functionalization of bio-based polyesters. *Trends Biotechnol.* **2016**, *34*, 316–328. [CrossRef] [PubMed]
3. Pellis, A.; Herrero Acero, E.; Gardossi, L.; Ferrario, V.; Guebitz, G.M. Renewable building blocks for sustainable polyesters: New biotechnological routes for greener plastics. *Polym. Int.* **2016**, *65*, 861–871. [CrossRef]
4. Gross, R.A.; Ganesh, M.; Lu, W. Enzyme-catalysis breathes new life into polyester condensation polymerizations. *Trends Biotechnol.* **2010**, *28*, 435–443. [CrossRef] [PubMed]
5. Nyyssola, A. Which properties of cutinases are important for applications? *Appl. Microbiol. Biotechnol.* **2015**, *99*, 4931–4942. [CrossRef] [PubMed]
6. Dutta, K.; Sen, S.; Veeranki, V.K. Production, characterization and applications of microbial cutinases. *Proc. Biochem.* **2009**, *44*, 127–134. [CrossRef]
7. Briggs, D.E.G. Molecular taphonomy of animal and plant cuticles: Selective preservation and diagenesis. *Philos. Trans. R. Soc. B* **1999**, *354*, 7–17. [CrossRef]
8. Kolattukudy, P.E. Polyesters in higher plants. *Adv. Biochem. Eng. Biotechnol.* **2001**, *71*, 1–4. [PubMed]
9. Gross, R.A. Overview: Polyester synthesis catalyzed by *Candida antarctica* lipase B and the cutinase from *Humicola insolens*. *Polym. Prepr.* **2006**, *47*, 263–264.
10. Pellis, A.; Ferrario, V.; Zartl, B.; Brandauer, M.; Gamerith, C.; Herrero Acero, E.; Ebert, C.; Gardossi, L.; Guebitz, G.M. Enlarging the tools for efficient enzymatic polycondensation: Structural and catalytic features of cutinase 1 from *Thermobifida cellulosilytica*. *Catal. Sci. Technol.* **2016**, *6*, 3430–3442. [CrossRef]
11. Carvalho, C.M.L.; Aires-Barros, M.R.; Cabral, J.M.S. Cutinase structure, function and biocatalytic applications. *Electron. J. Biotechnol.* **1998**, *1*, 160–173. [CrossRef]
12. Carvalho, C.M.L.; Aires-Barros, M.R.; Cabral, J.M.S. Cutinase: From molecular level to bioprocess development. *Biotechnol. Bioeng.* **1999**, *66*, 17–34. [CrossRef]
13. Poulose, A.; Boston, M. Enzyme Assisted Degradation of Surface Membranes of Harvested Fruits and Vegetables. U.S. Patent 5,298,265, 29 March 1994.
14. Andersen, K.E.; Borch, K.; Krebs, L.N.E.; Steffen, E.; Landvik, S.; Schnorr, K.M. Plant Extraction Process. WO Patent 2,006,111,163, 26 October 2006.
15. Regado, M.A.; Cristóvão, B.M.; Moutinho, C.G.; Balcão, V.M.; Aires-Barros, R.; Ferreira, J.P.M.; Xavier Malcata, F. Flavour development via lipolysis of milkfats: Changes in free fatty acid pool. *Int. J. Food Sci. Technol.* **2007**, *42*, 961–968. [CrossRef]
16. De Barros, D.P.C.; Fonseca, L.P.; Cabral, J.M.S.; Weiss, C.K.; Landfester, K. Synthesis of alkyl esters by cutinase in miniemulsion and organic solvent media. *Biotechnol. J.* **2009**, *4*, 674–683. [CrossRef] [PubMed]
17. Badenes, S.M.; Lemos, F.; Cabral, J.M.S. Transesterification of oil mixtures catalyzed by microencapsulated cutinase in reversed micelles. *Biotechnol. Lett.* **2010**, *32*, 399–403. [CrossRef] [PubMed]
18. Badenes, S.M.; Lemos, F.; Cabral, J.M.S. Kinetics and mechanism of the cutinase-catalyzed transesterification of oils in AOT reversed micellar system. *Bioprocess. Biosyst. Eng.* **2011**, *34*, 1133–1142. [CrossRef] [PubMed]
19. Flipsen, J.A.C.; Appel, A.C.M.; van der Hijden, H.T.W.M.; Verrips, C.T. Mechanism of removal of immobilized triacylglycerol by lipolytic enzymes in a sequential laundry wash process. *Enzym. Microb. Technol.* **1998**, *23*, 274–280. [CrossRef]
20. Ahn, J.Y.; Kim, Y.H.; Min, J.; Lee, J. Accelerated degradation of dipentyl phthalate by *Fusarium oxysporum f.* sp. *pisi* cutinase and toxicity evaluation of its degradation products using bioluminescent bacteria. *Curr. Microbiol.* **2006**, *52*, 340–344. [PubMed]
21. Kim, Y.H.; Lee, J.; Ahn, J.Y.; Gu, M.B.; Moon, S.H. Enhanced degradation of an endocrine-disrupting chemical, butyl benzyl phthalate, by *Fusarium oxysporum f. sp. pisi* cutinase. *Appl. Environ. Microbiol.* **2002**, *68*, 4684–4688. [CrossRef] [PubMed]
22. Kim, Y.H.; Lee, J.; Moon, S.H. Degradation of an endocrine disrupting chemical, DEHP [di-(2-ethylhexyl)-phthalate], by *Fusarium oxysporum f. sp. pisi* cutinase. *Appl. Microbiol. Biotechnol.* **2003**, *63*, 75–80. [CrossRef] [PubMed]

23. Chen, S.; Su, L.; Chen, J.; Wu, J. Cutinase: Characteristics, preparation, and application. *Biotechnol. Adv.* **2013**, *31*, 1754–1767. [CrossRef] [PubMed]

24. Soliday, C.L.; Kolattukudy, P.E. Primary structure of the active site region of fungal cutinase, an enzyme involved in phytopathogenesis. *Biochem. Biophys. Res. Commun.* **1983**, *114*, 1017–1022. [CrossRef]

25. Purdy, R.E.; Kolattukudy, P.E. Hydrolysis of plant cuticle by plant pathogens. Properties of cutinase I, cutinase II, and a nonspecific esterase isolated from *Fusarium solani pisi*. *Biochemistry* **1975**, *14*, 2832–2840. [CrossRef] [PubMed]

26. Yao, C.; Köller, W. Diversity of cutinases from plant pathogenic fungi: Different cutinases are expressed during saprophytic and pathogenic stages of *Alternaria brassicicola*. *Mol. Plant Microbe Interact.* **1995**, *8*, 122–130. [CrossRef]

27. Castro-Ochoa, D.; Peña-Montes, C.; González-Canto, A.; Alva-Gasca, A.; Esquivel-Bautista, R.; Navarro-Ocaña, A.; Farrés, A. An extracellular cutinase from *Aspergillus nidulans* induced by olive oil. *Appl. Biochem. Biotechnol.* **2012**, *166*, 1275–1290. [CrossRef] [PubMed]

28. Nyyssölä, A.; Pihlajaniemi, V.; Järvinen, R.; Mikander, S.; Kontkanen, H.; Kruus, K.; Kallio, H.; Buchert, J. Screening of microbes for novel acidic cutinases and cloning and expression of an acidic cutinase from *Aspergillus niger* CBS 513.88. *Enzym. Microb. Technol.* **2013**, *52*, 272–278. [CrossRef] [PubMed]

29. Maeda, H.; Yamagata, Y.; Abe, K.; Hasegawa, F.; Machida, M.; Ishioka, R.; Gomi, K.; Nakajima, T. Purification and characterization of a biodegradable plastic-degrading enzyme from Aspergillus oryzae. *Appl. Microbiol. Biotechnol.* **2005**, *67*, 778–788. [CrossRef] [PubMed]

30. Shishiyama, J.; Araki, F.; Akai, S. Studies on cutin-esterase II. Characteristics of cutin-esterase from *Botrytis cinerea* and its activity on tomato-cutin. *Plant Cell Physiol.* **1970**, *11*, 937–945.

31. Ettinger William, F.; Thukral Sushi, K.; Kolattukudy Pappachan, E. Structure of cutinase gene, cDNA, and the derived amino acid sequence from phytopathogenic Fungi. *Biochemistry* **1987**, *26*, 7883–7892. [CrossRef]

32. Chen, Z.; Franco, C.F.; Baptista, R.P.; Cabral, J.M.S.; Coelho, A.V.; Rodrigues, C.J.; Melo, E.P. Purification and identification of cutinases from *Colletotrichum kahawae* and *Colletotrichum gloeosporioides*. *Appl. Microbiol. Biotechnol.* **2007**, *73*, 1306–1313. [CrossRef] [PubMed]

33. Merz, J.; Schembecker, G.; Riemer, S.; Nimtz, M.; Zorn, H. Purification and identification of a novel cutinase from *Coprinopsis cinerea* by adsorptive bubble separation. *Sep. Purif. Technol.* **2009**, *69*, 57–62. [CrossRef]

34. Kodama, Y.; Masaki, K.; Kondo, H.; Suzuki, M.; Tsuda, S.; Nagura, T.; Shimba, N.; Suzuki, E.; Iefuji, H. Crystal structure and enhanced activity of a cutinase-like enzyme from *Cryptococcus* sp. strain S-2. *Proteins* **2009**, *77*, 710–717. [CrossRef] [PubMed]

35. Dimarogona, M.; Nikolaivits, E.; Kanelli, M.; Christakopoulos, P.; Sandgren, M.; Topakas, E. Structural and functional studies of a *Fusarium oxysporum* cutinase with polyethylene terephthalate modification potential. *Biochim. Biophys. Acta* **2015**, *1850*, 2308–2317. [CrossRef] [PubMed]

36. Soliday, C.L.; Kolattukudy, P.E. Isolation and characterization of a cutinase from *Fusarium roseum* culmorum and its immunological comparison with cutinases from *F. solani pisi*. *Arch. Biochem. Biophys.* **1976**, *176*, 334–343. [CrossRef]

37. Longhi, S.; Czjzek, M.; Lamzin, V.; Nicolas, A.; Cambillau, C. Atomic resolution (1.0 A) crystal structure of *Fusarium solani* cutinase: Stereochemical analysis. *J. Mol. Biol.* **1997**, *268*, 779–799. [CrossRef] [PubMed]

38. Nyon, M.P.; Rice, D.W.; Berrisford, J.M.; Hounslow, A.M.; Moir, A.J.G.; Huang, H.; Nathan, S.; Mahadi, N.M.; Bakar, F.D.A.; Craven, C.J. Catalysis by *Glomerella cingulata* cutinase requires conformational cycling between the active and inactive states of its catalytic triad. *J. Mol. Biol.* **2009**, *385*, 226–235. [CrossRef] [PubMed]

39. Lin, T.S.; Kolattukudy, P.E. Structural studies on cutinase, a glycoprotein containing novel amino acids and glucuronic acid amide at the N terminus. *Eur. J. Biochem.* **1980**, *106*, 341–351. [CrossRef] [PubMed]

40. Kold, D.; Dauter, Z.; Laustsen, A.K.; Brzozowski, A.M.; Turkenburg, J.P.; Nielsen, A.D.; Kolds, H.; Petersen, E.; Schitt, B.; de Maria, L.; et al. Thermodynamic and structural investigation of the specific SDS binding of *Humicola insolens* cutinase. *Protein Sci.* **2014**, *23*, 1023–1035. [CrossRef] [PubMed]

41. Sweigard, J.A.; Chumley, F.G.; Valent, B. Disruption of a *Magnaporthe grisea* cutinase gene. *Mol. Gen. Genet.* **1992**, *232*, 183–190. [PubMed]

42. Wang, G.Y.; Michailides, T.J.; Hammock, B.D.; Lee, Y.M.; Bostock, R.M. Affinity purification and characterization of a cutinase from the fungal plant pathogen *Monilinia fructicola* (Wint.) honey. *Arch. Biochem. Biophys.* **2000**, *382*, 31–38. [CrossRef] [PubMed]

43. Liebminger, S.; Eberl, A.; Sousa, F.; Heumann, S.; Fischer-Colbrie, G.; Cavaco-Paulo, A.; Guebitz, G.M. Hydrolysis of PET and bis-(benzoyloxyethyl) terephthalate with a new polyesterase from *Penicillium citrinum*. *Biocatal. Biotransform.* **2007**, *25*, 171–177. [CrossRef]

44. Sebastian, J.; Kolattukudy, P.E. Purification and characterization of cutinase from a fluorescent *Pseudomonas putida* bacterial strain isolated from phyllosphere. *Arch. Biochem. Biophys.* **1988**, *263*, 77–85. [CrossRef]

45. Davies, K.A.; Lorono, I.; Foster, S.J.; Li, D.; Johnstone, K.; Ashby, A.M. Evidence for a role of cutinase in pathogenicity of *Pyrenopeziza brassicae* on brassicas. *Physiol. Mol. Plant Pathol.* **2000**, *57*, 63–75. [CrossRef]

46. Parker, D.M.; Köller, W. Cutinase and other lipolytic esterases protect bean leaves from infection by *Rhizoctonia solani*. *Mol. Plant Microbe Interact.* **1998**, *11*, 514–522. [CrossRef]

47. Miyakawa, T.; Mizushima, H.; Ohtsuka, J.; Oda, M.; Kawai, F.; Tanokura, M. Structural basis for the Ca(2+)-enhanced thermostability and activity of PET-degrading cutinase-like enzyme from *Saccharomonospora viridis* AHK190. *Appl. Microbiol. Biotechnol.* **2015**, *99*, 4297–4307. [CrossRef] [PubMed]

48. Kitadokoro, K.; Thumarat, U.; Nakamura, R.; Nishimura, K.; Karatani, H.; Suzuki, H.; Kawai, F. Crystal structure of cutinase Est119 from *Thermobifida alba* AHK119 that can degrade modified polyethylene terephthalate at 1.76 Å resolution. *Polym. Degrad. Stab.* **2012**, *97*, 771–775. [CrossRef]

49. Roth, C.; Wei, R.; Oeser, T.; Then, J.; Foellner, C.; Zimmermann, W.; Straeter, N. Structural and functional studies on a thermostable polyethylene terephthalate degrading hydrolase from *Thermobifida fusca*. *Appl. Microbiol. Biotechnol.* **2014**, *98*, 7815–7823. [CrossRef] [PubMed]

50. Xu, H.; Yan, Q.; Duan, X.; Yang, S.; Jiang, Z. Characterization of an acidic cold-adapted cutinase from *Thielavia terrestris* and its application in flavor ester synthesis. *Food Chem.* **2015**, *188*, 439–445. [CrossRef] [PubMed]

51. Roussel, A.; Amara, S.; Nyyssola, A.; Mateos-Diaz, E.; Blangy, S.; Kontkanen, H.; Westerholm-Parvinen, A.; Carriere, F.; Cambillau, C. A Cutinase from *Trichoderma reesei* with a lid-covered active site and kinetic properties of true lipases. *J. Mol. Biol.* **2014**, *426*, 3757–3772. [CrossRef] [PubMed]

52. Maiti, I.B.; Kolattukudy, P.E.; Shaykh, M. Purification and characterization of a novel cutinase from nasturtium (*Tropaeolum majus*) pollen. *Arch. Biochem. Biophys.* **1979**, *196*, 412–423. [CrossRef]

53. Köller, W.; Parker, D.M. Purification and characterization of cutinase from *Venturia inaequalis*. *Phytopathology* **1989**, *79*, 278–283. [CrossRef]

54. Ferrario, V.; Ebert, C.; Knapic, L.; Fattor, D.; Basso, A.; Spizzo, P.; Gardossi, L. Conformational changes of lipases in aqueous media: A comparative computational study and experimental implications. *Adv. Synth. Catal.* **2011**, *353*, 2466–2480. [CrossRef]

55. Ferrario, V.; Siragusa, L.; Ebert, C.; Baroni, M.; Foscato, M.; Cruciani, G.; Gardossi, L. BioGPS descriptors for rational engineering of enzyme promiscuity and structure based bioinformatic analysis. *PLoS ONE* **2014**, *9*, e109354. [CrossRef] [PubMed]

56. Pellis, A.; Ferrario, V.; Cespugli, M.; Corici, L.; Guarnieri, A.; Zartl, B.; Herrero-Acero, E.; Ebert, C.; Guebitz, G.M.; Gardossi, L. Fully renewable polyesters via polycondensation catalyzed by *Thermobifida cellulosilytica* cutinase 1: An integrated approach. *Green Chem.* **2017**. [CrossRef]

57. Farmer, T.J.; Castle, R.L.; Clark, J.H.; Macquarrie, D.J. Synthesis of unsaturated polyester resins from various bio-derived platform molecules. *Int. J. Mol. Sci.* **2015**, *16*, 14912–14932. [CrossRef] [PubMed]

58. Bassanini, I.; Hult, K.; Riva, S. Dicarboxylic esters: Useful tools for the biocatalyzed synthesis of hybrid compounds and polymers. *Beilstein J. Org. Chem.* **2015**, *11*, 1583–1595. [CrossRef] [PubMed]

59. Pellis, A.; Corici, L.; Sinigoi, L.; D'amelio, N.; Fattor, D.; Ferrario, V.; Ebert, C.; Gardossi, L. Towards feasible and scalable solvent-free enzymatic polycondensations: Integrating robust biocatalysts with thin film reactions. *Green Chem.* **2015**, *17*, 1756–1766. [CrossRef]

60. Hunsen, M.; Azim, A.; Mang, H.; Wallner, S.R.; Ronkvist, A.; Xie, W.; Gross, R.A. A cutinase with polyester synthesis activity. *Macromolecules* **2007**, *40*, 148–150. [CrossRef]

61. Feder, D.; Gross, R.A. Exploring chain length selectivity in HIC-catalyzed polycondensation reactions. *Biomacromolecules* **2010**, *11*, 690–697. [CrossRef] [PubMed]

62. Stavila, E.; Arsyi, R.Z.; Petrovic, D.M.; Loos, K. *Fusarium solani pisi* cutinase-catalyzed synthesis of polyamides. *Eur. Polym. J.* **2013**, *49*, 834–842. [CrossRef]

63. Stavila, E.; Alberda van Ekenstein, G.O.R.; Loos, K. Enzyme-catalyzed synthesis of aliphatic-aromatic oligoamides. *Biomacromolecules* **2013**, *14*, 1600–1606. [CrossRef] [PubMed]

64. Binns, F.; Harffey, P.; Roberts, S.M.; Taylor, A. Studies leading to the large scale synthesis of polyesters using enzymes. *J. Chem. Soc. Perkin Trans.* **1999**, *1*, 2671–2676. [CrossRef]

65. Cantone, S.; Ferrario, V.; Corici, L.; Ebert, C.; Fattor, D.; Spizzo, P.; Gardossi, L. Efficient immobilisation of industrial biocatalysts: Criteria and constraints for the selection of organic polymeric carriers and immobilisation methods. *Chem. Soc. Rev.* **2013**, *42*, 6262–6276. [CrossRef] [PubMed]

66. Corici, L.; Ferrario, V.; Pellis, A.; Ebert, C.; Lotteria, S.; Cantone, S.; Voinovich, D.; Gardossi, L. Large scale applications of immobilized enzymes call for sustainable and inexpensive solutions: Rice husks as renewable alternatives to fossil-based organic resins. *RSC Adv.* **2016**, *6*, 63256–63270. [CrossRef]

67. Barth, M.; Oeser, T.; Wei, R.; Then, J.; Schmidt, J.; Zimmermann, W. Effect of hydrolysis products on the enzymatic degradation of polyethylene terephthalate nanoparticles by a polyester hydrolase from *Thermobifida fusca. Biochem. Eng. J.* **2015**, *93*, 222–228. [CrossRef]

68. Alisch-Mark, M.; Herrmann, A.; Zimmermann, W. Increase of the hydrophilicity of polyethylene terephthalate fibres by hydrolases from *Thermomonospora fusca* and *Fusarium solani f. sp. pisi. Biotechnol. Lett.* **2006**, *28*, 681–685. [CrossRef] [PubMed]

69. Donelli, I.; Taddei, P.; Smet, P.F.; Poelman, D.; Nierstrasz, V.A.; Freddi, G. Enzymatic surface modification and functionalization of PET: A water contact angle, FTIR, and fluorescence spectroscopy study. *Biotechnol. Bioeng.* **2009**, *103*, 845–856. [CrossRef] [PubMed]

70. Pellis, A.; Herrero Acero, E.; Weber, H.; Obersriebnig, M.; Breinbauer, R.; Srebotnik, E.; Guebitz, G.M. Biocatalyzed approach for the surface functionalization of poly(L-lactic acid) films using hydrolytic enzymes. *Biotechnol. J.* **2015**, *10*, 1739–1749. [CrossRef] [PubMed]

71. Mueller, R.J. Biological degradation of synthetic polyesters—ENZYMES as potential catalysts for polyester recycling. *Proc. Biochem.* **2006**, *41*, 2124–2128. [CrossRef]

72. Herrero Acero, E.; Ribitsch, D.; Steinkellner, G.; Gruber, K.; Greimel, K.; Eiteljoerg, I.; Trotscha, E.; Wei, R.; Zimmermann, W.; Zinn, M.; et al. Enzymatic surface hydrolysis of PET: Effect of structural diversity on kinetic properties of cutinases from *Thermobifida. Macromolecules* **2011**, *44*, 4632–4640. [CrossRef]

73. Pellis, A.; Gamerith, C.; Ghazaryan, G.; Ortner, A.; Herrero Acero, E.; Guebitz, G.M. Ultrasound-enhanced enzymatic hydrolysis of poly (ethylene terephthalate). *Biores. Technol.* **2016**, *218*, 1298–1302. [CrossRef] [PubMed]

74. Yang, S.; Xu, H.; Yan, Q.; Liu, Y.; Zhou, P.; Jiang, Z. A low molecular mass cutinase of *Thielavia. terrestris* efficiently hydrolyzes poly(esters). *J. Ind. Microbiol. Biotechnol.* **2013**, *40*, 217–226. [CrossRef] [PubMed]

75. Ronkvist, A.M.; Xie, W.; Lu, W.; Gross, R.A. Cutinase-catalyzed hydrolysis of poly(ethylene terephtalate). *Macromolecules* **2009**, *42*, 5128–5138. [CrossRef]

76. Pellis, A.; Silvestrini, L.; Scaini, D.; Coburn, J.; Gardossi, L.; Kaplan, D.; Herrero Acero, E.; Guebitz, G.M. Enzyme-catalyzed functionalization of poly (L-lactic acid) for drug delivery applications. *Process Biochem.* **2016**. [CrossRef]

77. Ribitsch, D.; Herrero Acero, E.; Greimel, K.; Dellacher, A.; Zitzenbacher, S.; Marold, A.; Diaz Rodriguez, R.; Steinkellner, G.; Gruber, K.; Schwab, H.; et al. A new esterase from *Thermobifida halotolerans* hydrolyses polyethylene terephthalate (PET) and polylactic acid (PLA). *Polymers* **2012**, *4*, 617–629. [CrossRef]

78. Pellis, A.; Haernvall, K.; Pichler, C.M.; Ghazaryan, G.; Breinbauer, R.; Guebitz, G.M. Enzymatic hydrolysis of poly (ethylene furanoate). *J. Biotechnol.* **2016**, *235*, 47–53. [CrossRef] [PubMed]

79. Perz, V.; Bleymaier, K.; Sinkel, C.; Kueper, U.; Bonnekessel, M.; Ribitsch, D.; Guebitz, G.M. Substrate specificities of cutinases on aliphatic–aromatic polyesters and on their model substrates. *New Biotechnol.* **2016**, *33*, 295–304. [CrossRef] [PubMed]

80. Silva, C.M.; Carnerio, F.; O'Neill, A.; Fonseca, L.P.; Cabral, J.S.M.; Guebitz, G.M.; Cavaco-Paulo, A. Cutinase—A new tool for biomodification of synthetic fibers. *J. Polym. Sci. Part A Polym. Chem.* **2005**, *43*, 2448–2450. [CrossRef]

81. Ribitsch, D.; Oracal Yebra, A.; Zitzenbacher, S.; Wu, J.; Nowitsch, S.; Steinkellner, G.; Greimel, K.; Doliska, A.; Oberdorfer, G.; Gruber, C.C.; et al. Fusion of binding domains to *Thermobifida cellulosilytica* cutinase to tune sorption characteristics and enhancing PET hydrolysis. *Biomacromolecules* **2013**, *14*, 1769–1776. [CrossRef] [PubMed]

82. Silva, C.; Da, S.; Silva, N.; Matamá, T.; Araújo, R.; Martins, M.; Chen, S.; Chen, J.; Wu, J.; Casal, M.; et al. Engineered *Thermobifida fusca* cutinase with increased activity on polyester substrates. *Biotechnol. J.* **2011**, *6*, 1230–1239. [CrossRef] [PubMed]

69

83. Araújo, R.; Silva, C.; O'Neill, A.; Micaelo, N.; Guebitz, G.M.; Soares, C.M.; Casal, M.; Cavaco-Paulo, A. Tailoring cutinase activity towards polyethylene terephthalate and polyamide 6,6 fibers. *J. Biotechnol.* **2007**, *128*, 849–857. [CrossRef] [PubMed]

84. Bilal, M.H.; Prehm, M.; Njau, A.E.; Samiullah, M.H.; Meister, A.; Kressler, J. Enzymatic synthesis and characterization of hydrophilic sugar based polyesters and their modification with stearic acid. *Polymers* **2016**, *8*, 80. [CrossRef]

85. Clark, J.H.; Farmer, T.J.; Herrero-Davila, L.; Sherwood, J. Circular economy design considerations for research and process development in the chemical sciences. *Green Chem.* **2016**, *18*, 3914–3934. [CrossRef]

4.2 Analysis of structural and functional properties of cutinases vs other serine hydrolases: a bioinformatics approach using molecular descriptors

The industrial optimization process of biocatalysts aims to expand the range of biocatalytic routes to be used in industrial synthetic processes and to improve the applicability of enzymes to meet the industrial needs in terms of operative conditions, product purity and cost-effectiveness.

The computational approach to this matter allows simplifying the screening process of new enzymes that in lab scale could be very expensive and time-consuming. *In silico* screening, through the use of appropriate bioinformatics software, can be an effective aid in reducing the number of experiments to be made in the laboratory, with a clear economic advantage. From this perspective, developing and testing new enzyme can be a way more efficient process. Through the last forty years, high computational cost quantomechanics (QM) methodologies have been used to understand the physicochemical properties of enzymes[52]. For this reason, enzymatic systems have always been studied only at the level of the catalytic residues, while combining molecular mechanics (MM) techniques to handle the remaining part of the protein structure, disregarding all the fine-grained electronic interactions and taking into account only the laws of classical mechanics to describe the atoms[53]. However, this approach turned out to be inconvenient because of the excessive simplification of the system while not reducing consistently the time required for the calculation[54].

The recent research in the field of bioinformatics resulted in the development of molecular descriptors that, as suggested by the name, describe quantitatively the characteristics of different kinds of molecular systems[55]. A molecular descriptor is the result of a logical and mathematical process that translates the protein structure in a numerical form useful to easily compare different structures in a dataset. Each amino acid establishes short and long-range interaction with other ones creating foreseeable and quantifiable perturbations in the surrounding environment. For this reason, molecular descriptors are required to formalize these data and correlate them to the physicochemical properties of the catalytic site. Various types of molecular descriptors have been developed distinguished on the basis of the specific type of interaction they focus on[56]. The molecular descriptor used in this thesis for the study of cutinases and other enzymes belonging to the family of serine hydrolases, is based on molecular interaction fields (MIFs): among them, GRID molecular descriptors[57], originally developed for drug-design oriented applications, are designed to seek for the highest interaction energy between a protein receptor and a candidate drug molecule. Nevertheless,

these descriptors are also useful tools for enzymatic catalysis because they can be used to evaluate the interactions responsible for the transition state stabilisation of a particular biocatalysed reaction.

GRID molecular descriptors and molecular interaction fields (MIFs) calculation

3D-QSAR approach is based on the determination and interpretation of the interactions between three-dimensional objects. According to Goodford[57] it is possible to evaluate the affinity of a system for a specific chemical functional group by calculating the interaction energy established with it in each point of a defined three-dimensional cage where the object to be studied is contained. The *probe* functional group is moved around the *target* molecule and the interaction energy is recorded. Typical chemical probes are water, methyl, aminic nitrogen, carboxyl, hydroxyl. This calculation results in the mapping of the space surrounding the target molecule, with the production of a three-dimensional matrix that associates each grid point to the interaction energy of that particular probe. The whole matrix (Figure 18) represents a molecular interaction field (MIF).
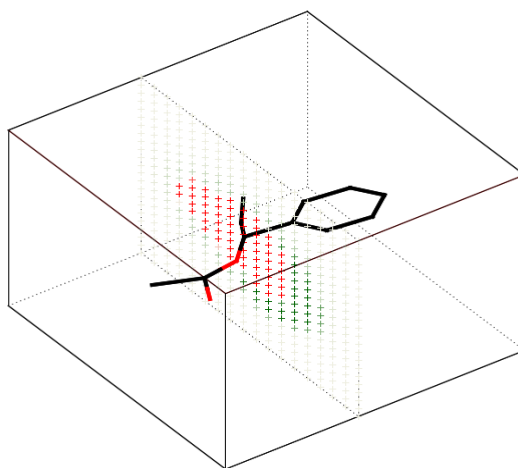
Figure 18. Molecular interaction fields. The box represents the dimension of the 3D grid. Interaction energies of the *probes* placed in the grid points are indicated in chromatic scale (green favourable interaction, red unfavourable interaction because of the steric hindrance)

The interaction energy for each point of the grid is calculated according to the following law (Eq. 1):

$$E_{xyz} = \sum_{i=1}^{n} E_{lj} + \sum_{i=1}^{n} E_{el} + \sum_{i=1}^{n} E_{hb}$$

Eq. 1

Each term of the equation refers to non-covalent interactions established between the chemical *probe* and the *n* atoms comprised in a sphere whose radius is defined by a cut-off distance. The three contributions represent the non-covalent Van der Waals interactions in Lennard-Jones form, the electrostatic interaction, and the H-bond interactions. The parameters used for the calculation of each term of the equation are empiric and fine-tuned for the probe functional group.

The molecular interaction field is a high density of information object and can be used for different purposes. Positive interaction energy corresponds to unfavourable *target-probe* interaction or when the *probe* is positioned inside the Van der Waals sphere of the atoms of the *target*. Conversely, using the grid points where interaction is more favourable (negative energy values) it is possible to analyse the macroscopic similitudes among different *target* objects. This approach has been used in this thesis to carry out a comparison between different serine hydrolase sub-families.

Chemometric analysis

GOLPE (Generating Optimal Linear PLS Estimations)[58] is a chemometric software used in 3D-QSAR studies, molecular interaction fields are used as independent variables source. In particular, the 3D matrix is converted into a single MIF-containing mono-dimensional vector. D-optimal selection seeks for the most informative variables while excluding the other ones. FDD (Fractional Factorial Design) is an optimization-targeted procedure that analyses the effect of the single variables on the predictivity of the model, maintaining the ones responsible for a positive contribution. Golpe also offers data pre-treatment tools used to clean the dataset while maintaining all the information resulted by MIF calculation.

The BioGPS descriptors and their application

In the optimization process of biocatalysts of industrial interest, enzyme manipulation plays a central role that is functional to the improvement of system properties which must be tuned on the specific application needs. In this perspective, computational methodologies help to reduce the costs in terms of time and money when it comes to enzyme activity screening. However, the rational re-design of an active site requires specific bioinformatics techniques capable of correlating protein structural features to the stabilization of the transition state. In

other words, a holistic approach to the structural and electronic features of the enzyme is needed, and BioGPS enables the user to watch at the enzyme in these terms.

BioGPS (*Global Positioning System in Biological Space*) makes use of a GRID-based approach to compare enzyme cavities (i.e. active sites) by means of a complex three-dimensional superimposition algorithm[54]. BioGPS method is based on UPCA (*Unsupervised Pattern Cognition Analysis*)[59] analysis and relies on the evaluation of physicochemical features in the active site who characterise the pre-organized reaction environment of the biocatalyst, in a similar way to the function of the solvent in a reaction medium. BioGPS-UPCA approach compares the binding sites of a protein dataset on the basis of a ligand and not looking at the features of the single amino acids. This action is performed by means of the definition of a molecular *fingerprint* that identifies each active site to be used for the calculation of *de novo* virtual structures by using FLAP (*Fingerprints for Ligands and Proteins*)[60]. The above-mentioned computational approach has been already successfully used in the field of drug design[61]. The complexity of the MIFs information is overcome by the multivariate statistical analysis which is able to simplify the handling of complex systems by identifying only on relevant variables in the starting matrix of values. This fact enables to represent the information in a mono-dimensional space making way easier the elaboration and the interpretation of the starting raw data. Together with MIFs, the algorithm allows also the calculation of pseudoMIFs, defined as a particular type of MIFs where the molecular interaction fields are a representation of electron density fields centred on the atoms of the chosen chemical probes instead of atoms of the enzyme. PseudoMIFs could be seen as the complementary counterpart of MIFs and it is useful to visualize the part of the active site occupied by a potential substrate (Figure 19). In the case of pseudoMIFs the interaction energies are not calculated for each point of the defined grid cage, conversely, they are generated in the form of a pseudopotential describing the areas with higher probe-chemical feature interactions[60].
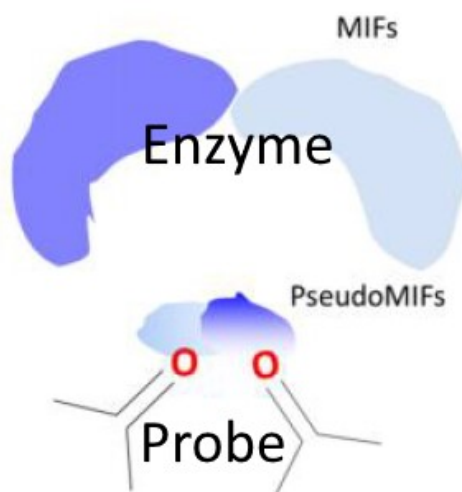
Figure 19. MIFs and pseudoMIFs. pseudoMIFs can be seen as the complementary part of MIFs. (BioGPS 16.06 User Manual)

On this basis, with reduced computational and time costs, entire enzyme sub-families and mutants can be efficiently compared without the need of relying on whatsoever precedent knowledge.

A typical flowchart of the operational procedure used with BioGPS could be described with the following steps:

1. Description of the active site environment by means of MIFs: all stacked enzyme cavities representing the dataset under consideration are described in the GRID force field and the complexity of the resulting MIFs is reduced in order to obtain a *Common Reference Framework*, a mathematical description of the protein cavities.

2. Superimposition step: a stochastic process allows the superimposition of the calculated MIFs using a quadruplet-based approach that can be tuned based on the specific operative conditions.

3. Scoring step: the outcoming results of the preceding step are used to quantify the entity of the similarity among different active sites. A standard output is produced based on the single chemical probes employed or, alternatively, on their combination (Figure 20).

4. Statistical interpretation of the numerical data obtained via appropriate software (i.e. GOLPE) and generation of a UPCA model (*Principal Component Analysis)*, a statistical method widely used to reduce the complexity of a dataset, correlating molecular descriptors with linearly dependent variables called Principal Components. This operation makes all the gathered data more

75

interpretable by the user, and macro-groups of physicochemically-correlated enzymes can be easily identified.
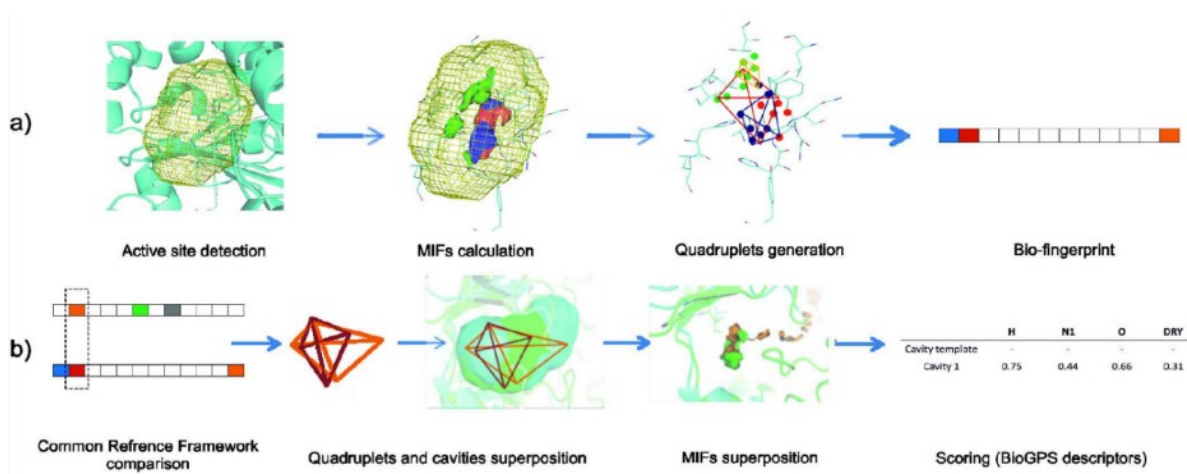
Figure 20. Schematic illustration of the generation of BioGPS molecular descriptors. (a) Starting from the GRID mapping of enzyme active site the BioGPS algorithm identifies points used for generating quadruplets and a Common Reference Framework. (b) In order to compare two cavities (active sites), the algorithm searches for similar quadruplets and then overlaps the corresponding 3D structures (all against all approach). Eventually, a series of probe scores are generated. (Ferrario et al. 2014)

Together with the mapping and MIF calculation phase, BioGPS *flappharm* algorithm can be used for the generation of a MIF-based "*pharmacophoric pseudomolecule*" whose displayed MIFs reflect the three-dimensional position of the specific functional groups of amino acids more frequently interacting with the particular probes chosen. The output structure is represented in the form of a grid cage and is prone to be superimposed to active sites to evaluate how and where it fits with the MIFs of the protein structures. This approach has been exploited for the calculation of the *catalophor* of a given serine-hydrolase sub-family.

The actual output of the catalophor calculation (MIFs) is completed with the generation of the above-mentioned pseudoMIFs, whose interpretation allows to estimate the positioning of a generic substrate within the active site cavity. The numerical scoring data obtained (*score by probe*, *S-Score* and *Model score*) can be exploited to evaluate the homogeneity of the whole dataset and to highlight analogies an differences among active sites in the same enzyme sub-family.

BioGPS as a tool for the study of serine hydrolases

BioGPS was exploited to highlight analogies and differences within a selection of enzymes belonging to the family of serine hydrolases, namely lipases, esterases, amidases, proteases and cutinases, the last one being an enzyme class of particular interest in relation to biocatalysed polycondensations, as stated in the reported review. All the enzymes of the dataset, with the exception cutinases, were already studied by means of BioGPS by Ferrario et al.[4]. Most of the serine hydrolases share a common catalytic triad Ser/His/Asp (or Glu), though hydrolysing different substrates (i.e. lipids, small esters, proteins) based on the sub-family they belong to.

Dataset composition

The dataset of serine-hydrolases was composed of 42 structures as used in the previous study with the addition of 9 protein structures belonging to the class of cutinases (E.C. 3.1.1.74). All the crystal structures were retrieved from the Protein Data Bank (PDB)[62]. In order to work only on protein data and discarding the other components of the structures (like water, duplicated protein chains, inhibitors, etc.) the PyMOL[63] software was used for pre-processing, leading to protein structures ready to be analysed by BioGPS[60]. The composition of the whole dataset is determined by 5 different enzyme classes, distinguished by their E.C. number: lipases (serine hydrolases defined as triacylglycerol lipase; E.C. 3.1.1.3), esterases (other carboxylic ester hydrolases but not triacylglycerol lipase; E.C. 3.1.1), proteases (serine endopeptidase; E.C. 3.4.21), amidases (amino peptidase and other hydrolases acting on carbon-nitrogen bonds other than peptide bonds; E.C. 3.4.11, E.C. 3.5.1, E.C. 3.5.2) and cutinases (acting on the polymeric structure of cutin formed by C16 or C18 hydroxy fatty acids; 3.1.1.74).

In Table 8, all the enzymes of the dataset are reported with the respective PDB code of the crystalline structure:

Enzyme class	PDB code	Source	Substrate
Cutinases	1AGY	*Fusarium solani*	cutin, short esters, PET, PBS
	3DCN	*Glomerella cingulata*	cutin, triacylglycerol
	3QPD	*Aspergillus oryzae*	cutin, long chain esters
	3WYN	*Thermobifida alba*	cutin, PET, PBS, PLA
	4CG1	*Thermobifida fusca*	cutin, PET
	4OYY	*Humicola insolens*	cutin, PET, PBS, PLA, PBAT
	4PSE	*Trichoderma reesei*	cutin, triacylglicerol
	4WFI	*Saccharomonospora virdis*	short-chain triacylglycerol, PET
	Thc_Cut1	*Thermobifida cellulosilytica*	PET, PEF, PBAT
Lipases	1CRL	*Candida rugosa*	triacylglycerol
	1DTE	*Humicola lanuginosa*	triacylglycerol
	1ETH	*Sus scrofa*	triacylglycerol
	1EX9	*Pseudomonas aeruginosa*	triacylglycerol
	1GPL	*Cavia porcellus*	triacylglycerol
	1K8Q	*Canis lupus familiaris*	triacylglycerol
	1LPB	*Homo sapiens*	triacylglycerol
	1TCA	*Candida antarctica*	triacylglycerol
	2FX5	*Pseudomonas mendocina*	triacylglycerol
	2NW6	*Burkholderia cepacia*	triacylglycerol
	2W22	*Geobacillus thermocatenulatus*	triacylglycerol
Esterases	1AUO	*Pseudomonas fluorescens*	broad specificity
	1BS9	*Penicillium purpurogenum*	xylanes acetates
	1C7J	*Bacillus subtilis*	p-nitrobenzyl esters
	1CLE	*Candida cylindracea*	cholesterol esters
	1JU3	*Rhodococcus sp.*	cocaine
	1QOZ	*Tricoderma reesei*	xylanes acetates
	1USW	*Aspergillus niger*	feroloyl-polysaccharide
	2ACE	*Torpedo californica*	acetylcoline

	PDB	Source	Substrate
	2H7C	*Homo sapiens*	CoA, palmitate and taurocholate
	2WFL	*Rauvolfia serpentine*	polyneuridine aldehyde
	3KVN	*Pseudomonas aeruginosa*	rhamnolipids
Proteases	1GVK	*Sus scrofa*	Ala-|-Xaa
	1NPM	*Mus musclus*	Lys/Arg-|-Xaa
	1PPB	*Homo sapiens*	Arg-|-Gly fibrinogen
	1QFM	*Sus scrofa*	Pro-|-Xaa (~30aa)
	1TAW	*Bos Taurus*	Lys/Arg-|-Xaa
	1TM1	*Bacillus amyloliquefaciens*	uncharged P1
	1YU6	*Bacillus licheniformis*	uncharged P1
	2XE4	*Leshmania major*	olygopeptides
	3F7O	*Peacelomyces lilacinus*	peptides
Amidases	1AZW	*Xantomonas campestris*	NH-Pro-|-Xaa
	1GM9	*Escherichia coli*	penicillin
	1HL7	*Microbacterium sp.*	γ-lactam
	1M21	*Stenotrophomonas maltophilia*	C terminal amide
	1MPL	*Streptomyces sp.*	L-Lys-D-Ala-|-D-Ala
	1MU0	*Thermoplasma acidophilum*	NH-Pro-|-Xaa
	1QTR	*Serratia marcescens*	NH-Pro-|-Xaa
	3A2P	*Arthrobacter sp.*	6-amino exanoate dimer
	3K3W	*Alcaligens faecalis*	penicillin
	3K84	*Rattus norvegicus*	fatty acid amide
	3NWO	*Mycobacterium smegmatis*	NH-Pro-|-Xaa

Table 8. PDB codes, sources and substrates of the serine-hydrolase dataset.

Crystalline structures coming from the Protein Data Bank were used after proper pre-processing and structure alignment (Figure 21) with PyMOL software with the exception of Thc_cut1 that has been obtained by homology modelling from 4CG1[4]. Structure alignment was performed based on the catalytic triad and oxyanion hole residues to ensure the proper spatial orientation of the active sites.
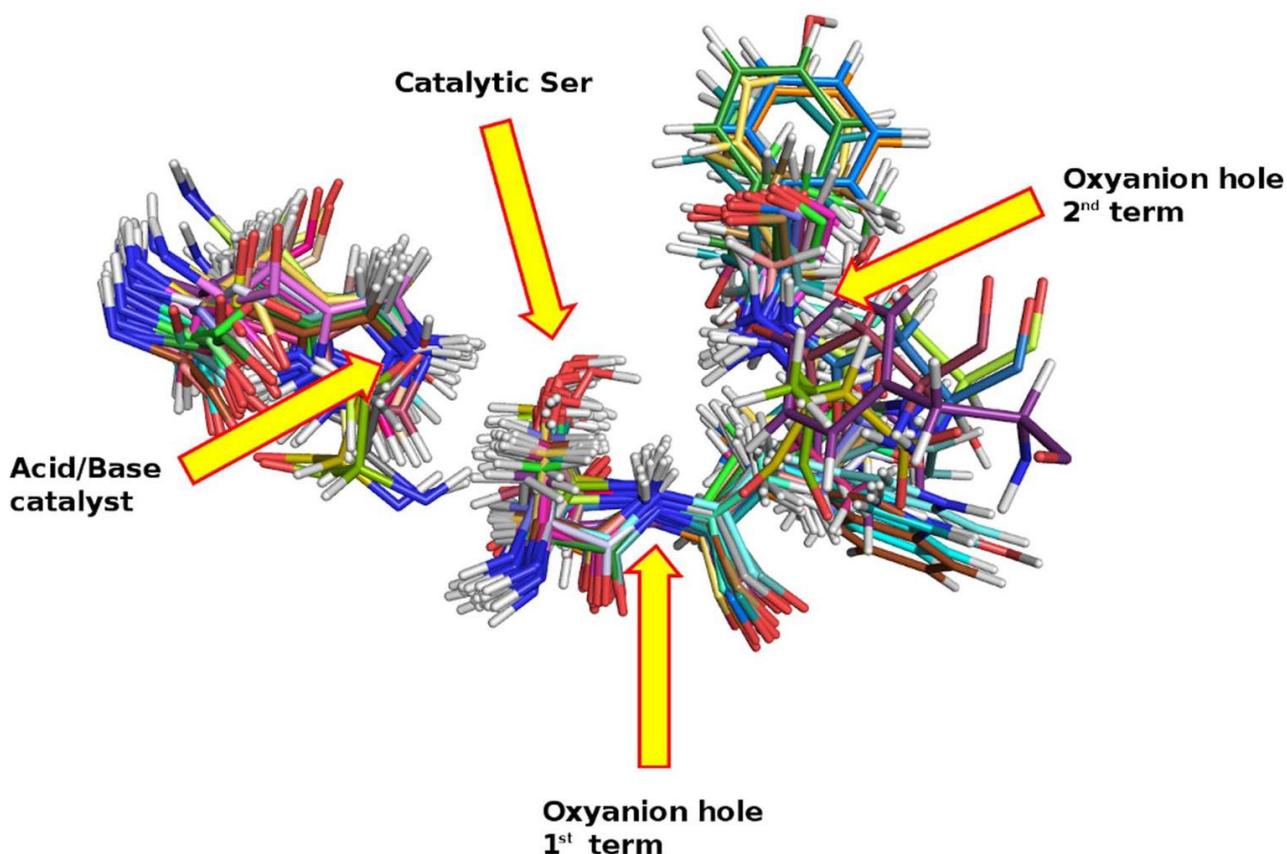
Figure 21. Superimposition of active site residues of the enzyme dataset. (Ferrario et al. 2014)

As stated before, FLAP algorithm was used for the calculation of molecular descriptors. FLAP exploits a *Common Reference Model* to evaluate and quantify the type and energy of the interactions established by the system *probe-target*.

In the present study, four chemical probes were taken into account for the generation of the molecular descriptors[64]:

- H probe describing the shape of the cavity surrounding the active site;
- O probe (carbonyl oxygen) describing H-Bond donor capabilities of the chosen cavity
- N1 probe (amidic nitrogen) describing H-Bond acceptor capabilities of the chosen cavity
- DRY probe (aromatic carbon) describing hydrophobic interactions with the chosen cavity

With the simultaneous generation of MIFs and pseudoMIFs, the said mapped properties were considered as density fields centred on each probe-interacting atom. Through an autonomous selection of the most representative points of the grid cages, a similarity-based quadruplet comparison between enzyme structures was made to project cutinase structures over the 4-

class serine hydrolase model previously reported[4] and a pharmacophoric pseudomolecule was generated for each class in order to extract the common physicochemical features of specific groups of protein structures.

4.2.1 BioGPS bioinformatics analysis and catalophores calculation

As previously demonstrated, the BioGPS bioinformatics tool allows to group enzyme structures according to the structural features of their active sites. A dataset of enzymes belonging to the serine-hydrolase class was previously analysed with this software, enabling the individuation of macro-clusters based on the physicochemical properties of the area surrounding the catalytic triad of the biocatalyst. The clusterization procedure via UPCA analysis showed that the structural properties explained by the BioGPS descriptors are correlated with the catalytic functions of each class of serine hydrolase.

Projecting on the UPCA plot a selection of enzymes belonging to the cutinase sub-family showed that the BioGPS analysis recognizes a high level of similarity between the active sites of cutinase 1 from *Thermobifida cellulosilytica* (Thc_cut1) and *Candida antarctica* lipase B (CaLB), which are projected in a region close both to the esterase and lipase group. Cutinase 1 is an enzyme of particular interest because has proven to be suitable for polycondensation reactions[3,6].

The active sites of CaLB and Thc_cut1 appeared to be similar in terms of hydrophobicity and they were positioned among esterases although close to the lipase cluster. Both Thc_cut1 and CaLB were clearly classified as esterases for their ability to establish H bonds and Thc_cut1 falls closer to the lipase group (Figures 22-26). These observations shed new light also on the behaviour of CaLB, whose hydrophobic properties of the active site are the main feature shared with lipases.
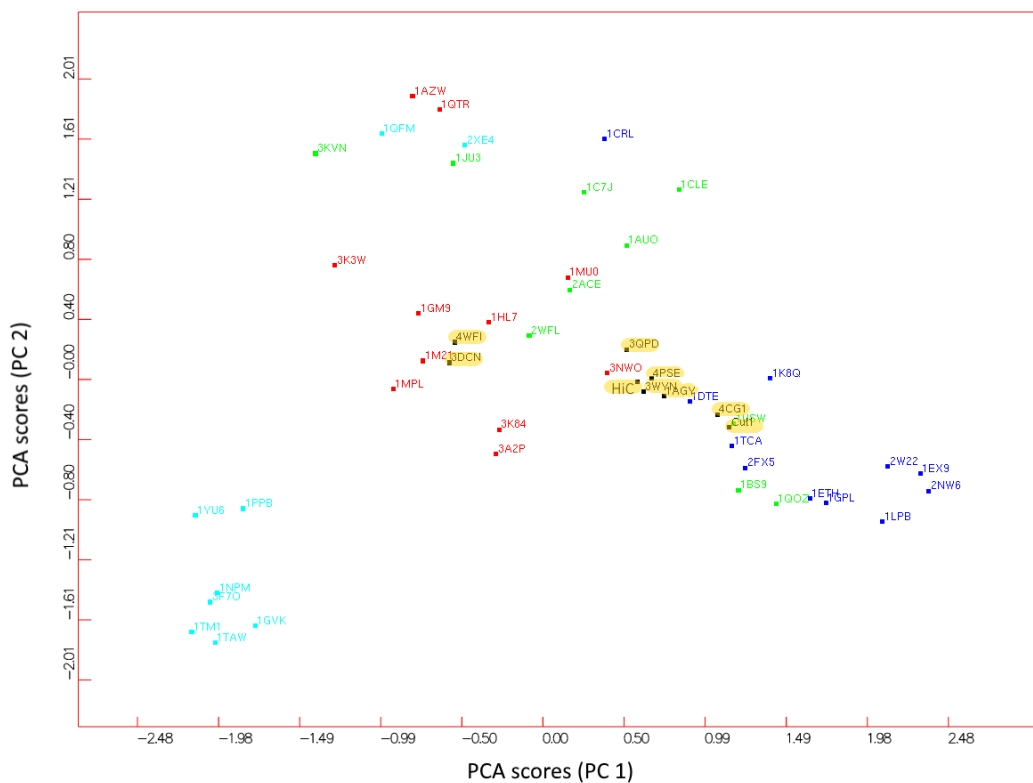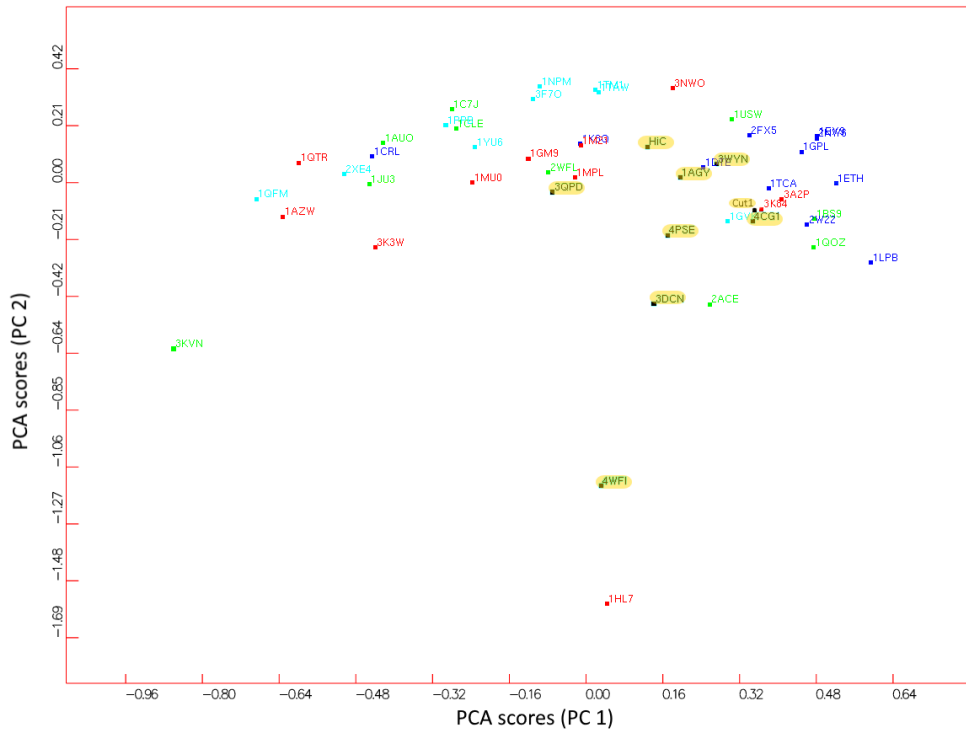
Figure 22. UPCA Model (Global score). Serine-hydrolases with cutinase projection. Blu: lipases; green: esterases; cyan: proteases; red: amidases; highlighted: cutinases. CaLB (1TCA) and Thc_cut1 (Cut1) are located close to each other.
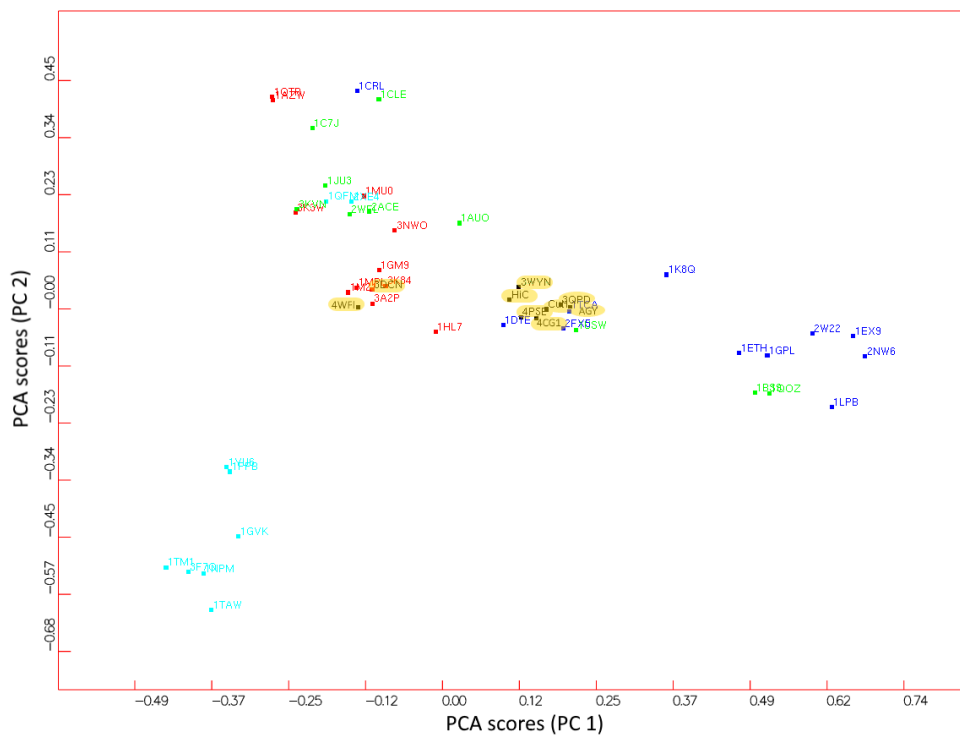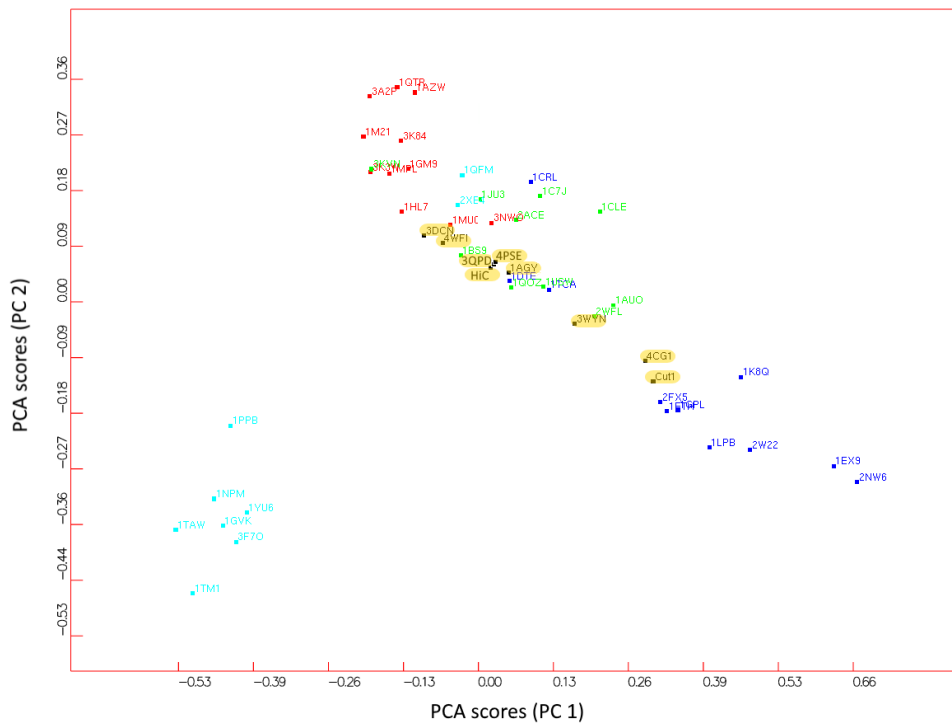

Figure 23. UPCA Model (hydrophobicity probe). Serine-hydrolases with cutinase projection. Blu: lipases; green: esterases; cyan: proteases; red: amidases; highlighted: cutinases.
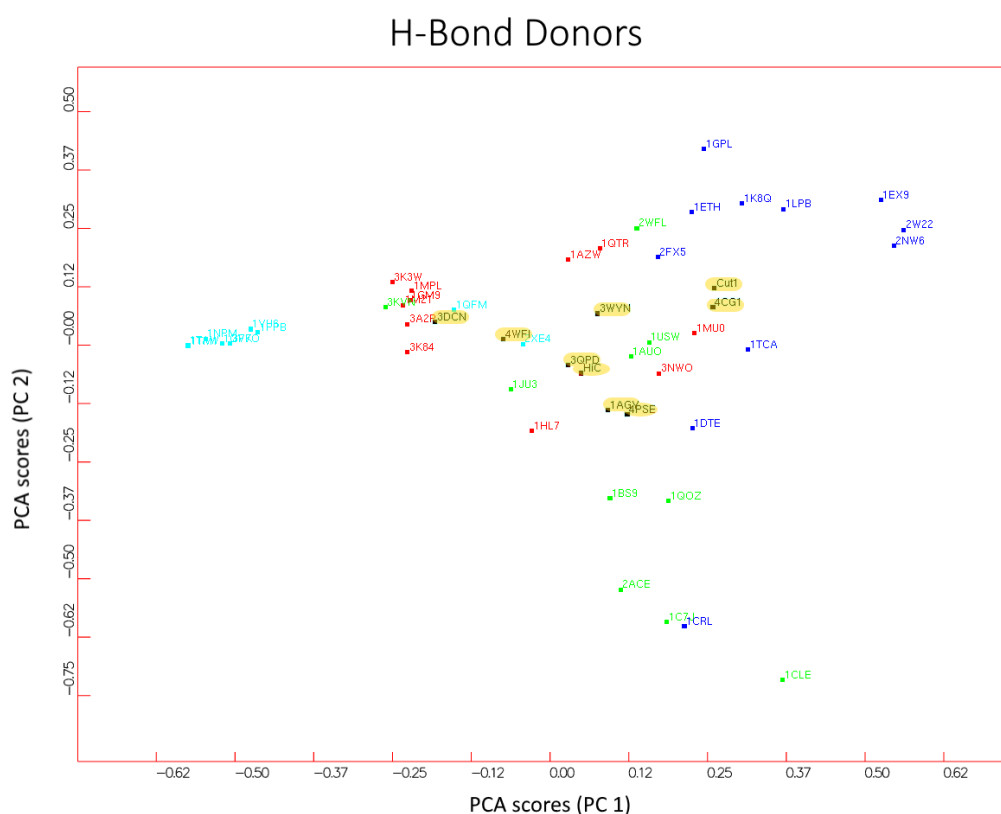
Figure 24. UPCA Model (shape probe). Serine-hydrolases with cutinase projection. Blu: lipases; green: esterases; cyan: proteases; red: amidases; highlighted: cutinases.

Figure 25. UPCA Model (H-bond acceptors probe). Serine-hydrolases with cutinase projection. Blu: lipases; green: esterases; cyan: proteases; red: amidases; highlighted: cutinases.

Figure 26. UPCA Model (H-bond donors probe). Serine-hydrolases with cutinase projection. Blu: lipases; green: esterases; cyan: proteases; red: amidases; highlighted: cutinases.

The analytical approach consists in a visual/statistical analysis that combines considerations based on the interpretation of images obtained with PyMOL software with numeric data generated by bioinformatics algorithms.

In particular, utilizing the GRID-based MIFs of BioGPS, the sub-families of serine-hydrolases composing the above-mentioned dataset, were processed separately to obtain the representative "catalophor" of each class that defined as a pharmacophoric pseudomolecule comprising a three-dimensional map of the more frequent physical-chemical features established by the amino acids of the enzyme active sites for the processed sub-family.

Exploiting different probes it was possible to evaluate the entity of the interaction between the couple probe-functional group on the surface of the biocatalyst. Four different probes were employed: H probe takes into account the active site shape, O probe that evaluates H-bond donor properties, N1 probe that evaluates the H-bond acceptor capabilities and the DRY probe accounting for hydrophobic interactions.

Following the probe-based mapping of the active site, the software calculates a score reflecting how frequent and strong such interactions are. Eventually, an S-Score value is obtained from the weighted average of the above-mentioned contributions of the singular components. The said S-Score represents how much the tridimensional picture of the

physicochemical features taken into account in a particular enzyme is similar to the algorithm-generated molecular interaction fields of the pharmacophoric pseudomolecule.

The adopted approach consists firstly in the GRID force field-based mapping of the active sites in order to quantify type and energy of the non-bonded interactions that could be established in the surrounding space. In the second stance, MIFs and PseudoMIFs are calculated using FLAP (Fingerprints for Ligands and Proteins) algorithm. PseudoMIFs are defined as a particular type of MIFs where the molecular interaction fields are a representation of electron density fields centred on the atoms of the above-mentioned probes instead of the atoms of the enzyme and, as stated before, could also be seen as the complementary counterpart of MIFs.

The average of the S-Scores of each subfamily of serine hydrolases is defined as Model Score. This value is important to evaluate how homogeneous are the accounted physicochemical features within a dataset.

A graphical representation of the deviation from the average values for each probe is provided below (Figure 27). Low values imply that the object enzyme obtained a score similar to the average in the model, conversely, higher values show stronger differences with the other elements in the same class. It is worth to say that similar values among different enzymes do not necessarily mean that the elements have shared features because the enzymes could also be equally different - but in different ways - from the generated pharmacophoric pseudomolecule (i.e. same distance in the UPCA model, but different positions).

The S-Score was calculated for each enzyme in the dataset and represents the weighted average of the contribution of the components (H, N1, O and DRY) in determining the entity of the superimposition of the MIFs of a particular enzyme with the ones of the pharmacophoric pseudomolecule. The catalophor is a spatial representation of MIFs generated by the different probes on the basis of the dataset elements.

Figure 27. S-scores represented by deviation from the average value, low values mean that the structure is well fitted within the dataset. A: lipases; B: esterases; C: proteases; D: amidases, E: cutinases; F: lipases + thc_cut1; G: lipases without CaLB; H: model scores, namely the weighted average of s-scores

Analysis of model score by components

The data here reported show that the contribution of the single probes in characterizing a serine-hydrolase subfamily slightly differs depending on the classes. In particular, no substantial differences were detected with regard to the hydrogen bond capabilities. More significative differences arise from the shape of the active site and the hydrophobicity. It is noteworthy that the contribution of the shape (H probe) is lower in the case of the cutinases compared to lipases (17.8% vs 20.0%, Figures 28-29). The rational basis of this behaviour can be found in the more superficial and wide active site of the cutinases, with a consequent

catalytic activity displayed towards a wider array of substrates. Furthermore, the algorithm shows a high importance of the hydrophobicity probe in the case of cutinases and lipases, where this feature contributes by a 28% in determining the Global Score value, showing that the hydrophobicity has a similar role for both the classes.
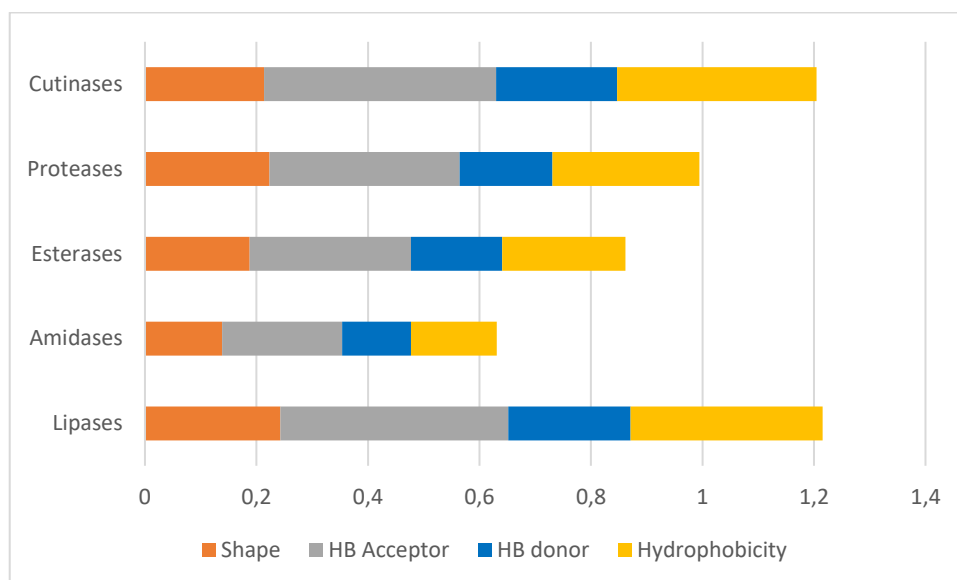
**Figure 28.** contribution of the various components in the determination of the model score.
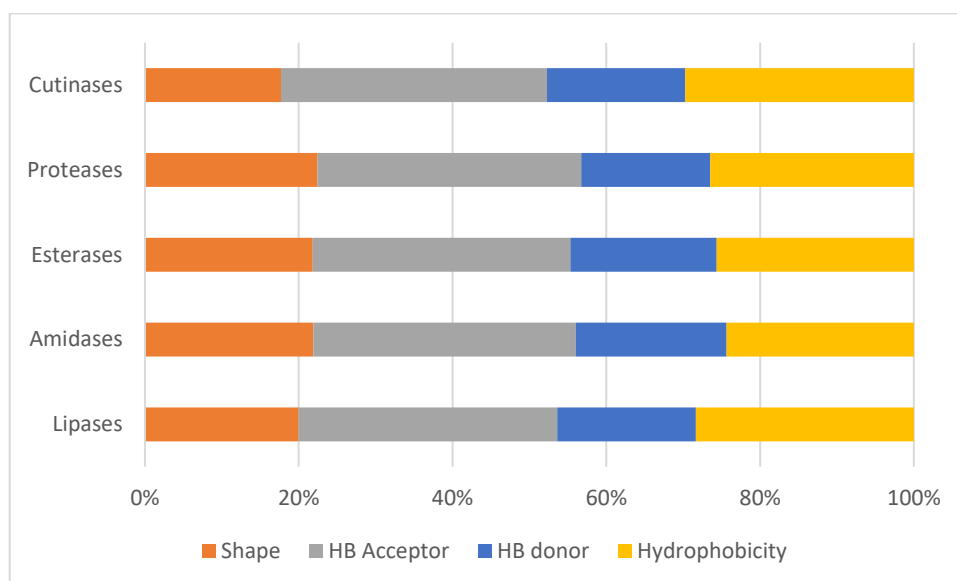
Figure 29. relative contribution to 100% of the given class of the various components in the determination of the model score.

In the cases of a low *model score* (see amidases, Figure 28), the molecular interaction fields (MIFs) associated to the more frequent pharmacophoric interactions in a particular dataset involve mostly the catalytic triad.; the reason lies on its being positioned in the same spatial configuration over the whole dataset. In such cases, the information given by the catalophor

lacks significance, in particular in the cases where the active sites are so heterogeneous that only the fingerprint of the catalytic triad is shown in the MIFs.

### 4.2.2 Analysis of the catalophores

Focusing on the catalophores calculated for each serine hydrolase sub-family (Figures 30-32), it results that cutinases are the more homogeneous class in the whole dataset used in this study. The S-Score value (Figure 27) for the mentioned class is 0.660, higher than the other classes. These enzymes are similar in terms of shape and molecular weight and are all able to hydrolyse cutin with the exception of structure 4WFI for which an evidence has not been proved yet[65]. Accordingly, this structure shows the lower score within the whole class. Another particular case is 4PSE, a cutinase where, atypically, a lid is expressed and surfactants are important for its catalytic activity[66].
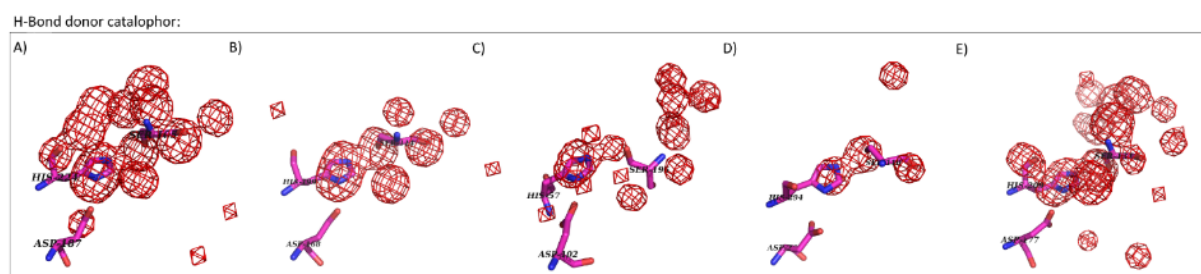
Figure 30. Catalophores obtained with O probe (H-Bond donors): A) lipases, B) estrases, C) proteases, D) amidases, E) cutinases.
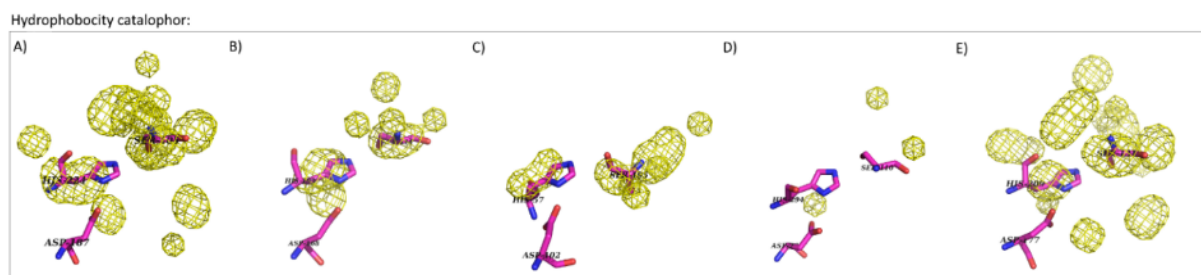
Figure 31. Catalophores obtained with DRY probe (hydrophobicity): A) lipases, B) estrases, C) proteases, D) amidases, E) cutinases.
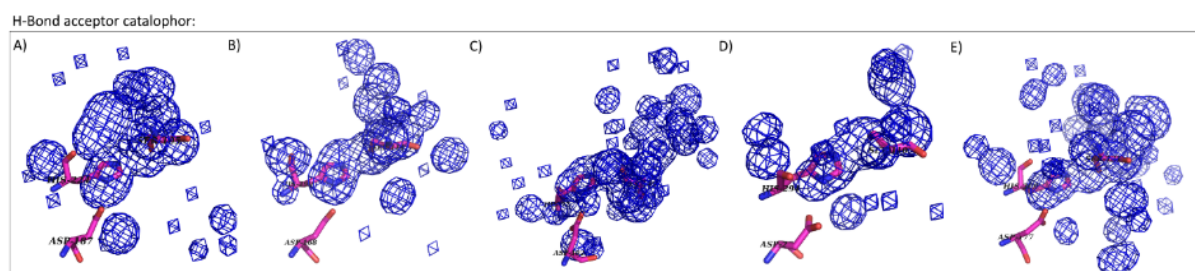

Figure 32. Catalophores obtained with N1 probe (H-Bond acceptors): A) lipases, B) estrases, C) proteases, D) amidases, E) cutinases.

Cutinase 1 structure (cutinase 1 from *Thermobifida cellulosilytica*, referred also as Thc_cut1) was produced by homology modelling from 4CG1 (cutinase from *Thermobifida fusca*) and shares with it the 99.23% of the sequence, the only differences are the amino acids 19 and 137 (Arg and Ser in 4CG1, Ser and Thr in Cut1)[6]. This sequence homology is reflected in the similar score associated with the two enzymes (Figure 27, E).

Cutinases vs esterases

A comparison between Thc_cut1 and 4OYY (*Humicola insolens* cutinase, referred also as HiC) focused on the score returned by the calculation shows that the two enzymes have a low analogy with the catalophor of cutinases, even though belonging to the same class (E.C. 3.1.1.74). In this respect, a precedent study based on sequence alignment demonstrated that the two aforementioned enzymes have only a 9% identity[6]. The same study, aimed to shed light on the nature of cutinases, pointed out that the physicochemical features of the active site of the cutinases Thc_cut1 and HiC have some common features shared by both lipases and esterases. Cutinases are, in fact, able to hydrolyse synthetic esters and emulsified triglycerides. Similarly to lipases and esterases, cutinases can catalyse esterification an transesterification reactions in low water activity media. To clarify such behaviour, a direct comparison between the catalophor of cutinases and esterases has been carried out and the single probe components were studied (Figure 33).
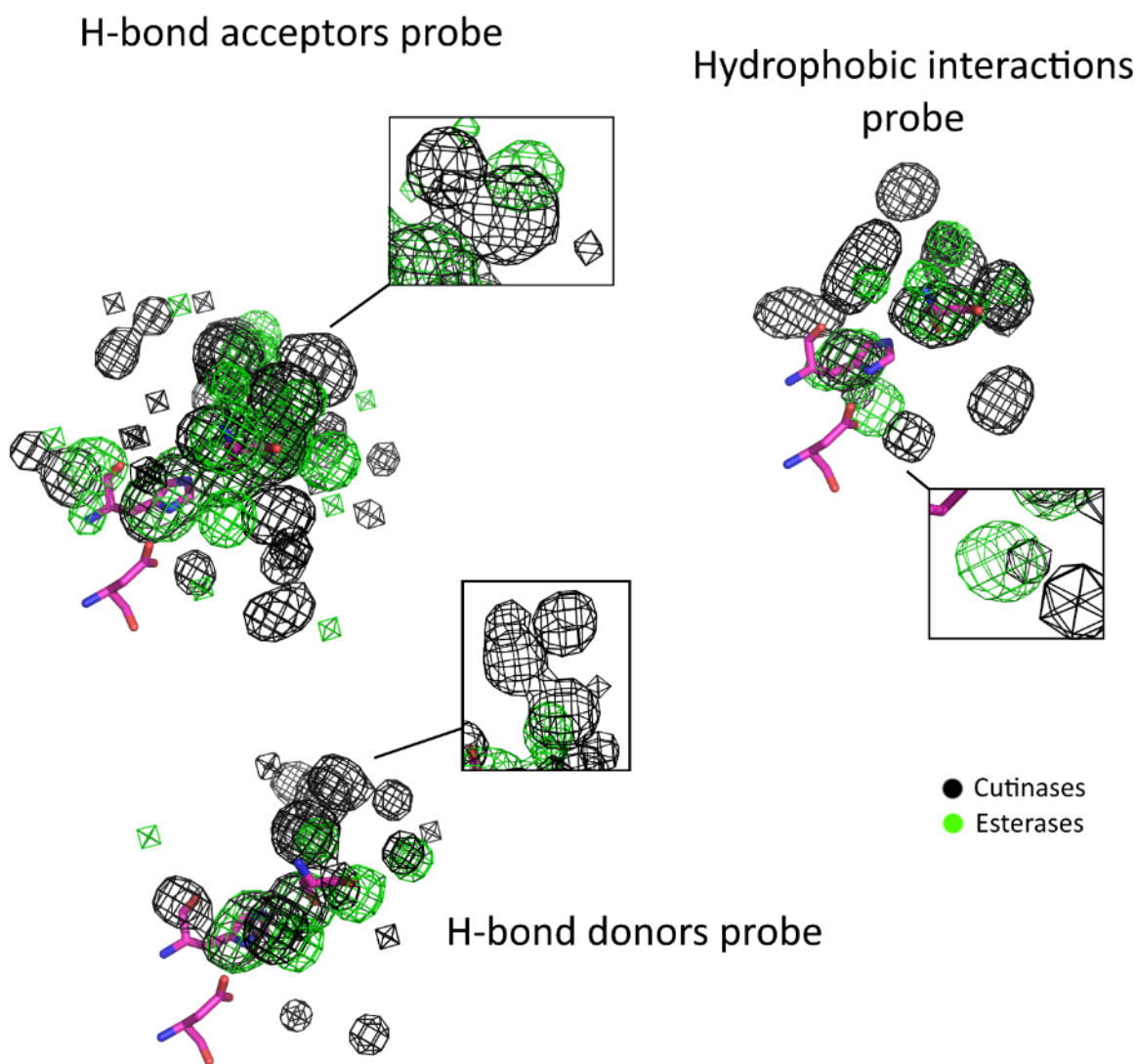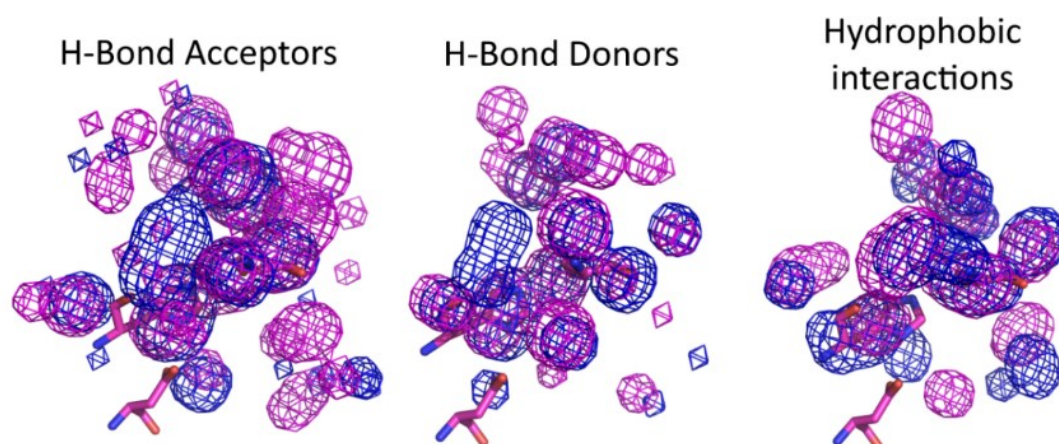
Figure 33. Superimposition of the catalophores of cutinases and esterases

Common MIFs of lipases and cutinases are mostly overlapping and the catalophor of cutinases is slightly more populated. A visual comparison with esterases is not very informative because of the low *model score* of esterases just like in the case of amidases; in these cases, the catalophor covers only the catalytic triad and on the oxyanion hole because of its being conserved among the processed structures. For this reason, the more informative catalophor of cutinases can hardly be compared with esterases.

Cutinases vs lipases

Because of the similar model score between cutinases and lipases, these two classes can be easily compared (Figure 34). The two catalophores are pretty different, the common fields centred on catalytic Ser and His are conserved, but the surrounding areas present substantial differences. In principle, it can be said that the cutinases share more similarity with esterases rather than the lipases. This conclusion is compatible with the higher structural analogy

between cutinases and esterases, due to the lack of a lid covering the active site and to the hydrophobicity of the natural substrates.

Figure 34. Superimposition of cutinases and lipases catalophores. Purple: cutinases; blue: lipases

Thc_cut1 comparison with CaLB

A more accurate comparison between CaLB and Thc_cut1 has been carried out to evaluate the different and shared features highlighted by the MIFs of the tested chemical probes. The picture of the MIFs centred on the active site of the two enzymes allows locating the parts of the active site where the physicochemical environment created by the aminoacidic residues is conserved or different between the two enzyme structures. As a visual example, it is here provided the structure of Cutinase 1 with all its catalophores (Figure 35) which will be dissected in shared and conserved parts with CaLB in the next picture (Figure 36).
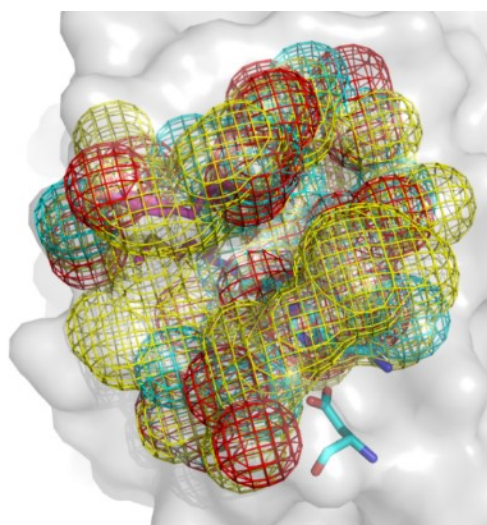
Figure 35. A comprehensive picture of the catalophores of cutinase in superimposition with cutinase 1 structure. Red: H-bond donors; yellow: hydrophobicity; cyan: H-bond acceptors. The cavity defining the active site is clearly visible.
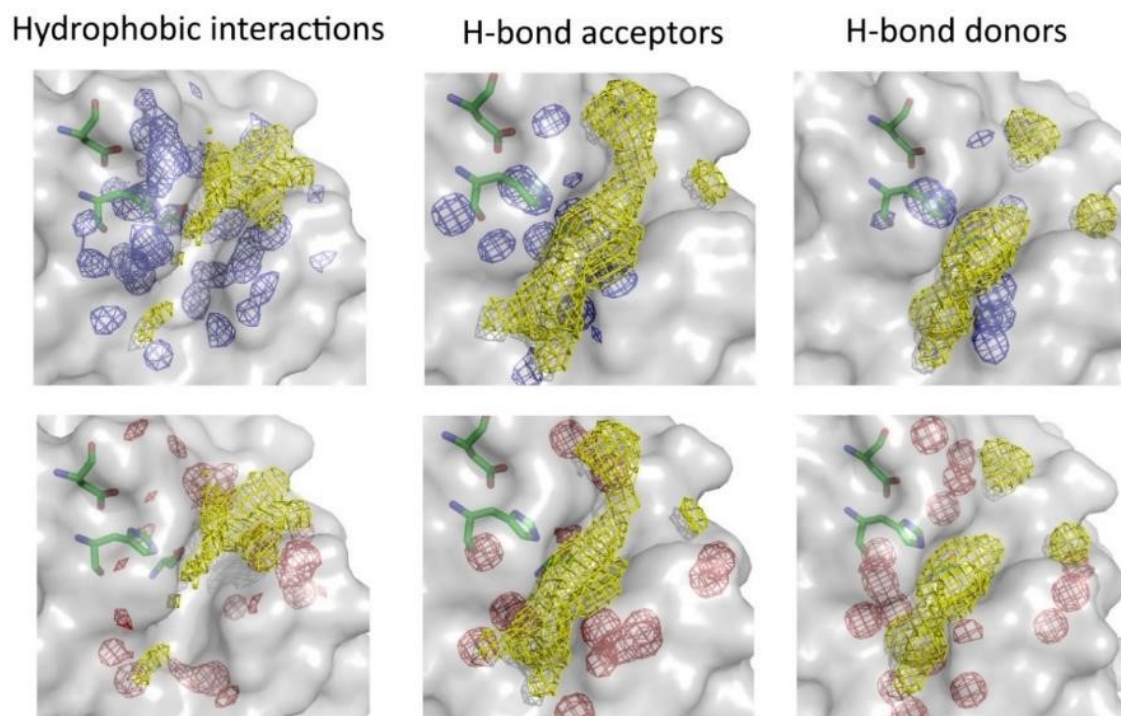
**Figure 36.** MIFs of cutinase 1 conserved (blue) and absent (red) in CaLB structure. The representation takes into account hydrophobic interactions and H-bond capabilities. The reference structure is cutinase 1, surface and catalytic triad are visible. The zones potentially occupied by functional groups of the substrate matching the mentioned probe are indicated in yellow and are represented by pseudoMIFs.

It is noteworthy that the hydrophobic interactions established in Figure 36 are very similar between CaLB and Thc_cut1, in that specific case the shared MIFs (blue grids) are widely represented. It can be argued that the great analogy of the catalytic sites in terms of hydrophobicity makes Thc_cut1 very similar to CaLB with regards to the nature of the accepted substrates and, at the same time, it is able to accept larger substrates because of the more superficial active site.

CaLB and Thc_Cut1 comparison with other serine hydrolase subfamilies

Due to the atypical lipase nature of CaLB (absence of the lid) which bring it near to the esterases in the UPCA model (Figure 22), a comparison between its MIFs and the ones of other serine hydrolases was carried out (Figure 37-38-40). The same procedure has been followed also for Thc_cut1. As stated above, the models of esterases and amidases are of hard interpretation and are less informative than the one of lipases because of the less populated catalophores.
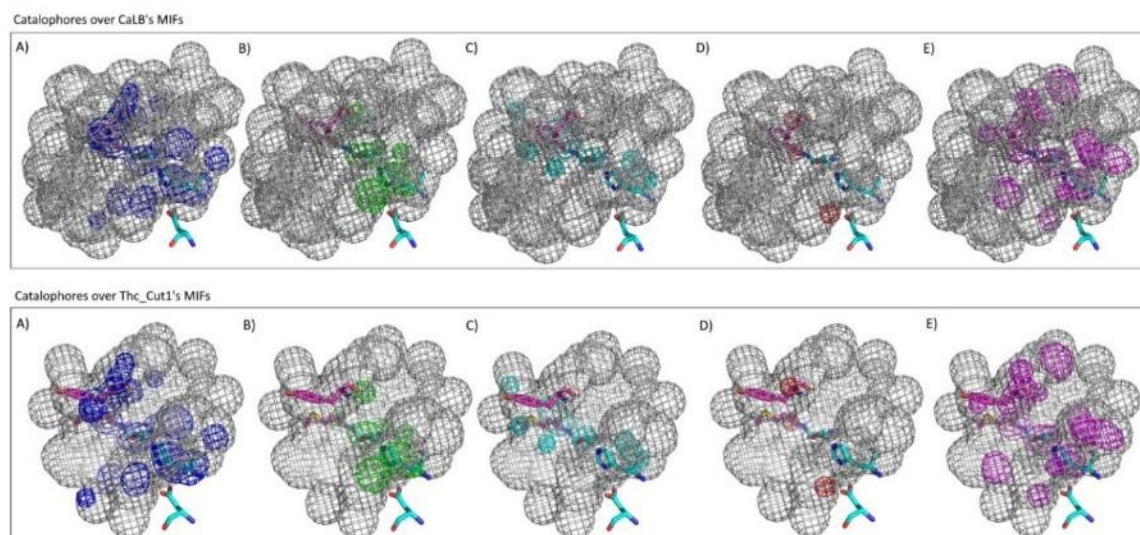
Figure 37. Hydrophobicity catalophor superimposed with CaLB and Thc_Cut1 MIFs. A) lipases B) esterases C) proteases D) amidases E) cutinases.

Focusing on the DRY probe, representing the hydrophobic interactions, no substantial differences amongst Thc_cut1 and CalB MIFs could be detected comparing them with other serine hydrolases subclasses. The superimposition is very good in all the cases.
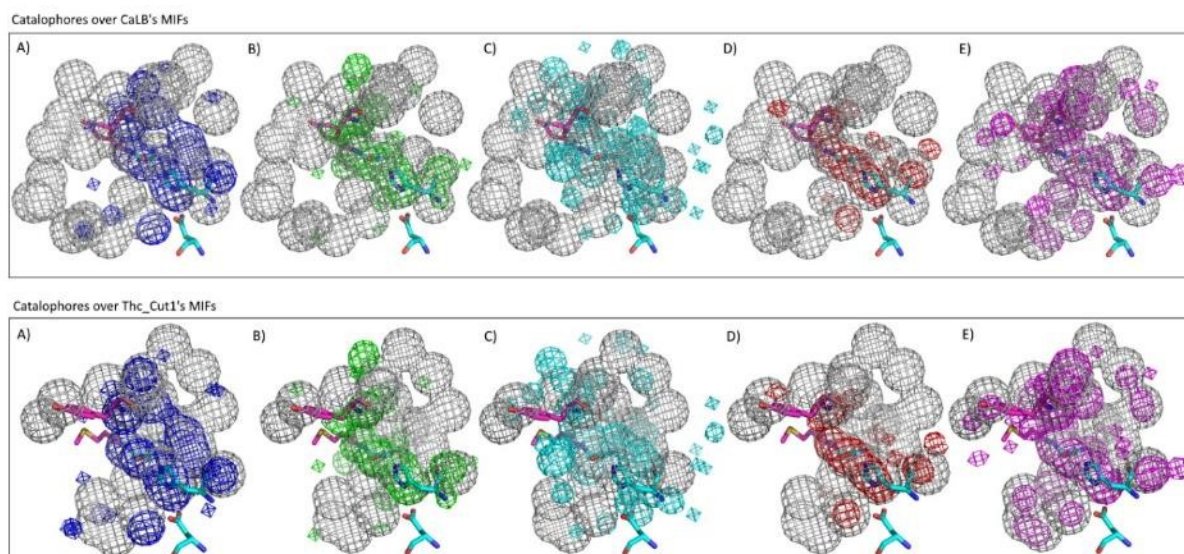
Figure 38. H-Bond acceptor catalophor superimposed with CaLB and Thc_Cut1 MIFs. A) lipases B) esterases C) proteases D) amidases E) cutinases.

The analysis of N1 probe, reflecting active site zones with H-bond acceptor capabilities, points out some noteworthy differences between the studied enzymes. With regards to the catalophores of lipases, esterases and amidases, in the case of CaLB there is no
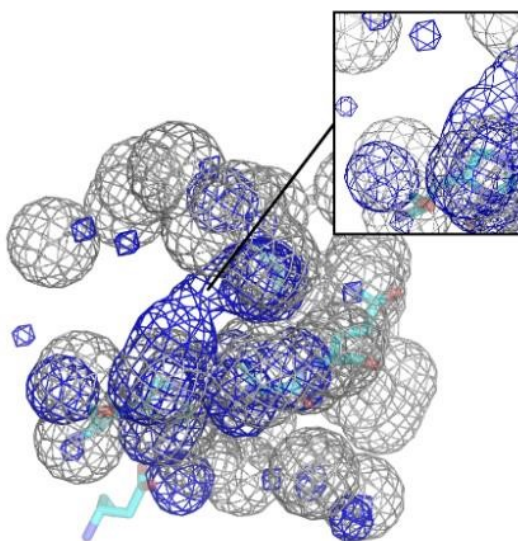
correspondence between its MIFs and the catalophor in some zones very close to the active site, this is more evident in the case of lipases (Figure 39).

However, on esterases and cutinases, the differences with CaLB are detectable in peripheral zones that may not be involved nor in the catalytic mechanism neither in the substrate binding. The aforementioned behaviour could be an evidence of the fact that CaLB has more shared features with esterases and cutinases rather than lipases.

Thc_cut1 MIFs are obviously highly superimposed with cutinases and there is also a good overlapping with esterases and lipases.

Figure 39. CaLB catalytic triad superimposed with H-bond acceptors component of lipase catalophores (blue) and CaLB H-bond acceptors MIFs (grey).In highlight the zone in the proximity of the active site where there is no correspondence between catalophor and MIFs.

The catalophor with the worst alignment with both enzymes is the one of proteases. This observation is confirmed by the UPCA model (Figure 22), where proteases are clearly separated from the other serine hydrolases.

A very similar behaviour to the one reported for H-bond acceptors, is present also in H-bond donor capabilities (O probe). An important note is the poor superimposition on certain portions near the oxyanion hole of Thc_cut1 on the esterase catalophor.
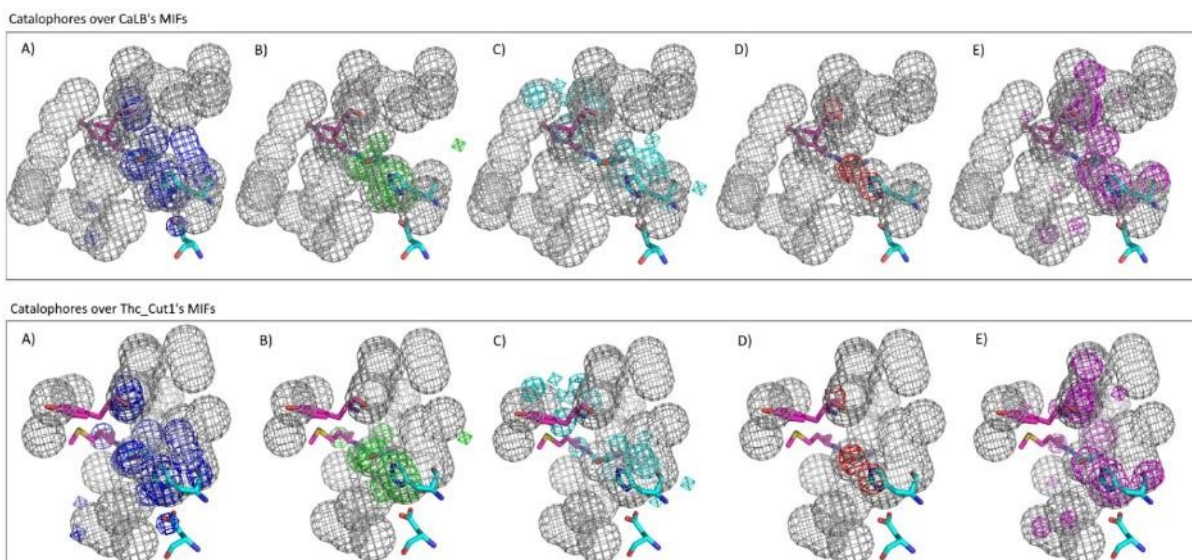
Figure 40. H-Bond donor catalophor superimposed with CaLB and Thc_Cut1 MIFs. A) lipases B) esterases C) proteases D) amidases E) cutinases.

Thc_cut1 and TLL comparison with lipases

The inclusion of Thc_cut1 in the lipase model (Figure 27, F) enables to directly compare this particular cutinase in a dataset of lipases in order to see how the outlier enzyme would fit on it. Looking at the model score value (0.616) of the above-mentioned model it is clear that this operation does not perturbate the value of the original model (0.621). For this reason, it can be concluded that Thc_cut1 has a minimum disturbing effect on the model, validating the hypothesis that there are shared features between the active site of Thc_cut1 and lipases, in particular CaLB.

Another conclusion that can be driven involves 1DTE and 1TCA, respectively *Thermomyces (Humicola) lanuginosa* lipase (TLL) e *Candida antarctica* lipase B (CaLB). TLL is a classical lipase exposing a lid that in the studied structure is in open conformation, a lid structure is not present in CaLB. The fact that the scores of the two enzymes are similar means that the TLL active site in open conformation has wide shared features with CaLB. This evidence shows the rational basis of the proximity of these enzymes in the UPCA model (Figure 22).
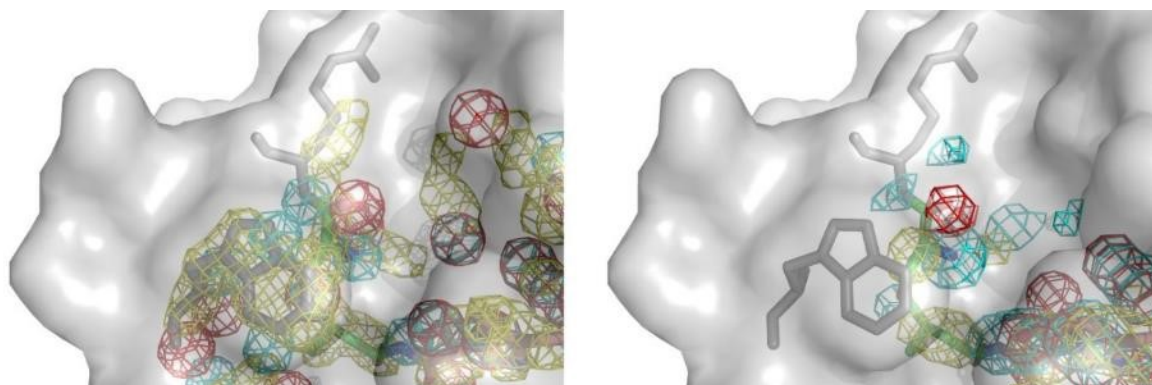
Figure 41. Active site of TLL with lid-forming amino acids indicated in grey sticks. On the left: MIFs of the enzyme. On the right: lipase catalophor. Yellow: hydrophobic interactions; red: H-bond donors; blue: H-bond acceptors.

By comparing the MIFs of TLL and lipase catalophor (Figure 41) it is clear that the mostly hydrophobic interactions given by lid-associated residues (R84 and W89)[67] are not represented in the catalophor, leading to the conclusion that the presence of a lid in that position is not a feature strictly required for classifying an enzyme as a lipase.

Comparison of lipases and esterases

The lipase dataset has the second high *model score* (Figure 27, F) right after the cutinases. All the lipases have in fact a very similar substrate specificity (see Table 8) because of their common activity towards triglycerides, albeit some differences depending on the aliphatic chain length. BioGPS software detects extended interactions for each one of the chemical probes tested because of a common substrate specificity and it is reflected in the higher overlapping of the MIFs of the single enzymes.

A one to one inspection of the scores obtained (Figure 27, F) reveals the presence of an outlier represented by *Candida rugosa* lipase (1CRL). This behaviour is in line with the data obtained from UPCA analysis positioning that enzyme on the cluster of esterases instead of lipases, in the proximity of cholesterol-esterase from *Candida cylindracea* (1CLE). The aforementioned enzymes, albeit the different substrate specificity, have only a 40% sequence homology[4].

Estarases

In the case of esterases, the homogeneity of the dataset is very low because of the different substrate specificity amongst enzymes. Nevertheless, the model score (0.354) is higher than

the one of amidases and H-bond acceptor capabilities (N1 probe) are well represented in the catalophor. In comparison with the class of amidases, it is noticeable a large presence of the components associated with hydrophobic interactions (DRY probe) and with the H-bond acceptors (O probe). This last point, directly correlated to the higher *model score*, shows that the physicochemical environment of the active sites of esterases is constant among the tested enzymes, notwithstanding their scattered-like disposition in the UPCA model; in fact, a more populated catalophor implies an higher analogy between the enzyme structures.

Another noteworthy point is the low score of the esterase from *Pseudomonas aeruginosa* (3KVN), which is also reflected in the UPCA model where this enzyme is located far away from the other esterases (Figure 22). The specific substrates of the above-mentioned enzyme are ramnolipids, but this fact does not classify it as a lipase because of its position in the UPCA model that is far away from them.

Lipases without CaLB

Taking into account the atypical, atypical features of CaLB (absence of a lid), a lipase model without this enzyme was generated in order to verify if CaLB is a perturbative factor in the model (Figure 27, G). Such operation produced in fact a model with a slightly (0.621 vs 0.634) higher score (i.e. more homogeneity among dataset elements) without influencing the relationship among the enzymes. Even though CaLB is missing a lid, it is well fitted within the other lipases. The reason is that BioGPS software does not recognize the lid as a critical feature when generating the catalophor by giving a marginal influence in the scoring procedure at the presence or absence of the lid, in the same way seen for TLL. This fact is noteworthy because demonstrates that the algorithm focuses mainly on the catalytic features of the enzyme rather than secondary lid-like structures.

Amidases

The UPCA model clearly showed that amidases share common feature with esterases because of the large overlapping of the elements in the plot. The subject of distinguishing the particular structural features of amidases and esterases has already been addressed in the literature. The active sites of the 11 amidases used for the catalophor calculation show a strong heterogeneity driven by the different substrate specificity (Figure 27, H). Consequently, the model score (0.219) is the lowest of all the serine hydrolases subfamilies studied. Nevertheless, observing at the shape and disposition of the common molecular interaction fields shown in the catalophor for the singular probes it is possible to conclude

that the interactions where the enzyme residues act as H-bond acceptors towards the substrate (i.e. backbone carbonyl groups) show a common scheme that can be found more frequently if compared with other types of interactions involving this enzyme subfamily. This interaction pattern is visible in the three-dimensional representation of the catalophor (Figure 37-38-40).

Proteases

The protease class occupies its specific position in the UPCA model, separated from the other enzyme subfamilies. The dataset here employed is quite heterogeneous and a visual inspection of the catalophor highlights the presence of numerous and repeated H-bond acceptor interactions (N1 probe, Figure 40). Some of these interactions are likely to be established with carbonyl groups of the substrate.

The two proteases already marked as outliers in the previous UPCA analysis (1QFM and 2XE4) show the same behaviour here, returning the lowest score and so the highest deviation from the average of the dataset (Figure 27, C). The unusual position of these two enzymes is well represented in the global PCA model (Figure 22).

Lipases vs amidases

Lipases catalophor has been directly compared with amidases (Figure 42). As it was pointed out for cutinases/esterases comparison, the low model score of amidases leads to a catalophor where the represented MIFs are mostly positioned over the catalytic triad, being a common behaviour for all the elements of the dataset.

The graphical and score analysis shows that the hydrophobic interactions in lipases play a more important role rather than in amidases, and this is to be expected due to the different nature of the enzymes. Conversely, hydrogen bond acceptors and donors are more represented in amidases.
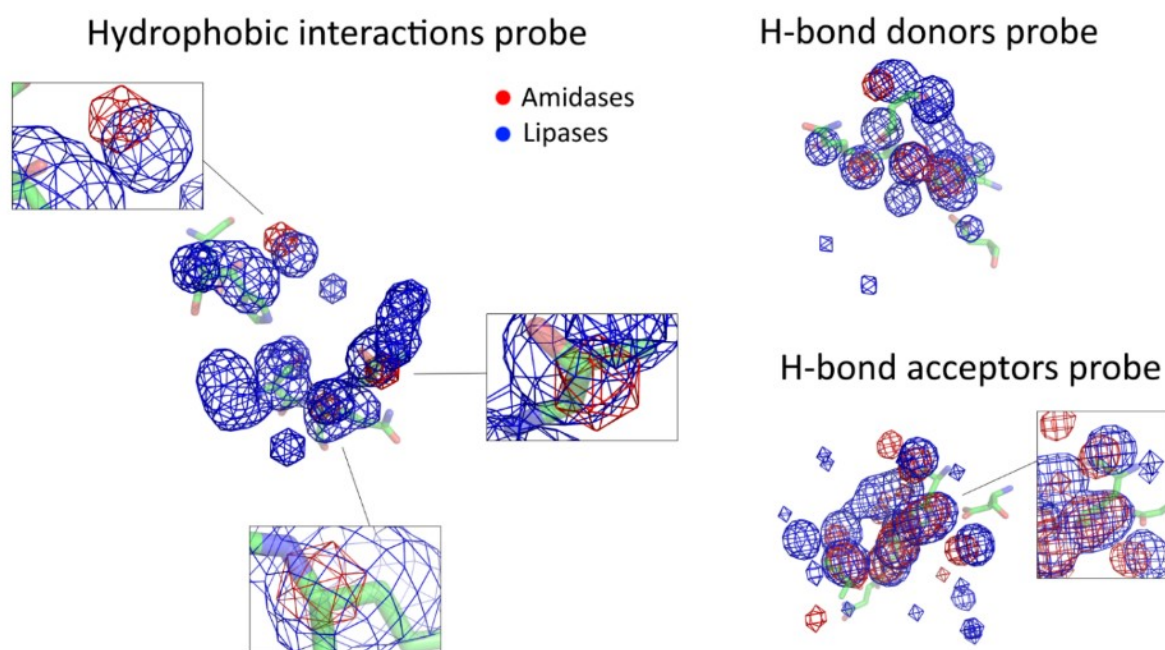
Figure 42. Superimposition of the catalophores of lipases (blue) and amidases(red).

4.2.3 *Analysis of a mutant of Thc_cut1: an application of BioGPS to a case study*

In an attempt to enhance the synthetic capabilities of Thc_cut1 in the field of the production of aliphatic polyesters, the enzyme was modified *in silico* aiming to boost the accessibility of the active site, to allow longer polymeric chains to enter the active site[68]. The residue mutations were proposed by dr. Ferrario and involve 3 amino acids in the entrance of the active site. The chosen strategy was to replace the more hindering residues with other ones with lower steric effects, improving at the same time the efficiency of the immobilization of the enzyme on epoxydic supports thanks to the replacing of a Lys residue next to the catalytic triad that could promote the a wrong orientation of the enzyme in the immobilization phase. The mutated residues were Trp156, Leu158, Lys160 that were respectively replaced with Gly, Ala and Leu.

Activity studies reported in the present work show a total loss of activity, and this behaviour was inspected by the means of a bioinformatic analysis with BioGPS software.

An extensive discussion on the adopted approach to model the *in silico* mutant and to produce the actual enzyme is beyond the purposes of this thesis.

The bioinformatic analysis here proposed, pointed out a possible rational basis of the complete loss of activity.

The comparison between Thc_cut1 wild type and its mutant have been carried out focusing in particular on the pseudoMIFs of the DRY probe, related to hydrophobicity. Hydrophobic interactions are here way more informative than H-bond capabilities. DRY probe pseudoMIFs highlights the zone that a hypothetic hydrophobic substrate could occupy in the active site to establish efficient hydrophobic interactions. In the case of the mutant, the PseudoMIFs appear to be split in two parts (Figure 43).
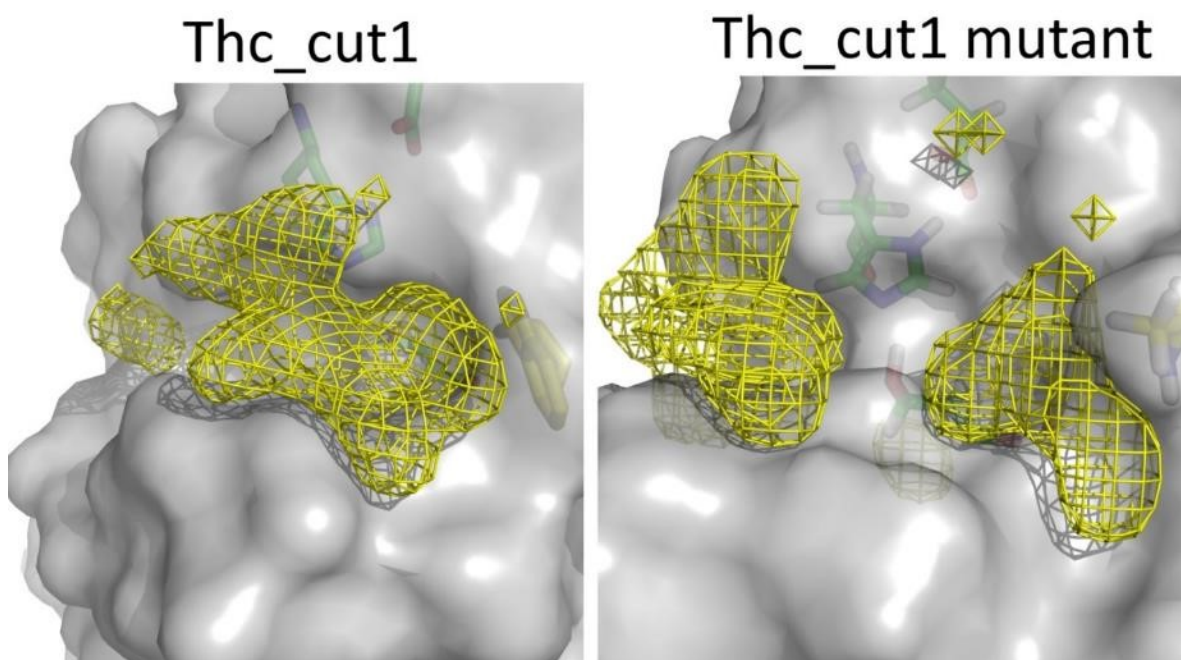
Figure 43. Hydrophobicity pseudoMIFs of Thc_cut1 and its mutant.

In the same way previously used with Thc_cut1 vs. CaLB, the MIFs of the enzymes were compared, shedding light on shared and different features. By means of this operation, the reason for the anomalous disposition of the pseudoMIFs has proven to be the removal of Trp156 residue, responsible for conferring some important hydrophobic interactions with the substrate (Figure 44). Noteworthy, the influence of the other two mutated amino acids were not evaluated because they do not fall in the working cavity due to their relative distance from the active site. Other differences that can be noted are artefacts generated by the process of minimization and dynamization of the mutated enzyme structure and do not need to be taken into account.

A projection of the mutant on the UPCA model did not lead to significant results, the same behaviour was found during the attempt of comparing the scoring of the mutated Thc_cut1 with other enzyme classes (Fig. 45). In this case, the visual inspection turned out to be the most effective way to drive conclusions on the different catalytic activity found for the two enzymes.
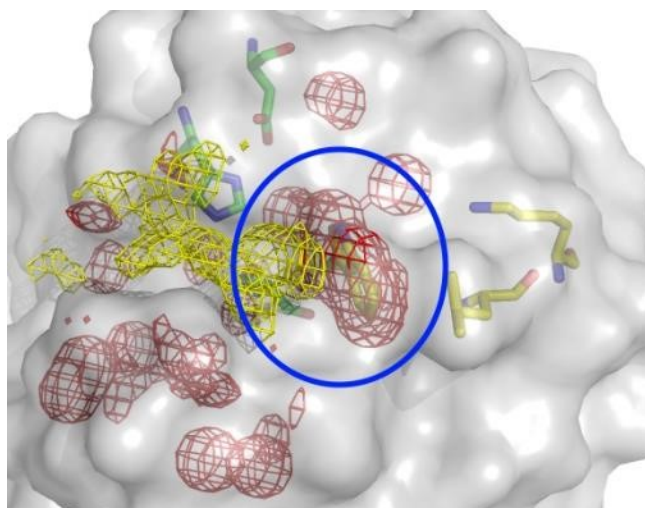
Figure 44. Red: differences between Thc_cut1 and its mutant. Yellow: Hydrophobicity pseudoMIFs of Thc_cut1. Trp156 is highlighted.
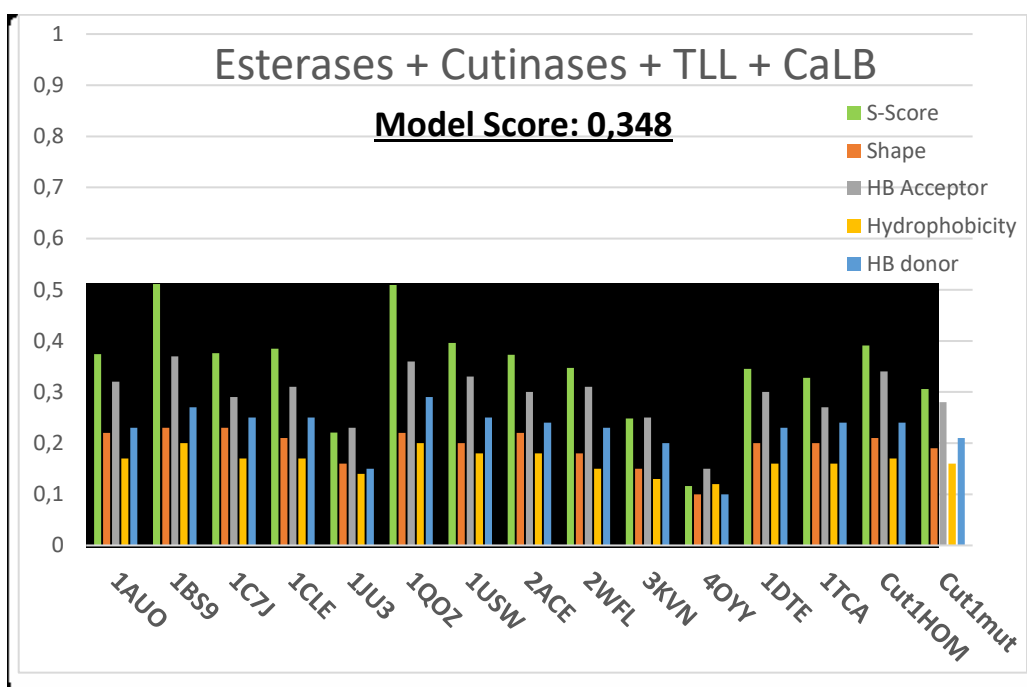
Figure 45. Values obtained with the model comprising esterases, CaLB, TLL, cutinases and Thc_cut1 mutant.

4.2.4 Molecular dynamics to understand the effect of temperature and pressure on CaLB and Thc_cut1

Note: see Annex 2 for the full research paper.

Another step of our investigation was to shed light on the influence of conformational changes in determining the dissimilar behaviour of CaLB and Thc_cut1 at different temperature and pressure. In fact, our research group demonstrated that the activity of

101

Thc_cut1 is higher at low temperature and environmental pressure, while CaLB requires vacuum for achieving maximum yield in polycondensation reactions. For these reasons, Thc_cut1 represents a valid alternative to CaLB, allowing the reaction to take place in mild conditions, increasing the overall sustainability of the biocatalysed process[3]. Molecular Dynamics simulations were run under different conditions of temperature and pressure for 10 ns by using the software GROMACS[69] version 4 OPLS force field[70] definitions and explicit water as a solvent. Three simulations were sun for each enzyme according to the conditions defined in Table 9:

Simulation	Temperature	Pressure
1	300 K	1000 mbar
2	343 K	1000 mbar
3	343 K	70 mbar

Table 9. Temperature and pressure settings of the MD simulations

Each one structure was compared on the basis of RMSF calculated on the Cα of the proteins (Figure 46).
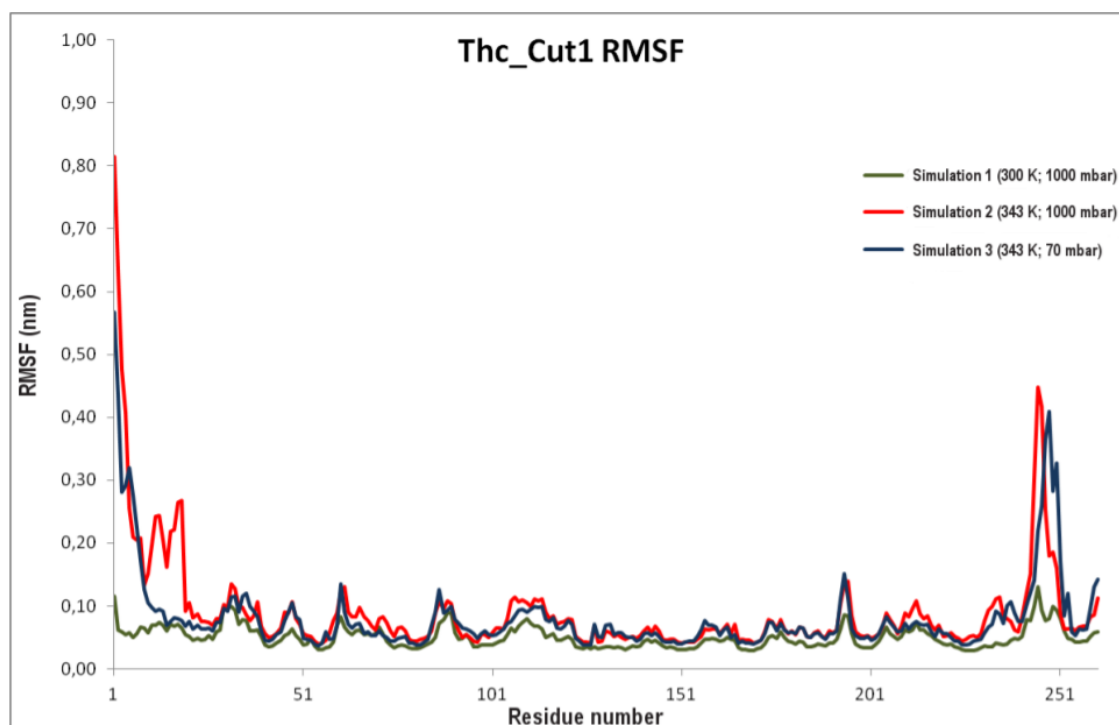
Figure 46: Thc_cut1RMSF analysis and comparison. The 3 different simulation conditions are highlighted in different colours which are indicated together with the simulation conditions in the chart legend.

The RMSF analysis pointed out that the protein has similar behaviour under all the conditions tested, with an obvious higher average mobility at 343 K because of the higher temperature. More interesting differences are noticeable for the terminal part of the peptide chain. The overall conformational stability of Thc_cut1 is also confirmed by observing the superimposed dynamized structures.
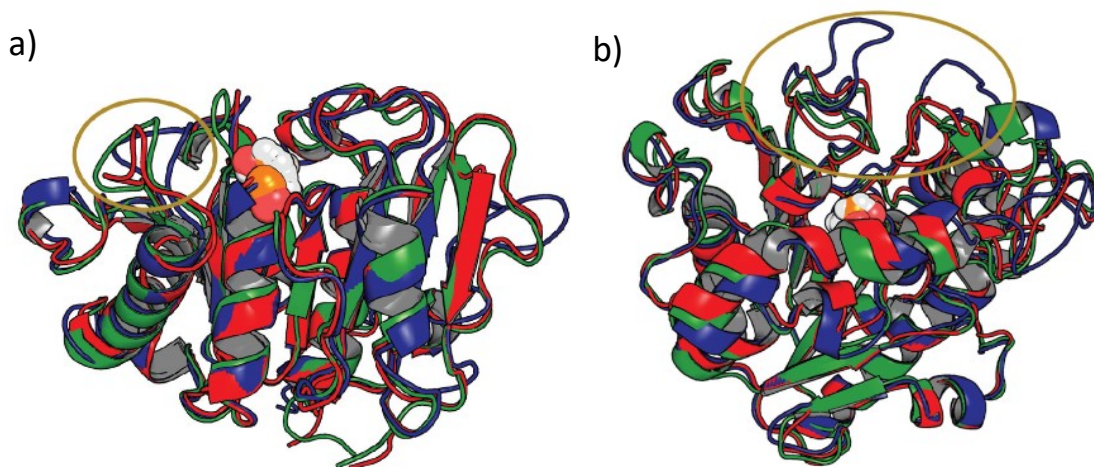
Figure 47. Superimposition of the structures of **a)** Thc_cut1 and **b)** CaLB resulting from the 3 MD simulations, refer to **Table X**: green, conditions 1; red, conditions 2; blue, conditions 3. Catalytic serines are shown in sphere mode; residues 86-91 close to the active site are marked by a circle.

Noteworthy there are also some differences not directly highlighted by RMSF analysis and mainly related to sidechain movements in the area surrounding the active site (residues 86-91, Figure 47). At 343 K and 70 mbar (conditions 3 in table 9) the active site appears to be less accessible than at environmental pressure as a direct consequence of conformational changes involving the said residues, although it is difficult to correlate these observations with the negative effect of high temperature and vacuum on the enzyme. No disruptive conformational changes were observed in the tested conditions. RMSF analysis carried out on Cα of CaLB (Figure 48) showed clear differences in the enzyme mobility, even more evident by superimposing the structures (Figure 47).
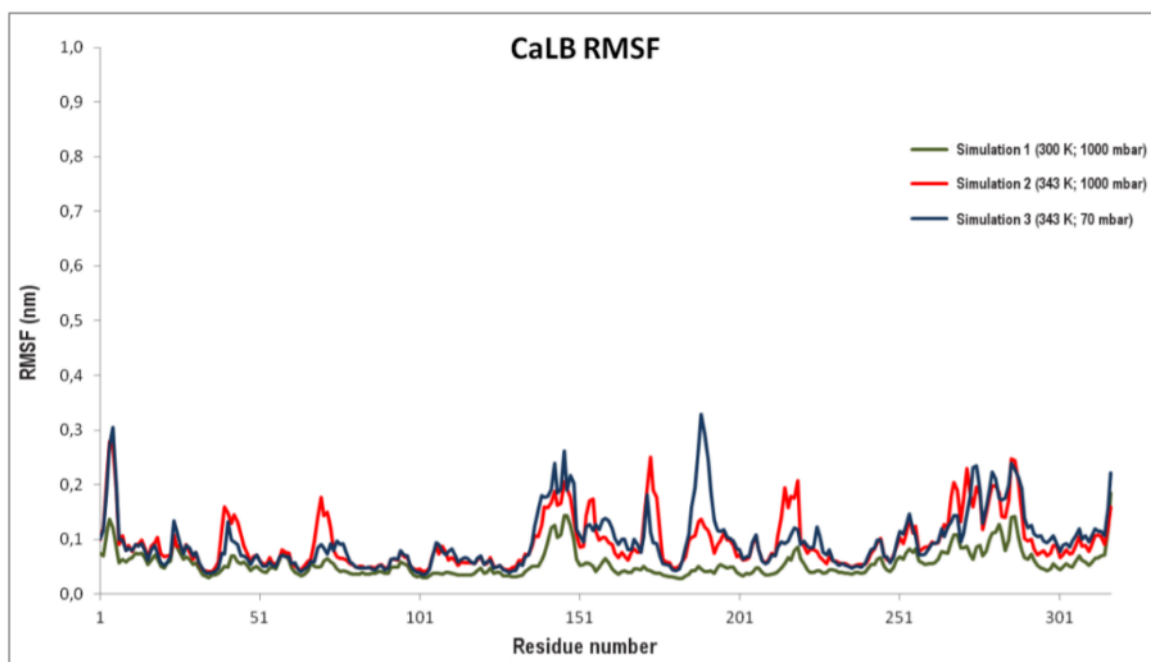
Figure 48. CaLB RMSF analysis. The three MD simulations are represented in different colours together with the simulation conditions in the chart legend.

The protein loops located at the entrance of the active site (residues 138-143 and 187-193) change their conformations on passing from environmental conditions to high temperature and low pressure, enlarging the active site entrance. Notably, this behaviour was not detected in the simulation run at high temperature and atmospheric pressure (343K and 1000 mbar).

These data are in accordance with what observed with the BioGPS analysis that pointed out different H-bond capabilities of CaLB if compared with other lipases. In fact, the effects of temperature and pressure appear to be strictly linked to the role of water inside active sites. The influence of water molecules inside CaLB active site, a critical aspect in biocatalysed polycondensations, has been already discussed by other authors[71,72]. Future engineering strategies of CaLB should follow this direction, while taking into account the positive features displayed by Thc_cut1.

5. Materials and methods

Materials

The solvents were standard laboratory grade. Alcohol, organic acid, and other reagents were purchased from either Aldrich Chemical Co. (Milwaukee, Wisconsin, United States) or Sigma-Aldrich (St. Louis, MO, USA) and used as received if not otherwise specified. Samples of rice husk (Carnaroli type) were kindly donated by Riseria Cusaro (S.r.L.) (Binasco, Italy) and derive from Italian rice varieties. The organic composition, previously determined [10], is the following: 46.5% cellulose, 31.9% lignin and 22.1% of pentosanes (hemicellulose). SiO2 constitutes about 20% of the global weight. The milled RH has a water adsorption capacity of 42.6% w/w, determined by weight difference. Lipase B from Candida antarctica (CaLB, batch LCN02115 with an activity of 4005 U mL^{-1} purchased from Novozymes (Bagsvaerd, Denmark) and Laccase C was purchased from ASA-Spezialenzyme (Wolfenbüttel, Germania)

Milling of rice husk

Rice husk was milled using a Rotor mill ZM 200 (Retsch S.r.l., Bergamo, Italy) according to a procedure already described.14 The raw material was separated by size using sieves of 450 and then 200 mm. The wet particles were weighed and then dried in an oven at 120 °C for 6 h. The milled RH (size 0.2–0.4 mm) had a density of 0.437 g mL^{-1}.

SEM Microscopy

Samples were metallized with the S150A Sputter Coater instrument (Edwards High Vacuum, Crawley, West Sussex, UK) before being observed with the Leica Stereoscan 430i scanning electron microscope (Leica Cambridge Ltd., Cambridge, UK) integrated with an Si detector (Li) PENTAFET PLUS TM, with an ATW TM window (Oxford Instruments, Oxfordshire, England) for microanalysis.

Rice husk moisture determination

A sample of rice husk was weighed in a tared weighing bottle. After drying for 2 hours in the oven at 105 °C followed by cooling in a desiccator in vacuum conditions. The bottle was replaced again in the oven for 1 hour. The process was repeated, followed by cooling and weighing as above for successive periods until constant weight was reached. Moisture content was determined as follows:

$$\%_{moisture} = \frac{m_{wet} - m_{dry}}{m_{wet}}$$

Oxidation of rice husk with sodium periodate

A total of 2.0 g of rice husk (particle size 0.2-0.4 mm) previously washed with a mixture of H2O:ethanol 50:50 (3 x 3 mL) was placed in a syringe with septum. Then, 50 mL of a 0.20 M $NaIO_4$ solution was added and the mixture was allowed to react under stirring on the blood rotator for 22 h in the dark and at 25 °C. The solid support became dark brown. At the end of the reaction, the rice husk was filtered and rinsed with deionized water (3 x 10 mL) until neutrality.

Oxidation of raw rice husk with laccase-mediator system (LMS)

This protocol is referred to the first carbonyl content evaluation here reported and at the covalent immobilization sample obtained with laccase C oxidized, non-AHP rice husk. 500 mg of washed rice husk were washed and put into a 50 mL flask in 10 mL phosphate buffer 0.1 M pH 5. Laccase C (20 U/mL or 100 U/mL) or Novozym S1003 (20 U/mL) were added to the reaction mixture together with 10 mM TEMPO radical (except for one sample). The buffer solution was added to bring the volume at 25 mL and the suspension was stirred for 48 hours at 50 °C. The product was washed with deionized water 5 x 10 mL. The same method was followed with AHP pre-treated samples with a rice husk concentration of 0.2-1.0 U/mg_{RH}.

Functionalization of oxidized rice husk with HMDA diamine spacer

A total of 40 mL of a 0.9 M solution of hexamethylenediamine in methanol was added to rice husk samples and the mixture reacted for 72 h at 25 °C by stirring on an orbital stirrer. After this time, the rice husk was filtered and washed with methanol (2 x 40 mL).

Activation of amine functionalized rice husk with glutaraldehyde

Prior to immobilization, the amine-functionalized rice husk was activated by adding 50 mL of a 1.25% (v/v) glutaraldehyde solution in 0.05 M phosphate buffer at pH 8 and the suspension was allowed to react for 5 h at 25 °C. At the end of activation, the rice husk was filtered and washed with 0.05 M phosphate buffer at pH 8 (2 x 50 mL).

Candida antarctica lipase B immobilization via diamine linker and glutaraldehyde activation

A solution of Lypozyme CaLB 1350 TBU/mL in phosphate buffer 0.5 M pH 8 was prepared. To ensure 10.000 TBU/g_{RH} of enzyme 2.23 mL of this solution were taken and 300 mg of rice husk were added together with 0.5 mL of PEG-3000 solution at the concentration of 2

mg/mL in phosphate buffer. The suspension was put in orbital stirrer for 48 hours at environmental temperature. A sample of the same starting solution was prepared and conserved to determine the protein concentration. After the immobilization, the supernatant was separated and tested with Bradford assay for protein loading determination. The rice husk was then washed with phosphate buffer 6 x 10 mL.

Alkaline hydrogen peroxide pre-treatment of rice husk (ammonium hydroxide)

A set of 500 mg samples of 0.2-0.4 mm washed rice husk were prepared in different flasks. Hydrogen peroxide and ammonium hydroxide were added accordingly to the proportion indicated in the text and the volume was brought to 30 mL with deionized water where necessary. The reaction proceeded for 4 hours in orbital stirrer at 50 °C. Moderate foam production was noticed and manual mixing was occasionally necessary. The products were filtered and washed several times with deionized water until neutrality of the washing solution was reached. Consequently, the products were dried for 6 hours at 120 °C.

Alkaline hydrogen peroxide pre-treatment of rice husk (sodium hydroxide)

1.0 g of rice husk were put in a 100 mL flask. 33.3 mL deionized water were added with 16.7 mL of hydrogen peroxide 30% solution. Approximately 11 mL NaOH 5 M were slowly added to adjust pH at 11.5, the final concentration of hydrogen peroxide in the reaction mixture was calculated to be 8.2%. When pH 10.5 is exceeded, a severe formation of foam was noticed and the reaction became highly exothermic. Manual mixing was often necessary during the first 15 minutes of the reaction. The flask was moved in orbital stirrer and reacted 4 hours at 50 °C. A blank reaction was carried out in the same conditions without the addition of hydrogen peroxide. The products were filtered and washed several times with deionized water until neutrality of the washing solution was reached. Consequently, the products were dried for 6 hours at 120 °C.

Laccase C activity assay with ABTS (2,2'-azino-bis(3-ethylbenzothiazoline-6-sulphonic acid))
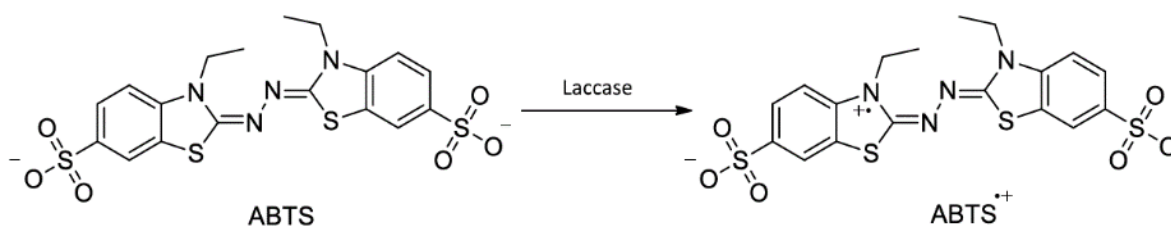
Figure 49. ABTS oxidation by laccase.

ABTS solutions are unstable because of spontaneous oxidation by atmospheric oxygen. The solution must be hence used right away from its preparation. 2 mL of ABTS 0.02 M solution were prepared dissolving 21.9 mg of reagent in pH 3 citrate buffer 0.05 M. A 0.500 mg/mL solution of lyophilized laccase C was prepared in the same citrate buffer and diluted to 0.125 mg/mL. These concentrations were chosen in order to obtain absorbance values within the observable range of the instrument and reaction times in the range of 1-2 minutes. 0.100 mL of ABTS solution 0.02 M and 0.900 mL of citrate buffer were added in a UV/vis spectrometry cuvette and the sample was used as a reference. Wavelength was set at 420 nm and *time drive* mode was selected. The analytical samples were prepared adding 0.100 mL of ABTS solution and 0.850 mL of citrate buffer. Blank value was acquired by registering the absorbance value of this sample. 0.050 mL of enzyme solution 0.125 mg/mL were then added and the sample solution was quickly mixed before putting it in the instrument. The absorbance change caused by ABTS oxidation was monitored for 3 minutes and the experiment was repeated 5 times obtaining the best linear interval between 1-2 minutes with $R^2=1$.
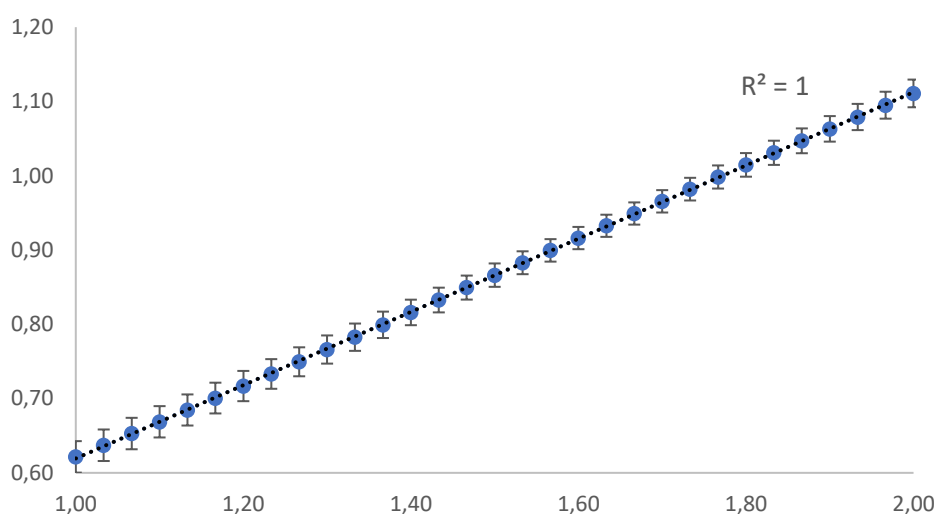
Figure 50. Time/absorbance chart obtained with laccase C activity assay

The activity value as U/mL was calculated using the following law:

$$Activity \; ^{U}/_{mL} = \frac{^{\Delta A}/_{min}}{36} \times \frac{V_{tot}}{V_{enz}}$$

The activity is referred to the starting enzyme solution of 0.125 mg/mL. The activity value for the lyophilized enzyme was calculated to be 2176 U_{ABTS}/g.

Lipase hydrolytic activity assay with tributyrin

The activity of enzymatic preparations was assayed by following the tributyrin hydrolysis and by titrating, with 0.05 M sodium hydroxide (NaOH), the butyric acid that was released during the hydrolysis. An emulsion composed of 1.5 mL tributyrin, 5.1 mL gum arabic emulsifier (0.6% w/v) and 23.4 mL water was prepared in order to obtain a final molarity of tributyrin of 0.17 M. Successively, 2 mL of 0.1 M sodium phosphate buffer (Nap), pH 7.0, was added to 30 mL of tributyrin emulsion and the mixture was incubated in a thermostated vessel at 30 °C, equipped with a mechanical stirrer. After pH stabilization, 20 mg of the immobilized biocatalyst. The consumption of 0.05 M NaOH was monitored for 14 min. One unit of activity was defined as the amount of immobilized enzyme required to produce 1 µmol of butyric acid per min at 30 °C. One tributyrin unit (TBU) of lipase activity was defined as the amount of enzyme which produced 1 µmol of butyric acid per minute under the given assay conditions.

Determination of the Leaching of the Enzymes after Covalent Immobilization

At the end of the test for enzymatic activity, the biocatalyst was removed by filtration and the pH of the suspension was monitored for residual enzymatic activity.

Lipase synthetic activity assay with propyl laurate

The synthetic activity was evaluated with the esterification of lauric acid to propyl laurate using 1-propanol. 6 mmol of lauric acid and 0.450 mL of 1-propanol were put together in a glass vial. The solution was kept at a constant temperature of 55 °C and stirred in an orbital shaker. At time t=0, 0.1 mL were withdrawn and weighted. 50 mg of biocatalyst were added and the mixture was stirred for 15 minutes taking 0.1 mL of solution at regular intervals, weighted and diluted with 7 mL of ethanol under continuous stirring. 3 drops of phenolphthalein were added. The samples were then titrated with 0.1 M KOH in ethanol until colour change. An enzyme unit was defined as the amount of biocatalyst required to produce 1 µmol of propyl laurate per min at 55 °C in solvent-less conditions. The acid value at a given time was calculated with the following law:

$$AV = \frac{MM_{KOH} \times M_{KOH} \times V_{KOH}}{m_{sample}}$$

MM_{KOH} is the molecular mass of potassium hydroxide, M_{KOH} is the molarity of the KOH solution in ethanol and V_{KOH} is the mL volume of solution used for the titration, m_{sample} is the mass of the sample at a given time. The percentual formation of propyl laurate was calculated with the following law:

$$\%_{propyl\ laurate} = 100 \times \frac{AV_0 - AV_t}{AV_0}$$

Propyl laurate quantity was calculated as follows:

$$\mu mol_{propyl\ laurate} = \frac{\%_{propyl\ laurate} \times 6000}{100}$$

The activity value was calculated as follows:

$$Activity = \frac{\mu mol_{propyl\ laurate}}{m_{biocatalyst} \times t}$$

The t value is the time in minutes at which the sample was taken.

Carbonyl content assay with tributyrin

The content of carbonyl groups was determined by reaction with hydroxylamine chlorhydrate. Carbonyl groups react with the hydroxylamine forming an oxime and the hydrochloric acid released was then titrated with sodium hydroxide. 25 mL of a 0.25 M solution of hydroxylamine and chlorhydrate, the pH was brought to pH 3.20 ± 0.05 with HCl. About 200 mg of rice husk were added to the solution and the suspension was allowed to react for 2 hours under stirring. Consequently, the reaction mixture was titrated with 0.1 M NaOH to bring the pH back to 3.20 by neutralization of the hydrochloric acid formed. At the end of the titration, the supernatant was separated by filtration and the rice husk was dried for 6 hours in the oven at 120 °C to determine the exact anhydrous weight of the analysed sample. To remove any interferences, a blank reaction consisting of non-oxidized rice husk was treated with the same method. The content of carbonyl groups was calculated using the following formula:

$$mmol_{CO}/g_{carrier} = \frac{V_{NaOH} \times C_{NaOH}}{m_{dry\ carrier}}$$

Where V_{NaOH} is the volume in mL necessary to adjust the pH of the reaction mixture back to 3.20, C_{NaOH} is the concentration of NaOH and $m_{dry\ carrier}$ is the mass of the dried samples.

Enzyme structures used in the bioinformatics analysis

All the protein structures used as the dataset for BioGPS model generation were retrieved from the Protein Data Bank[62] (PDB) and pre-processed by using the software PyMOL. All molecules but the proteins were deleted (i.e. water molecules, inhibitors, glycosylation residues, etc.). The original protein structure coordinates (from the PDB) were used as inputs, without any previous superimposition. The same approach was used for the structure

of *Humicola insolens* cutinase (HiC)[73] (PDB code 4OYY) whereas the structure of cutinase from *Thermobifida cellulosilytica* (Thc_cut1) comes from an already published homology model[6]. In the same way of Thc_cut1, his mutant has underwent dynamization, see following paragraphs.

Structure alignment procedure

PyMOL alignment was carried out on alpha-carbons of the catalytic triad and oxyanion hole residues using the function pair_fit. The target residues for lipases, amidases, esterases and proteases were retrieved from a previous study of Gardossi and co-workers[4]. In the case of cutinases, the aligned residues are reported in Table 10.

Enzyme class	PDB code	Catalytic triad	Oxyanion hole	S-Scores in cutinases model
Cutinases	1AGY[74]	H188/S120/D175	S42/Q121	0.711
	3DCN[75]	H204/S136/D191	S57/Q137	0.346
	3QPD[76]	H194/S126/D181	S48/Q127	0.792
	3WYN[77]	H247/S169/D215	M170/Y99	0.899
	4CG1[78]	H208/S130/D176	M131/Y60	0.979
	4OYY[73]	H173/S105/D160	-	0.370
	4PSE[66]	H229/S164/D216	T90	0.538
	4WFI[65]	H254/S176/D222	-	0.328
	Thc_Cut1[6]	H209/S131/D177	Y61/M132	0.975

Table 10. residues used for cutinases structure alignment

In the particular case of the 3DCN (*Glomerella cingulata* cutinase) structure, the acid-base catalyst His 204 was not considered during the alignment procedure because its position in the catalytic machinery is very unusual, as reported by Nyon et al. [75]. Therefore, including this residue in the alignment would have turned out in a misalignment of the whole active site due to the perturbative effect of that His residue.

To avoid sub-optimal alignment between pdb structures, the best way for achieving productive alignment turned out to be the PyMOL-guided superimposition of structures, which was performed considering the critical residues for the catalytic activity, namely the like the catalytic triad and the oxyanion hole. Whole-enzyme based alignment was not possible due to the heterogeneity of the protein structures.

The enzyme active sites were analysed by calculating the GRID molecular interaction fields in order to provide a detailed description of molecules. GRID probes H, O, N1 and DRY (which represent respectively the shape, H-bond donor and acceptor capabilities, hydrophobic interactions) were used to investigate the protein structure.

BioGPS model

The BioGPS (Global Positioning System in Biological Space) model was obtained as already published[21] using BioGPS software version 16.01. BioGPS is based on the "Common Reference Framework" composed by two main steps: the characterization of the protein active sites and their comparison. The active site of each enzyme was automatically detected by the FLAP algorithm[60]. First the algorithm reduces the complexity of the pseudo-MIFs selecting a number of representative points using a weighted energy-based and space-coverage function. Then it generates all possible combinations of four points; each combination is termed "quadruplet". All possible quadruplets for each mapped active site were generated and stored into a biofingerprint (bitstring). Each active site was then compared within the Common Reference Framework using an "all against all" approach where each enzyme active site is compared with itself and with all the other enzyme active sites. At the end, the algorithm generates a set of Tanimoto scores[79] represented by square matrixes, namely a series of probe scores (one for each original probe) together with a global score. The set of Tanimoto scores was used as an input for the UPCA algorithm which generated the final BioGPS statistical model by generating the multidimensional space (Principal Components – PCs) which differentiated each enzyme active site on the bases of their similarities and differences.

Projection of cutinases

The two cutinases Hic and Thc_cut1, were projected into the BioGPS model. These two enzymes were processed as described in the previous section. Each cutinase was compared with itself and with all the other enzymes. Finally the Tanimoto scores[79] (see the ESI† for details) were used for the projections of the two cutinases into the BioGPS model computed for the 41 ser-hydrolases.

Catalophor calculation

FLAPpharm, the algorithm used for this purpose, offers the possibility of aligning autonomously protein structures before the catalophor calculation, using as a target the whole working cavity defined on the enzyme surface that comprises active site and surrounding area. This kind of work-flow turned out to be ineffective due to the fact that maximum cavity overlapping could not correspond to efficient catalytic residues superimposition. For this reason, structure alignment was user-guided according to the procedure described above.

The preliminary mapping of the working cavity on the surface of the enzymes that defines the working-cavity. FLAPsite algorithm – using the GRID force field - was exploited for this purpose. After proper structures alignment, the centroid of the cavities were placed in the catalytic serine of the protein structure, and two values defining the shape and size of the cavities (parameters called *extension* and *thickness*) were set to 9 and 9, a value slightly higher than the one used in our previous work. The size of the cavities was increased in order to achieve a broad mapping of the catalophoric zones. Some other attempts of cavity generation with different size and shape were performed, leading to irregularly shaped cavities or to accessory lobes that have to be discarded.

FLAPsite algorithm was executed for each enzyme and the output cavities were saved as separate pdb structures consisting of a set of points with specific coordinates.

After cavity definition, FLAPpharm catalophor calculation was performed for each sub-class of hydrolases and for some mixed datasets, always skipping the algorithm-based alignment step.

The output of the algorithm is composed by the pseudoMIFs for each enzyme and by a pdb structure containing the catalophor MIFs represented by the common fields between the MIFs of the enzymes in the dataset. The outputs - deriving from GRID-based force field mapping with the determination of type and energy of interactions - are presented in terms of the probes employed: H probe takes into account active site shape; O probe reveals the H-bond donor capabilities; N1 probe the H-bond acceptor ones; DRY probe evaluates the hydrophobic interactions.

Together with the pdb files generated by the algorithm and containing the grid cages, a scoring file containing values called "S-score" global and split in the probe components values are generated. Where necessary, FLAPpharm command-line was used to compare pairwise protein structures in terms of similarity and differences of molecular descriptors i.e. intersection and difference MIFs.

All the pdb files obtained were processed in PyMOL using the *gridiso* plugin. Energy cutoff was set to -0.1.

Molecular dynamics

The structure of CaLB (PDB 1TCA), Thc_cut1 (homology model) and his mutant were protonated at pH 7.0 using the PDB2PQR[80] server based on the software PROPKA[81]. Subsequently, each protonated enzyme structure was defined into an OPLS force field[70]. Each protein was inserted in a cubic box of 216 nm^3 and solvated with an explicit solvent

(TIP4 water type)[82]. Thus, each enzyme system was minimized using the software GROMACS[69] version 4 using the steepest descendent algorithm for 10,000 steps. Afterwards, each enzyme was simulated under three different conditions: (1) 300 K and 1000 mbar; (2) 343 K and 1000 mbar; and (3) 343 K and 70 mbar. Each MD simulation was performed for 10 ns with the software GROMACS version 4 defining a NVT environment; the Particle Mesh Ewald (PME) algorithm[83] was used for the calculation of electrostatic interactions, the v-rescale algorithm[84] for temperature and the Berendsen algorithm[84] for pressure were also employed. The outcome of each MD simulation was analysed by calculating the Root Mean Square Fluctuation (RMSF), which indicates the average movement of the protein residues during simulation. The calculation was performed on the protein Cα using the g_rmsf tool of the GROMCS 4 package.

6. Conclusions

This study reports an overview on the potential of rice husk as an inexpensive, although chemically complex and mechanically resistant biomaterial. Investigations on the optimization of the immobilization protocol have been carried out by means of enzymatic oxidative routes. The data here reported show that there is the potential for moving towards a new paradigm in enzyme immobilization, replaced the petrochemical-based resins commonly used for these purposes, reducing the environmental impact of biobased chemical industry. Keeping in mind that 10% of the bulk chemical market of today, being about 330 Mton per year, will be manufactured using immobilized enzymes in the next few decades at a cost of 100 US $ per ton, this would mean a turnover of 3.3 billion US $ (http://www.unep.org/yearbook/2014/). In addition, in solvent-free systems that can increase the environmental sustainability of chemical processes, there is the common issue of mass transfer limitations caused by the high viscosity of the reaction medium. In these cases, low protein loading on the carrier is an advantage because using a large number of enzymatic units concentrated in a small volume would turn into a low process efficiency. This is the reason why obtaining stable and covalent biocatalyst formulations with low specific activity has to be seen as an advantage because the enzyme is "diluted" on a wider surface enabling to overcame mass transfer limitations. In the present study we have demonstrated the applicability of functionalized rice husk as a renewable carrier for the covalent immobilization of two asparaginases and *Candida antarctica* lipase B. Moreover, we have

developed an efficient protocol for the delignification of rice husk, thus obtaining an increased hydrophilicity of the material while preserving its robustness. The pre-treatment with hydrogen peroxide in alkaline conditions followed by biocatalysed cellulose oxidation led to an innovative type of functionalized carrier, characterized by low density and high water retention capacity. These properties enabled the enhancement of the activity of the immobilized lipase (25-30 %) in comparison with the raw-rice husk . Notably, the activation of rice husk using sodium periodate has been replaced by the oxidation by laccases, laying the foundations for the fully renewable synthesis of biobased polyesters. The possibility of immobilizing enzymes on large volumes of inexpensive renewable carriers opens new perspectives for overcoming the environmental impact of fossil-based carriers, while boosting the economic viability of processes nowadays hampered by the high cost of immobilized biocatalysts.

Secondly, a thorough structural study of serine hydrolases was carried out based on Unsupervised Pattern Cognition Analysis (UPCA) of GRID-based BioGPS descriptors. BioGPS allowed to project a selection of cutinases on a model previously published by this research group, confirming that the pre-organized physicochemical environment in the active site of Cutinase 1 from *Thermobifida cellulosilytica* is very similar to the one of *Candida antarctica* Lipase B, while offering increased capabilities in terms of the size of the substrate accepted, thanks to a superficial and wide active site. This method was used also to calculate the "catalophor" of different serine hydrolase subfamilies enabling to extract the structural features that distinguish the various sub-families of serine hydrolases. More importantly, this approach allows comparing entire enzyme classes. Notably, the hydrophobicity of the active site turned out to be a major factor in classifying an enzyme as a lipase or as a cutinase. Our analysis pointed out that cutinases have some shared features with both lipases and esterases that justifies their capability of catalysing transesterification reactions in low water activity media. The catalophor approach was also conveniently exploited for determining that CaLB, notwithstanding the absence of a lid covering the active site, shares many features with the other lipases; we also demonstrated that the presence of a lid is not a feature represented in the catalophor of lipases, making its presence not necessarily required to classify an enzyme as a lipase. Our approach was also used to clarify the structural reasons for the lack of activity in a mutant of Thc_cut1. In addition, molecular dynamics studies were carried out to investigate the different response of CaLB and Thc_cut1 to different pressure and temperature conditions, revealing that a loop in the

proximity of the active site responsible of the advantageous features that make Thc_cut1 able to work in mild temperature and pressure conditions.

7. Bibliography

1 M. Cespugli, S. Lotteria, L. Navarini, V. Lonzarich, L. Del Terra, F. Vita, M. Zweyer, G. Baldini, V. Ferrario, C. Ebert and L. Gardossi, *Catalysts*, 2018, **8**, 471.

2 V. Ferrario, A. Pellis, M. Cespugli, G. Guebitz and L. Gardossi, *Catalysts*, 2016, **6**, 205.

3 A. Pellis, V. Ferrario, M. Cespugli, L. Corici, A. Guarneri, B. Zartl, E. Herrero Acero, C. Ebert, G. M. Guebitz and L. Gardossi, *Green Chemistry*, 2017, **19**, 490–502.

4 V. Ferrario, L. Siragusa, C. Ebert, M. Baroni, M. Foscato, G. Cruciani and L. Gardossi, *PLoS ONE*, 2014, **9**, e109354.

5 L. Corici, V. Ferrario, A. Pellis, C. Ebert, S. Lotteria, S. Cantone, D. Voinovich and L. Gardossi, *RSC Advances*, 2016, **6**, 63256–63270.

6 A. Pellis, V. Ferrario, B. Zartl, M. Brandauer, C. Gamerith, E. Herrero Acero, C. Ebert, L. Gardossi and G. M. Guebitz, *Catalysis Science & Technology*, 2016, **6**, 3430–3442.

7 Ellen MacArthur Foundation, *Towards the Circular Economy*, .

8 McKinsey Global Institute, *Resource Revolution: Meeting the World's*, .

9 *IUPAC Technical Reports and Recommendations*, .

10 T. Narancic, R. Davis, J. Nikodinovic-Runic and K. E. O' Connor, *Biotechnology Letters*, 2015, **37**, 943–954.

11 R. A. Gross, M. Ganesh and W. Lu, *Trends in Biotechnology*, 2010, **28**, 435–443.

12 S. Kobayashi, *Proceedings of the Japan Academy, Series B*, 2010, **86**, 338–365.

13 J. Kadokawa and S. Kobayashi, *Current Opinion in Chemical Biology*, 2010, **14**, 145–153.

14 U. Hanefeld, L. Gardossi and E. Magner, *Chem. Soc. Rev.*, 2009, **38**, 453–468.

15 L. Cao, A. Fischer, U. T. Bornscheuer and R. D. Schmid, *Biocatalysis and Biotransformation*, 1996, **14**, 269–283.

16 K.-E. Jaeger, B. W. Dijkstra and M. T. Reetz, *Annual Review of Microbiology*, 1999, **53**, 315–351.

17 J. Uppenberg, M. T. Hansen, S. Patkar and T. A. Jones, *Structure*, 1994, **2**, 293–308.

18 I. Høegh, S. Patkar, T. Halkier and M. T. Hansen, *Canadian Journal of Botany*, 1995, **73**, 869–875.

19 S.-W. Tsai, *Journal of Molecular Catalysis B: Enzymatic*, 2016, **127**, 98–116.

20 M. Martinelle and K. Hult, *Biochimica et Biophysica Acta (BBA) - Protein Structure and Molecular Enzymology*, 1995, **1251**, 191–197.

21 S. Kim, C. Jiménez-González and B. E. Dale, *The International Journal of Life Cycle Assessment*, 2009, **14**, 392–400.

22 C. Korupp, R. Weberskirch, J. J. Müller, A. Liese and L. Hilterhaus, *Organic Process Research & Development*, 2010, **14**, 1118–1124.

23 A. Kumar, A. S. Kulshrestha, W. Gao and R. A. Gross, *Macromolecules*, 2003, **36**, 8219–8221.

24 Y. Shen, X. Chen and R. A. Gross, *Macromolecules*, 1999, **32**, 2799–2802.

25 F. Binns, P. Harffey, S. M. Roberts and A. Taylor, *Journal of the Chemical Society, Perkin Transactions 1*, 1999, 2671–2676.

26 A. Pellis, L. Corici, L. Sinigoi, N. D'Amelio, D. Fattor, V. Ferrario, C. Ebert and L. Gardossi, *Green Chemistry*, 2015, **17**, 1756–1766.

27 R. DiCosimo, J. McAuliffe, A. J. Poulose and G. Bohlmann, *Chemical Society Reviews*, 2013, **42**, 6437.

28 M. B. Ansorge-Schumacher and O. Thum, *Chemical Society Reviews*, 2013, **42**, 6475.

29 C. F. Thurston, *Microbiology*, 1994, **140**, 19–26.

30 H. Claus, *Micron*, 2004, **35**, 93–96.

31 L.-E. Andréasson and B. Reinhammar, *Biochimica et Biophysica Acta (BBA) - Enzymology*, 1979, **568**, 145–156.

32 R. Bourbonnais, M. G. Paice, I. D. Reid, P. Lanthier and M. Yaguchi, *Appl. Environ. Microbiol.*, 1995, **61**, 1876–1880.

33 A. I. Cañas and S. Camarero, *Biotechnol. Adv.*, 2010, **28**, 694–705.

34 S. Camarero, D. Ibarra, M. J. Martinez and A. T. Martinez, *Applied and Environmental Microbiology*, 2005, **71**, 1775–1784.

35 S. Lotteria, S. Master thesis, University of Trieste.

36 P. Alvira, E. Tomás-Pejó, M. Ballesteros and M. J. Negro, *Bioresource Technology*, 2010, **101**, 4851–4861.

37 T. Kudanga, G. S. Nyanhongo, G. M. Guebitz and S. Burton, *Enzyme and Microbial Technology*, 2011, **48**, 195–208.

38 I. Patel, R. Ludwig, D. Haltrich, T. Rosenau and A. Potthast, *Holzforschung*, , DOI:10.1515/hf.2011.035.

39 D. da Silva Perez, S. Montanari and M. R. Vignon, *Biomacromolecules*, 2003, **4**, 1417–1425.

40 N. Guigo, K. Mazeau, J.-L. Putaux and L. Heux, *Cellulose*, 2014, **21**, 4119–4133.

41 V. C. Coletta, C. A. Rezende, F. R. da Conceição, I. Polikarpov and F. E. G. Guimarães, *Biotechnology for Biofuels*, 2013, **6**, 43.

42 I. Migneault, C. Dartiguenave, M. J. Bertrand and K. C. Waldron, *BioTechniques*, 2004, **37**, 790–802.

43 C. Zhao, Q. Shao, B. Li and W. Ding, *Energy & Fuels*, 2014, **28**, 6392–6397.

44 S. B. Kim and Y. Y. Lee, *Applied Biochemistry and Biotechnology*, 1996, **57**–**58**, 147–156.

45 B. E. Dale, in *Annual Reports on Fermentation Processes*, Elsevier, 1985, vol. 8, pp. 299–323.

46 J. E. A. M. van den Meerakker, *Journal of The Electrochemical Society*, 1990, **137**, 1239.

47 WO2016156009, 2016.

48 A. B. Díaz, A. Blandino, C. Belleli and I. Caro, *Industrial & Engineering Chemistry Research*, 2014, **53**, 10870–10875.

49 Zhixuan Wang , Jiaying Li , John P. Barford , Klaus Hellgradt, Gordon McKay, *IJOEAR*.

50 A. Ma'ruf, B. Pramudono and N. Aryanti, Las Vegas, Nevada, USA, 2017, p. 020013.

51 Y. Chen and X. Cheng, *Journal of Forestry Research*, 2008, **19**, 159–163.

52 Cramer C.J., *Essential in Computational Chemistry: Theories and Models*, Wiley., 2005.

53 A. Warshel and M. Levitt, *Journal of Molecular Biology*, 1976, **103**, 227–249.

54 V. Ferrario, C. Ebert, A. Svendsen, W. Besenmatter and L. Gardossi, *Journal of Molecular Catalysis B: Enzymatic*, 2014, **101**, 7–15.

55 P. Braiuca, C. Ebert, A. Basso, P. Linda and L. Gardossi, *Trends in Biotechnology*, 2006, **24**, 419–425.

56 Todeschini R., Consonni V., *Molecular Descriptors for Chemoinformatics: Volume I*, Weinheim: Wiley-VCH, Weinheim: Wiley-VCH., 2009.

57 P. J. Goodford, *Journal of Medicinal Chemistry*, 1985, **28**, 849–857.

58 *MIA s.r.l. - Perugia*, .

59 P. C. Boutros and A. B. Okey, *Briefings in Bioinformatics*, 2005, **6**, 331–343.

60 M. Baroni, G. Cruciani, S. Sciabola, F. Perruccio and J. S. Mason, *Journal of Chemical Information and Modeling*, 2007, **47**, 279–294.

61 J. P. Brincat, E. Carosati, S. Sabatini, G. Manfroni, A. Fravolini, J. L. Raygada, D. Patel, G. W. Kaatz and G. Cruciani, *Journal of Medicinal Chemistry*, 2011, **54**, 354–365.

62 H. M. Berman, J. Westbrook, Z. Feng, G. Gilliland, T. N. Bhat, H. Weissig, I. N. Shindyalov and P. E. Bourne, *Nucleic Acids Res.*, 2000, **28**, 235–242.

63 *The PyMOL Molecular Graphic System, Version 1.5.0.3, Schrodinger LLC*, .

64 A. Svendsen, Ed., *Understanding Enzymes: Function, Design, Engineering, and Analysis*, Pan Stanford, 2016.

65 T. Miyakawa, H. Mizushima, J. Ohtsuka, M. Oda, F. Kawai and M. Tanokura, *Applied Microbiology and Biotechnology*, 2015, **99**, 4297–4307.

66 A. Roussel, S. Amara, A. Nyyssölä, E. Mateos-Diaz, S. Blangy, H. Kontkanen, A. Westerholm-Parvinen, F. Carrière and C. Cambillau, *Journal of Molecular Biology*, 2014, **426**, 3757–3772.

67 S. Das, T. Karmakar and S. Balasubramanian, *J Phys Chem B*, 2016, **120**, 11720–11732.

68 N. Piovesan, Master thesis, University of Trieste.

69 D. Van Der Spoel, E. Lindahl, B. Hess, G. Groenhof, A. E. Mark and H. J. C. Berendsen, *J Comput Chem*, 2005, **26**, 1701–1718.

70 W. L. Jorgensen and J. Tirado-Rives, *Journal of the American Chemical Society*, 1988, **110**, 1657–1666.

71 Z. Marton, V. Léonard-Nevers, P.-O. Syrén, C. Bauer, S. Lamare, K. Hult, V. Tranc and M. Graber, *Journal of Molecular Catalysis B: Enzymatic*, 2010, **65**, 11–17.

72 P. Spizzo, A. Basso, C. Ebert, L. Gardossi, V. Ferrario, D. Romano and F. Molinari, *Tetrahedron*, 2007, **63**, 11005–11010.

73 D. Kold, Z. Dauter, A. K. Laustsen, A. M. Brzozowski, J. P. Turkenburg, A. D. Nielsen, H. Koldsø, E. Petersen, B. Schiøtt, L. De Maria, K. S. Wilson, A. Svendsen and R. Wimmer, *Protein Science*, 2014, **23**, 1023–1035.

74 S. Longhi, M. Czjzek, V. Lamzin, A. Nicolas and C. Cambillau, *J. Mol. Biol.*, 1997, **268**, 779–799.

75 M. P. Nyon, D. W. Rice, J. M. Berrisford, A. M. Hounslow, A. J. G. Moir, H. Huang, S. Nathan, N. M. Mahadi, F. D. A. Bakar and C. J. Craven, *Journal of Molecular Biology*, 2009, **385**, 226–235.

76 Z. Liu, Y. Gosser, P. J. Baker, Y. Ravee, Z. Lu, G. Alemu, H. Li, G. L. Butterfoss, X.-P. Kong, R. Gross and J. K. Montclare, *Journal of the American Chemical Society*, 2009, **131**, 15711–15716.

77 K. Kitadokoro, U. Thumarat, R. Nakamura, K. Nishimura, H. Karatani, H. Suzuki and F. Kawai, *Polymer Degradation and Stability*, 2012, **97**, 771–775.

78 C. Roth, R. Wei, T. Oeser, J. Then, C. Föllner, W. Zimmermann and N. Sträter, *Applied Microbiology and Biotechnology*, 2014, **98**, 7815–7823.

79 D. J. Rogers and T. T. Tanimoto, *Science*, 1960, **132**, 1115–1118.

80 T. J. Dolinsky, J. E. Nielsen, J. A. McCammon and N. A. Baker, *Nucleic Acids Res.*, 2004, **32**, W665-667.

81 H. Li, A. D. Robertson and J. H. Jensen, *Proteins: Structure, Function, and Bioinformatics*, 2005, **61**, 704–721.

82 H. W. Horn, W. C. Swope, J. W. Pitera, J. D. Madura, T. J. Dick, G. L. Hura and T. Head-Gordon, *J Chem Phys*, 2004, **120**, 9665–9678.

83 U. Essmann, L. Perera, M. L. Berkowitz, T. Darden, H. Lee and L. G. Pedersen, *The Journal of Chemical Physics*, 1995, **103**, 8577–8593.

84 H. J. C. Berendsen, J. P. M. Postma, W. F. van Gunsteren, A. DiNola and J. R. Haak, *The Journal of Chemical Physics*, 1984, **81**, 3684–3690.

8. Annex 1

List of pubblications

- Ferrario V., Pellis A., Cespugli M., Guebitz G. M., Gardossi L., "Nature Inspired Solutions for Polymers: Will Cutinase Enzymes Make Polyesters and Polyamides Greener?", *Catalysts*, **2016**, 6, 205.
- Pellis A., Ferrario V., Cespugli M., Corici L., Guarneri A., Zartl B., Herrero A. E., Ebert C., Guebitz G. M., Gardossi L., "Fully renewable polyesters via polycondensation catalyzed by Thermobifida cellulosilytica cutinase 1: an integrated approach", *Green Chemistry*, **2017**, 19, 490-502.
- Cespugli, M, Lotteria S., Navarini L., Lonzarich V., Del Terra L., Vita F., Zweyer M., Baldini G., Ferrario V., Ebert C., Gardossi L." Rice Husk as an Inexpensive Renewable Immobilization Carrier for Biocatalysts Employed in the Food, Cosmetic and Polymer Sectors", *Catalysts*, **2018**, 8, 471.

List of scientific contributions at conferences

- Poster and oral communication: Cespugli M., Ferrario V., Ebert C., Pellis A., Siragusa L., Guebitz G.M., Gardossi L., "In silico screening of cutinases for polycondensation using structure-based bioinformatic analysis and BioGPS descriptors". COST Training School "Systems Biocatalysis" April 27-30 **2016**, Siena.
- Contribution for presentation: Pellis A., Ferrario V., Guarneri A., Acero E. H., Corici L., Cespugli M., Ebert C., Guebitz G. M., Gardossi L., "Thermobifida cellulosilytica Cutinase (Thc_cut1) as a Powerful Tool for the Synthesis and Functionalization of Biobased Polyesters". Biocat Hamburg, August 28- September 1 **2016**, invited lecture (Lucia Gardossi)
- Poster: Cespugli M., Ferrario V., Ebert C., Pellis A., Siragusa L., Guebitz G.M., Gardossi L., "In silico screening of cutinases for polycondensation using structure-based bioinformatic analysis and BioGPS descriptors". Novacam winter School **2017**, Padova.
- Poster: Cespugli M., Lotteria S., Corici L., Ferrario V., Pellis A., Ebert C., Gardossi L., "Solventfree synthesis of esters and polyesters using renewable immobilization carriers". BNCM Conference **2017**, Rostock

- Oral communication: Workshop "I chimici per le biotecnologe". "In silico screening of enzymes for polycondensation using structure-based bioinformatic analysis and BioGPS descriptors". February **2018**, Bologna.
- Oral communication: Workshop Nazionale del Gruppo Interdivisionale GREEN CHEMISTRY della Società Chimica Italiana,. "Sustainable chemo-enzymatic functionalization of rice husk for fully renewable biocatalysed processes", June **2018**, Milan.

9. Annex 2

Manuscript: Fully renewable polyesters via polycondensation catalyzed by *Thermobifida cellulosilytica* cutinase 1: an integrated approach

Fully renewable polyesters *via* polycondensation catalyzed by *Thermobifida cellulosilytica* cutinase 1: an integrated approach†

Alessandro Pellis,[a] Valerio Ferrario,[b] Marco Cespugli,[b] Livia Corici,‡[c] Alice Guarneri,[b] Barbara Zartl,[a] Enrique Herrero Acero,[d] Cynthia Ebert,[b] Georg M. Guebitz[a,d] and Lucia Gardossi*[b]

The present study addresses comprehensively the problem of producing polyesters through sustainable processes while using fully renewable raw materials and biocatalysts. Polycondensation of bio-based dimethyl adipate with different diols was catalyzed by cutinase 1 from *Thermobifida cellulosilytica* (Thc_cut1) under solvent free and thin-film conditions. The biocatalyst was immobilized efficiently on a fully renewable cheap carrier based on milled rice husk. A multivariate factorial design demonstrated that Thc_cut1 is less sensitive to the presence of water in the system and it works efficiently under milder conditions (50 °C; 535 mbar) when compared to lipase B from *Candida antarctica* (CaLB), thus enabling energy savings. Experimental and computational investigations of cutinase 1 from *Thermobifida cellulosilytica* (Thc_cut1) disclosed structural and functional features that make this serine-hydrolase efficient in polycondensation reactions. Bioinformatic analysis performed with the BioGPS tool pointed out functional similarities with CaLB and provided guidelines for future engineering studies aiming, for instance, at introducing different promiscuous activities in the Thc_cut1 scaffold. The results set robust premises for a full exploitation of enzymes in environmentally and economically sustainable enzymatic polycondensation reactions.

Introduction

United Nations Environment Programme (UNEP) has calculated that the natural capital costs of polymers and plastics used in the consumer goods industry are over $75 bn per year. Interestingly, over 75% of the known and quantifiable impacts associated with plastic use are located in the upstream portion of the supply chain across all sectors, namely impacts generated from the extraction of raw materials to the manufacturing of plastic feedstock.[1]

[a] University of Natural Resources and Life Sciences, Institute for Environmental Biotechnology, Konrad Lorenz Strasse 20, 3430 Tulln an der Donau, Austria
[b] Laboratory of Applied and Computational Biocatalysis, Department of Scienze Chimiche e Farmaceutiche, Università degli Studi di Trieste, Piazzale Europa 1, 34127 Trieste, Italy. E-mail: gardossi@units.it
[c] SPRIN S.p.a., Via Flavia 23/1, 34148 Trieste, Italy
[d] Austrian Centre of Industrial Biotechnology GmbH, Division Enzymes and Polymers, Konrad Lorenz Strasse 20, 3430 Tulln an der Donau, Austria
†Electronic supplementary information (ESI) available. See DOI: 10.1039/c6gc02142e
‡Current address: Institute of Chemistry Timisoara of Romanian Academy, Mihai Viteazul 24, 300223 Timisoara, Romania.

The dimension of the problem is even more evident when considered that about 4–6% of the world's oil production is used to produce 311 million tons of polymers and plastics (http://www.plasticseurope.org) out of a global 7% of petroleum consumption ascribable to the whole chemical sector.[4] Even if global recycling rates rose from today's 14% to more than 55% – which would be higher than the rate achieved today by even the best performing countries – annual requirements for polymeric products would still double by 2050.[2] Moreover, there are several applications – within the plastic stream – where recycling strategies appear not effective because of technical or economic reasons. Examples can be found in the cosmetic and the lubricant sectors.[3] The present study addresses comprehensively the problem of producing polyesters through sustainable processes while using renewable raw materials and biocatalysts, namely enzymes. Among polymers, polyesters are a widely used class with applications ranging from clothing to food packaging and from the car industry to biomedical applications. A number of hydrolases, and lipase B from *Candida antarctica* in particular, were reported to catalyze the synthesis of polyesters *via* polycondensation or ring opening polymerization. Enzymes are attractive sustainable alternatives to toxic catalysts used in polyconden-

sation, such as metal catalysts and tin in particular. They may work also in solvent-free systems and enable the synthesis of functionalized as well biodegradable polyesters with a controlled architecture through highly selective processes at temperatures ranging between 40 °C and 90 °C, whereas conventional polycondensations are carried out at $T > 150$ °C.[4] Enzymatic synthesis generally leads to polymers with a moderate molecular weight as compared to products obtainable via conventional chemical synthesis, but this drawback has been circumvented by using two-step procedures, where an initial enzymatic polymerization leads to oligomers and the second step is carried out at a higher temperature and/or at a lower pressure after removal of the biocatalyst.[5] Furthermore, the synthesis of oligomers and short telechelic prepolymers with functional ends represents an effective strategy for obtaining polymers with a higher molecular weight.[6] It must be underlined that short polyesters (<2500 Da) with highly regular structures have been used in coating and adhesive applications[7] and that biodegradable oligomers can have intrinsic interesting properties as film forming in cosmetic formulations.[8]

In the present study we report on a comprehensive approach for the sustainable synthesis of polyesters, which encompasses renewability of both raw materials and immobilized enzymes, solvent use reduction, as well as energy consumption.[8,9] Since 30% of the environmental impact of polymers and plastics is ascribable to greenhouse gas emissions from raw material extraction and processing, we focused on the esters of adipic acid and 1,4-butandiol (BDO), two renewable bio-based monomers available at an industrial scale.[9–11] Indeed, there is a wide range of structurally different bio-based chemical building blocks already available via fermentation or chemical transformation of a renewable carbon. They are contributing to the growth of the bio-based plastic market and to the mitigation of the environmental impact of fossil-based plastics.[10]

In order to fulfill sustainability criteria, polycondensation reactions were carried out under solvent-free conditions and exploiting thin-film systems that were demonstrated to overcome viscosity by promoting optimal heat and mass transfer, thus enabling the use of lower operational temperatures.[5,12,13] Attention was paid also to the environmental impact of the immobilization procedure: hydrolases were immobilized efficiently on a renewable lignocellulosic carrier based on milled rice husk,[14] without any further chemical functionalization of the solid matrix.

Integrated experimental and computational investigations were used to study the applicability of cutinase 1 from *Thermobifida cellulosilytica* (Thc_cut1)[15,16] in polycondensations, with the objective of enlarging the portfolio of biocatalysts in polyester synthesis. Cutinases are fungal enzymes involved in plant pathogenesis caused by the depolymerization of cutin, a three-dimensional polymer of inter-esterified hydroxyl and epoxy–hydroxy fatty acids with chain lengths mostly between 16 and 18 carbon atoms.[17] Because of their ability to accept long chain substrates, cutinases are also effective in catalyzing *in vitro* polymer synthesis. Recently, a

cutinase from *Fusarium solani pisi* showed consistent synthetic activity for the production of polyamides,[18] whereas cutinase from *Humicola insolens* (HiC) was used in the polycondensation of linear dicarboxylic acids and their esters (*e.g.* adipic acid, diethyl sebacate)[19] and its application in the ring opening polymerizations of lactones.[20] We have recently reported that Thc_cut1 efficiently catalyzes the polycondensation of dimethyl adipate with different polyols leading to higher M_w (~1900) and M_n (~1000)[15] when compared to the performances of other hydrolases such as CaLB or *Humicola insolens* cutinase (HiC).[19] These observations stimulated the study presented here, where experimental and bioinformatics investigations provide a more detailed understanding of the functional properties of Thc_cut1, disclosing specific features that differentiate this serine-hydrolase from other enzymes previously used in similar polycondensation reactions, namely CaLB and HiC.

Finally, the design of the experiment study sheds light on the response of Thc_cut1 under operational conditions. Molecular dynamic simulations supported the experimental study, revealing how Thc_cut1 displays optimal efficiency under milder experimental conditions as compared to CaLB, thus enabling saving energies in terms of heating and vacuum application.

Overall, the present study provides the first comprehensive analysis of the feasibility of fully renewable and economically sustainable polyesters via enzymatic catalysis. There is robust evidence that the next generation of sustainable polymers and plastics calls for a change of paradigm and a closer integration between chemistry and biotechnologies.

Results and discussion

BioGPS bioinformatics analysis of Thc_cut1 *versus* serine hydrolase superfamily

Recent computational investigations[15] disclosed the structural features that make Thc_cut1 readily accessible to substrates and optimally suited for covalent immobilization. As lipases and other cutinase enzymes, it presents hydrophobic superficial regions around the active site. The wide and superficial active site of Thc_cut1 makes this hydrolase a promising catalyst for enlarging the scope of enzymatic polycondensation by synthesizing new polyesters with a larger molecular weight. The scaffold of Thc_cut1 also represents a potential starting point for further engineering strategies aiming at the synthesis of novel classes of polymers.

In the present study, we analysed cutinase 1 from *Thermobifida cellulosilytica* by means of the BioGPS bioinformatics tool[21] recently developed in our group with the objective of identifying differences and similarities with respect to CaLB and cutinase from *Humicola insolens* (HiC), two hydrolases previously employed in polycondensation reactions.[19,20]

BioGPS (Global Positioning System in Biological Space) molecular descriptors[21–24] are based on GRID derived molecular descriptors and are able to describe, mathematically, the

environment of enzyme active sites both in geometrical and electrostatic terms. Active sites were mapped using the GRID force field for evaluating the energy of non-bonded interactions and then for generating pseudo-MIFs (Molecular Interaction Fields).[25] Different probes were employed for the study of four different properties: H probe, that maps the active site shape; O probe, that evaluates H-bond donor properties; N1 probe, that accounts for H-bond acceptor capabilities; and the DRY probe, that evaluates hydrophobic interactions. The magnitude of the interaction of the N1 and O probes also includes, implicitly, information about the charge contribution, since these probes already have a partially positive and negative charge respectively.

The three-dimensional structure of HiC was taken from PDB (Protein Data Bank)[26] and corresponds to the PDB code 4OYY.[27] For Thc_cut1, an already published homology model was used[15] since the crystal structure of this enzyme is not available yet. The BioGPS descriptors for the two cutinases were calculated by using BioGPS software version 2.1 using the procedure already published. For CaLB, the 1TCA[28] crystal code of PDB was used.

With the pseudo-MIF procedure, the mapped properties are considered as electron-density like fields centered on each atom, corresponding to specific probe types (*i.e.* the interaction energies coming from the GRID N1 probe were centered on the carbonyl oxygen as a H-bond acceptor). Afterwards, the algorithm reduces the complexity of the pseudo-MIFs selecting a number of representative points using a weighted energy-based and space-coverage function. A preliminary visual comparison between the three enzymes comes from the alignment of the corresponding pseudo-MIFs reported in Fig. 1.

The visual comparison of pseudo-MIF can simply suggest a higher degree of similarity between CaLB and Thc_cut1, whereas HiC differs significantly, especially for a less extended ability to establish H-bonds. This type of mapping provides some focused information although it cannot give comprehensive analysis of functional differences, since they depend on a complex combination of all structural and electrostatic factors and, more importantly, on their interactions.

Therefore, in order to move beyond the approach based on the visual inspection and to draw an unbiased picture of structural and functional similarities, the properties of the two cutinases were statistically compared using a mathematical model calculated on a set of 41 serine-hydrolases, which also contains CaLB. The model was computed by analyzing statistically the information contained in the BioGPS descriptors of each hydrolase[21] using Unsupervised Pattern Cognition Analysis (UPCA).[29] The complete procedure used for the calculation of the UPCA model is available in the Materials and Methods section and the set of the 41 Ser hydrolases enzymes that includes amidases, peptidases, esterases and lipases is available in Table S1 in the ESI.† The approach is based on the concept that catalytic properties depend not only on structural features but especially on the ability of active sites to establish electrostatic interactions.[30,31] The BioGPS tool mapped the active sites of all the serine-hydrolases and the information
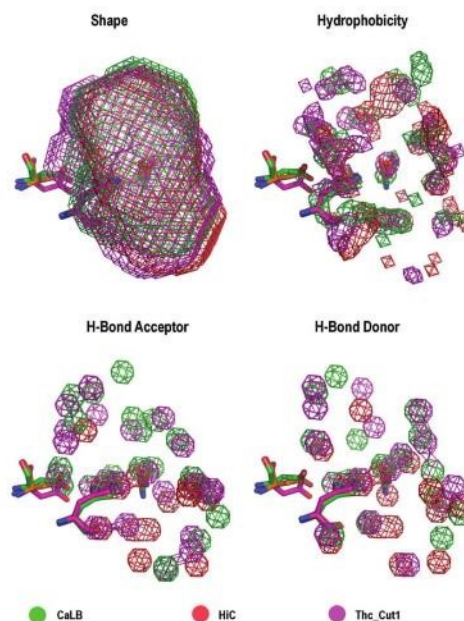

Fig. 1 Comparison of the active site properties of CaLB, HiC and Thc_cut1. Four active site properties are compared: shape, hydrophobicity, H-bond acceptor capabilities and H-bond donor capabilities. The catalytic triads (represented in stick mode) are superposed for active site orientation. PseudoMIFs are represented as wireframes and coloured in green, red and pink for CaLB, HiC and Thc_cut1 respectively.

contained in the molecular descriptors was analyzed by means of the UPCA approach. Fig. 2 reports the Global Score analysis, which encompasses all properties analyzed by the four probes. The statistical analysis sorted all hydrolases and grouped them into functionally distinct clusters, thus confirming that the structural properties explained by the BioGPS descriptors are correlated with catalytic functions of each class of serine-hydrolase.

The main advantage of this approach is represented by the visual representation of differences and similarities and it was used for "projecting" the properties of the two cutinases, calculated with the BioGPS tool, into the UPCA domain (Fig. 2). The BioGPS analysis recognizes a high level of similarity between the active sites of Thc_cut1 and CaLB (1TCA), which are projected in a region close to the esterase cluster but at the edge of the lipase group. This result supports the previous data obtained for Thc_cut1 and CaLB through molecular dynamics simulations, which indicated the absence of mobile domains responsible for interfacial activation.[15]

BioGPS information was also dissected into the UPCA plots computed for each single probe and they are reported in the ESI (Fig. S1†). The active sites of CaLB, Thc_cut1 and HiC

126
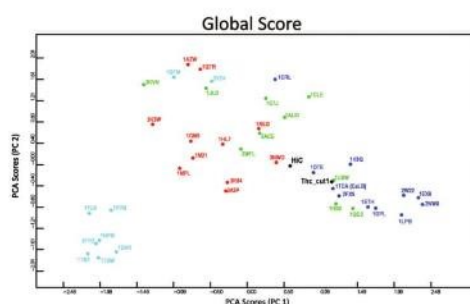
Fig. 2 Projection of cutinases from *Thermobifida cellulosilytica* (Thc_cut1) and from *Humicola insolens* (HiC) in the BioGPS model obtained through Unsupervised Pattern Cognition Analysis (UPCA). Ser hydrolases are clustered on the basis of the global similarity scores computed using the BioGPS descriptors. They are labelled according to their PDB code. Lipases are indicated in blue, esterases in green, amidases in red and proteases in cyan.

appear similar in terms of hydrophobic properties and they are positioned among esterases although close to the lipase cluster. Both Thc_cut1 and CaLB are clearly classified as esterases for their ability to establish H bonds and Thc_cut1 falls closer to the lipase group. In terms of H bond capabilities, HiC moves far away from lipases and the other two enzymes, confirming the differences observed in Fig. 1. These observations shed new light also on the behaviour of CaLB, which is recognized similar to lipases only in terms of hydrophobic properties.

Fully renewable immobilized Thc_cut1 applied in polycondensations

In our previous investigations of polycondensations of different diesters and polyols catalyzed by CaLB[12] we have demonstrated that viscosity represents a major bottleneck for solvent free enzymatic polycondensation. Optimal mass transfer and the homogeneous dispersion of the enzyme in the reaction mixture are essential for achieving a reasonable elongation of the oligomers. Although a mono-molecular dispersion of the native enzyme would lead to the highest reaction rate, immobilization of the enzyme is mandatory in order to avoid contamination of the product with the free protein

and also to assure the recycling of the biocatalyst for the economics of the process.[5,7,20] We have also demonstrated that immobilized formulations characterized by a low loading of the CaLB protein are more effective as long as they are used in larger amounts to promote the dispersion of the enzyme and its accessibility.[12] However, a fully renewable and economically viable synthesis of bio-based polyesters must take into account waste production, energy consumption as well as the environmental impact of all raw materials, including immobilized biocatalysts. On that respect, it has been reported that fossil based methacrylic carriers account for a relevant part of greenhouse gas emissions due to the biocatalyst.[32] In a recent study, we have proposed rice husk (RH) as a renewable alternative carrier suitable for immobilization of CaLB and other hydrolases.[33] This inexpensive and massively available biomass (globally 100 Mt per year) is composed of SiO_2 and three different biopolymers, namely cellulose, hemicellulose and lignin.[34] A preliminary analysis of the sustainability of immobilization protocols employing rice husk has been previously reported.[15] Besides being fully renewable, at the end of its proposed applications RH can still be used as a carbon source for anaerobic digestion for biogas production, as a cellulose source for bioethanol fermentation, burnt for generating energy or exploited in different manufacturing sectors[35] in accordance with the circular economy principles.[36]

It must be noted that in our previous study all attempts of adsorbing CaLB on rice husk particles in aqueous buffer were unsuccessful (<5% adsorbed). Therefore, CaLB was covalently immobilized on rice husk particles, which were oxidized at the cellulosic component and later functionalized with a hexamethylene spacer. Looking for simpler and economical protocols for covalent immobilization, in the present study we verified that Thc_cut1 can be adsorbed in moderate yield (36% in 24 h) on rice husk particles (rThc_cut1) with a diameter in the range of 200–400 μm. In order to prevent protein leaching, the enzyme was cross-linked using glutaraldehyde. Interestingly, Table 1 shows that, despite the low loading, rThc_cut1 has a higher hydrolytic activity as compared to a reference formulation obtained by immobilizing a much higher amount of cutinase (about 7 folders) on a commercial epoxy-activated methacrylic resin.

Two different drying methods, namely freeze-drying and evaporation at environmental pressure and at 30 °C for 48 h, led to comparable enzymatic activity, although the lyophilization allows for a more extensive dehydration (ESI, Table S2†).

Table 1 Activity of Thc_cut1 immobilized on rice husk (rThc_cut1) and on epoxy-methacrylic resin Sepabeads EC-EP/M (iThc_cut1)

Enzymatic Preparation	Protein loading (mg g$_{dry}$$^{-1}$)	Loaded protein (%)	Drying method	Hydrolytic activity^a (U g^{-1})	Water content (% w/w)
rThc_cut1	4	36	Air-dried	35 ± 5	4
Lyo_rThc_cut1			Freeze drying	35 ± 3	0.2
iThc_cut1	10	99	Air-dried	13 ± 2	3
Lyo_iThc_cut1			Freeze drying	12 ± 3	0.2

^{a} Calculated *via* the PNPB hydrolytic assay. All determinations were conducted in duplicates.

127

Table 2 Polycondensation of DMA with BDO catalyzed by different formulations of Thc_cut1 after 24 h

Entry	Enzymatic preparation	Amount (% w/w)	P (mbar)	$M_w{}^a$	$M_n{}^a$	PD^a	Conv.^{b} (%)
1	rThc_cut1	10	1000	594	434	1.37	64
2	rThc_cut1	10	70	230	222	1.04	18
3	rThc_cut1	30	70	487	343	1.42	62
4	Lyo_rThc_cut1	10	1000	587	384	1.53	62
5	Lyo_rThc_cut1	10	70	224	203	1.10	13
6	iThc_cut1	10	1000	1923	985	1.95	86[13]
7	iThc_cut1	10	70	480	290	1.66	48
8	Lyo_iThc_cut1	10	1000	1120	656	1.71	78
9	Lyo_iThc_cut1	10	70	319	275	1.16	43

^{a} Calculated *via* GPC calibrated with low molecular weight polystyrene standards 250–70 000 Da. ^{b} Calculated *via* ^{1}H-NMR by comparing the ratio between the signals of methylene groups adjacent to –OH of BDO and the methylene groups of DMA (assumed as constant). All reactions were performed in duplicates.

The preparations were applied and compared in the polycondensation of dimethyl adipate (DMA) and 1,4-butanediol (BDO), two bio-based monomers widely used in polymer synthesis. Polycondensations were conducted using a thin-film solvent-free system[4] at 70 °C and working either at atmospheric pressure or at 70 mbar.

The results in Table 2 indicate that by working with 10% of formulations of rThc_cut1 with a very low loading of protein it is possible to achieve in 24 h more than 64% of conversion and oligomers made by up to 7 units. The complete characterization of the products is available in the ESI (Fig. S2–S15†). Unexpectedly, working under reduced pressure and with very dry preparations does not translate into higher conversions or elongation. Rather, there is a negative effect of reduced pressure, whereas the effect of water is less evident. When working under vacuum (entry 3) it is necessary to use a triple amount of the biocatalyst for reaching conversions observed in

entry 1 that was carried out at 1000 mbar. ESI-MS analysis in Fig. 3 confirms this trend.

The same behavior was observed in the polycondensations catalyzed by Thc_cut1 immobilized on epoxy methacrylic resins, indicating that the effect is not dependent on the nature of the carrier.

The negative effect of vacuum emerged also from the study of the polycondensation of DMA with ODO (see ESI Fig. S16–S24† for complete characterization of products). Also in this case using 30% w/w of the biocatalyst at 70 mbar leads to comparable conversion (44%) with the 10% w/w 1000 mbar reaction (39%) (Table 3).

This behavior appears to be in contradiction with all previous reports on polycondensation catalyzed by CaLB,[7,12,37] where the application of vacuum had the beneficial effect of promoting the removal of the leaving nucleophile (either alcohol or water), thus preventing the reversing of the reaction and promoting higher yields and molecular weights.

Indeed, the experiments performed using CaLB immobilized on the same epoxy activated methacrylic resin (Table 4, entries 1 and 2) confirmed that it is necessary to apply vacuum for achieving satisfying yield and elongation when traces of water are still present in the enzymatic preparation (3%). Also in the case of Novozym® 435 (NZ 435®), the enzymatic preparation most widely used in previous polycondensation studies, it is evident that the reduced pressure exerts a dramatic effect
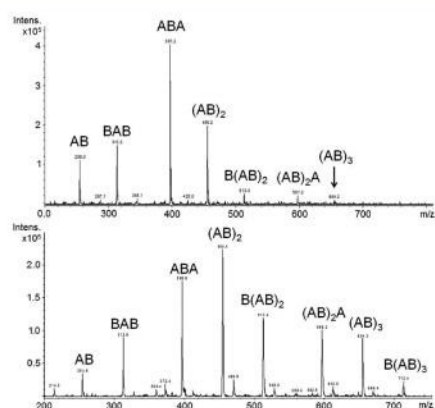
Fig. 3 ESI-MS positive ion mass spectrum of the polycondensation products of DMA with BDO catalyzed by 10% w/w rThc_cut1 at 24 h and 70 mbar (top) and 1000 mbar (bottom).

Table 3 Polycondensation of DMA with ODO using the rThc_cut1 preparation as a catalyst

Entry	Amount (% w/w)	Vacuum (mbar)	$M_w{}^a$	$M_n{}^a$	PD^a	Conv.^{b} (%)
1	10	1000	508	393	1.29	44
2	10	70	354	289	1.22	8
3	30	70	447	298	1.50	39

^{a} Calculated *via* GPC calibrated with low molecular weight polystyrene standards 250–70 000 Da. ^{b} Calculated *via* ^{1}H-NMR by comparing the ratio between the polyol methylene groups adjacent to –OH area and the internal methylene groups area of DMA (assumed as constant). All reactions were performed in duplicates.

Table 4 Polycondensation of DMA with BDO catalyzed by 10% (w/w) of different formulations of CaLB after 24 h of reaction

Entry	Biocatalyst	H_2O % (w/w)	p (mbar)	M_w	$M_n{}^a$	PD^a	Conv.^{b} (%)
1	iCaLB	3	1000	888	528	1.68	76[15]
2	iCaLB	3	70	6947	3162	2.20	90
3	NZ 435®	1	1000	1040	561	1.85	78[15]
4	NZ 435®	1	70	8357	1759	4.75	96
5	LyoNZ435®	0.1	1000	999	608	1.64	76
6	LyoNZ435®	0.1	70	8250	2438	3.38	94

^{a} Calculated *via* GPC calibrated with low molecular weight polystyrene standards 250–70 000 Da. ^{b} Calculated *via* ^{1}H-NMR by comparing the ratio between the signals of methylene groups adjacent to –OH of BDO and the methylene groups of DMA (assumed as constant). All reactions were performed in duplicates.

on the elongation of the polyester, even when the enzyme is employed in a highly dried form (0.1% w/w). It must be noted that a higher M_n obtained using Novozym® 435 is a consequence of the detachment and dispersion of the enzyme adsorbed on the acrylic support, as also experimentally demonstrated in previous studies.[5] We previously demonstrated that both CaLB and Thc_cut1 can be recycled effectively for at least ten cycles when covalently immobilized either on RH or on epoxy methacrylic resins, with negligible protein leaching.[4,14,15]

Globally, the data here reported suggest that CaLB and Thc_cut1 are differently affected by experimental conditions. These differences show no direct dependence on the immobilization carrier, the substrate or the dehydration method.

Therefore, to the best of our knowledge, this is the first report on the complexity of effects of experimental variables on the efficiency of enzymes in enzymatic polycondensation and we considered that the issue had to be analyzed in detail by means of a design of the experiment approach.

Multivariate analysis of the effect of experimental variables on polycondensation catalyzed by immobilized Thc_cut1

In a traditional investigative approach, 'one factor at a time' is varied, with the remaining factors held constant. This method provides an estimate of the effect of the single variable under selected fixed conditions, but if the variables do no act additively (*i.e.* they interact), the resulting information is incomplete and the real optimum of a system can be identified only with difficulty or by chance.[38] By using statistical experimental designs (*i.e.* factorial design), sets of experimental conditions are selected according to a systematic plan, so that statistical analysis of data provides information about the impact of factors or their interactions on the response considered.[39]

In the present study we used a fractional factorial design to quantitatively evaluate the effect of temperature, pressure and water on diol conversion and product elongation (M_n). These experimental variables were studied in the context of the polycondensations of DMA with two different diols: BDO and ODO. A fractional factorial design was planned by setting a low and a high value for each variable, thus defining the experimental domain to be explored. Additionally, a central point – corresponding to intermediate levels of the variables – was run for each diol twice. Table 5 reports the plan of the experi-

Table 5 Scheme of the experimental design developed for evaluating the effect of experimental conditions on the polycondensation (24 h) of DMA with BDO or ODO catalyzed by immobilized Thc_cut1

T (°C)	P (mbar)	H_2O (μL)	Yield (%)	M_n (Da)
		BDO		
30	70	0	85	901
70	1000	0	66	514
70	70	10	22	359
30	1000	10	50	417
50	535	5	96	1893
50	535	5	90	1266
		ODO		
70	70	0	6	271
30	1000	0	54	423
30	70	10	66	716
70	1000	10	53	434
50	535	5	85	1315
50	535	5	85	1221

ments, consisting of 12 polycondensation reactions, and the obtained experimental results.

The effect of moisture was studied by adding defined volumes of water to the reaction mixture. It must be noted that the water activity is the actual informative parameter affecting polycondensation and it is expected to vary as a function of the diol and also throughout the course of the reaction. In order to acquire more accurate information on the free water available in the systems and its distribution among the different phases at least at the starting of the reactions, the vapor pressure was measured in the gas phase using a humidity sensor. In principle, at equilibrium, the "free" water should be the same in all phases of the closed system, so that by measuring the vapor pressure (or RH) in the gas phase we know the a_w value of the system and, ultimately, the water available for promoting undesired hydrolytic reactions or for increasing the hydration state of the enzyme.[40]

The system containing ODO reached constant values of vapor pressure after 24 h of equilibration whereas for BDO the system took 96 h to reach equilibrium (Table 6). Most probably this behavior depends on the presence of traces of water in the highly hygroscopic BDO. The distribution of such water between the different phases occurred very slowly, as suggested by a progressive increase of RH from 34% (24 h) to 49% (96 h).

Table 6 a_w measured in the sealed vessels containing the reaction mixtures and the immobilization carrier. Values refer to systems made with 0.006 mol of each monomer in a 50 mL round-bottom flask equilibrated at 30 °C until constant readings

Monomer mixture	Water added 0 μL	Water added 5 μL	Water added 10 μL
DMA-BDO (96 h)	a_w 0.49	a_w 0.63	a_w 0.61
DMA-ODO (24 h)	a_w 0.34	a_w 0.35	a_w 0.51

Overall, the data in Table 6 indicate that at the starting of the reactions all different systems studied with the factorial design had a_w values ranging between 0.34 and 0.63.

Fig. 4 reports a global visual representation of the data obtained with BDO and ODO, with the results displaced at the edges of the cubes. The two centers report the average of values obtained from the replicates using BDO and ODO and provide information on the effect of the diol structure.
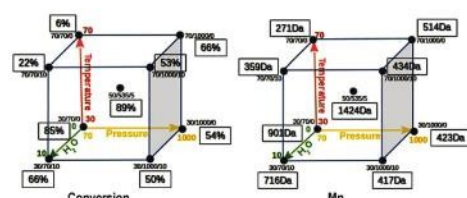
Data clearly indicate that immobilized Thc_cut1 displays the best performances at intermediate values of all experimental variables considered in the study.

The variable importance plots (VIP plots) explain the effect of each single variable and, most importantly, of their interactions (Fig. 5). They were calculated by linear regression for both responses, where the effect corresponds to the difference between the averages of responses obtained at a high and low level of each experimental factor. Details are available in the ESI, Fig. S52.†
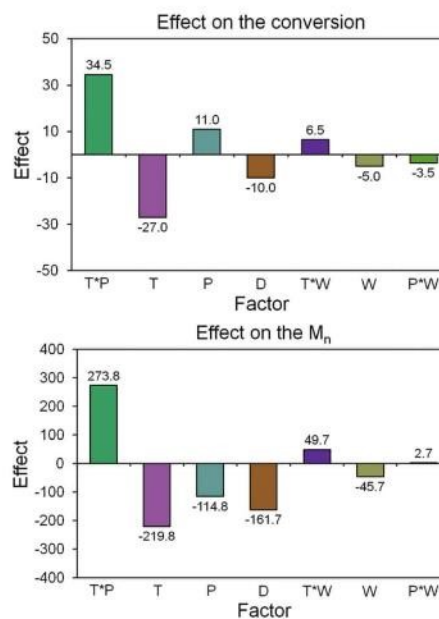
Temperature is the factor that exerts a major and detrimental effect on the reaction, indicating that Thc_cut1 prefers milder temperatures to 70 °C. At 30 °C the enzyme is efficient but most probably the temperature is insufficient for increasing the fluidity of the reaction mixture, so that 50 °C appears to be a suitable temperature for the chosen reactions.

Interestingly, pressure does not exert a great effect on conversion and M_n but rather the interaction between pressure and temperature causes the most negative effect on the reactions. The results of the design indicate that the enzyme is severely affected by vacuum at high temperature, whereas the negative effect of vacuum is not relevant at low temperature.

It is note worthy that the chemometric approach disclosed the disruptive effect of this interaction, whereas the mono-

Fig. 5 Analysis of effect of variables and of their interactions on reaction conversion and M_n.

variate analysis of the preliminary data induced to attribute a negative effect on the vacuum alone.

The structure of the diol is also relevant for the elongation of the reaction, whereas the conversion is not much affected. This finding suggests that the bulkiness of the substrates gains increasing importance as the reaction proceeds and the molecular weight of the oligoesters grows. It must be also taken into account that BDO is a viscous liquid, whereas ODO is a solid (melting point between 57 and 61 °C) that is suspended in the DMA and melts upon heating at 50 °C. The corresponding intermediate products of ODO are more viscous, thus hampering the elongation of the oligoesters.

Unexpectedly, the water added to the system does not exert a major effect on M_n, and polycondensation proceeds even in the presence of small volumes of water (5 μL for 0.006 moles of each monomer), at a mild temperature (50 °C) and under vacuum (535 mbar). In summary, these findings indicate that immobilized Thc_cut1 works optimally under conditions quite different from those employed so far for the polycondensation reactions catalyzed by CaLB. A comprehensive review by Gross and co-workers[20] reported a list of polycondensations catalyzed by CaLB carried out between 70 and 95 °C and most studies underlined how heating must be used in combination with high vacuum for removing traces of water or the leaving nucleophile (i.e. alcohol or water), thus promoting the shifting of equilibrium towards synthesis.[5,12]

Fig. 4 Tridimensional representation of conversions and M_n obtained in the reactions of the factorial design. Numbers reported in the cubic space represent the average of values obtained from the corresponding reactions carried out with BDO and ODO.

Indeed, Table 4 above reports that CaLB immobilized on epoxy methacrylic resins leads to polyesters of DMA and BDO with M_ws of almost 7000 Da and M_n above 3000 Da when working at 70 °C and 70 mbar, whereas at atmospheric pressure M_n falls dramatically to 528 Da. In order to further compare the behavior of CaLB with Thc_cut1 we carried out the same polycondensation catalyzed by CaLB at 50 °C. The results are reported in the ESI (Fig. S48–S51†). Although the conversion of the diol was 90%, surprisingly ESI mass spectrometry shows the formation of polyesters with M_ws lower than 1000 Da. More importantly, the spectra pointed out the formation of hydrolytic products as well cyclic polyesters. After 72 h of reaction the elongation does not improve but rather the formation of hydrolysis products is even more evident. Apparently CaLB is more sensitive to traces of water, which affects the equilibrium of the reaction.

Molecular dynamics simulations of CaLB and Thc_cut1 at different temperatures and pressure

In the next step of the investigation we intended to investigate whether conformational changes are on the basis of the different behaviour of CaLB and Thc_cut1. Molecular Dynamics simulations were run under different conditions of temperature and pressure for 10 ns by using the software GROMACS version 4, OPLS force field definitions and explicit water as a solvent. Each enzyme was subjected to three different simulations (6 MD simulation in total) in terms of temperature and pressure conditions that are highlighted in Table 7.

Each enzyme structure was analyzed and compared on the basis of RMSF calculated on the protein Cα. The RMSF analysis of Thc_cut1 (see ESI Fig. S46†) shows that the enzyme has a similar behaviour under all conditions, with a slightly higher average enzyme mobility at 343 K, as normally expected. More relevant conformational mobility differences are observable for the terminal parts of the protein chain. The overall conformational stability of Thc_cut1 is also confirmed by the superimposition of the structures resulting from the three simulations (Fig. 6). On the other hand, Fig. 6 highlights some differences not revealed by the RMSF analysis and mainly related to side chain movements in an area flanking the active site corresponding to residues 86–91.

At 343 K and 70 mbar (blue structure) the active site appears slightly less accessible than at atmospheric pressure (red structure), as a consequence of conformational changes of residues 86–91, although it is difficult to establish a direct link between these observations and the negative effect of high temperature and vacuum on the enzyme. Nevertheless, the MD

Fig. 6 Superimposition of the structures of Thc_cut1 resulting from the three different MD simulations: condition 1 (300 K, 1000 mbar) in green, condition 2 (343 K, 1000 mbar) in red; condition 3 (343 K; 70 mbar) in blue. Catalytic serines are represented in sphere mode; residues 86–91 in the proximity of the enzyme active site are highlighted in the yellow circle.

simulations did not show fast and disruptive conformational changes caused by the combination of high temperature and vacuum.

RMSF analysis performed on the Cα of CaLB (see ESI Fig. S47†) shows clear differences in the enzyme behaviour under different simulated conditions. Such differences are even more evident by superimposing the structures (Fig. 7).

Fig. 7 Superimposition of the structures of CaLB resulting from the three different MD simulations: condition 1 (300 K, 1000 mbar) in green, condition 2 (343 K, 1000 mbar) in red; condition 3 (343 K, 70 mbar) in blue. Catalytic serines are represented in sphere mode; residues 86–91 in the proximity of the enzyme active site are highlighted in the yellow circle.

Table 7 Temperature and pressure settings of the 3 MD simulations performed on each enzyme

Simulation	Temperature	Pressure
1	300 K	1000 mbar
2	343 K	1000 mbar
3	343 K	70 mbar

Fig. 7 indicates that the protein loops at the active site entrance, corresponding to residues 138–143 and 187–193 (highlighted in the yellow circle), change their conformations on passing from physiological conditions (green structure: 300 K; atmospheric pressure) to high temperature and low pressure (343 K, 70 mbar; in blue) that widen the active site shape. Notably, no enlargement of the active site is observable in the simulation run at high temperature and atmospheric pressure (343 K, 1000 mbar; in red).

Although MD simulations provide some preliminary important hints on the stability of ThC_cut1 and the accessibility of the active sites of both hydrolases, the different effects of temperature and pressure on the two enzymes appear strictly linked to the role of water inside active sites. BioGPS analysis reported above clearly indicates that the H-bond capabilities of CaLB are different from what was observed for most lipases.

It must be noted that several authors have already discussed the possible effect of water molecules entrapped in the stereospecificity pocket of CaLB[40,41] and this issue appears of crucial importance for the optimal exploitation of this enzyme in polycondensations. Future engineering strategies of CaLB might follow that direction, also taking inspiration from the positive features displayed by Thc_cut1.

Conclusions

Enzyme catalyzed reactions, because of their selectivity and efficiency, have the potential to confer advanced and unique properties to polyesters, while boosting a sustainable innovation towards more benign polymers and synthetic processes. Here we demonstrated the feasibility of fully renewable enzymatic synthesis of polyesters by addressing comprehensively the environmental, technological and economic constraints. Bio-based monomers were used in polycondensations catalysed by a cutinase enzyme (Thc_cut1) immobilized on renewable and inexpensive carriers made by using milled rice husk following a simple and economic protocol of adsorption and crosslinking thus overcoming the environmental impact of conventional fossil-based immobilization carriers. The biocatalyst works efficiently in solvent-free systems and under very mild reaction conditions (50 °C) as compared to conventional polycondensations employing toxic metals (T > 150 °C). As compared to lipase B from *Candida antarctica*, Thc_cut1 is less sensitive to the presence of water in the system and this feature makes achieving chain elongation possible at a pressure closer to atmospheric pressure without observing hydrolytic reactions. Moreover, by operating under thin-film conditions, mass and heat transfer are optimized, with consequent energy saving.

These findings set robust premises for further exploitations of this cutinase enzyme in different environmentally and economically sustainable synthesis of biorenewables.[42]

Future investigations might address engineering strategies to enlarge the specificity and catalytic properties of Thc_cut1.

The accessible and superficial active site of Thc_cut1 makes this enzymatic scaffold very attractive for polymer synthesis and transformation of bulky substrates in general. Information coming from BioGPS bioinformatics analysis provides guidelines for future engineering studies aiming, for instance, at introducing different promiscuous activities in the Thc_cut1 scaffold. On that respect, Bio_GPS analysis disclosed the similarities between Thc_cut1 and CaLB, which share the hydrophobic nature of lipases but appear to be functionally closer to esterases.

Methods

Chemicals and reagents

EC-EP/M Sepabeads were kindly donated by Resindion S.r.l., (Mitsubishi Chemical Corporation, Milan, Italy). Dimethyl adipate (DMA) was purchased from Sigma-Aldrich. 1,4-Butanediol (BDO), and 1,8-octanediol (ODO) were purchased from Merck. All other chemicals and solvents were also purchased from Sigma-Aldrich at reagent grade, and used without further purification if not otherwise specified. The samples of rice husk (carnaroli type) were kindly donated by Riseria Cusaro S.r.L. (Binasco, Italy).

Enzymes

The recombinant *Thermobifida cellulosilytica* cutinase 1 (Thc_cut1) was produced and purified as previously described.[43] The organism used for the expression was *E. coli*. Novozym® 435 was purchased from Sigma-Aldrich (product code: L4777) containing *Candida antarctica* lipase B immobilized on macroporous acrylic resin, exhibiting a synthetic activity of 11 700 PLU U per g propyl laurate units). Lipozyme CaLB (protein concentration of 8 mg mL^{-1}) was a kind gift from Novozymes (DK).

Protein structures

All the protein structures used as the dataset for BioGPS model generation (Table S1 in the ESI†) were retrieved from the Protein Data Bank (PDB)[26] and preprocessed by using the software PyMOL.[44] All molecules but the proteins were deleted (*i.e.* water molecules, inhibitors, glycosylation residues, *etc.*). The original protein structure coordinates (from the PDB) were used as inputs, without any previous superimposition.

The same approach was used for the structure of *Humicola insolens* cutinase (HiC) (PDB code 4OYY)[27] whereas the structure of cutinase from *Thermobifida cellulosilytica* (Thc_cut1) comes from an already published homology model.[15]

BioGPS model

The BioGPS (Global Positioning System in Biological Space) model was obtained as already published[21] using BioGPS software version 2.1. BioGPS is based on the "Common Reference Framework" composed by two main steps: the characterization of the protein active sites and their comparison. The active site of each enzyme was automatically detected by the FLAPsite

132

algorithm.[23] First the algorithm reduces the complexity of the pseudo-MIFs selecting a number of representative points using a weighted energy-based and space-coverage function. Then it generates all possible combinations of four points; each combination is termed "quadruplet". All possible quadruplets for each mapped active site were generated and stored into a biofingerprint (bitstring). Each active site was then compared within the Common Reference Framework using an "all against all" approach where each enzyme active site is compared with itself and with all the other enzyme active sites. At the end, the algorithm generates a set of Tanimoto scores[45] represented by square matrixes, namely a series of probe scores (one for each original probe) together with a global score. The set of Tanimoto scores was used as an input for the UPCA algorithm which generated the final BioGPS statistical model by generating the multidimensional space (Principal Components – PCs) which differentiated each enzyme active site on the bases of their similarities and differences.

Projection of cutinases

The two cutinases Hic and Thc_cut1, were projected into the BioGPS model. These two enzymes were processed as described in the previous section. Each cutinase was compared with itself and with all the other enzymes. Finally the Tanimoto scores[45] (see the ESI† for details) were used for the projections of the two cutinases into the BioGPS model computed for the 41 ser-hydrolases.

Milling of rice husk

Rice husk was milled using a Rotor mill ZM 200 (Retsch S.r.l., Bergamo, Italy) according to a procedure already described.[14] The raw material was separated by size using sieves of 450 and then 200 mm. The wet particles were weighed and then dried in an oven at 120 °C for 6 h. The density of RH before milling was 0.153 g mL^{-1} whereas the milled RH (size 0.2–0.4 mm) had a density of 0.437 g mL^{-1}. The full characterization of rice husk has been previously reported.[14]

Immobilization of Thc_cut1 on milled rice husk (200–400 µm diameter)

The rice husk powder (200–400 µm) was washed with an ethanol/distilled H$_2$O mixture (2×) 10 min each step (4 mL g^{-1} dry material). Then the particles were rinsed with distilled H$_2$O (2 times). The moisture content was determined as described above and an amount corresponding to 1 g of dry rice husk powder was suspended in 10 mL of 0.4 mg mL^{-1} enzyme solution in 0.1 M Tris-HCl buffer pH 7.0 at room temperature for 24 h on a rotating wheel. The progress of the immobilization was monitored by evaluating the residual protein concentration in the supernatant after 4, 8 and 24 h and data are reported in the ESI.† The supernatant containing the unbound enzyme was discharged and the cutinase adsorbed on the rice husk was subjected to a cross-linking step using 5 mL solution of glutaraldehyde 1.5% in potassium phosphate buffer 0.1 M pH 8.0, for 4 h at room temperature. The enzyme preparation was extensively washed with 0.1 M Tris-HCl buffer

pH 7 in order to remove all the non-bound protein on the support, monitoring UV absorbance of washing solutions. The preparation was left to dry on a Büchner filter for 48 h at 30 °C and atmospheric pressure prior to use (if not otherwise specified).

Immobilization of Thc_cut1 on epoxy activated carrier

The epoxy-activated beads were washed with ethanol (2 times) and double distilled H$_2$O (2 times) prior to use. A total of 1.0 g of dry epoxy-activated beads were suspended in 10 mL of 1 mg mL^{-1} enzyme solution in 0.1 M Tris-HCl buffer pH 7 at 21 °C for 24 h on a blood rotator. The samples were withdrawn over time. The progress of the immobilization was monitored by evaluating the residual activity and the protein concentration in the supernatant. It must be noted that Tris-HCl buffer was selected as immobilization medium because native Thc_cut1 was produced in this same buffer and the exchange of buffer would cause a loss of enzymatic activity (data not shown). After the immobilization, the enzyme preparations were extensively washed with 0.1 M Tris-HCl buffer pH 7 in order to remove all the non-covalently bound protein adsorbed on the support. Finally, in order to block the unreacted epoxy groups, the enzymatic preparations were incubated in 45 mL of 3 M glycine for 24 h at 21 °C as previously reported.[15] The enzyme preparations were extensively washed with 0.1 M Tris-HCl buffer pH 7.

Moisture determination

0.2 g of immobilized enzymatic preparation was weighed in a tarred weighing bottle (A), dried for 6 h at 120 ± 5 °C, cooled down in a dessicator until a constant weight was reached and then weighed again (B). The moisture content was calculated as follows:

$$\text{Moisture content } (\%) = [(A - B)/A] \times 100$$

Activity assay for immobilized enzymes

Activity was measured at 21 °C using PNPB as a substrate. The final assay mixture was made up of 0.1 mL of the substrate solution (86 µL of PNPB and 1000 µL of 2-methyl-2-butanol), 11 mL of 100 mM Tris-HCl buffer at pH 7 and 20 mg of immobilized enzyme preparation. The increase of the absorbance at 405 nm due to the hydrolytic release of p-nitrophenol (ε 405 nm = 9.36 mL (µmol cm)$^{-1}$) was measured over time with a HACH Lange benchtop spectrophotometer using plastic cuvettes. A blank was included using beads where glycine was used instead of an enzyme as a blocker for the epoxy-activated beads. The activity was calculated in units (U), where 1 unit is defined as the amount of the enzyme required to hydrolyze 1 µmol of the substrate per minute under the given assay conditions.

Protein quantification

Protein concentrations were determined by using the BioRad protein assay (Bio-Rad Laboratories GmbH, Vienna, Cat. No: 500-0006). Briefly, 10 µL of the sample was added into the

wells of a 96-well micro-titer plate (Greiner 96 Flat Bottom Transparent Polystyrene). As soon as all the samples were placed into the wells, 200 µL of the prepared BioRad reaction solution were added to the wells (BioRad Reagent diluted 1 : 5 with mQH$_2$O). The plate was incubated for 5 min at 21 °C and 400 rpm. The buffer for protein dilution (0.1 M Tris-HCl pH 7) was used as a blank and BSA (bovine serum albumin) as the standard. The absorption after 5 min was measured at $\lambda = 595$ nm and the concentration calculated from the average of triplicate samples and blanks.

Enzymatic polycondensation using a thin-film reaction system

The thin-film enzymatic polycondensations were conducted as previously reported by Pellis *et al.*[6] Reactions based on the factorial design were carried out using equimolar amounts (0.006 mol) of diester and diol (0.006 mol) and 10% w/w of immobilized iThc_cut1. The reactions were conducted in 50 mL round-bottom flasks connected to a rotary evaporator, applying reduced pressure when requested. The reactions were operated with a Rotavapor R-215 (BÜCHI) connected to a vacuum pump Vac® V-513 (BÜCHI) and a pressure controller V-800 (BÜCHI). Temperature was controlled by means of a Waterbath B-480 (BÜCHI). After 24 h, the reaction mixture was recovered with THF and products were characterized after filtration of the biocatalyst and evaporation of THF, without any further treatment.

Measurement of water activity

Water activity of the reaction system was determined at 30 °C by using a hygrometer (DARAI-Trieste, Italy) operated and calibrated as previously reported.[19] The monomers, the porous immobilization carrier without the enzyme and different volumes of water were added, mixed and thermostated at 30 °C in the same round-bottom flasks used for carrying out the reactions. We assumed that the very small amount of protein linked to the carrier binds to a negligible percentage of water if compared with the huge bead surface and therefore does not affect the a_w of the system. The humidity sensor was maintained in contact with the gas phase within the sealed vessels and the values of relative humidity (RH) were measured until constant readings (a_w), namely the achievement of equilibrium.

The relative humidity at equilibrium is correlated with a_w by the following equation: ERH = $a_w \times 100$.

GPC

The samples were dissolved in THF (250 ppm BHT as inhibitor). Gel permeation chromatography was carried out at 30 °C on an Agilent Technologies HPLC System (Agilent Technologies 1260 Infinity) connected to a 17 369 6.0 mm ID × 40 mm L H$_{HR}$-H, 5 µm guard column and a 18 055 7.8 mm ID × 300 mm L GMH$_{HR}$-N, 5 µm TSK gel liquid chromatography column (Tosoh Bioscience, Tessenderlo, Belgium) using THF (250 ppm BHT as inhibitor) as an eluent (at a flow rate of 1 mL min^{-1}). An Agilent Technologies G1362A refractive index detector was employed for detection. The molecular weights of the

polymers were calculated using linear polystyrene calibration standards (250–70 000 Da).

^{1}H-NMR

Nuclear magnetic resonance ^{1}H measurements were performed on a Bruker Avance II 400 spectrometer (resonance frequencies 400.13 MHz for ^{1}H) equipped with a 5 mm observe broadband probe head (BBFO) with z-gradients. CDCl$_3$ was used as an NMR solvent if not otherwise specified.

Electrospray ionization mass spectrometry (ESI-MS)

The crude reaction mixtures were analyzed on an Esquire 4000 (Bruker) electrospray positive ionization by generating the ions in an acidic environment. Around 10 mg of the sample was dissolved in 2 mL of methanol containing 0.1% v/v formic acid. The generated ions were positively charged with m/z ratio falls in the range of 200–1000. The subsequent process of deconvolution allows the reconstruction of the mass peaks of the chemical species derived from the analysis of the peaks generated.

Planning of the factorial design

The factorial design was planned using the software MODDE 8.0.2 (MSK Umetrics). Polycondensations were carried out on a thin film and under solvent-less conditions using Thc_cut1 immobilized on epoxy methacrylic resin and following the procedures described above. Experiments were run following a random sequence. The independent variables considered were temperature, pressure and added water. They were studied at two levels (+1 and −1). Temperature = (70 °C; 30 °C); pressure = (1000 mbar; 70 mbar); and H$_2$O = (10 µL; 0 µL). The factorial design is composed by the combination of the different levels of the three variables. The effect of the diols (BDO and ODO) was evaluated by dividing the factorial design into two blocks, one for each diol. For each block, a further central point was added, corresponding to the combination of the combination of each independent variable taken at an intermediate level (level 0: $T = 50$ °C; $p = 535$ mbar; H$_2$O = 5 µL). The responses measured for each experiment were the conversion of the diol (calculated by NMR spectroscopy as described above) and the M_n of the product (calculated by GPC analysis). The effects of factors on responses were calculated by multiple linear regression.

Molecular dynamics simulations

The structure of CaLB (PDB 1TCA) and Thc_cut1 (homology model)[15] were protonated at pH 7.0 using the PDB2PQR server[46] based on the software PROPKA.[47] Subsequently, each protonated enzyme structure was defined into an OPLS force field.[48] Each protein was inserted in a cubic box of 216 nm^3 and solvated with an explicit solvent (TIP4 water type).[49] Thus, each enzyme system was minimized using the software GROMACS version 4[50] using the steepest descendent algorithm for 10 000 steps. Afterwards, each enzyme was simulated under three different conditions: (1) 300 K and 1000 mbar; (2) 343 K and 1000 mbar; and (3) 343 K and 70 mbar. Each MD simu-

lation was performed for 10 ns with the software GROMACS version 4 defining a NVT environment; the Particle Mesh Ewald (PME) algorithm[31] was used for the calculation of electrostatic interactions, the v-rescale algorithm64 for temperature and the Berendsen algorithm[52] for pressure were also employed.

The outcome of each MD simulation was analyzed by calculating the Root Mean Square Fluctuation (RMSF), which indicates the average movement of the protein residues during simulation. The calculation was performed on the protein $C\alpha$ using the g_rmsf tool of the GROMCS 4 package.

Acknowledgements

Notes and references

1 UNEP, *Valuing Plastics: The Business Case for Measuring, Managing and Disclosing Plastic Use in the Consumer Goods Industry*, United Nations Environment Programme (UNEP), Nairobi, Kenya, 2014.

2 Ellen MacArthur Foundation, *The new plastics economy: rethinking the future of plastics*, 2016.

3 UNEP, *Plastic in Cosmetics*, United Nations Environmental Programme (UNEP), Nairobi, Kenya, 2015.

4 J. H. Clark, T. J. Farmer, L. Herrero-Davila and J. Sherwooda, *Green Chem.*, 2016, **18**, 3914–3934.

5 A. Pellis, L. Corici, L. Sinigoi, N. D'Amelio, D. Fattor, V. Ferrario, C. Ebert and L. Gardossi, *Green Chem.*, 2015, **17**, 1756–1766.

6 I. Bassanini, K. Hult and S. Riva, *Beilstein J. Org. Chem.*, 2015, **11**, 1583–1595.

7 F. Binns, P. Harffey, S. M. Roberts and A. Taylor, *J. Chem. Soc., Perkin Trans. 1*, 1999, 2671–2676.

8 M. B. Ansorge-Schumacher and O. Thum, *Chem. Soc. Rev.*, 2013, **42**, 6475–6490.

9 A. A. Koutinas, A. Vlysidis, D. Pleissner, N. Kopsahelis, I. Lopez Garcia, I. K. Kookos, S. Papanikolaou, T. H. Kwanb and C. Sze Ki Lin, *Chem. Soc. Rev.*, 2014, **43**, 2587–2627.

10 A. Pellis, E. Herrero Acero, L. Gardossi, V. Ferrario and G. M. Guebitz, *Polym. Int.*, 2016, **65**, 861–871.

11 A. Pellis, E. Herrero Acero, V. Ferrario, D. Ribitsch, G. M. Guebitz and L. Gardossi, *Trends Biotechnol.*, 2016, **34**, 316–328.

12 L. Corici, A. Pellis, V. Ferrario, C. Ebert, S. Cantone and L. Gardossi, *Adv. Synth. Catal.*, 2015, **8**, 1763–1774.

13 G. Cerea, L. Gardossi, L. Sinigoi and D. Fattor, *World Patent* WO/2013110446A1, 2013.

14 L. Corici, V. Ferrario, A. Pellis, C. Ebert, S. Lotteria, S. Cantone, D. Voinovich and L. Gardossi, *RSC Adv.*, 2016, **6**, 63256–63270.

15 A. Pellis, V. Ferrario, B. Zartl, M. Brandauer, C. Gamerith, E. Herrero Acero, C. Ebert, L. Gardossi and G. M. Guebitz, *Catal. Sci. Technol.*, 2016, **6**, 3430–3442.

16 A. Pellis, A. Guarneri, M. Brandauer, E. Herrero Acero, H. Peerlings, L. Gardossi and G. M. Guebitz, *Biotechnol. J.*, 2016, **11**, 642–647.

17 P. Sieber, M. Schorderet, U. Ryser, A. Buchala, P. Kolattukudy, J. P. Métraux and C. Nawrath, *Plant Cell*, 2000, **12**, 721–737.

18 E. Stavila, R. Z. Arsyi, D. M. Petrovic and K. Loos, *Eur. Polym. J.*, 2013, **49**, 834–842.

19 D. Feder and R. A. Gross, *Biomacromolecules*, 2010, **11**, 690–697.

20 R. A. Gross, M. Ganesh and W. Lu, *Trends Biotechnol.*, 2010, **8**, 435–443.

21 V. Ferrario, L. Siragusa, C. Ebert, M. Baroni, M. Foscato, G. Cruciani and L. Gardossi, *PLoS One*, 2014, **9**, e109354.

22 M. Baroni, G. Cruciani, S. Sciabola, F. Perruccio and J. S. Mason, *J. Chem. Inf. Model.*, 2007, **47**, 279–294.

23 S. Henrich, O. M. Salo-Ahen, B. Huang, F. F. Rippmann, G. Cruciani and R. C. Wade, *J. Mol. Recognit.*, 2010, **23**, 209–219.

24 L. Siragusa, S. Cross, M. Baroni, L. Goracci and G. Cruciani, *Proteins*, 2015, **83**, 517–532.

25 P. Braiuca, L. Knapic, V. Ferrario, C. Ebert and L. Gardossi, *Adv. Synth. Catal.*, 2009, **351**, 1293–1302.

26 H. M. Berman, J. Westbrook, Z. Feng, G. Gilliland, T. N. Bhat, H. Weissig, I. N. Shindyalov and P. E. Bourne, *Nucleic Acids Res.*, 2000, **28**, 235–242.

27 D. Kold, Z. Dauter, A. K. Laustsen, A. M. Brzozowski, J. P. Turkenburg, A. D. Nielsen, H. Koldso, E. Petersen, B. Schiott, L. De Maria, K. S. Wilson, A. Svendsen and R. Wimmer, *Protein Sci.*, 2014, **23**, 1023–1035.

28 J. Uppenberg, M. T. Hansen, S. Patkar and T. A. Jones, *Structure*, 1994, **2**, 293–308.

29 P. C. Boutros and A. B. Okey, *Briefings Bioinf.*, 2005, **6**, 331–343.

135

30 M. H. M. Olsson, W. W. Parson and A. Warshel, *Chem. Rev.*, 2006, **106**, 1737–1756.

31 A. Warshel, P. K. Sharma, M. Kato, Y. Xiang, H. Liu and M. H. Olsson, *Chem. Rev.*, 2006, **106**, 3210–3235.

32 R. DiCosimo, J. McAuliffe, A. J. Pouloseb and G. Bohlmann, *Chem. Soc. Rev.*, 2013, **42**, 6437–6474.

33 S. Kim, C. Jimenez-Gonzalez and B. E. Dale, *Int. J. Life Cycle Assess.*, 2009, **14**, 392–400.

34 N. K. Sharma, W. S. Williams and A. Zangvil, *J. Am. Ceram. Soc.*, 1984, **67**, 715–720.

35 L. M. Contreras, H. Schelle, C. R. Sebrango and I. Pereda, *Water Sci. Technol.*, 2012, **65**, 1142–1149.

36 W. R. Stahel, *Nature*, 2016, **531**, 435–438.

37 C. Korupp, R. Weberskirch, J. J. Muller, A. Liese and I. Hilterhaus, *Org. Process Res. Dev.*, 2010, **14**, 1118–1124.

38 P. Braiuca, C. Ebert, A. Basso, P. Linda and L. Gardossi, *Trends Biotechnol.*, 2006, **24**, 419–425.

39 R. V. Ulijn, L. De Martin, P. J. Halling, A. E. M. Janssen, L. Gardossi and B. D. Moore, *Biotechnol. Bioeng.*, 2002, **80**, 509–515.

40 V. Léonard-Nevers, Z. Marton, S. Lamare, K. Hult and M. Graber, *J. Mol. Catal. B: Enzym.*, 2009, **59**, 90–95.

41 P. Spizzo, A. Basso, C. Ebert, L. Gardossi, V. Ferrario, D. Romano and F. Molinari, *Tetrahedron*, 2007, **63**, 11005–11010.

42 M. C. Franssen, P. Steunenberg, E. L. Scott, H. Zuilhofac and J. P. Sanders, *Chem. Soc. Rev.*, 2013, **42**, 6491–6533.

43 E. Herrero Acero, D. Ribitsch, G. Steinkellner, K. Gruber, K. Greimel, I. Eiteljoerg, E. Trotscha, R. Wei, W. Zimmermann, M. Zinn, A. Cavaco-Paulo, G. Freddi, H. Schwab and G. M. Guebitz, *Macromolecules*, 2011, **44**, 4632–4640.

44 *The PyMOL Molecular Graphic System. Version 1.5.0.3*, Schrodinger LLC.

45 D. J. Rogers and T. T. Tanimoto, *Science*, 1960, **132**, 1115–1118.

46 T. J. Dolinsky, J. E. Nielsen, J. A. McCammon and N. A. Baker, *Nucleic Acids Res.*, 2004, **32**, W665–W667.

47 H. Li, A. D. Robertson and J. H. Jensen, *Proteins*, 2005, **61**, 704–721.

48 G. A. Kaminski, R. A. Friesner, J. Tirado-Rives and W. L. Jorgensen, *J. Phys. Chem. B*, 2001, **105**, 6474–6487.

49 H. W. Horn, W. C. Swope, J. W. Pitera, J. D. Madura, T. J. Dick, G. L. Hura and T. Head-Gordon, *J. Chem. Phys.*, 2004, **120**, 9665–9678.

50 B. Hess, C. Kutzner, D. V. D. Spoel and E. Lindahl, *J. Chem. Theory Comput.*, 2008, **4**, 435–447.

51 U. Essmann, L. Perera, M. L. Berkowitz, T. Darden, H. Lee and L. G. Pedersen, *J. Chem. Phys.*, 1995, **103**, 8577–8593.

52 H. J. C. Berendsen, J. P. M. Postma, W. F. van Gunsteren, A. Di Nola and J. R. Haak, *J. Chem. Phys.*, 1984, **81**, 3684.

136

10. Aknowledgements

I would like to acknowledge first and foremost professor Lucia Gardossi and Cynthia Ebert for all the help they gave me during these years and for guiding me with great passion for their work.

I express gratitude to my family, friends and to all the master degree students who shared with me this journey.